Retrofitted Solar Domestic Hot Water System for Single-Family Electrically-Heated Houses

Development and testing

Ricardo Bernardo

Doctoral Dissertation

Keywords

Solar domestic hot water, retrofitting, single family electrically heated houses, high solar fraction, photovoltaic thermal concentrating hybrids, PVT, parabolic reflectors, CPC thermal collector.

English language corrected by Leslie Walke, CommunicAID

Printed by Media-Tryck, Lund University, Sweden

Report No EBD-T--13/17
Retrofitted Solar Domestic Hot Water System for Single-Family Electrically-Heated Houses
Department of Architecture and Built Environment, Division of Energy and Building Design, Lund University, Lund

ISSN 1651-8136
ISBN 978-91-85147-55-7

Lund University, Lund Institute of Technology
Department of Architecture and Built Environment
Division of Energy and Building Design
P.O. Box 118
SE-221 00 Lund
Sweden

Telephone: +46 46 - 222 73 52
Telefax: +46 46 - 222 47 19
E-mail: ebd@ebd.lth.se
Hompage: www.ebd.lth.se

Abstract

In Sweden, there are roughly half a million single-family houses that use electric heating for both domestic hot water production and space heating. Since electricity is the most expensive energy source in Sweden, it is interesting to install a high solar fraction solar thermal system to reduce the domestic hot water energy use in these houses. One of the most significant bottlenecks for deployment of solar heating technology is economic profitability due to high investment costs. During this investigation a system that retrofits existing domestic hot water electric storages was developed. This has the potential to significantly reduce the investment costs regarding both material and installation. Three different collectors were also tested. Their suitability to be part of the retrofitted solar domestic hot water system was addressed. These were a one-axis tracking photovoltaic/thermal (PV/T) concentrating hybrid and two stationary compound parabolic concentrating (CPC) collectors with the same geometry. One of the CPC collectors was a thermal collector while the other was a PV/T hybrid collector. The aim for PV/T concentrating hybrid collectors is to produce heat and electricity at a lower cost than conventional alternatives. The CPC-thermal collector design aims to adapt the solar production to the yearly consumption profile in order to achieve a higher annual solar fraction without increasing the stagnation periods.

Outdoor measurements were carried out to characterise the collectors. For the retrofitted system, several system configurations were theoretically analysed by means of simulation models using TRNSYS software. A prototype of the retrofitted system was built and the simulation model was revised and validated against measurements. The validated model was further used to optimize the performance of the system and to carry out a sensitivity analysis. Furthermore, an add-on retrofitting unit that is able to connect solar collectors to existing hot water electric storages was also designed and built.

Measurement results showed that the efficiency values of the tracking concentrating PV/T hybrid are lower than those of conventional flat plate collectors and PV modules. The usable incident irradiation on the one-axis tracking concentrating surface is also lower than the usable irradiation in-

cident on a stationary optimally tilted flat surface. Even though the studied hybrid has potential for improvement, the combination of low efficiencies with low usable irradiation levels makes it difficult for concentrating PV/T hybrids to compete with conventional alternatives, especially in countries where the annual beam irradiation values are low. The geometry of the tested stationary CPC-PV/T hybrid collector was shown not to be the most appropriate for hybrid applications. The measured incidence angle modifier effects were also high. The studied CPC-thermal collector system was found to achieve a higher annual solar fraction than a conventional flat plate collector system while making use of less absorber surface, one of the most expensive components in the collector. It is concluded that the CPC-thermal collector is adequate to be part of the retrofitting solar domestic hot water system in Swedish single-family houses. The decrease in absorber area together with the increase in performance must compensate for the additional cost of extra materials such as reflectors, glass and frames.

The investigation of the retrofit system showed that an annual solar fraction of 58% can be achieved in Sweden when a 200-litre hot water heater is retrofitted and 6 m^2 of flat plate collectors is used. The investment cost of the developed retrofit solution was estimated to be reduced by roughly one third compared with a conventional solar domestic hot water system. This means that the developed retrofit system achieves a comparable performance with conventional solar domestic hot water systems in single-family houses with a significant reduction in investment cost. The developed retrofitting solution is therefore considered to have the potential to become a competitive solution in the solar domestic hot water market.

Contents

Nomenclature

Latin

$A_{active\ elect.}$	Electrically active glazed area of the hybrid	m^2
$A_{active\ thermal}$	Thermally active glazed area of the hybrid	m^2
A_{total}	Total glazed collector area	m^2
$b_{0\_electric}$	Electric incidence angle modifier coefficient	-
$b_{0\_thermal}$	Thermal incidence angle modifier coefficient	-
C	Geometrical concentration ratio	-
C_p	Heat capacity	J/kg/°C
f_{comf}	Fraction between the penalty function and the total domestic hot water (DHW) load of the DHW reference system	-
FF	Fill Factor	-
F'	Collector efficiency factor for the absorber	-
$F'U_0$	Heat loss coefficient when $(T_m-T_{amb})=0$	$W/m^2/°C$
$F'U_1$	Temperature dependence of the heat loss coefficient	$W/m^2/°C^2$
$F'U_u$	Wind speed dependence of the heat loss coefficient	$Ws/m^3/°C$
$F'(\tau\alpha)_n =$	Zero loss efficiency for beam radiation at normal incidence angle	-
G	Global solar radiation	W/m^2
G_b	Beam solar radiation	W/m^2
G_d	Diffuse solar radiation	W/m^2
I	Current	A
I_L	Light generated current	A
I_{mp}	Current at maximum power point	A
I_{sc}	Short circuit current	A
I_0	Diode leakage current in the absence of light	A
k	Boltzmann's constant	J/K
$K_b(\Theta)$	Beam incidence angle modifier	-
$K_{b\_electric}(\Theta)$	Electric beam incidence angle modifier	-
$K_{b\_thermal}(\Theta)$	Thermal beam incidence angle modifier	-
K_d	Diffuse incidence angle modifier	-
K_T	Dependence of beam electric efficiency on temperature	%/°C
L	Length of the pipes	m
$\dot{m}$	Mass flow	kg/s
n	Idealist factor of the diode	-
q	Thermal energy rate	W

$q_{electric}$	Electric power	W/m^2
$q_{thermal}$	Thermal energy rate	W/m^2
q_C	Absolute value of the electronic current	C
Q_{aux}	Required auxiliary energy to meet the load	kWh
$Q_{aux,error}$	Error between the modelled and measured auxiliary energy	%
$Q_{aux,meas}$	Measured auxiliary energy	kWh
$Q_{aux,mod}$	Modelled auxiliary energy	kWh
$Q_{aux,ref}$	Required auxiliary energy of the reference system to meet the DHW load without the use of solar collectors	kWh
$Q_{DHW,meas}$	Measured energy provided by the SDHW system	kWh
$Q_{DHW,mod}$	Modelled energy provided by the SDHW system	kWh
$Q_{energy,miss}$	Energy that was not provided to the load	kWh
$Q_{losses-aux}$	Thermal losses from the auxiliary storage	kWh
$Q_{losses-retrofit/stnd}$	Thermal losses of the retrofitted storage or the standard solar storage	kWh
$Q_{penalty,ref}$	Penalty function of the solar domestic hot water system	kWh
$Q_{penalty}$	Penalty function of the domestic hot water system without solar collectors	kWh
Q_{pumps}	Required energy to run the pumps in the system	kWh
Q_{total}	Required auxiliary energy to meet the load including the energy required by the pumps	kWh
R_L	Load resistance	Ω
R_s	Series resistance	Ω
R_{sh}	Shunt resistance	Ω
SF_{ext}	Extended solar fraction	-
$SF_{ext,ref}$	Extended solar fraction relative to a reference system	-
SF_i	Solar fraction indicator	-
t_i	Initial time of the integrating period	h
t_f	Final time of the integrating period	h
T	Temperature of the solar cell	°C
T_{amb}	Ambient temperature	°C
$T_{aux,ret}$	Thermostat temperature of the heater of the retrofitted hot water storage	°C
T_{cold}	Temperature of the incoming cold water from the discharge in the SDHW system	°C
T_{hot}	Hot water temperature delivered by the SDHW system	°C
$T_{hot,comf}$	Hot water temperature requirement	°C
T_{in}	Inlet fluid temperature to the collector	°C
T_m	Mean fluid temperature in the absorber	°C
T_{out}	Outlet fluid temperature from the collector	°C
T_{set}	Temperature setting of the auxiliary heater	°C
T_{solar}	Solar hot water temperature in the upper part of the retrofitted tank	°C
u	Wind speed near the collector	m/s

U	Voltage	V
UA_{HX}	Overall heat transfer coefficient of the heat exchanger	W/K
U_{aux}	Heat loss factor of the new auxiliary storage	W/m^2/°C
U_{bottom}	Heat loss factor of the bottom part of the retrofitted hot water storage	W/m^2/°C
U_{mid}	Heat loss factor of the middle part of the retrofitted hot water storage	W/m^2/°C
U_{pipes}	Heat loss factor of the pipes	W/m^2/°C
U_{top}	Heat loss factor of the upper part of the retrofitted hot water storage	W/m^2/°C
V	Volume	m^3
V_{aux}	Volume of the new auxiliary storage	litres
V_{mp}	Voltage at maximum power point	V
V_{oc}	Open circuit voltage	V
V_{sol}	Volume of the retrofitted hot water storage	litres
$\dot{V}$	Flow rate	m^3/s
$\dot{V}_p$	The highest flow rate at which the flow meter shall function without the maximum permissible errors being exceeded	m^3/s
x	Power of the penalty function	-
$(mC)_e$	Effective thermal capacitance including piping for the collector array per collector area	J/m^2/°C

Greek

α	Absorptance coefficient	-
η	Efficiency	-
$\eta(\Theta)$	Efficiency at incidence angle θ	-
$\eta_{b\_electrical}$	Beam electric efficiency	-
$\eta_{b\_thermal}$	Beam thermal efficiency	-
$\eta_{0b}(0)$	Zero loss efficiency for beam radiation at normal incidence angle	-
$\eta_{0b}(\Theta)$	Zero loss efficiency for beam radiation at incidence angle θ	-
θ	Angle of incidence of the beam radiation with the normal to the collector plane	Angular degrees
θ_t	Transverse angle of incidence onto collector	Angular degrees
θ_l	Longitudinal angle of incidence onto collector	Angular degrees
ρ	Density	kg/m^3
τ	Transmittance coefficient of the glass	-
$(\tau\alpha)$	Effective transmission-absorption of the solar radiation	-
$(\tau\alpha)_n$	Effective transmission-absorption of the beam radiation at normal incidence angles	-
σ_T	Standard deviation of the temperature measurement	°C

Δ_T	Heat-carrier temperature change	K

Abbreviations

CPC	Compound parabolic concentrator
DHW	Domestic hot water
IAM_t	Transversal incidence angle modifier for beam radiation
IAM_l	Longitudinal incidence angle modifier for beam radiation
IPCC	Intergovernmental Panel for Climate Change
PV/T	Photovoltaic/Thermal hybrid
RRR	Resources/Reserves Ratio
SDHW	Solar domestic hot water system

Acknowledgements

This Ph.D. thesis has been supported by the Swedish Energy Agency and the Marie Curie Program, SolNet-Advanced Solar Heating and Cooling for Buildings which is the first coordinated international Ph.D. education program in Solar Thermal Engineering.

I wish to thank Björn Karlsson (Mälardalen University) for the valuable discussions and positive attitude. His creative thinking and broad perspective of the solar energy field was important when putting the results of this investigation into a context. Åke Blomsterberg (Lund University) is acknowledged for contributing with a critical review of the work and proofreading this manuscript.

For being a friend since I arrived at the department, I am grateful to my colleague Henrik Davidsson (Lund University). He has been one of the great contributors in teaching me Swedish and more importantly "Skånska", the interesting dialect spoken in the South of Sweden. I am grateful to Johan Nilsson (Lund University) for valuable discussions and close support during challenging times, especially at the beginning of the project. I would like to thank Håkan Håkansson (Lund University) for the support with measurements. Bengt Perers (Technical University of Denmark) is acknowledged for helping with my practical work. He was one of the persons from whom I have learned most in terms of collector testing. His help on the simulation software and interpretation of the results was also important. Chris Bales (Dalarna University) is acknowledged for valuable feedback regarding published articles and parts of the thesis. I thank Simon Furbo (Technical University of Denmark) for helpful discussions regarding the methods and results of the study. I am grateful to Bengt Hellström (Lund University) for his help on critically evaluating the research work. Peter Krohn (Vattenfall AB) is acknowledged for his help in installing the data monitoring system. I would also like to thank Gunilla Kellgren (Lund University) for all the help and support during the project. I thank Niko Gentile (Lund University), João Gomes (Solarus AB) and Christian Gruffman (Vattenfall AB) for their positive attitude in our common projects. Leslie Walke is acknowledged for proof reading the

thesis in terms of the English language and Ilgot Liljedahl (Media-Tryck) for taking care of the layout.

To everyone at the Division of Energy and Building Design, I wish to express my gratitude for making me feel welcome right from the start. The biggest reward when working abroad is the culture and social experience; these people have been important in this.

Finally, it is with particular pleasure that I express my gratitude to my family for all the help and support during this period. My wonderful grandparents have been tireless in keeping me in touch with home, despite the distance. They have mailed me a bit of everything from Portugal, such as newspapers, wine and even my favourite cake. They have been very interested in hearing me refute many of the Swedish myths common in southern Europe. Some of their favourites are the non-existence of polar bears and that the temperature reaches 25°C in the summer. I am also especially grateful to my parents and grandfather for being a constant and active source of information related to the research subject. Finally I want to express my gratitude to my "sambo" (partner) Jennie for always supporting me with her contagious joy and positive attitude. She helped make this journey such an amazing one.

1 Introduction

In this section the background, main objectives, method and limitations of the research work are addressed. The latest developments regarding the availability of conventional fuels and climate change issues are briefly presented. The climate and energy policies of the European Union and Sweden in particular are also discussed. The background of energy use in Swedish buildings is described with the focus on electrically heated single-family houses. Finaly, the risk of legionella growth in solar domestic hot water systems is discussed with the focus on the developed retrofitted system.

1.1 Background

1.1.1 Conventional fuels, climate change and solar energy

Climate change and the scarcity of energy resources are two of the biggest challenges we will face in the near future (European Renewable Energy Council, 2010). Growth and implementation of renewable energies directly depend on the conclusions drawn concerning these issues. Relevant statements from official organizations are presented in this sub-chapter in the form of quotes in order to avoid misinterpretations.

Two of the main conventional fuels that play major roles in our energy supply are oil and nuclear energy. The central questions regarding these fuels concern their cost and availability in the future. Fossil fuels prices have drastically increased, especially in the last decade, see Figure 1.1. The vertical axis illustrates the price in U.S. dollars per energy equivalent to one barrel of oil. One can see a steep increase in prices from the year 2000 with a decrease in 2008 due to the world economic crises. According to the Federal Institute for Geosciences and Natural Resources, "*in the long term, higher oil prices seem unavoidable because the production of oil from increasingly complex and less accessible deposits is more difficult, and therefore*

more expensive" (Federal Institute for Geosciences and Natural Resources, 2011).

In Figure 1.2 and Table 1.1 data is shown concerning the present and predicted future availability of non-renewable fuels. Figure 1.2 represents the historical production profile of oil and gas liquids since 1930 including a forecast scenario up until 2050. As shown, it is estimated that a peak in production will be reached in the next few years. The Federal Institute for Geosciences and Natural Resources also states that "*no increase in the production of conventional oil alone is expected overall*" and that "*unlike uranium, coal and natural gas, the situation for crude oil is critical because production from a technical point of view will already begin to decline even when there are still large remaining reserves and resources.*"

In Table 1.1, the estimated available resources/reserves ratio at the end of 2005 is presented. These indicators point to the scarcity of conventional oil. According to Kjell Aleklett, Professor of Physics at Uppsala University in Sweden, we have now (2013) probably "consumed almost half of the conventional oil available on Earth" (Aleklett, 2012). Also, J. Peter Gerling (Federal Institute for Geosciences and Natural Resources, Germany) wrote the following in the Survey of Energy Resources of the World Energy Council in 2007: "*The evidence suggests that the peak of world discovery was in the 1960s, meaning that the corresponding peak of production for 'Conventional Oil' is approaching. The world started using more than it found in 1981 and that gap has widened since. From a geological point of view, the remaining potential for conventional oil can provide for a moderate increase in oil consumption over the next 10 to 15 years. Demand will then have to be met by other fuels. The timing of the peak currently attracts much debate, but is considered less important than the vision of the long decline that comes into view on its far side. Certainly, countries that begin to address the issue and implement the necessary changes will find themselves enjoying huge advantages over those which continue to live in the past and have blind faith in unspecified technological solutions, or the ability of an open market to deliver.*

The world will not finally run out of oil for very many years, if ever, but the onset of decline may prove to be a discontinuity of historic proportions, given the key role oil plays in modern economies. The transition to decline threatens indeed to be an age of great economic and geopolitical tension." In the latest released version of the same document it is concluded that "*crude oil is the only non-renewable energy resource which will no longer be able to keep up with growing demand in future decades. The timely development of alternative energy systems will therefore be necessary given the long time periods involved in bringing about major changes in the energy sector*" (Federal Institute for Geosciences and Natural Resources, 2011).

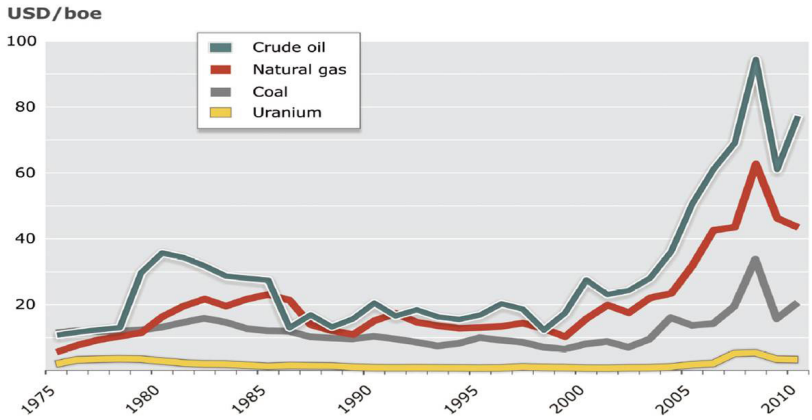

Figure 1.1 *Development of nominal fossil fuel prices in recent decades in USD per barrel of oil equivalent (Federal Institute for Geosciences and Natural Resources, 2011).*

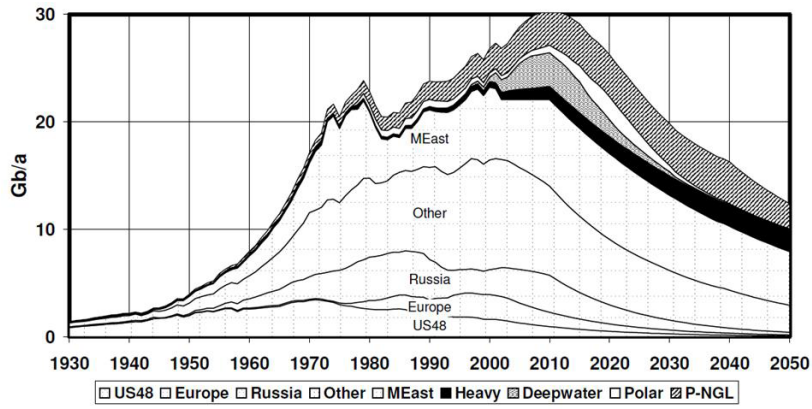

Figure 1.2 *Production profile of oil and gas liquids, 2003 base case scenario. (Aleklett and Campbell, 2003).*

Table 1.1 Resources/Reserves Ratio – an indicator of the future availability of conventional geo-fuels at the end of 2005 (World Energy Council, 2007).

Fuel	Resources		Reserves		R/RR
Conventional oil	82	billion tons	162	billion tons	0.5
Conventional natural gas	207	trillion m3	179	trillion m3	1.2
Hard coal	4079	billion tons	746	billion tons	5.5
Brown coal/lignite	1025	billion tons	207	billion tons	5
Uranium	12.8	million tons	1.9	million tons	6.7

When it comes to uranium availability for nuclear power the conclusion is different. If investment were made to exploit undiscovered resources, the available resources of uranium are expected to last many hundreds of years. Hence, it is estimated that nuclear power development will not be directly constrained by uranium resources in the next generations (Federal Institute for Geosciences and Natural Resources, 2011). Other opposing views consider that the costs of treating radioactive wastes for the next generations and the risk for public health should also be taken into account when the energy cost produced by this technology is calculated. If so, the numbers for profitability would not be as positive as they normally appear (European Renewable Energy Council, 2010).

When it comes to climate change, one of the most important sources of information is the Intergovernmental Panel for Climate Change (IPCC). This organization was created in 1988 by the United Nations Environment Programme and the World Meteorological Organization to provide a reliable and impartial investigation of the facts concerning worldwide climate change. The last assessment report was released in 2007 (IPCC, 2007). Some of the main conclusions from that report were: *"Warming in the climate system is unequivocal..."; "Most of the observed increase in global average temperature (...) is very likely due to increase in greenhouse gas concentrations"; "Continued greenhouse gas emissions (...) would induce many changes that would very likely be larger than those observed..."* Figure 1.3 shows a comparison between observed changes in surface temperature and simulated results by climate models. The models take into account either natural or both natural and anthropogenic factors. The results indicate the influence of human activity on the increase in the surface temperature.

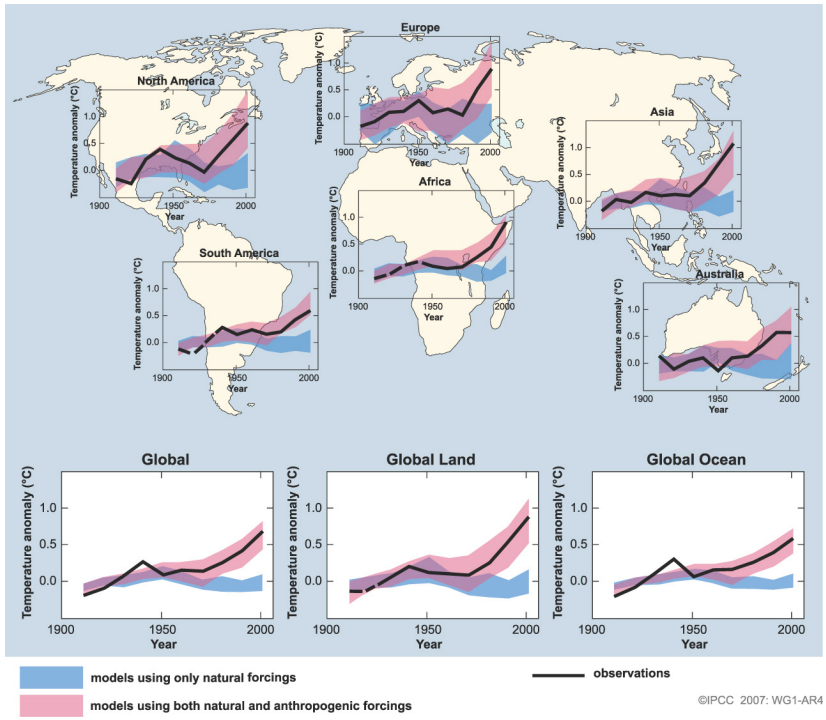

Figure 1.3 *Comparison between measured data and model results on the global and continental surface temperature change (IPCC, 2007).*

Many questions were raised regarding this report which resulted in continual scientific investigations. The next assessment report is currently under development. However, some of the latest findings that will be assessed in that report have already been released. The main conclusion is that the new data strengthens the conclusions of Assessment Report 4 (2007). Moreover, they indicate that the current CO_2 concentration levels are higher and have increased more rapidly than expected and that measured sea-level rise is slightly higher than previously estimated (IPCC Working Group I, 2010). In August 2010, IPCC proffered the following statement (Dr Rajendra Pachauri, chairman of the IPCC at a press conference at the United Nations in New York):

"By overwhelming consensus, the scientific community agrees that climate change is real. Greenhouse gases have increased markedly as a result of human activities and now far exceed pre-industrial values."

According to the IPCC, the temperature rise in the case of doubled CO_2 emissions is between 2°C and 4.5°C, with the most probable being 3°C of warming. However, a recent study from The Norwegian Research Council indicates that this might be an overestimation. The Norwegian investigation estimated a probable increase of 1.9°C. Professor Terje Berntsen (University of Oslo, Norway) who conducted the study emphasises that *"the project's findings must not be construed as an excuse for complacency in addressing human-induced global warming. The results do indicate, however, that it may be more within our reach to achieve global climate targets than previously thought"* (The Research Council of Norway, 2013).

Further, impacts of climate change in wildlife have been documented. In a recent article in *Science*, Chen et. al (2011) described how wildlife has been rapidly shifting in latitude or in altitude as a result of climate change. The larger distances covered by the species were associated with larger levels of global warming.

After discussing the latest developments concerning two of the most important non-renewable fuels it seems that climate change adds up to what was already clear. The energy sector is a major concern today. Profound changes need to be made not only to reduce our energy use but also to change the way energy is produced. The overall conclusion from the Survey of Energy Resources (2010), is that "*there is no shortage of energy resources in the world either today or for decades to come. It is the way we are using these resources that has to change to ensure sustainable energy future*" (World Energy Council, 2010).

Figures show that all renewable energy sources could provide 3078 times the current global annual energy needs. The energy potential of every source is shown in Figure 1.4. These are the theoretical potentials, i.e. the total available energy of each source at the earth's surface. They correspond to the upper limit of what can be exploited. Solar energy is the renewable energy source with by far the largest potential. All the renewable energy sources depend, in one way or another, on the constant solar energy incident on the surface of the Earth. By itself it is enough to ensure 2850 times the annual global energy needs. In just one day the solar energy incident on the surface of the Earth equals the global energy needs during eight years.

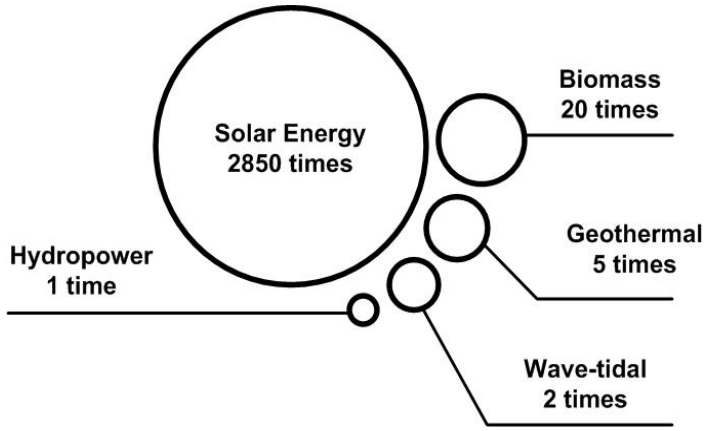

Figure 1.4 *Theoretical potential of renewable energy sources compared with the annual global energy needs (European Renewable Energy Council, 2010). The representations are not to scale.*

Taking into consideration only the theoretical potential of solar energy can be misleading. Together with the theoretical potential, it is also crucial to evaluate the technical and economic potentials as well (European Renewable Energy Council, 2010). The technical potential considers the limitations of the existing technology in exploiting a certain energy source. Among other things, it takes into account the geographical locations where the energy can be explored, technical limitations and the final efficiency of energy conversion. The economic potential weighs the price of exploiting the renewable energy source against the total energy produced and its cost. It also accounts for future benefits of exploiting renewable energy sources. These can be the decrease in greenhouse gases emissions, influence on the health and wellbeing of society and the value of energy supply independence.

The technical potential and the economic potential must be evaluated in a dynamic way. Both these potentials may vary significantly with time. Certain technical challenges may be easily solved in the near future due to a steep learning curve of the technology used to exploit an energy source. The same applies to the analysis of economic potential. The energy price that the renewable energy source replaces might change significantly in the near future. Also, factors like future introduction of direct costs per released quantity of greenhouse gases can be taken into account. When evaluated dynamically, solar energy is one of the sources with larger technical and economical potentials (European Renewable Energy Council, 2010).

In total, the estimated incident radiation on a horizontal surface in Lund (Sweden) during a year is roughly 1000 kWh/m^2,year. In Figure 1.5, the estimate of the distribution of the global incident irradiation on an optimally oriented surface for the whole of Europe is shown. The distribution of the global incident irradiation on a surface located in Lund (Sweden) for various tilts and orientations is shown in Figure 1.6. The figure shows that the larger variation in the global incident irradiation on the surface occurs while the tilt angle is changed from 45° to a vertical position of 90°. This is mainly explained by the fact that a higher tilt angle excludes a large part of the diffuse annual radiation which represents roughly half of the annual radiation in Lund. Also, the incident radiation in the summer is reduced for higher tilt angles.

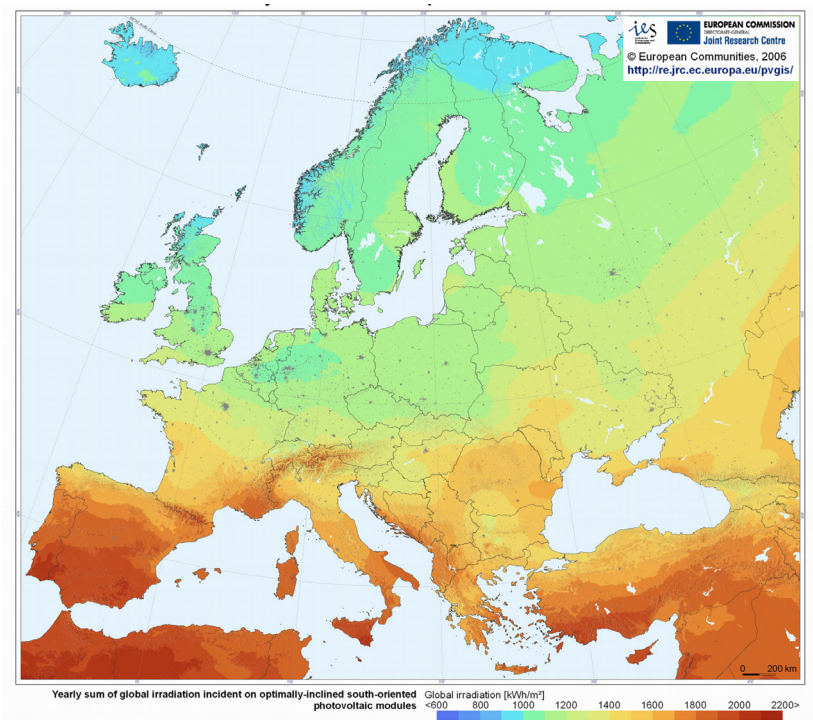

Figure 1.5 *Yearly sum of global irradiation incident on an optimally oriented surface kWh/m^2/year (European Commission, 2006).*

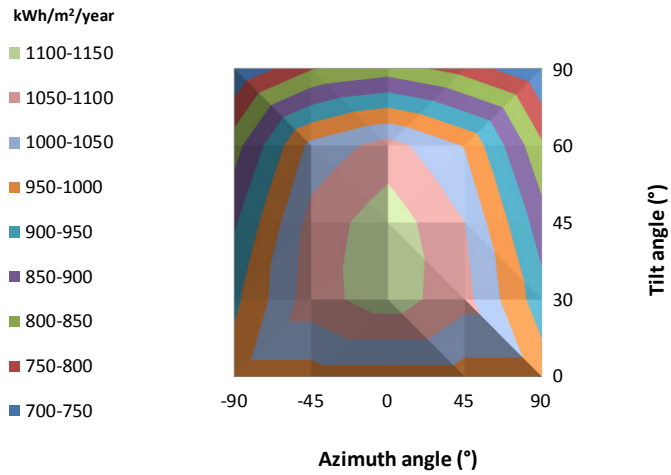

Figure 1.6 *Yearly global irradiation incident on a surface set at different tilts and orientations in Lund, Sweden.*

1.1.2 Single-family electrically-heated houses in Sweden

In light of the previously discussed issues, in 2007 the European Union adopted an energy and climate change policy with ambitious targets for 2020. For instance, it aims to reduce greenhouse gas emissions by 20%, reduce energy use by 20% and meet 20% of the energy needs by means of renewable sources in comparison with the corresponding values in 1995 (European Union, 2007). Sweden has gone even further and is aiming to meet 50% of its total energy need by renewable energy sources. Also, by 2020 the Swedish transport sector is aiming to cover 10% of its needs using renewable energy (Government Bill, 2008; Blomsterberg, 2012).

Building new energy efficient buildings has the potential to lower the future energy demand in the residential sector. However, the biggest energy saving potential today lies in renovating the existing building stock. The residential and service sectors represent approximately 40% of the total energy use in Sweden, with the biggest share used for space heating and domestic hot water (Swedish Energy Agency, 2012b). In Sweden there are around half a million single family houses that use only electricity for heating (directly or with a water based system) (Swedish Energy Agency, 2011b). As shown in Figure 1.7 and Figure 1.8, the total electricity use in such houses is high. The average electricity use in 2011 for electrically-

heated single-family houses was equal to 17 400 kWh/year. If expressed per floor area, the average electricity use was roughly 128 kWh/m^2/year.

This high number of electrically-heated houses combined with the cold Swedish climate and electricity driven industry leads to one of the highest electricity consumptions per capita in the world. Sweden is the 4th biggest electricity consumer per capita in the world just behind Iceland, Norway and Canada (International Energy Agency Statistics, 2009). This fact becomes even more relevant if one takes into account the electricity price and its trend. In Figure 1.9, the Swedish energy prices for different energy sources are presented. As shown, the most expensive energy source in Sweden is electricity used for heating. Also, the price of electricity for single family houses with electric heating has almost doubled since the year 2000.

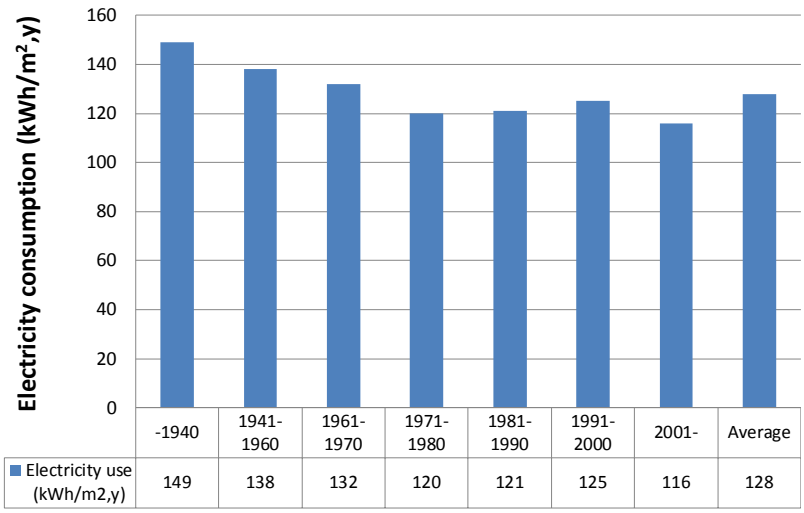

Figure 1.7 *Average use of electricity in 2011 (including electricity for household purposes) in single-family houses heated exclusively with electricity (directly or with a water based system). The electricity use is expressed per square meter of heated floor area (including non-residential floor area) and by year of completion (Swedish Energy Agency, 2011b).*

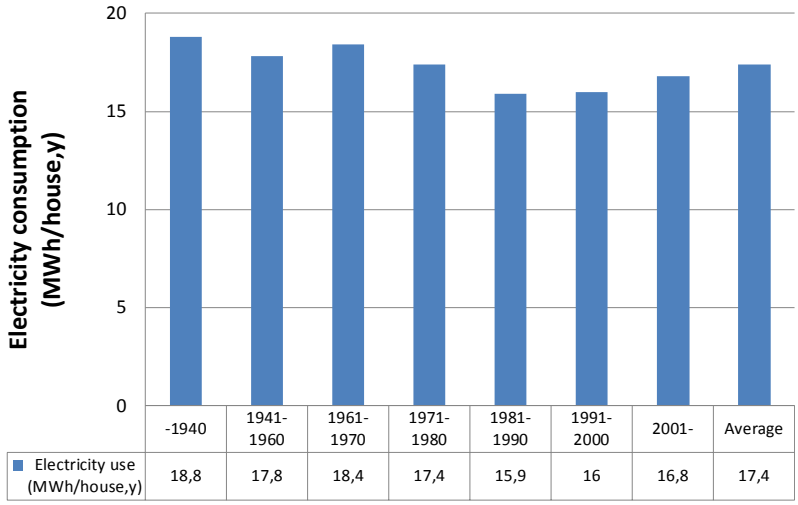

Figure 1.8 *Average use of electricity (including electricity for household purposes) in single-family houses in 2011, heated exclusively with electricity (directly or with a water based system). The electricity use is expressed per house and by year of completion (Swedish Energy Agency, 2011b).*

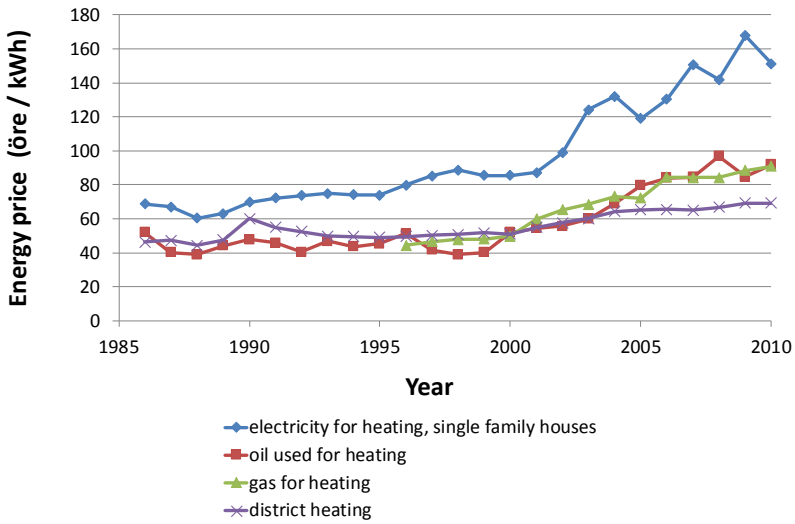

Figure 1.9 *Real energy prices for housing in Sweden including energy taxes and value added taxes expressed in öre/kWh (Swedish Energy Agency, 2011a) (1 öre = 0.01 Swedish crown).*

The electricity market has become more international, as trading is vital to ensure a stable and secure electricity supply. In 2011, 73% of the electricity used in the Nordic market was traded in the Nord Pool´s market (Swedish Energy Agency, 2012b). Nord Pool is the Nordic power exchange market created to improve pricing transparency and exchange. This market is also increasingly trading with other countries like Poland, Germany and other central European countries. These countries produce a big share of their electricity with coal fired power plants. Hence, the Swedish electricity price is increasingly affected by the fuel prices and availability in the rest of Europe. Also, the policy of the European Union and Sweden to ensure that 10% of the energy use in the transport sector comes from renewable sources will probably promote the implementation of electric vehicles. This means that a part of the demand for fossil fuels may shift to electricity, increasing its consumption. Thus, it is likely that the electricity price will continue to rise.

In summary, the current electricity consumption in Swedish single-family electrically-heated houses is a combination of the following factors, creating concerns for the future:

- around half a million single-family electrically-heated houses have a high electricity consumption;
- electricity used for heating is the most expensive energy source in Sweden;
- the price of electricity has been rising at a high rate during recent years;
- The electricity price is generally expected to continue rising.

An increasing number of installed heat pumps are contributing to a decrease in the space heating load. On the other hand the household electricity consumption increased by 58% since 1970, from 3800 to 6000 kWh/house,year. Almost half the Swedish single family houses are equipped with some kind of heat pump, the most common being the air-to-air heat pump (Swedish Energy Agency, 2011b). However, such heat pumps do not influence the domestic hot water energy load.

The number of houses that are estimated to use a separate hot water boiler for domestic hot water production is roughly 450 000. These represent houses with only direct electric heating and houses with a combination of bio fuel (wood, pellets, etc) and direct electric heating (see Table 1.2) (Swedish Energy Agency, 2011b). In such houses, a heat pump supported water based system for both space heating and domestic hot water could be installed. However, extensive installation work is needed as well as a large investment cost. For this reason, a simple and cost efficient solar hot water system for domestic hot water production can be a competitive

choice. By retrofitting the existing hot water storage, the initial cost of the solar thermal system can be reduced both in material and installation costs. One of the principal technical problems with a solar thermal system is the stagnation periods during the summer. This can be partly prevented by using a load-adapted thermal collector that achieves a higher annual solar fraction without increasing the stagnation periods. Beyond thermal collectors, a PV/T (Photo Voltaic/Thermal) hybrid collector may be integrated in the retrofitted system instead. This saves electricity not only for domestic hot water production but also for household appliances. Other alternatives are the installation of a PV system and energy renovation measures such as new energy efficient windows and extra insulation where it is most needed.

When the project was started, the main challenge with PV systems was the high cost of the solar cells. Therefore, it was interesting to concentrate the radiation on the solar cells in order to replace expensive cell area by cheaper reflector material. During recent years the market price of solar cells has drastically decreased which means that the demand for using a high concentration factor became less significant.

Table 1.2 Total number of Swedish single-family houses that are estimated to use a separate hot water storage for domestic hot water production (Swedish Energy Agency, 2011b).

Type of heating system	Number of single-family houses
Only direct electric heating	206 000
Bio fuel and direct electric heating	254 000
Total number of single family houses	460 000

1.1.3 Risk of legionella growth in the developed retrofitted solar thermal system

Legionella bacteria occur naturally in water and can infect human beings via inhalation which, under certain conditions, may potentially lead to death. Legionella grows for example in domestic hot water systems and it is therefore important to analyse the risks in solar domestic hot water systems. Some studies that have addressed the topic of legionella growth in solar thermal systems are reviewed in this section. A direct adaptation, and sometimes transcriptions, of these investigations is presented. The risk of legionella growth in the developed retrofitted solar domestic hot water system is discussed.

The main factors promoting the bacterial growth are summarized below (Wolferen, 2011 & Rogers et. al, 1994):

- Water environment where the bacteria live;
- Bacteria thrive in stagnated water;
- Oxygen since the bacteria are aerobic;
- Temperature. The bacteria grow between 20°C and 50°C where the optimum temperature for growth is roughly between 30°C and 40°C. Above 60°C the bacteria die after a certain period of exposure depending on the temperature;
- Residence time. Longer times favour bacterial growth;
- Acidity. The bacteria can grow between a PH of 5.5 and 9.2 and survive a PH of 2.2 for 5 min;
- The bacteria feed on nutrients present in sediments and other bio-films.

There are EU directives and recommendations that establish the common ground for national regulations and guidelines. Most of the countries in Europe have no specific regulation for solar domestic hot water systems and legionella growth. It is common that the general rules for hot water installations apply. Some countries such as France, Germany and the United Kingdom have low restrictions for hot water installations with storage volume below 400 litres where the risk is considered to be very low (Cabeza, 2005). Further, it is common that national branch organizations establish their own regulations, so that domestic hot water products and installations can be covered by warranties and insurances. These regulations often have more demanding measures for controlling the bacterial growth in hot water systems.

There are no specific rules regarding legionella in Sweden. The building code legislation for hot water installations applies. The temperature of circulating hot water in the installation must not fall below 50°C. It is recommended that the temperature of hot water in storage tanks should not be less than 60°C. The Swedish Industrial Rules (Swedish Industrial Rules, 2011) is a quality marking of the hot water installation issued by companies, organizations, insurances and manufacturers in the field to minimize the risk of water injuries, legionella growth, burning injuries and poisoning. These rules cover the Swedish Building Code plus additional requirements. The Swedish Social Board (2013) has analogous recommendations. A hot water installation carried out in accordance with these rules is to be considered as carried out professionally and can be covered by warranties and insurances. For hot water storage the following applies:

- Temperature in the storage tank higher than 60°C;

- Temperature of the outgoing hot water to the installation higher than 55°C;
- Temperature in all the hot water pipes higher than 50°C;
- Regarding for example heat pumps where the temperature of the water in the boiler does not reach 60°C, a safety function that heats up the boiler automatically at least once per week should be in place.

Several control measures have been studied in order to limit bacterial growth. The one most practical and commonly used in domestic hot water systems seems to be thermal disinfection. Thermal control measures can be applied in order to decrease the bacterial concentration to a safe level. If the whole system needs to be disinfected, weekly flushing of hot water can be applied. Otherwise, reheating of the storage is normally performed (Table 1.3). The legionella risk assessment in The Netherlands mentions that, in case of a hot water storage maintaining water at a temperature between 25°C and 45°C and performing weekly thermal disinfection, *"legionella may occasionally occur in concentrations above the detection limit. If that happens there is no reason to expect dangerous concentrations which need corrective measures"* (Wolferen, 2001). Karl Leidig states in "Risk of Legionnaires' disease in solar water heaters – status report" (Leidig, K., 2001) that this general thermal prevention does not offer 100% protection against legionella occurrence but prevents an uncontrolled bacterial growth.

Table 1.3 Flushing time and re-heating time as a function of temperature (Wolferen, 2001).

Temperature	Flushing time in case of weekly flushing of the whole system	Re-heating time of the storage
60°C	20 min.	10 min.
65°C	10 min.	1 min.
70°C	5 min.	10 s.

Darelid's work at a Swedish hospital concluded that *"Complete eradication of Legionella from the hot water system does not seem necessary. This is often an unrealistic goal as Legionella can survive ... at temperatures up to 70˚C and ... the bacteria can reach the hospital through the cold water supply"* (Darelid et. al, 2002). Such a conclusion is supported by the investigation carried out by Marchesi et. al (2011) stating that *"Once legionella has colonised a water system, our observations support the consensus that eradication is usually unachievable."*

In the document "Legionella in Combisystems Tanks", Cabeza (2005) concludes that *"from all the information gathered from many countries, reports, papers and legislation, the main conclusion of this report is that solar tanks are not more dangerous than other water tanks"*. From this point of view, guidelines and regulations for regular hot water installations, such as heat pump systems, should also apply for solar thermal systems. The Swedish Industrial Rules (2001) recommends that "if the heating device in the storage produces a temperature lower than 60°C (e.g. heating with heat pumps), a safety function that heats up the boiler automatically at least once per week should exist (for example with an electric water heater)". The Dutch risk assessment also supports this recommendation. However, in most of the traditional solar thermal systems, it is not possible to heat up the whole storage to 60°C since the auxiliary heater is not placed at the bottom.

Taking into account the literature review, and from the point of view of safety against legionella growth, the developed retrofitted system should be able to implement the following control measures:

- Auxiliary heater volume kept at 60°C;
- Hot water provided at a temperature higher than 50°C;
- Heat all the storage volumes to 60°C for 10-20 minutes if the stored temperature of the water is below 60°C during a period of one week;

1.2 Objectives

The objectives of the present work are:

- to develop and test a solar thermal system for domestic hot water production where the existing electric water heater storage is retrofitted. This includes a theoretical estimation of the annual performance of several retrofitting configurations and a comparison with a conventional solar domestic hot water system. Also, practical testing of the developed system is included in the investigation;
- to test and evaluate two compound parabolic concentrator (CPC) collectors that may be suitable to be integrated in the developed retrofitted system. These CPC collectors have the same geometry however, one of them is a PV/T hybrid and the other one a thermal collector. The PV/T hybrid produces both heat and electricity. The thermal collector aims at achieving higher annual performances than conventional collectors without increasing the stagnation periods.

- to test and evaluate a third collector, a tracking concentrating PV/T hybrid with a higher concentration factor. At the beginning of the project (2008) the difference between the price of solar cells and reflective material was significantly higher than it is today making it attractive to use higher concentration factors. This tracking hybrid was not thought to be integrated in single-family houses but it was considered technically interesting and worth investigating as an independent study.

1.3 Method

A solar domestic hot water system was developed by retrofitting the existing electric water heater storage. Hence, no significant changes need to be carried out in houses with existing electric hot water storages when the new solar thermal system is installed. Also, since the solar hot water tank is one of the most expensive components of a solar thermal system, retrofitting the existing tank can lower the investment cost. By means of TRNSYS simulations, different configurations for the retrofitted system design were analysed. At this stage, the simulation models were simplified to some extent since an appropriate technical solution for retrofitting was not yet achieved. A prototype of the retrofitted system was built and tested in the laboratory according to the configuration which achieved the highest annual solar fraction in the theoretical study. During the test period necessary technical changes in the retrofitting configuration were carried out and therefore the simulation model was adjusted. This model was validated against measurements and further used to optimize the system performance. Sensitivity analysis studies were also carried out. Finally, an add-on unit containing the necessary components for the retrofitting was developed. This unit is used to connect, in a simple way, new solar collectors to most types of electrical storage tanks. This has the potential to make the installation of the system more flexible and cheaper. The costs of the developed retrofitted system and a standard solar domestic hot water system were estimated. These were used to carry out a straightforward payback time analysis based on an illustrative example.

Two compound parabolic concentrating (CPC) collectors that may be suitable to be integrated in the retrofitted system were tested. The collectors have a low concentration factor of 1.5 and the same design. The CPC-thermal collector was tested and a validated model of the collector was created. This was used to estimate the annual production of a solar domestic hot water system using the CPC-thermal collector in comparison with using conventional flat plate collectors. The electrical parameters of the CPC-PV/T hybrid collector were measured which made it possible to derive conclusions on its design.

A tracking concentrating PV/T hybrid collector with a concentration factor of eight was also analysed. A validated model of this collector was created and its annual production was compared with that of conventional solar thermal collectors and PV modules working side-by-side. Because of its higher concentration factor, this hybrid has the potential to produce energy at lower costs and it was considered to be technically interesting to be tested. This was especially attractive at the beginning of the project (2008) when the difference between the prices of solar cells and reflector material was significantly higher than what it is now. This was a fairly independent study from the investigations described above.

1.4 Limitations

In order to quantitatively compare the retrofitted system to a conventional solar domestic hot water system, two figures are needed regarding both systems: annual energy savings (solar fraction) and system costs.

The annual performance of the retrofitted system was estimated using a model validated against measurements. On the other hand, the annual performance of the conventional system was only estimated theoretically. Nevertheless, the goal was to achieve a high performance for the retrofitted system independently of the performance achieved by a conventional system. Also, there is extensive literature regarding the performance of standard solar domestic hot water systems.

The economic analysis was performed in a straightforward manner using the payback method. For a detailed economic analysis, additional factors than the ones considered should be taken into account such as the cost of the auxiliary energy, its predicted trend during the system lifetime, maintenance costs, replacement costs, subsidies, intrest on loans, inflation, discount rate and residual value at the end of the system's lifetime. Also, it is difficult to quantify how much technical developments on the integration of all retrofitting components into one add-on unit would decrease the cost. In addition, the space occupied by the introduction of the extra add-on unit is a qualitative parameter which makes it difficult to predict its importance on the market. Important information when it comes to the costs of the add-on unit is still missing. These costs depend not only on the production costs but also on the market volume that could be achieved.

Since the frame of the investigation was to retrofit an existing hot water boiler, its age and condition are relevant for the lifetime of the system. Under certain circumstances it may be better to consider the existing boiler not to be appropriate for the retrofit. These could be a combination of its

age and condition, for example. These factors were however not investigated in the present study.

The model of the retrofitting system was validated against measurements performed under certain test conditions which aimed to approximate the normal functioning of the system as if it were installed in a representative single family house in Sweden. This was a difficult task since different houses have significantly different consumption patterns and annual loads. The domestic hot water load in such houses is commonly very irregular with high peaks in consumption during short periods. However, in order to simplify the test procedure, the load was simplified to seven different draw-offs per day which causes a significant decrease in peak consumption. Also, the model which was validated against measurements performed in Sweden was used to estimate the system performance in the Portuguese and Zambian climates. This can increase inaccuracies of the model which were not investigated.

Another limitation of the investigation relates to the lack of a sensitivity analysis of the comparison between the CPC-thermal collector system and different types of flat plate collector systems. Such analysis would provide a broader insight into the relative performance of the CPC-thermal collector system. Also, the CPC-PV/T hybrid collector was solely tested regarding its electrical parameters without estimating the annual outputs. An investigation of the thermal performance and a total system analysis were not performed.

2 Measuring equipment and simulation software

The monitoring equipment and their accuracies are described in this chapter. Identical measurement equipment was used for collector testing and to test the retrofitted system. The error propagation was estimated. Finally, the simulation software, TRNSYS, used in combination with the optimization tool, GenOpt, is described.

2.1 Measuring equipment and accuracies

The monitoring system used in the collector testing managed three temperature sensors, one flow meter, two pyranometers and one I-V curve measuring device. The measuring points are illustrated in Figure 1 and Figure 2 in Article I, Figure 2 in Article II and Figure 2 in Article III. The monitoring system used for testing the retrofitted system managed 19 temperature sensors, five flow meters, two pyranometers, two electricity meters, and the discharge control systems. These are illustrated in Figure 1 in Article V. Discharge was controlled and data collected by a number of loggers, the “brain” of the monitoring system. The sensors, their accuracies, and how the respective data was collected and stored are described below.

Temperature sensors of type Pt100 four-wire model class A manufactured by "Pentronic" (Pentronic, 2009) were used. The sensor was placed so that the fluid came in direct contact with the sensor while flowing upwards (Figure 2.1), thereby giving good contact between the fluid and the sensor. The resistance of each sensor was monitored at 0°C by the manufacturer. Different sensors had slightly different resistances. Subsequently, to increase the measurement accuracy, the sensors with the closest resistance according to the tests carried out by the manufacturer were paired in order to read difference in temperatures more accurately. This was the case, for example, for the inlet and outlet temperatures of the collector. The sensors comply with the standard IEC60751 (2008) valid for a Pt100 temperature sensor of class A with a maximum permitted error given by Equation 2.1.

$$\sigma_T = \pm(0.15 + 0.002 \cdot T)\ (°C) \qquad \text{Equation 2.1}$$

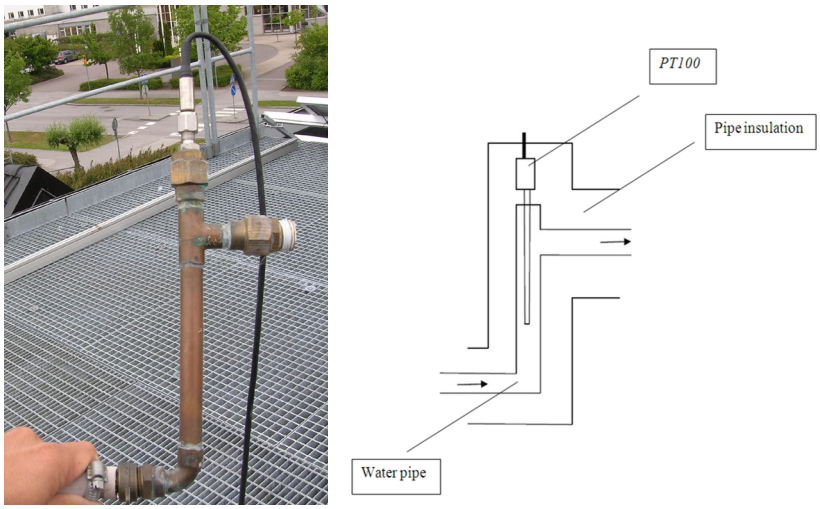

Figure 2.1 Pt100 sensor and its placing.

Flow meters of 9V-MP115 model manufactured by Kamstrup (Kamstrup, 2009) were used (Figure 2.2). The device sends 5760 electric pulses per litre volume. The flow meters comply with the EN1434 standard where the maximum permitted error for flow meters of class 1 is given by Equation 2.2. $\dot{V}_p$ is the highest flow rate, at which the flow meter functions without the maximum permissible errors being exceeded and $\dot{V}$ is the actual flow rate.

Figure 2.2 Flow meter.

$$\sigma_F = \pm\left(1 + 0.01 \cdot \frac{\dot{V}_p}{\dot{V}}\right)(\%) \qquad \text{Equation 2.2}$$

Two pyranometers measured the global and diffuse incident irradiation. CM10 model pyranometers manufactured by Kipp & Zonnen were used. The uncertainty of the irradiation measurement was 1.4%, given by the manufacter (Kipp & Zonnen, 2009). The equipment is illustrated in Figure 2.3.

Figure 2.3 Global and diffuse irradiation sensors.

The I-V curve measurement was carried out with a custom-made I-V recorder and the relative uncertainty was assumed to be 1% of the total measured power, based on experience.

The electricity meters were manufactured by ABB. The device transmitted 100 electric pulses per kWh unit consumed by the electric heater. The accuracy of the measurement was 1%, given by the manufacter (ABB, 2009).

The discharge control system comprised a custom-made relay control unit. This unit was controlled by output signals from the logger, which opened and closed the magnetic taping valves. The magnetic on/off valves and the relay box are shown in Figure 2.4.

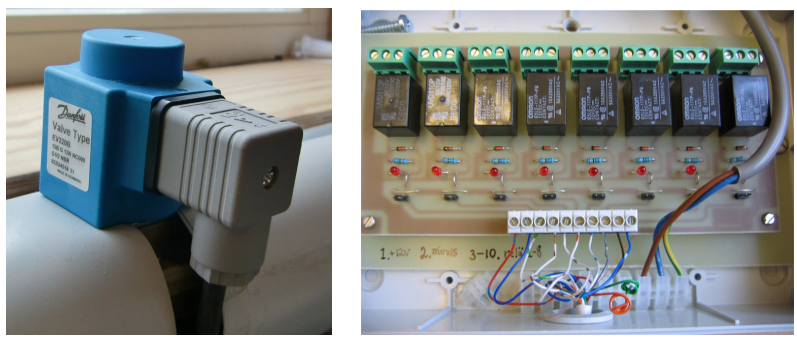

Figure 2.4 Magnetic discharge valves and the relay control unit.

The logger system comprised a CR1000 model, two multiplexers AM16/32, and one digital input/output expansion model SDM-IO16 manufactured by Campbell Scientific (Campbell Scientific, 2009). The CR1000 logger was the "brain" of the logger system. It controlled the AM16/32, the SDM-IO16 and the discharge control system, while recording all the monitored data. The multiplexers were a simple expansion of the available temperature inputs of the main logger. The input/output expansion model recorded the flow data and sent inputs to the discharge relay unit box. A simplified domestic hot water load profile in a typical Swedish single-family house, illustrated in Figure 1 in Article IV, was provided to the main logger, CR1000. For every discharge according to that profile, the logger sent electric impulses to open the discharge valves using the relay unit. The logger integrated the energy provided by the system to the user. When that energy output matched the load data of the consumption pattern for a certain period, the main logger shut down the discharge valves. The logger registered information every ten seconds and stored the average value of the irradiation and temperatures, or integrated the value of the flow, every five minutes. The logger system is illustrated in Figure 2.5.

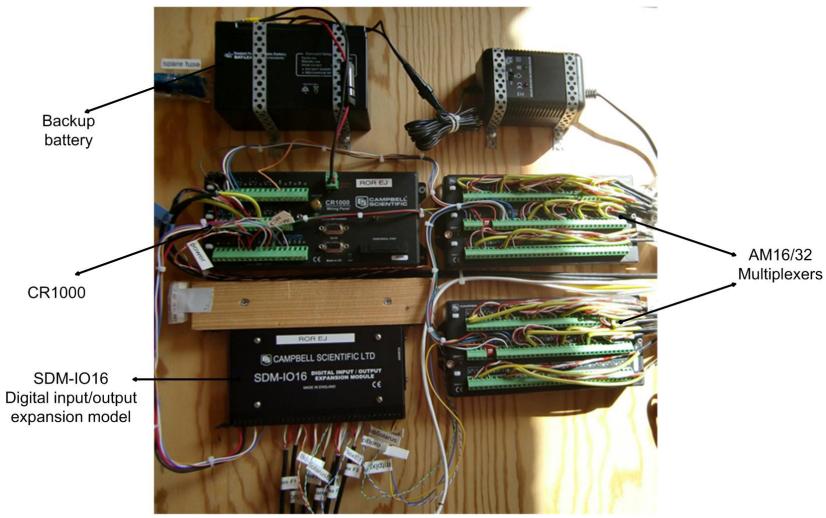

Figure 2.5 *Logger system comprising a CR1000 model, two AM16/32 multiplexers and one SDM-IO16 digital input/output expansion model.*

2.2 Error propagation

The well-known formula described in Equation 2.3 and Equation 2.4 was used for calculating the error propagation of independent variables (x, y …). This formula follows the American Standard of Measurements in Laboratory (Ku, 1966).

$$u = f(x, y, \dots) \qquad \text{Equation 2.3}$$

$$\sigma_u = \sqrt{\left(\frac{\partial u}{\partial x}\right)^2 \cdot \sigma_x^2 + \left(\frac{\partial u}{\partial y}\right)^2 \cdot \sigma_y^2 + \cdots} \qquad \text{Equation 2.4}$$

Equation 2.5 to Equation 2.10 were applied for the collector testing. The temperature dependence of the heat capacity of the water was taken into account in the calculations. When estimating the thermal performance of the collectors, the independent variables are the flow rate, $\dot{V}$, the temperature difference, Δ_T, and the irradiation, G. The error propagation of the thermal efficiency and power was calculated according to Equation 2.5 to 2.7. The error propagation of the electric efficiency and power was calculated according to Equation 2.8 to 2.10. The values of the error propagation for the collector testing are presented together with the measurements in Chapters 3, 4 and 5.

$$\eta_{b\_thermal} = \frac{q}{G_b \cdot A_{total}} = \frac{\rho \cdot C_p \cdot \dot{V} \cdot \Delta_T}{G_b \cdot A_{total}} \text{ (-)} \qquad \text{Equation 2.5}$$

$$\sigma_{\eta_{b\_thermal}} = \sqrt{\left(\left(\frac{\rho \cdot C_p \cdot \Delta_T}{G_b \cdot A_{total}}\right)^2 \cdot \sigma_{\dot{V}}{}^2 + \left(\frac{\rho \cdot C_p \cdot \dot{V}}{G_b \cdot A_{total}}\right)^2 \cdot \sigma_{\Delta_T}^2 + \left(-\frac{\rho \cdot C_p \cdot \dot{V} \cdot \Delta_T}{A_{total}} \cdot \frac{1}{G_b^2}\right)^2 \cdot \sigma_{G_b}^2\right)} \text{ (-)}$$

Equation 2.6

$$\sigma_q = \sqrt{\left(\left(\rho \cdot C_p \cdot \Delta_T\right)^2 \cdot \sigma_{\dot{V}}{}^2 + \left(\rho \cdot C_p \cdot \dot{V}\right)^2 \cdot \left(\sigma_{Thot}{}^2 + \sigma_{Tcold}{}^2\right)\right)} \text{ (W)}$$

Equation 2.7

$$\eta_{b\_electrical} = \frac{q_{electric}}{G_b \cdot A_{total}} \text{ (-)} \qquad \text{Equation 2.8}$$

$$\sigma_{\eta_{electrical}} = \sqrt{\left(\left(\frac{1}{G_b \cdot A_{total}}\right)^2 \cdot \sigma_{q_{electric}}{}^2 + \left(-\frac{q_{electric}}{A_{total}} \cdot \frac{1}{G_b^2}\right)^2 \cdot \sigma_{G_b}^2\right)} \text{ (-)}$$

Equation 2.9

$$\sigma_{q_{electric}} = 0.01 \cdot q_{electric} \text{ (W)}$$ Equation 2.10

Regarding the retrofitted system, the measured and modeled auxiliary energies were compared for different time-periods as part of the validation of the simulation model. Another measured parameter was the energy tapped from the system to the user. The error propagation for both these parameters is described below.

The energy tapped from the system was calculated according to Equation 2.11, where $\dot{V}$ is the discharged volume during a time period, T_{hot} is the hot water temperature delivered by the SDHW system, and T_{cold} is the temperature of the incoming cold water from the discharge. Assuming the temperature difference, (T_{hot}-T_{cold}) constant and equal to Δ_T, the error propagation of the measured tapped energy, $Q_{aux,meas}$, was calculated as in Equation 2.12. The standard deviation of the temperature difference, σ_{Δ_T}, is given by the square root of the sum of the squares of the errors for each temperature measurement (Equation 2.13). The values of the error propagation for the testing of the retrofitted system are presented together with the measurements in Chapter 7.

$$Q_{DHW,meas} = \rho \cdot C_p \cdot \int_{t_i}^{t_f} \dot{V}(T_{hot} - T_{cold})\, dt \text{ (kWh)}$$

Equation 2.11

$$\sigma_{Q_{DHW,meas}} = \sqrt{\left(\left(\rho \cdot C_p \cdot \Delta_T\right)^2 \cdot \sigma_V{}^2 + \left(\rho \cdot C_p \cdot V\right)^2 \cdot \sigma_{\Delta_T}^2\right)} \text{ (kWh)}$$

Equation 2.12

$$\sigma_{\Delta_T} = \sqrt{(\sigma_{Thot}{}^2 + \sigma_{Tcold}{}^2)} \text{ (K)}$$ Equation 2.13

2.3 Simulations with TRNSYS software

The simulation analyses performed in this work were carried out using TRNSYS (Transient Systems Simulation Software) (Klein et al., 2006). The software was developed by the University of Wisconsin, U.S.A. It has been commercially available since 1975 and is widely used by the research community. It is used for applications such as renewable energy systems, low-energy buildings, ventilation systems, etc. One of the biggest advantages of this software is its flexibility in connecting many different available components. Consequently, one of the trade-offs is its complexity. The modular nature of the software, together with the open source code of the components, has been one of the reasons for its success among researchers. It is possible to create new components that match the user needs and most of the common programming languages can be used for this (TRNSYS, 2010).

The simulations performed on the PV/T hybrid collectors were carried out using Winsun (Winsun Educational Software, 2009). This is a TRNSYS-based software, developed by Bengt Perers (Technical University of Denmark), which estimates energy outputs from user-specified collectors. The simulation model was validated against measured outputs. The software only takes into account the collector, not the whole system.

In addition to the PV/T hybrid collector analysis, the performance of a conventional flat plate collector system was compared with that of a CPC thermal load-adapted collector system. For this evaluation, a TRNSYS model of the entire solar thermal system was built, but only the collector model was validated. The model includes detailed measured data on the incidence angle modifiers. This information was added in the collector model by means of high-grade polynomial equations to increase its accuracy.

TRNSYS was also used to model solar thermal systems corresponding to different retrofitting configurations of existing water heaters (Article IV). At this point, the evaluation was theoretical and no models had yet been validated. These simulation results were used to compare the performances of the different systems.

A Generic Optimisation Program (GenOpt) (Lawrence Berkeley National Laboratory, 2011) was used together with TRNSYS. GenOpt is an optimisation program that minimises a user-selected target function given by a simulation program, in this case TRNYS. The value of the target function may depend on several user-defined independent variables with a range of user-defined inputs for each variable. The optimisation algorithm can also be selected by the user. The Hooke-Jeeves algorithm (Wetter, 2011) was used since it can perform global and local searches for the minimum

value of the target function. This algorithm can also identify continuous variables only limited by a maximum and minimum value.

This optimisation tool was used for optimising the flow on the collector loop of the simulated systems. The algorithm performed iterations with different values of the collector flow until a maximum annual solar fraction was reached. GenOpt was also used to validate the model of the tested retrofitted system against measurements. The target function was defined as the absolute difference between the simulated and measured auxiliary energies. The algorithm iterated the target function by changing several system parameters until a minimum was found.

One observed limitation with this optimisation process is that local minimums are sometimes found instead of the absolute minimum of the target function. Therefore, it was observed that for target functions depending on several independent variables, such as the model validation described in Article V, the optimisation should start with realistic values for each variable of the target function.

3 Testing of the tracking PV/T concentrating hybrid

A tracking PV/T concentrating hybrid was tested and the simulation model validated against measured data. The annual performance was estimated for different climates. The hybrid performance was compared with that of conventional flat plate collectors and PV modules working side-by-side. In order to understand how to characterise a photovoltaic/thermal hybrid (PV/T) collector, both photovoltaic and solar thermal technologies should be understood separately.

In this chapter, a short description of the simplified working principles of solar cells and solar collectors is included, which was compiled from literature. This will make it easier to comprehend the effects of their combination and interaction in a hybrid collector. For further details about photovoltaics, the reader is referred to Wenham et al. (2007), Green (1998) and Fahrenbruch & Bube (1983). For details on solar thermal processes the reader is referred to Duffie & Beckman (2006).

3.1 Characterisation of solar cells

Photovoltaics is generally known as the process of converting solar radiation into electricity using solar cells. This is possible because of the electronic properties of semiconductors. Photons with energy lower than the band gap energy pass through the semiconductor as if it were transparent. On the other hand, photons with energy greater than the band gap energy use their energy to break covalent bonds and create electron-hole pairs (Figure 3.1). Once the electron is excited, the p-n doped junction provides charge separation which gives direction to the current. Those electrons can then circulate around an electric circuit and produce electric power.

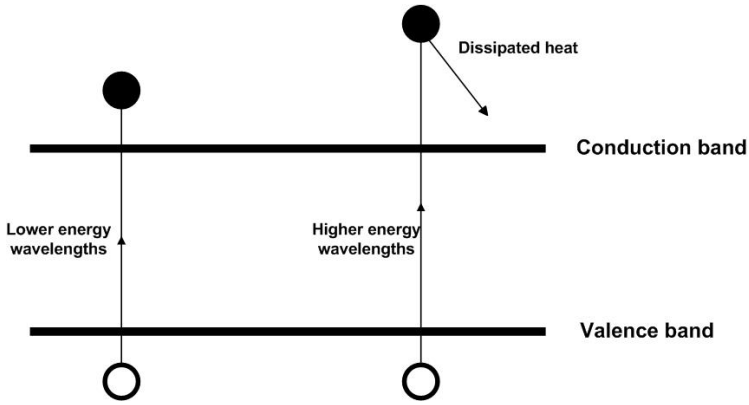

Figure 3.1 *Creation of electron-hole pairs and dissipation of heat for different energies of the wavelength of the photon (adapted from Wenham et al., 2007).*

Creating an electrically equivalent model based on separate electrical components whose performance is well known helps to understand the electronic behaviour of a solar cell. One of the simplest models consists of a current generator in parallel with a diode. Since no solar cell is ideal, a shunt resistance and a series resistance are also included in the model. The result is the "one-diode equivalent circuit of a solar cell" shown in Figure 3.2. This model assumes that both the temperature and illumination are evenly distributed over the cell.

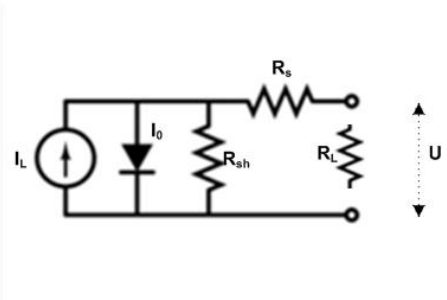

Figure 3.2 *Equivalent circuit of a solar cell (adapted from Wenham et al., 2007).*

A solar cell is characterised by its current-voltage characteristic curve (I-V curve). Using the following mathematical model that describes the previous equivalent electric circuit of a solar cell, theoretical I-V curves can be generated (Green, 1998):

$$I = I_L - I_0 \cdot \left[e^{\left(\frac{q_C (U + I \cdot R_S)}{nkT} \right)} - 1 \right] - \frac{U + I \cdot R_S}{R_{sh}} \text{ (A)} \qquad \text{Equation 3.1}$$

I represents the current, U represents the voltage over the load, I_L is the light-generated current, I_0 is the diode leakage current density in the absence of light, n is the idealist factor of the diode, q_C is the absolute value of the electronic current, k is the Boltzmann constant, T is the absolute temperature, R_s is the series resistance of the cells, R_{sh} is the shunt resistance and the load is represented by R_L.

Using these I-V curves, three parameters can be estimated that characterise the performance of a solar cell for given irradiance, operating temperature, and area. These are the short-circuit current I_{sc}, the open-circuit voltage V_{oc} and the fill factor *FF*. I_{sc} is the maximum current at zero voltage and is directly proportional to the available sunlight. V_{oc} is the maximum voltage at zero current while the fill factor *FF* is a measure of the quality of a cell. The higher the fill factor, the higher the efficiency of the cell. The power output for a certain operating condition can be calculated as the product of the current and voltage. The fill factor is defined as in Equation 3.2 (Green, 1998).

$$FF = \frac{V_{mp} I_{mp}}{V_{oc} I_{sc}} \text{ (-)} \qquad \text{Equation 3.2}$$

The product $V_{mp}I_{mp}$ represents the maximum power point of the solar cell while $V_{oc}I_{sc}$ represents the maximum power if the cell were ideal. Consequently, this coefficient corresponds to the fraction of the maximum efficiency that the cell can ideally reach. In order to make best use of the cells, the load should match this maximum power point regardless of the light conditions. In the case of grid connected systems, this can be achieved with a maximum power point tracker normally built into the inverter.

A simple overview of the efficiency of a cell as a function of the incident irradiation, working temperature, series and shunt resistances is described below. This was carried out by generating theoretical I-V curves while varying the previous parameters and comparing them with the I-V curves of a reference case. The data used in the calculations for the reference case is shown in Table 3.1. The estimated I-V curve for the reference case is shown in Figure 3.3 while the other cases are illustrated in Figures 3.4- 3.7.

Table 3.1 Data used to generate theoretical I-V curves for the reference case.

Reference case		
I_{sc}	(A)	4
G	(W/m^2)	1000
T	(K)	293
U_0	(V)	0.65
R_s	(Ω)	0.008
R_{SH}	(Ω)	50
q_C	(C)	1.6E-19
n	(-)	1
k	(J/K)	1.38E-23

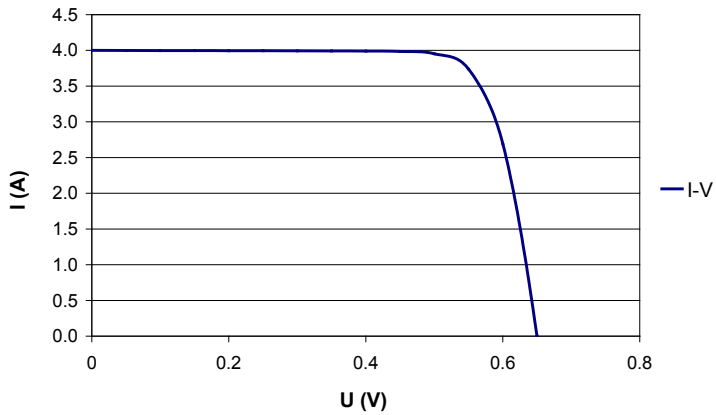

Figure 3.3 Estimated I-V curve corresponding to the reference case.

3.1.1 Effects of variation in irradiation

The results for the various irradiation levels and the corresponding power outputs are shown in Figure 3.4. As expected, higher irradiation levels cause an increase in the short circuit current since more electrons are collected into the circuit.

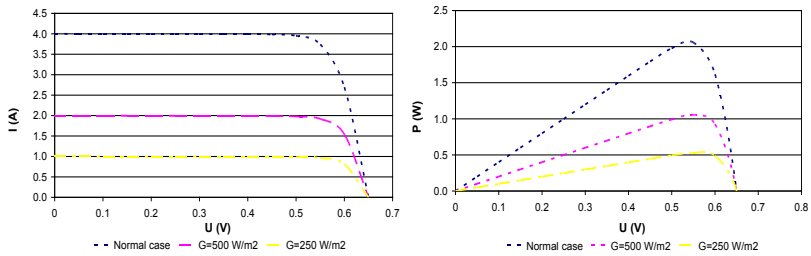

Figure 3.4 *I-V curves and corresponding power outputs for three different irradiation levels.*

3.1.2 Effects of variation in temperature

The I-V curves and the variation in power output with temperature are illustrated in Figure 3.5. The main effect of the temperature rise is the voltage drop, which reduces the cell power output. As temperature increases, more electrons are able to "escape" through the p-n junction and recombine. It is desirable to operate at as low a temperature as possible, since the power output of solar cells is increased and thermal cycles and stress are reduced (Green, 1998).

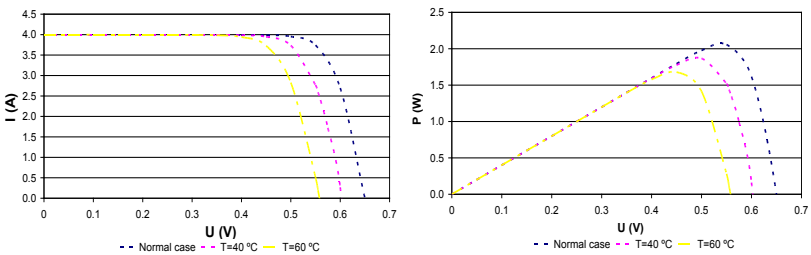

Figure 3.5 *I-V curves and corresponding power outputs for three different temperatures.*

3.1.3 Effects of variation in series resistance

The influence on the I-V curves, using three different values of series resistance, was estimated. The results are shown in Figure 3.6. The main contributors to the series resistance (R_s) are the bulk resistance of the semiconductor material, the fingers, busbars, the metallic contacts, and the resistance between the metallic contacts and the semiconductor. This

resistance represents all the non-ideal connections in a solar cell. Consequently, the higher the value of this resistance, less power is extracted from the solar cell.

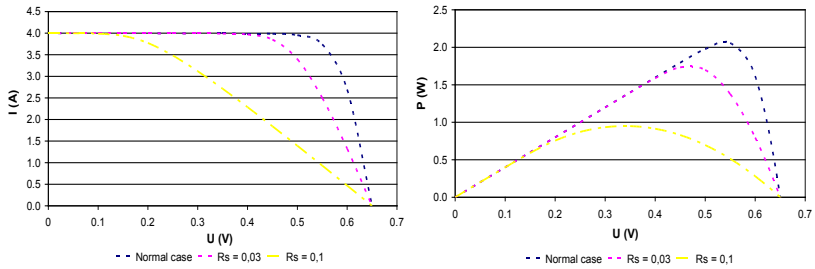

Figure 3.6 *I-V curves and corresponding power outputs for three different series resistances.*

3.1.4 Effects of variation in shunt resistance

The shunt resistance (R_{SH}) corresponds to *p-n* junction imperfections and impurities near the junction. The ideal circuit should include an infinite shunt resistance that "forces" the current in the circuit and prevents its leakage through the junction. However, the shunt resistance has finite values and the smaller the shunt resistance, the bigger the current drop (Figure 3.7).

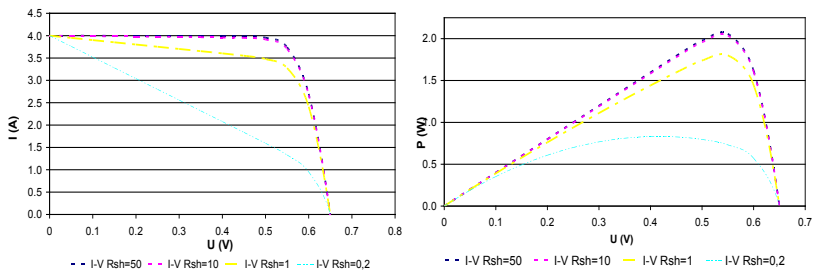

Figure 3.7 *I-V curves and corresponding power outputs for three different shunt resistances.*

A PV cell cannot use all incoming photon energy to create electricity. It absorbs only radiation with energy higher than the band gap energy. For instance, a silicon solar cell absorbs roughly all radiation for wavelengths below the band gap of 1.1 μm (Green, 1998). This energy is used to pro-

duce electricity at variable efficiencies. Photons with higher energy than the band gap energy cannot be fully used, as they will give off their excess energy as heat to the surroundings. For photons with energy below the band gap, the cell behaves as though it was transparent, and this radiation is transmitted through the cell. Consequently, most of the incident radiation is converted into heat. The part of the light spectrum that can be used to excite electrons and produce electricity is rather small. This explains why a conventional commercial solar cell has an efficiency of 10% to 20% for transforming all the available radiation into electricity. Considering the high price of the solar cells, it may be attractive to use concentrating solar light modules with the aim of increasing cost efficiency the electric outputs per cell area.

3.2 Characterisation of solar thermal collectors

Solar thermal collectors use the incoming energy from the sun to produce heat. This heat can be used for several applications, ranging from pool heating to electricity generation from steam. In steady state, the performance of a solar collector can be described as a simple energy balance that indicates the distribution of incident solar energy into useful energy gain, thermal losses and optical losses. Consequently, the useful energy output of a collector is the difference between the absorbed solar radiation and the thermal loss which, divided by the incoming radiation at a normal angle to the collector plane, corresponds to the instantaneous steady-state collector efficiency. This is described by Equation 3.3 (Duffie and Beckman, 2006). The steady-state test method complies with ISO 9806-1 (1994), ISO 9806-3 (1995) and ASHRAE 93-77 (1978). For this test method, the collector parameters are obtained by measurements at normal incidence angles, stable radiation conditions and temperatures, while separate testing is needed for estimating the incidence angle modifier. For greater accuracy, a second-order heat loss term and the thermal capacity can also be added. This test method normally requires longer test periods, especially in climates such as that in Sweden. A typical result from such tests is shown in Figure 3.8.

$$\eta = \frac{q}{G} = F' \cdot (\tau\alpha)_n - F' \cdot U_0 \cdot \frac{(T_m - T_{amb})}{G} \quad (-) \qquad \text{Equation 3.3}$$

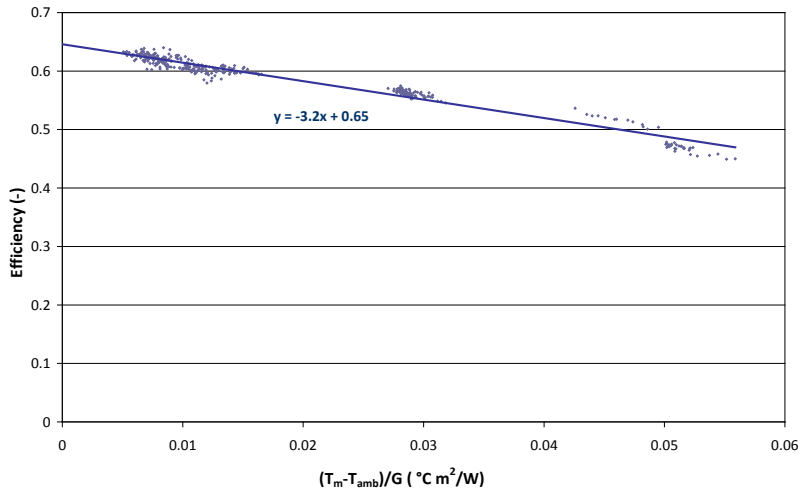

Figure 3.8 *Example of a collector thermal efficiency obtained by steady-state testing.*

This thermal efficiency line is one characteristic of a thermal collector that is obtained for a wide range of working temperatures. Each illustrated measurement point corresponds to the "instantaneous" efficiency during a time interval at normal incidence angle. This was determined from Equation 3.3 and plotted as a function of $(T_m\text{-}T_{amb})/G$. If U_0, F' and $(\tau\alpha)_n$ were all constant, the plots of the efficiency versus $(T_m\text{-}T_{amb})/G$ would correspond to a straight line with "zero interception" $F'(\tau\alpha)_n$ and slope $-F'U_0$, as shown in Figure 3.8. However, in reality, the performance line is a curve since $-F'U_0$ depends on the temperature as the thermal losses do not increase linearly with temperature. Also, the previous efficiency equation does not take into account other factors such as variable wind speeds. More complete dynamic models can be built, such as the one exemplified in Equation 3.4 (Perers, 1993; Fisher et al., 2004).

$$q_{thermal} = F'(\tau\alpha)_n K_b(\theta) G_b + F'(\tau\alpha)_n K_d G_d - F'U_0(T_m - T_{amb}) - \\ - F'U_1(T_m - T_{amb})^2 - F'U_u u(T_m - T_{amb}) - (mC)_e \, dT_m/dt \ (\mathrm{W/m^2})$$

Equation 3.4

The most important component of a modern flat plate solar thermal collector is probably the selective absorber. This type of absorber aims to increase the heat collection performance and is characterised by high absorption for shorter wave solar radiation and low emissivity for long-wave

heat radiation from the absorber. This means that energy absorbed from the sun is maximised and the heat losses from the absorber minimised.

Different solar collectors feature different performances. Theoretical collector performances are exemplified in Figure 3.9 for three different collector designs: an unglazed collector, a glazed collector with a selective surface, and a glazed collector with a selective surface and a Teflon insulator film. These were carried out using "Solar Collector" software (Solar Collector, 2010). By analysing the figure, it can be concluded that the choice of the most appropriate collector depends on the working remperature. If the collector is expected to work at low temperatures, the least expensive collector, the unglazed collector, achieves the highest efficiency. On the other hand, at high temperatures, the most expensive collector corresponding to the glass cover, selective absorber and Teflon film performs best. A detailed cost-performance analysis should be carried out in order to find the most suitable collector for a desired application.

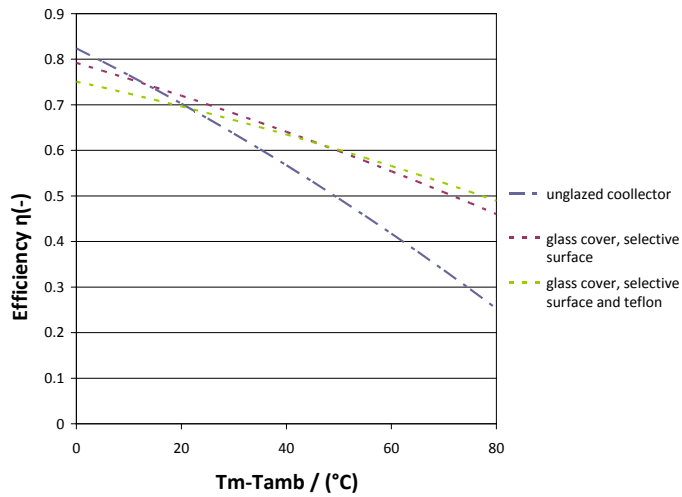

Figure 3.9 *Thermal efficiency curves obtained by theoretical simulations for three different collectors at a constant irradiation level and normal incidence angles.*

3.3 Concentrating Photovoltaic / Thermal (PV/T) technology

One of the most important aspects to take into account when studying photovoltaic/thermal hybrids is the interaction between electrical and

thermal outputs. When an electric load is connected to the electric circuit, electric and thermal power is extracted. This means that part of the incoming irradiation is transformed into electricity by the PV cells instead of being absorbed by the thermal receiver. Consequently, the thermal output decreases nearly as much as the extracted electrical output. Figure 3.10 shows the measured power outputs of a hybrid when an electric load is connected to the PV modules during part of the day.

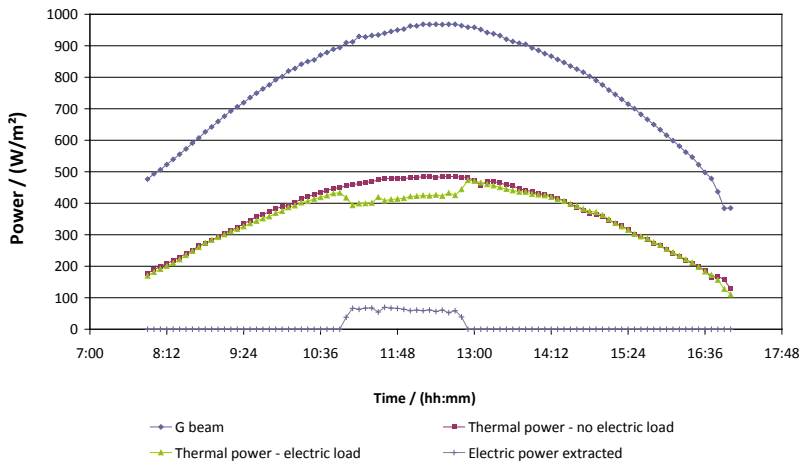

Figure 3.10 *Measured interaction of the hybrid electric and thermal outputs during two clear days with and without electric load. Thermal and electric power outputs expressed per glazed area (A_{total}=4.6 m²) (Bernardo et al., 2008).*

Replacing expensive solar cell material with cheaper reflectors may reduce the costs per energy output unit. Above certain concentration factors, the use of reflectors generally requires cooling of the PV cells, which is important to prevent damage to the cells and maintain their efficiency (Nilsson et al., 2007). Usually, a photovoltaic/thermal (PV/T) concentrating hybrid tracks and concentrates light into a water/air-cooled photovoltaic module working as a thermal absorber (Figure 3.11). Consequetly, not only electricity is generated from the absorber but also heat. Ideally, the thermal absorber uses the energy that the PV cells are not capable of transforming into electricity – both the excess energy used to excite the electrons when the photon energy is higher than the energy band gap, and the photon energy that is not great enough to excite electrons.

Generally, the performance of a typical solar cell decreases by 0.4% per centigrade of temperature increase (Wenham et al., 2007). As discussed in

the previous section, the performance of a solar collector also deteriorates with increasing operating temperature. This is because the thermal losses to the surroundings increase with the temperature difference between the absorber and the ambient temperature. Consequently, the production of both heat and electricity is favoured by lowering the operating temperature. Another issue to take into account is the higher temperature of the cells compared to the temperature of the cooling medium at high irradiance. This is a result of the heat conduction resistance between cells and fluid. Therefore it is important for the absorber to have as high conduction as possible.

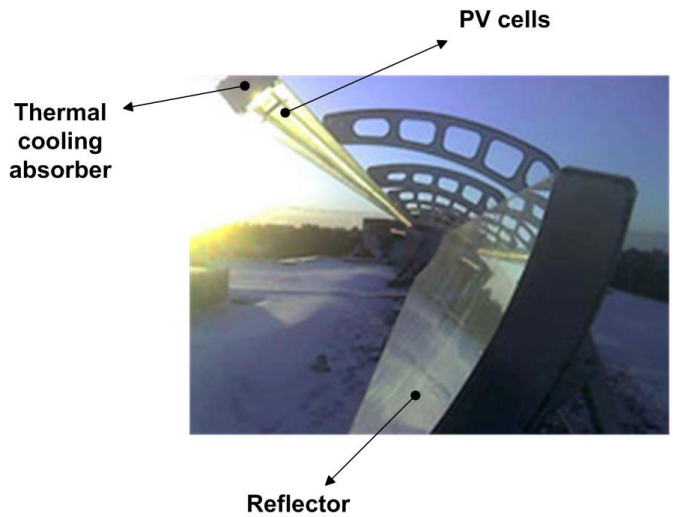

Figure 3.11 Concentrating PV/T hybrid (Menova Energy, 2010).

In a PV/T hybrid, the absorber is made of solar cells instead of the selective surface as in conventional solar thermal collectors. This implies higher thermal emittance and thereby a higher U-value. Also, the optical efficiency is reduced because the absorbance of the PV cells is lower than that of a selective surface. The reflectance factor, light scattering and common shape imperfections of the reflector further reduce the optical efficiency. When an electric load is connected to the PV cells, heat production is lowered because part of the radiation is converted into electricity. The use of concentrators will also reduce electricity production because of the non-uniform concentration profile of the irradiation. Ultimately, a cost analysis is necessary to determine whether the concentrating system reduces the cost of produced energy (Arvind & Tiwari, 2010; Arvind et al., 2009).

3.4 Description of the PV/T concentrating hybrid design and experimental setup

This photovoltaic/thermal parabolic concentrating system tracks and concentrates light into a water-cooled photovoltaic module working as a thermal absorber (Figure 3.12). The PV/T system consists of a photovoltaic module, thermal absorber, parabolic reflector, tracking system, glazed protection, and supporting structure (Figure 3.13). The photovoltaic cells are made of monocrystalline silicon and have a nominal efficiency of 16% at 25°C (Absolicon Solar Concentrator AB, 2008). The total surface area of the cells is 0.33 m². Water runs inside the aluminium thermal absorber where the cells are laminated. The parabolic reflector is made of a silver-coated plastic film laminated on a steel sheet. The geometrical concentration ratio of the reflector, *C*, is 7.8 (Figure 3.12). The reflector is 40 cm longer than the absorber at the edges to also make use of the direct radiation in the morning and afternoon. The tracking is carried out by rotating the structure around a horizontal axis oriented in the east-west direction. The tilt angle is adjusted periodically according to the calculated position of the sun. The parabolic trough is covered by a 4.6 m² glass pane with a measured transmission coefficient of 90% (Bernardo et al., 2008).

In this study, two glazed areas were defined: total glazed area and active glazed area. For this particular hybrid, the total glazed area (A_{total}) was 4.6 m². Active glazed area was defined as the maximum glazed area that the system can make use of. This excludes surface areas where it is impossible for the incoming irradiation to reach the absorber, such as frames and gaps between solar cells and reflector edges, which are longer than the absorber (Figure 3.12). The electric and thermal active glazed areas are different because the thermal absorber is wider than the cells. The electric active glazed area ($A_{active\ elect.}$) is 3.5 m², while the thermal active glazed area ($A_{active\ thermal}$) is 3.7 m².

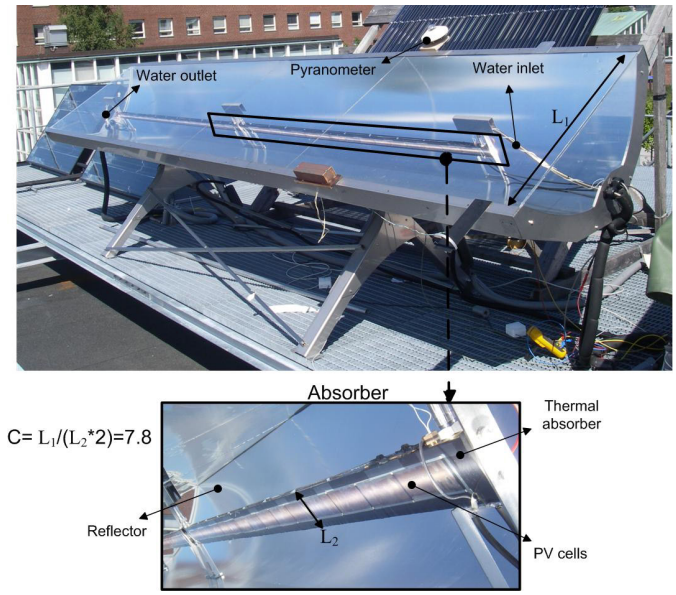

Figure 3.12 *PV/T concentrator trough and photovoltaic cells laminated on one side of the thermal absorber.*

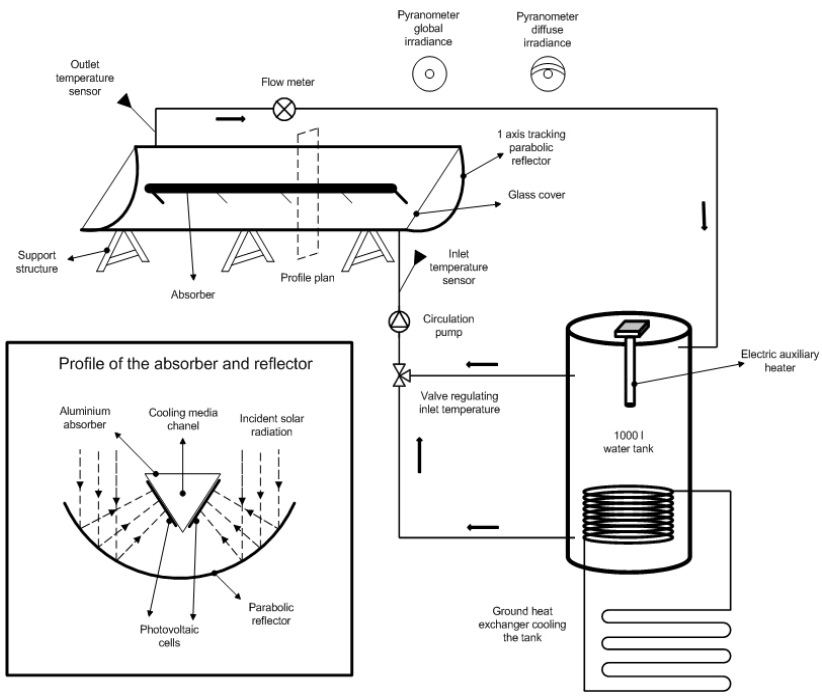

Figure 3.13 *Schematic diagram of the experimental setup system and its monitoring points.*

3.5 Test method and modelling procedure

The testing and modelling procedure is described by the following steps:

a) Simultaneous monitoring of heat and electricity production;
b) Characterisation of the thermal collector according to the steady-state test method (Fisher et al., 2004);
c) Characterisation of the photovoltaic module at high irradiances and variable working temperatures;
d) Measurement of the thermal and electrical incidence angle modifier during one day with stable high solar intensity;
e) Using the previous tested parameters to generate a model capable of describing the thermal and electrical outputs;
f) Validation of the model by comparison between measurements and model outputs during days with varying weather conditions.

Both the electrical and thermal outputs were recorded every six minutes for different temperature conditions in the collector. The maximum electric power output extracted by the hybrid was calculated, based on periodic I-V curve measurements. Using this value, together with the incident beam radiation, the system beam electrical efficiency as a function of working temperature was determined. The useful diffuse radiation was neglected in these calculations because it is the result of the measured diffuse radiation on the glazed surface during high radiation conditions minus nearly half of the diffuse radiation lost in the longitudinal direction by the cell at the edge of the absorber. Furthermore, only the fraction 1/C of the diffuse radiation can be used by the reflector. This results in a total usable diffuse radiation of roughly 5 W/m^2. In this specific case, since the structure is closed, it was not possible to measure the cell temperature directly. Instead, the temperature of the outlet water running inside the thermal absorber at the moment of the electrical efficiency measurement was recorded. This was the temperature limiting the whole electric output, as the cells are series connected.

Since there was no electric load continuously connected to the hybrid, the incoming solar radiation was used to produce heat. This output was calculated using Equation 3.5 (Duffie & Beckman, 2006). The thermal power was then obtained by subtracting the measured electric power from this heat output. The beam incidence angle modifier for the thermal and electric efficiency was calculated with Equation 3.6 and Equation 3.7 (Duffie & Beckman, 2006). The thermal incidence angle modifier (IAM) was defined as the ratio between the measured zero loss efficiency at a certain incidence angle and the zero loss efficiency at normal incidence angle determined from the measurements. The electric incidence angle

modifier was defined as the ratio between the measured electric power at a certain incidence angle and temperature and the estimated power of the hybrid at the same temperature for a normal incidence angle. Only variations in the longitudinal direction along the collector were taken into account, since the tracking system was considered to keep the projected solar height on the transverse direction nearly coincident with the normal of the collector. The IAM measurements are a combination of all angular effects such as decrease of transmission in the glazing for high incidence angles and shading effects by the edges.

$$q = \rho \cdot C_p \cdot \dot{V} \cdot (T_{out} - T_{in}) \quad (\mathrm{W}) \qquad \text{Equation 3.5}$$

$$K_{b\_thermal}(\theta) = \frac{\eta_{0b}(\theta)}{\eta_{0b}(0)} = \frac{\eta(\theta) + \frac{F'U(\Delta T)}{G_b}}{F'(\tau\alpha)_n} = \frac{\eta(\theta) + \frac{F'U_0(T_m - T_{amb}) + F'U_1(T_m - T_{amb})^2}{G_b}}{F'(\tau\alpha)_n} \text{ (-)} \qquad \text{Equation 3.6}$$

$$K_{b\_electric}(\theta) = \frac{q_{electric}(\theta)}{G_b \cdot [\eta_{b\_electrical}(25°C) - \eta_{b\_electrical} \cdot K_T \cdot (T_{out} - 25°C)]} \text{ (-)} \qquad \text{Equation 3.7}$$

The function commonly used to fit the incidence angle modifier data between 0° and 60° is given by Equation 3.8 (Duffie and Beckman, 2006). Between 60° and 90° the function was assumed to be linear (Perers, 1993). The incidence angle modifier coefficient, b_0, shapes the curvature of the function, setting higher or lower incidence angle modifier values for the same incidence angle.

$$K_b(\theta) = 1 - b_0 * \left(\frac{1}{\cos(\theta)} - 1 \right) \text{ (-)} \qquad \text{Equation 3.8}$$

The hybrid was continuously tested at the Energy and Building Design Laboratory of the Faculty of Engineering (LTH), Lund University in Sweden (latitude 55°44'N, longitude 13°12'E) during the period 1 June 2008 to 13 September 2008.

By analyzing the measured data, the hybrid parameters were determined and simple mathematical models, capable of describing its behaviour and estimate its outputs for any geographic location, were used. The monitored parameters and the equations that were used in the model are Equations 3.9-3.12 (Duffie and Beckman, 2006).

$$q_{thermal} = F'(\tau\alpha)_n K_{b\_thermal}(\theta) G_b + F'(\tau\alpha)_n K_d G_d - F'U_0(T_m - T_{amb}) - F'U_1(T_m - T_{amb})^2 \text{ (W/m}^2\text{)}$$ Equation 3.9

$$K_{b\_thermal}(\theta) = 1 - b_{0\_thermal} * \left(\frac{1}{\cos(\theta)} - 1 \right) \text{(-)}$$ Equation 3.10

$$q_{electric} = \left[\eta_{b\_electrical}(25°C) \cdot K_{b\_electric} \cdot G_b + \eta_{b\_electrical}(25°C) \cdot K_d \cdot G_d \right] \cdot \left[1 - K_T \cdot (T_{out} - 25°C) \right] \text{ (W/m}^2\text{)}$$ Equation 3.11

$$K_{b\_electric}(\theta) = 1 - b_{0\_electric} * \left(\frac{1}{\cos(\theta)} - 1 \right) \text{ (-)}$$ Equation 3.12

The hybrid parameters were then fed into Winsun (Winsun Software, 2009), a TRNSYS-based simulation software that estimates the annual thermal and electrical outputs using the described models.

In order to compare the hybrid performance with a conventional side-by-side system made of standard thermal collectors and photovoltaic modules, simulations were also carried out for these standard components. It was assumed that the produced heat would be used for domestic hot water applications, since this could be the largest potential market for these hybrids (Affolter et al., 2004). Therefore, the mean collector temperature of the cells was set to 40°C. Since the cold water temperature was 10°C, the output temperature was 70°C. Consequently, the hybrid solar cells, but not the individual PV module, would work at 70°C, the temperature that limits the electric output. As the PV module is independent of the flat plate collector, it can work at different temperature. This was assumed to be a relatively low temperature of 30°C. The diffuse incidence angle modifier (K_d) was theoretically calculated as being the inverse of the geometrical concentration ratio (1/C where C=7.8) (Winston et al., 2005). All the parameters for the side-by-side system were assumed to be common values for standard components.

3.6 Measurement results and PV/T concentrating hybrid characterisation

3.6.1 Electrical performance

Figure 3.14 shows the electrical beam efficiency as a function of the water outlet temperature. The measured electrical efficiency was 6.4% at 25°C water outlet temperature while the temperature dependence of the electric efficiency was 0.3 %/K. The measured total peak power was 61 ± 0.6 W/m² of total glazed area at 28°C inlet and 39°C outlet water temperature and 997 ± 14 W/m² incident beam radiation.

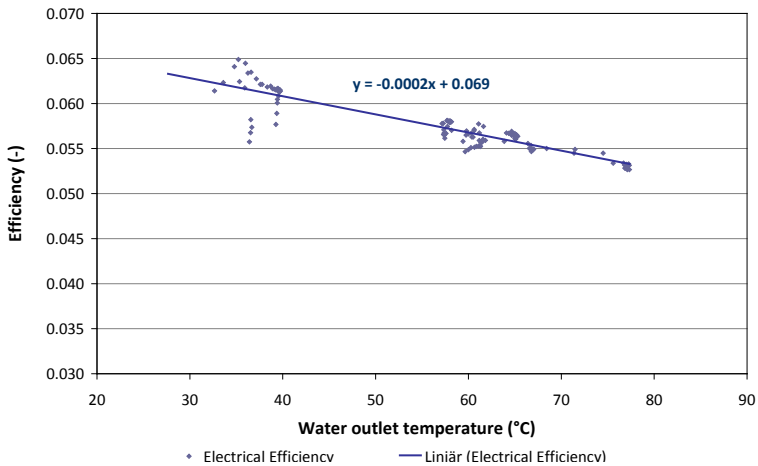

Figure 3.14 *Measured electrical beam efficiency per total glazed area for different working temperatures and beam irradiation higher than 900 W/m².*

3.6.2 Thermal performance

The measured thermal beam efficiency as a function of the working temperature and incident radiation is presented in Figure 3.15. Using linear approximation, the hybrid beam zero loss efficiency $F'(\tau\alpha)_n$ and the heat loss coefficient $F'U_0$ were determined. These were 0.45 and 1.9 W/(m²K) of total glazed area, respectively. The measured thermal peak power was 435 ± 13 W/m² of total glazed area at the same conditions described above.

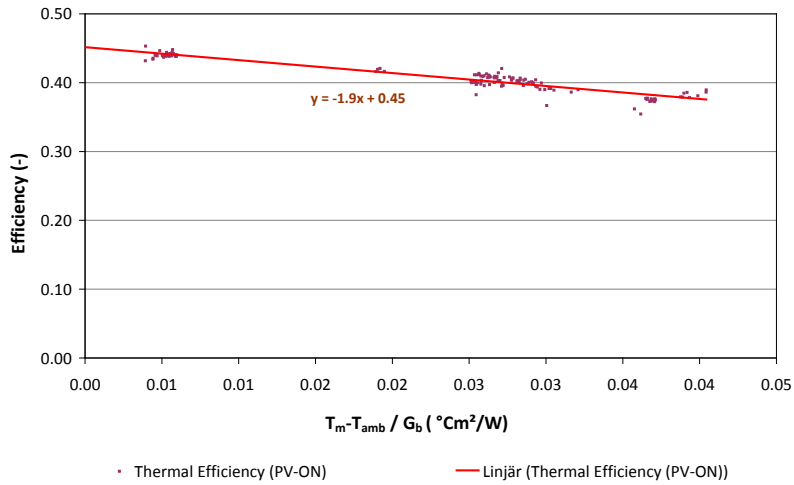

Figure 3.15 *Measured thermal beam efficiency per total glazed area for different working temperatures and beam irradiation higher than 900 W/m².*

3.6.3 Incidence angle modifier

During the morning and afternoon, the reflection losses at the glass cover and absorber increase due to higher angles of incidence. This effect causes a drop in the thermal and electrical outputs. The measured incidence angle modifier of the thermal and electrical efficiency as a function of the angle of incidence is presented in Figure 3.16. The measured b_0 fitting the thermal and electric data was 0.14 and 0.28 respectively, showing that higher angles of incidence have a greater impact on the electrical performance.

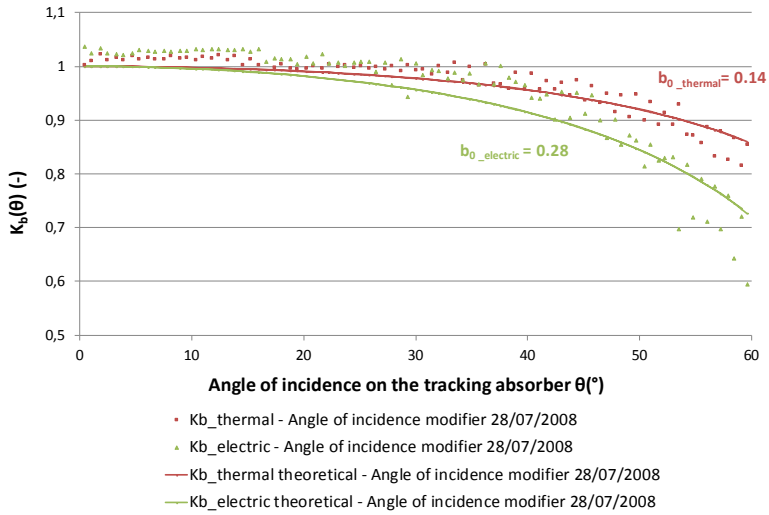

Figure 3.16 *Measured thermal and electrical incidence angle modifier for beam radiation during one clear day and θ<60°.*

3.7 Model validation

The hybrid measured parameters and the presumed parameters corresponding to conventional PV modules and thermal collectors are summarised in Table 3.2 and Table 3.3. The corresponding generated thermal and electric power outputs, illustrated for one day in Figure 3.17 and Figure 3.18, show that good agreement between the hybrid model and measurements was achieved even during variable radiation conditions.

Table 3.2 Parameters for electricity production used in the simulations, expressed by total glazed area. The hybrid parameters were measured, while the ones for the PV module were assumed.

Model electrical parameters	$\eta_{b\_electric}$ (25°C) (-)	K_d (-)	K_T (%/K)	$b_{0\_electric}$ (-)
Hybrid Electric	0.064	0.13	0.3 %/K	0.28
PV module	0.16	0.9	0.4 %/K	0.10

Table 3.3 Parameters for hot water production used in the simulations, expressed by total glazed area. The hybrid parameters were measured, while the ones for the flat plate collector were assumed.

Model thermal parameters	$F'(\tau\alpha)_n$ (-)	K_d (-)	U_0 (W/(m²K))	U_1 (W/(m²K²))	$b_{0\_thermal}$ (-)
Hybrid Thermal (PV-ON)	0.45	0.13	1.9 W/(m²K)	0 W/(m²K²)	0.14
Flat plate collector	0.8	0.9	3.6 W/(m²K)	0.014 W/(m²K²)	0.15

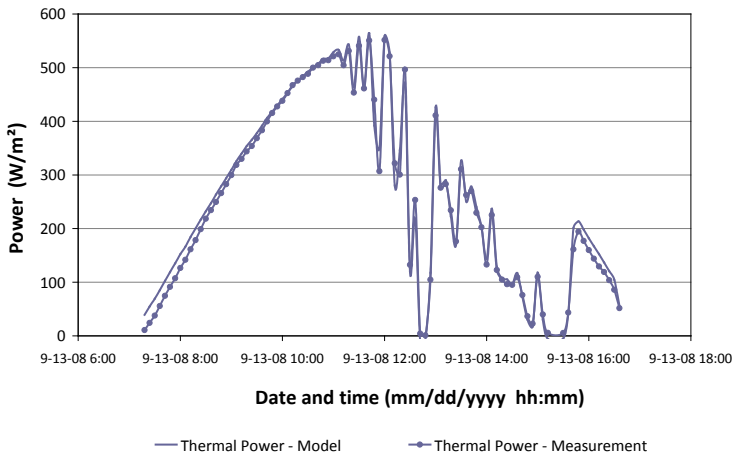

Figure 3.17 Thermal model and measurements during unstable irradiation day.

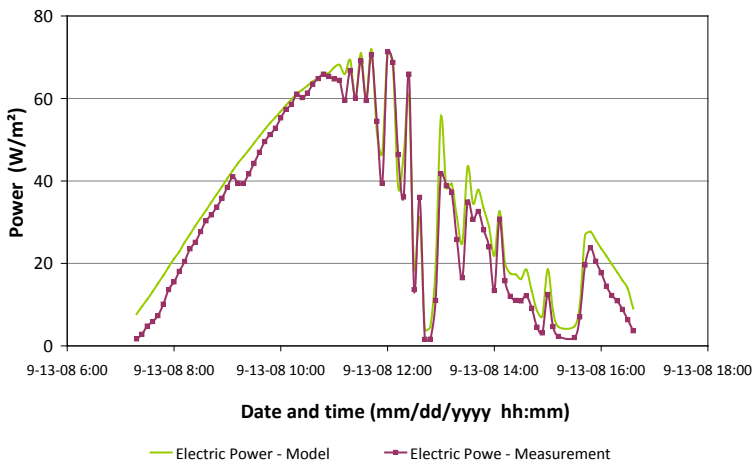

Figure 3.18 Electrical model and measurements during unstable irradiation day.

3.8 Performance analysis

Following the measurement test method described above, a performance analysis is proposed in this section. This consists of estimating the hybrid annual performance for different climates and comparing it with separate conventional PV modules and thermal collectors.

3.8.1 Tracking system

The tested hybrid is thought to work with its tracking axis oriented in an east-west direction. Simulations were carried out to estimate the received irradiation by a tracking surface with the axis horizontally oriented in both east-west and north-south directions for several climates at different latitudes. The results are given in Table 5 in Article I. It can be concluded that it is better to track the sun around an axis in the north-south direction, regardeless of the geographical position (10% to 20% better). This effect is even more relevant when the system is moved closer to the equator where the sun reaches higher altitudes. All the following simulations take this result into account, estimating the annual outputs as if the hybrid were tracking the sun in a more productive way, with its axis in the north-south direction.

Concentrating solar systems can only make use of a fraction of the incident diffuse light. In contrast, non-concentrating systems, like standard PV modules and flat plate collectors, use the global irradiation. For the next calculation, it was assumed that the tested concentrator could make use of the incoming beam irradiation plus ($1/C$) of the diffuse irradiation (G_b+G_d/C) on the collector plane (Winston et al., 2005). This comparison is presented in Table 5 in Article I. The conclusion is that the global irradiation incident on a static surface is higher than the beam irradiation plus a fraction of the diffuse incident on a one-axis tracking concentrating surface for this concentration ratio. This means that, regardeless of its location, a non-concentrating fixed collector receives more usable irradiation than the studied tracking concentrating one (roughly 20% to 40% in this case). Closer to the equator, where the beam irradiation values are higher, this result becomes less evident and becomes even clearer as the concentration ratio increases.

3.8.2 Annual performance

Based on the system parameters previously presented in Table 3.2 and Table 3.3, the total annual performance for the hybrid and the traditional side-by-side system was calculated for three different climates. These re-

sults are presented in Table 3.5. For Stockholm, the estimated electric and thermal annual outputs per total glazed area were 45 kWh/m^2/yr and 188 kWh/m^2/yr, respectively. The outputs of the stand-alone PV module and thermal collector were 165 kWh/m^2/yr and 402 kWh/m^2/yr, respectively.

Table 3.5 Electric and thermal outputs of the hybrid and conventional side-by-side-system for domestic hot water application expressed per square metre of total glazed area.

Annual outputs per total glazed area (kWh/m^2/yr)	**Stockholm (lat=59.2°N)**	**Lisbon (lat=38.7°N)**	**Lusaka (lat=15.4°S)**
Hybrid electric annual output (kWh/m^2/yr)	45	83	103
Hybrid thermal annual output (kWh/m^2/yr)	188	457	613
(Side-by-side system) PV module annual output (kWh/m^2/yr)	165	265	308
(Side-by-side system) thermal collector annual output (kWh/m^2/yr)	402	888	1144

3.8.3 Hybrid concentrator vs. standard PV module based on cell area

The main goal when building a concentrating PV/T hybrid is to increase annual electrical production per cell area, commonly the most expensive component of the collector. The production per cell area of the hybrid and the traditional PV module, and the ratio between the two, is presented in Table 3.6. The results show that the concentrating hybrid cells produce 3.6 to 4.4 times more electricity than a PV module with the same cell area.

Table 3.6 PV/T north-south concentrating hybrid and traditional PV module electric output comparison based on cell area. PV module inclination from the horizontal was set to near optimum values of 40º in Stockholm, 30º in Lisbon and 20º in Lusaka. A_{cells_hybrid}=0.33m^2.

Electric annual output per cells area (kWh/m^2/yr)	**Stockholm (lat=59.2°N)**	**Lisbon (lat=38.7°N)**	**Lusaka (lat=15.4°S)**
Hybrid tracking N-S (70°C)	627	1156	1422
Traditional static PV module (30°C)	173	279	325
Output ratio (Hybrid/PV module)	3.6	4.1	4.4

3.9 Discussion

A relatively high concentration factor aims to improve cost efficiency, since solar cells are commonly the most expensive component of a PV/T concentrating hybrid. For higher concentration factors, a lower fraction of the diffuse radiation can be used. Consequetly, the applicability of the hybrid in climates with a large fraction of diffuse radiation, such as that in Sweden, decreases. Furthermore, since higher temperatures decrease the electrical and thermal efficiency, producing low-temperature heat is more adequate. More importantly, temperatures close to 100°C are dangerous for the integrity of the solar cells in this hybrid. This is a disadvantage if the hybrid is to be used in a solar domestic hot water system where stagnation periods are likely to occur during the summer. Higher concentration factors also increase the size of the hybrid and so decrease the possibility of integration on the roof of a single family house.

The temperature profiles of the model were qualitatively compared with measurements during the tested period (Figure 3.17 and Figure 3.18). The difference in temperatures is thought to be primarily due to the inaccuracy in modelling the incidence angle modifier, especially for higher incidence angles in the morning and afternoon periods (Figure 3.16). Another possible contributor may be that the diffuse radiation was neglected when calculating the measured efficiency, which would decrease the modelled efficiency and production. The measurements of the electrical efficiency showed a larger dispersion compared with the thermal efficiency measurements, probably related to the sensitivity of solar cells to uneven distribution of radiation and to the accuracy of the tracking system (Figure 3.14).

The tracking system analysis showed that a one-axis tracking system should rotate around an axis aligned in the north-south direction, regardless of its geographical location. If tilted towards the equator, the performance is further improved. Furthermore, the tested hybrid was shown to receive less usable radiation than a standard flat fixed collector on an annual basis. Consequently, the measured low hybrid efficiencies, together with low usable annual radiation, generate low annual outputs per glazed area when compared with conventional alternatives. However, the output per cell area was increased approximately four times compared with a conventional PV module with the same cell area. The optical efficiency is one of the factors that directly influence the final electric efficiency. The ideal thermal optical efficiency of the hybrid was theoretically estimated in the discussion chapter in Article I. This analysis helps to understand why concentrating hybrids commonly feature lower efficiencies than conventional thermal collectors and PV modules. For future development, hybrid design still has margin

for improvement for most of its components. It is very important that cells under concentration have very high efficiency and homogenous irradiation; the glass cover should have very high transmittance while optical errors in the reflector should be avoided and reflectance maximised.

4 Testing of the CPC-themal collector system

4.1 Background

One of the most important goals to be achieved by a solar thermal system is a high annual solar fraction (Mills & Morrison, 2003; Helgesson et al., 2002). Generally, in geographical regions further away from the equator, the solar contribution profile peaks during the summer months and decreases during the winter period. On the other hand, the domestic hot water load is fairly constant over the year. This means that the annual production and consumption profiles do not match. Consequently, the annual solar fraction of the system is reduced. The optical efficiency of the tested CPC-thermal collector decreases during the summer period making it possible to increase the collector area and, thereby the annual solar fraction, without increasing the stagnation periods. The main objective of this investigation was to evaluate the performance of the CPC-thermal collector system and compare it with that of a conventional flat plate collector system.

4.2 Collector design

A solar collector design in which a relatively expensive selective absorber material was replaced by a cheaper reflector was studied. A compound parabolic concentrator (CPC) collector with a geometrical concentration factor of 1.5 had been previously developed (Helgesson et al., 2004; Adsten et al., 2004). The collector consists of a reflector, a bi-facial selective absorber and a support structure. The reflector has an optical axis normal to the collector glass which defines the irradiation acceptance interval of the reflector (Figure 4.1). Once the incident radiation is outside this interval, the reflectors do not redirect the incoming beam radiation to the absorber and the optical efficiency of the collector is reduced. Consequently, the optical efficiency of the collector changes throughout the year depending

on the projected solar height. The tilt determines the amount of annual irradiation kept within the acceptance interval. As a result, by varying the tilt, the collector area can be increased without increasing the stagnation periods in the summer when the collector has lower optical efficiency. Further details about the design of the collector and the experimental setup can be found in Article II. Related concepts to this collector have been reported by Kothdiwala et al. (1995), Tripanagnostopoulos et al. (2004), Chaves & Pereira (2000), Mills & Morrison (2003).

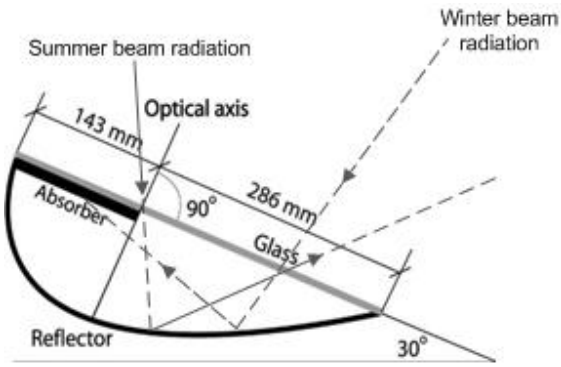

Figure 4.1 Sketch of the CPC-thermal collector profile (Helgesson, 2004).

4.3 Evaluation method and model

Several measurements were carried out on the CPC-thermal collector in order to calculate the necessary parameters for the annual performance simulations. A simplified version of the quasi-dynamic test method for determination of the optical and thermal characteristics with multiple linear regressions was used (Perers, 1993; Perers, 1997; Duffie & Beckman, 2006). In this test method, wind and long wave radiation factors of the dynamic test method were not included. Measurements were carried out between August and October. However, only measurements correspondent to periods when the incident radiation was inside the acceptance angle were used. The collector parameters were then fed into a TRNSYS model (Klein S., 2006). The collector model was validated and used to estimate the performance of the CPC-thermal collector system in comparison with that of a flat plate collector system.

In order to accurately determine the collector incidence angle modifiers, measurements were carried out for the longitudinal and transversal direction. Firstly, the influence of the glazing was measured in the longitudinal direction while the transversal incident angle was kept constant. Since

this measurement did not provide data of sufficient quality, a theoretical expression of the incident angle modifier on a glass, according to Fresnel and Snell's laws, was used. This was previously shown to be a fair approximation for the incidence angle of the tested collector in the longitudinal direction (Helgesson, 2004). Secondly, the dependence of the reflector was measured on the transversal plane when the longitudinal incidence angle was constant during a clear day at the autumn equinox (Figure 4.2). The bi-axial model uses the projected transverse incidence angle, θ_t, for describing the influence of the reflector and the incidence angle, θ, for the influence of the glazing. For further details on the measurement procedure, refer to Helgesson (2004) and Article II. Since large variations of the incidence angle modifier are expected within a short angle interval around the optical axis, measurements were carried out at a relatively short time interval of six minutes. The measured incidence angle modifier curves were then modelled by high-grade polynomial equations. This increases the accuracy of the model. Two TRSNSYS models were created: one describing a solar domestic hot water system using the tested CPC-thermal collector and a second system using a standard flat plate collector. Only the CPC-thermal collector model was validated while the other parameters were assumed, and based on literature (Helgesson, 2004; Hobbi & Siddiqui, 2009). The main components of the system are shown in Figure 4.3 and the parameters of the collectors in Table 4.1. The system parameters are described in Article II. The accuracies of the measurements were the same as previously described for the thermal properties of the tested PV/T hybrid.

The domestic hot water load profile was built based on that described by Widén et al., (2009) but scaled to the latest data on Swedish total hot water consumption (Stengård, 2009). The daily profile was made of seven different water draw-offs. The annual hot water consumption variation effect was also introduced (Swedish Energy Agency, 2009). These are shown in Figure 5 and Figure 6 in Article II. The total annual hot water provided by the system corresponded to 2050 kWh/year.

By simulation iterations, the maximum collector area that maximises the annual solar fraction but limits the stagnation periods under a certain limit was determined. In order to quantify the stagnation periods, a deterioration factor was assumed. This factor took into account not only the number of stagnation hours but also how much the collector outlet temperature increased over 100°C during that period. The limit was set to 5000°Ch/year. The deterioration factor is described in more detail in Article II and is further considered in the discussion chapter.

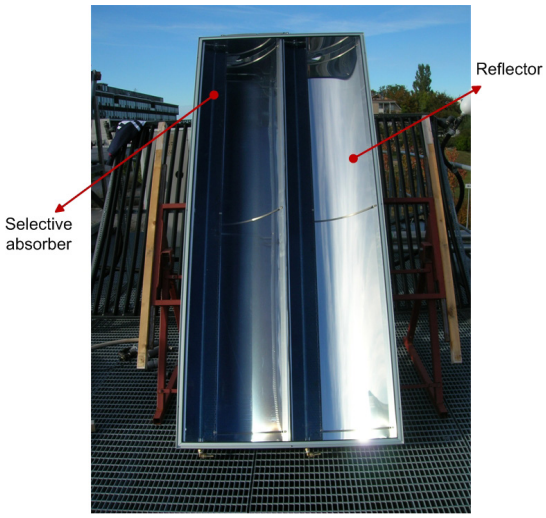

Figure 4.2 *CPC-thermal collector turned 90° during the autumn equinox.*

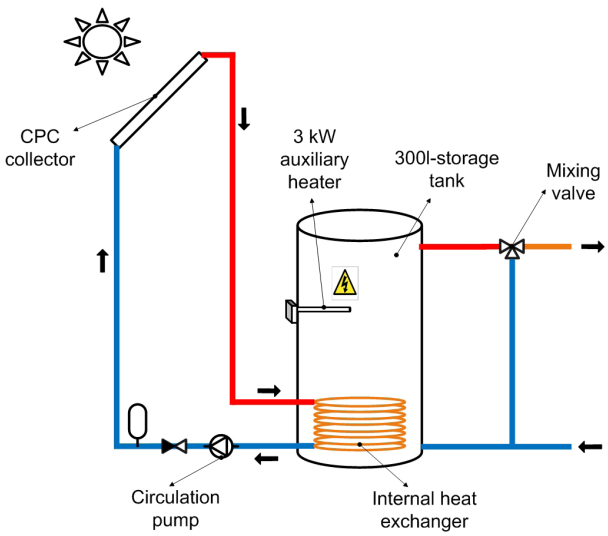

Figure 4.3 *Main components of the solar domestic hot water system model.*

4.4 Measurement results and collector characterisation

The CPC-thermal collector parameters, estimated using multi linear regression on the measured data, and the parameters assumed to be representative for conventional flat plate collectors, are presented in Table 4.1.

Table 4.1 Measured parameters of the CPC-thermal collector and presumed parameters of a typical flat plate collector.

Parameters and units	CPC collector (measured)	Flat plate collector (presumed)
$F'(\tau\alpha)_n$ (-)	0.64	0.8
$F'(\tau\alpha)_n K_d$ (-)	0.31	0.72
$F'U_0$ (W/m^2/K)	2.8	3.6
$F'U_1$ (W/m^2/K^2)	0.035	0.014
$b_{o\_thermal}$ (-)	-	0.2
$(mC)_e$ (J/m^2/K)	1923	8000

Figure 4.4 shows the longitudinal and transversal beam incidence angle modifiers describing the influence of glazing and reflector, respectively.

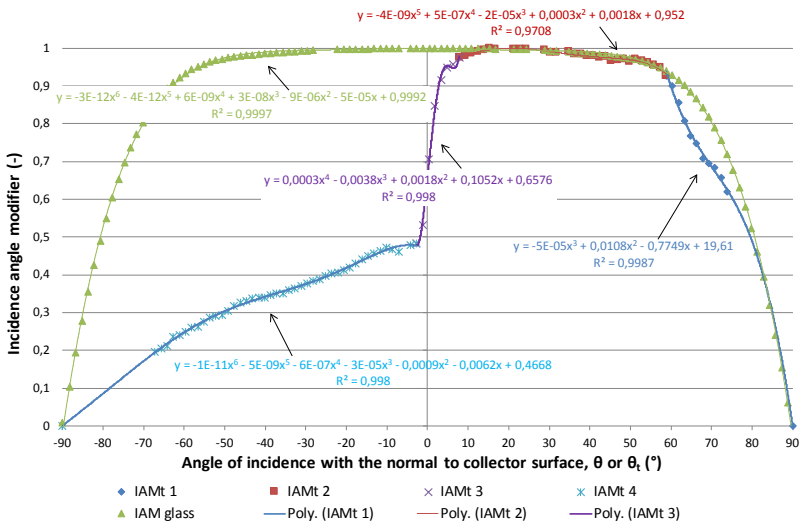

Figure 4.4 *Measured transversal incidence angle modifier as a function of θ_t describing the reflector influence and modelled by four polynomial equations for different intervals. Theoretical incidence angle modifier as a function of θ describing influence of the glass.*

4.5 Model validation

To validate the CPC-thermal collector model, the measured and modelled power outputs were compared during the test period (Figure 4.5). From the analysis of Figure 4.5, it can be concluded that good agreement was found between the model and the measurements. In Figure 4.6 the modelled and measured power output were compared during a day with variable irradiation conditions. The CPC-thermal collector model was the only one validated.

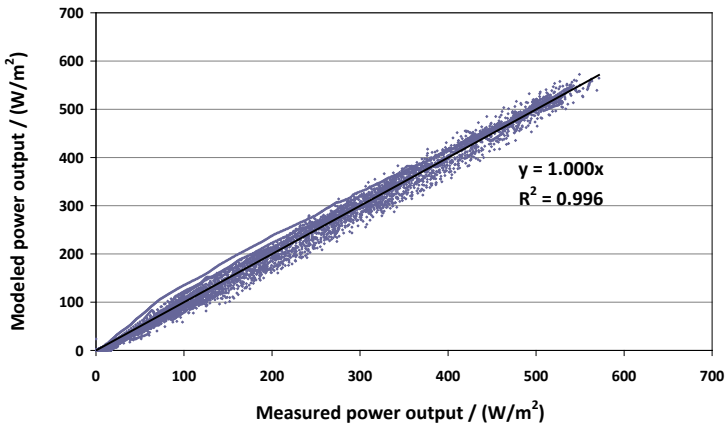

Figure 4.5 *Modelled and measured power output data during the period of testing (August-October).*

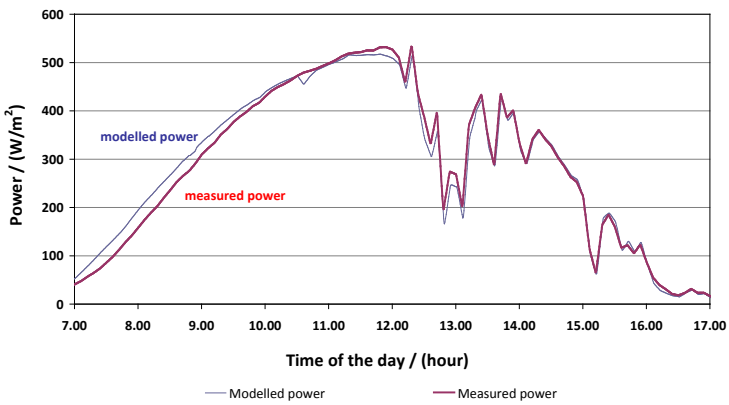

Figure 4.6 *Modelled and measured power output on the 20 September 2009.*

4.6 Performance analysis

The maximum solar fraction achieved by both systems, for several different tilts, is presented in the left axis in Figure 4.7. The corresponding maximum collector area that limits the deterioration factor under 5000°Ch/year is shown in the right axis of the same figure.

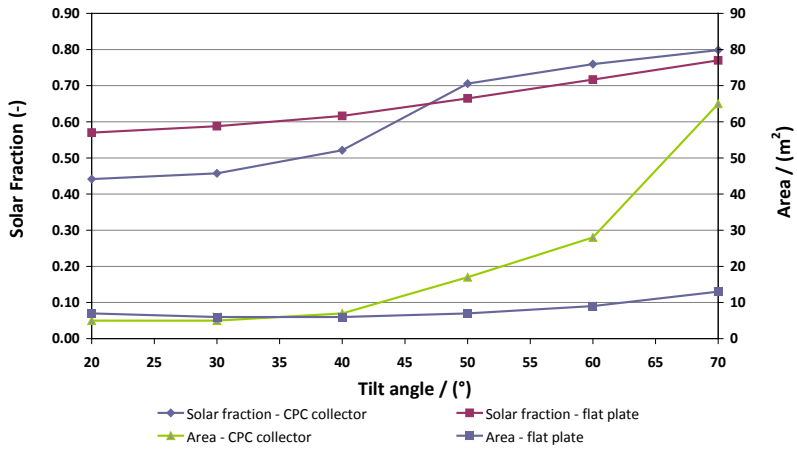

Figure 4.7 *Annual solar fraction and corresponding collector areas for the CPC-thermal collector system and a flat plate collector system.*

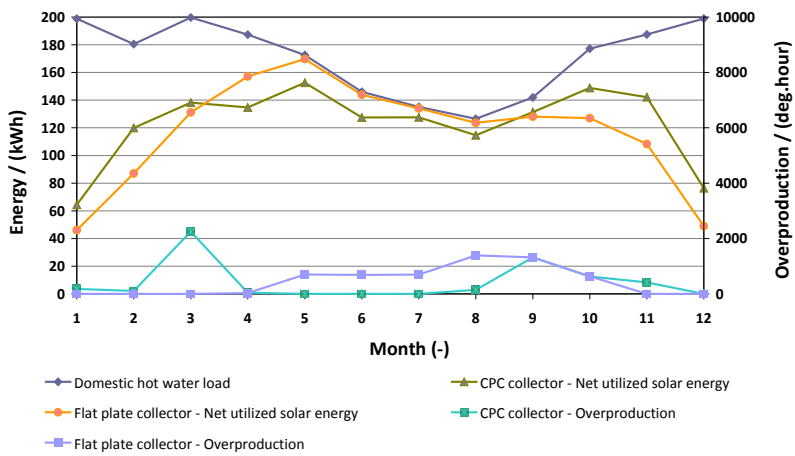

Figure 4.8 *Energy and deterioration factor profiles during the year for 50° tilt. The CPC-thermal and the flat plate collector areas were 17 m^2 and 7 m^2, respectively.*

An analysis of the simulation results shows that, at 50˚ tilt, the load-adapted system achieves a solar fraction of 71% using 17 m^2 of collector area compared to 66% and 7 m^2 of a flat plate collector system. In Figure 4.8, the annual production profile of the two solar domestic hot water systems is presented for 50˚ tilt. It can be noted that the decreased solar production in the CPC-thermal collector system during the summer and the stagnation periods moved to the spring and autumn periods. When the CPC-thermal collector system achieves higher solar fractions than the flat plate collector system, it requires at least 2.4 times greater collector glazed area. Taking into account that the selective absorber surface of the CPC collector is 1/3 of its total glazed area (Figure 4.1), the CPC collector makes use of roughly 20 % less absorber area.

4.7 Discussion

Some limitations in the test method can be noted. Since the measurements that estimated the collector parameters and validated the model were carried out between August and October, the variation in projected solar height during that period was limited. Ideally, the model should be validated with measurements carried out from the summer to winter solstice. Also, the "b_0 equation" was used by the multi linear regression when calculating the collector parameters. This is an approximation since, in predicting the performance of the collector, the described biaxial incidence angle modifier shown in Figure 4.4 was used. In addition, the effect of the gables in the longitudinal direction was not included, which decreases the accuracy of the model, especially during morning and afternoon and for shorter collectors. Furthermore, a deterioration factor was assumed as a design parameter instead of economics or solar fraction. Considerations regarding this factor can be read in the discussion chapter in Article II.

Since the concentration ratio of the tested CPC-thermal collector is relatively low (1.5), the collector could be built with a compact design. This is advantageous for integration on roofs of single family houses. Due to the low concentration factor, a larger fraction of the diffuse radiation can be used, as exemplified in the measured parameters. This is advantageous since, in Sweden, roughly half of the annual radiation is in fact diffuse (Kjellsson, 2009). The negative aspect is the fact that the reduction in absorber area compared with a flat plate collector is relatively small, which indicates that the cost-efficiency increase may be limited.

Helgesson (2004) reached analogous results; 15 m^2 of the same CPC-thermal collector reached an annual solar fraction of 71% at an optimal angle of roughly 50˚ tilt. For the same conditions, 6.5 m^2 of a

flat plate system achieved an annual solar fraction of 56% at the same tilt. This means that the CPC-thermal collector used 23% less absorber area than the flat plate collector with an increase in solar fraction of 15 percentage points.

The simulation results from this investigation showed that the optical efficiency decrease during the summer caused the production of the CPC-thermal collector system to be lower than that of the flat plat collector system during that period. This may indicate a margin of improvement on the shape of the CPC-thermal collector in such way that the decrease in optical efficiency during the summer period is less abrupt. The cost decrease due to 20% lower absorber area combined with the solar fraction increase of 5 percentage points should compensate for extra costs of the increased reflector and glazed area. The required performance data for carrying out a cost analysis that compares the flat plate and CPC-thermal collector systems was provided in this investigation. However, the estimated differences in absorber area and annual performance between the systems were not found to be large.

5 Measurements on the electrical incidence angle modifiers of an asymmetrical photovoltaic/thermal compound parabolic concentrating-collector

The electrical properties of an asymmetrical compound parabolic concentrating (CPC) photovoltaic/thermal (PV/T) hybrid collector were investigated. The geometrical design of this hybrid collector is the same as the previously tested CPC-thermal collector (Article II) with photovoltaic cells laminated on both sides of the absorber. The thermal absorber is new but the collector geometry is still the same and is described in Figure 1 in Article II. The CPC-PV/T hybrid collector is shown in Figure 5.1. The main objective of this study was to measure the electrical efficiency and incidence angle modifiers of the hybrid collector.

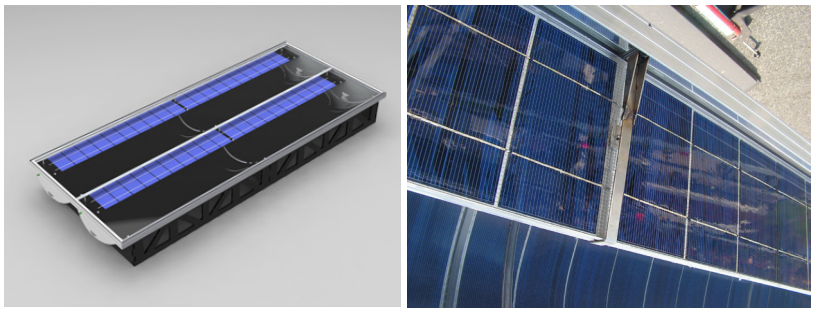

Figure 5.1 *Left: illustration of the hybrid. Right: picture of the PV/T absorber.*

5.1 Experimental setup and hybrid design

Figure 5.2 describes the electrical arrangement of the solar cells in one PV/T module. Since the two receivers are identical, only one of the receivers was tested. The figure shows the collector viewed from the top. The backside, i.e. the part that utilises the reflector, is equipped with the same PV cell arrangement. One string consists of 38 PV cells. Both the front and the backside of the receiver consist of two PV strings each so the total number of PV cells per receiver is 152 cells. The total area of PV cells on a receiver was approximately 0.58 m^2 and the active glazed area was approximately 0.87 m^2 per receiver. For this hybrid collector, the active glazed area was defined as the glazed area directly on top of the cells and reflector, excluding edges, spaces between cells, and parts where there was no reflector. Figure 5.2 shows the electrical connection in red and the water connections in blue. T_{in} and T_{out} represent the temperature sensors placed at the inlet and outlet of the water running inside the collector. T_{mid} was calculated as the average temperature between T_{in} and T_{out}. The same figure also shows the size of the different electric components in the collector. The total size of the collector is 2.31 m by 0.955 m. The length of the thermal receiver is 2.290 m and the height is 0.158 m. The size of the PV cells is 0.148 m by 0.026 m. The active width of the reflector is 0.292 m. The parts of the collector which are excluded by the active glazed area are indicated in the figure. The total active width of the trough is 0.44 m, i.e. the sum of the active reflector height and the height of the PV cells.

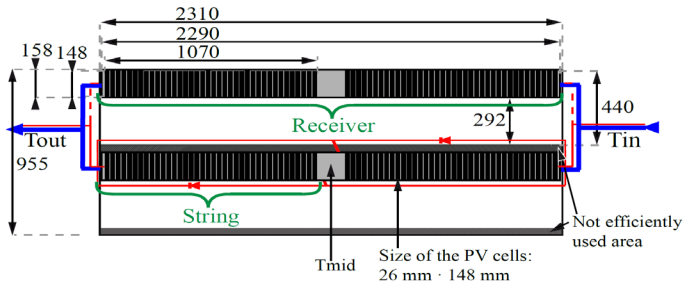

Figure 5.2. *Top view of an illustration of the PV/T hybrid collector. The water connections are shown in blue and the electrical connections in red. The collector measures are in millimetres.*

5.2 Test method

The first step in the testing procedure was to analyse the electrical efficiency and temperature dependence of the hybrid collector. This was performed while the incidence angle maximised the electrical output, i.e. close to a normal incidence angle. Once the temperature dependence was determined, the incidence angle modifier could be measured. This was done by measuring I-V curves. Since the investigated collector has a closed structure, the cell temperature could not be measured directly. Instead, as for the previously tested hybrid, the temperature of the water outlet was measured.

The transverse incidence angle modifier (IAM_t) was defined by the reduction in electrical efficiency in relation to its maximum value, caused by variations in the incidence angle between the sun and the normal to the collector in the transverse direction (θ_t). This is exemplified in the left illustration in Figure 5.3. In order to measure IAM_t for different transverse angles, the longitudinal angle was kept equal to zero. This was measured by directing the collector towards the solar azimuth for various tilt angles.

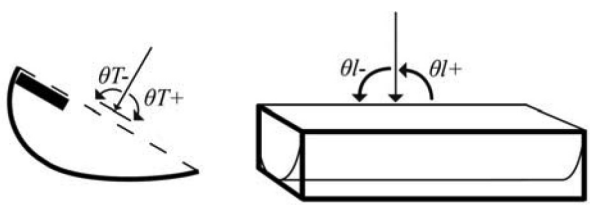

Figure 5.3 *Transversal incidence angle (left) and longitudinal incidence angle (right).*

The measured incidence angle modifier is only valid for the direct radiation. However, even on clear days, there is always a percentage of diffuse light that contributes to the measured power output, which becomes relevant for low concentrating collectors such as this one. The fraction of useful diffuse radiation in relation to the total diffuse radiation incident on the glazed cover of the collector varies with its tilt. This fraction was calculated by summing the theoretical contributions from the front and backside of the receiver and dividing this by the diffuse radiation as measured by the pyranometer. The variation in the fraction of the useful diffuse radiation was relatively small for the tilt interval used during the tests, and was set to 50%. This calculation is described in more detail in Article III.

The longitudinal incidence angle modifier (IAM_l) was measured while keeping a constant θ_t, which corresponds to the measured maximum value of IAM_t.

5.3 Results

The results from the electrical efficiency dependence on the temperature and the incidence angle modifier are described below. In Article III, a theoretical estimation of the maximum output of the collector was also described.

5.3.1 Dependence of the electrical efficiency on temperature

The estimated electrical efficiency of the PV/T hybrid collector per cell area and per active glazed area at 25°C was 21% and 14%, respectively (Figure 5.4). The maximum electrical power of the tested collector was 241 ± 2.4 W or 139 ± 1.4 W/m^2 per active glazed areas. The measured dependence of electrical efficiency on temperature (K_T) was -0.4%/K.

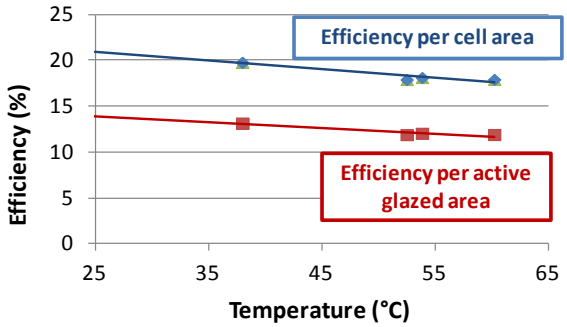

Figure 5.4 *Electrical efficiency dependence on the water outlet temperature expressed per cell area and active glazed area.*

5.3.2 Incidence angle modifiers for beam radiation

Figure 5.5 shows the electrical transverse incidence angle modifier, IAM_t, and Figure 5.6 shows the longitudinal incidence angle modifier, IAM_l, for beam radiation. The measured values are adjusted for temperature variations. The sharp variation around 0° for the IAM_t is explained by the radiation shifting from outside to inside the acceptance angle. The IAM_l for the front and backside receivers is shown in yellow and green respectively. As shown, the front receiver behaves like a flat plate solar panel. The backside receiver is maily responsible for the efficiency drop during low incidence angles in the longitudinal direction.

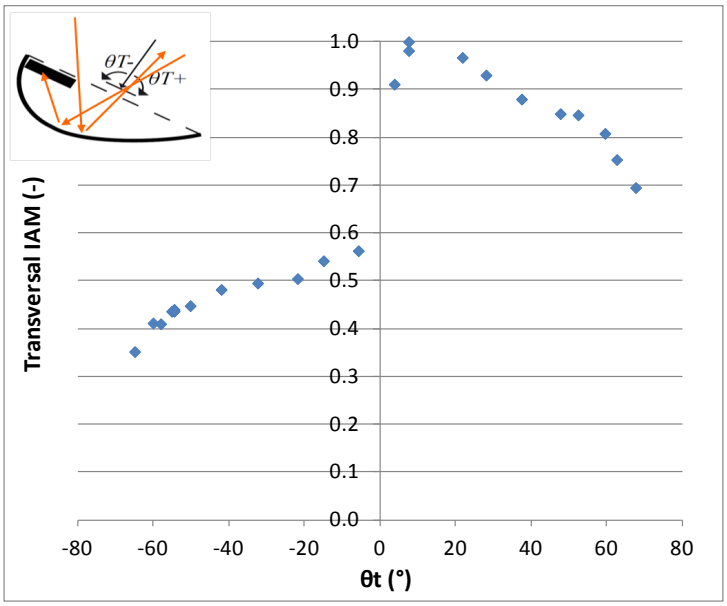

Figure 5.5 *Electrical transverse incidence angle modifier (IAM_t) for beam radiation.*

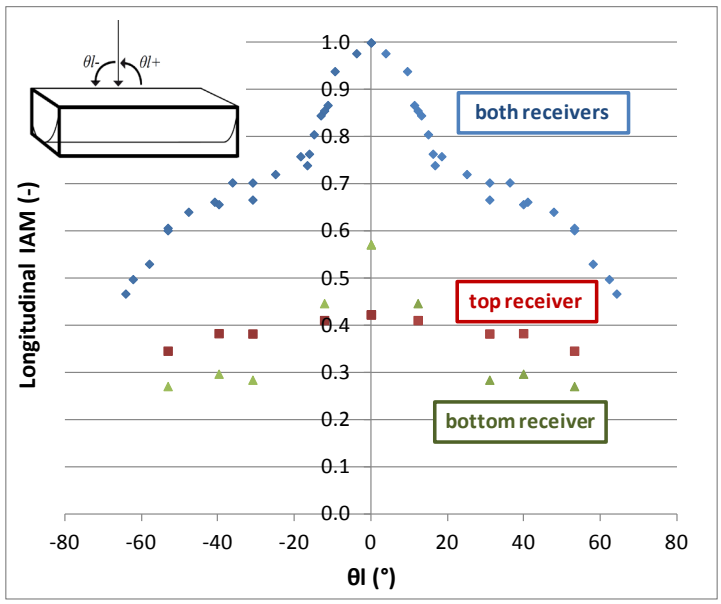

Figure 5.6 *Electrical longitudinal incidence angle modifier (IAM_l) in blue. The IAM_l for the backside and front of the receiver are shown in green and red, respectively.*

5.4 Discussion

The measured results of the electrical efficiency and the incidence angle modifiers provide valuable information for further improvements of the collector design. It also provides necessary information to model the electrical production of the hybrid at different climatic and operating conditions. As shown in Figure 5.4, a limitation of this study is the small amount of measured data for the efficiency dependence on the temperature. However, the values were found to be in good agreement with the literature (for example in Wenham et al., 2007).

Figure 5.5 shows that, if the collector is installed in a tracking axis rotating around an axis aligned in the east-west direction, the projected solar height over the day should be maintained between 5° and 10° for maximum output. The decrease in the longitudinal incidence angle modifier is caused by the shading due to the reflector edges (Figure 5.1, left). When $0°<\theta_l<30°$ the decrease in the IAM_l is apparent (Figure 5.6). This corresponds to partial shading on the first cell placed at the edge of the backside receiver (Figure 6 in Article III). At around $\theta_l=30°$, the cell on the edge placed on the backside of the receiver is totally shaded, which makes the bypass diode "shut down" that string. Shading more cells when $\theta_l>30°$ will not imply a significant further decrease in production on that string, and so the total efficiency decrease is diminished. If there was no bypass diode installed on each string, the decrease would be twice as large, since the strings are connected in series. Total IAM would decrease to about 0.5 and not just to the 0.75 as seen in the figure. This is even clearer if the output of the cells on the backside of the absorber is studied. This output falls from 0.58 to 0.29, i.e. a 50% reduction. As shown in Figure 5.6, the front side is less affected by the shading. The IAM_t shown in Figure 5.5 is in agreement with previous measurements for the thermal production of a solar thermal collector with the same geometry (Figure 7 in Article II).

During a large period of the day, output is significantly reduced by the reflector edges, as shown by the IAM-measurements. For periods when $-20°<\theta_l<20°$, high beam-radiation conditions and for an optimum angle of θ_t around 5°, the solar cells on the backside of the receiver produce more energy than the ones on the front. The maximum difference is shown in Figure 5.6 at $\theta_l=0°$ when the cells on the back are responsible for 58% of the collector output while the cells on the front are responsible for 42%. In the other periods, the solar cells on top of the receiver produce more energy. This represents a margin of improvement on the design of the hybrid collector. By removing the cells on the edge, turning the edge cells 90°, dividing the string into three or four parts, and tracking the collector around an axis oriented in the north-south direction, the collector performance can be significantly improved.

6 Retrofitted solar thermal systems – theoretical analysis

6.1 Background

According to the Technology Roadmap of the Solar Heating and Cooling Program (International Energy Agency, 2012), one of the biggest bottlenecks in the deployment of solar heating technology is the economic profitability, because of the high investment cost (Hang et al., 2012; Dayan, 1997; Tsilingiris, 1996; Eicker & Pietruschka, 2009). The solar storage is one of the most expensive components in a solar water heating system (Hang et al., 2012). Some of the main goals in attaining larger market volumes are a system cost reduction of 30% and development of standardised kits and plug-and-function systems (International Energy Agency, 2012).

Retrofitting existing domestic hot water (DHW) storages using add-on docking units has the potential to help meeting these goals. The investment cost can be significantly reduced both in material and installation (International Energy Agency, 2012; Bernardo et.al, 2012; Eicker & Pietruschka, 2009). In Sweden alone, approximately half a million single-family electrically-heated houses use conventional electrically-heated water storage for domestic hot water production (Swedish Energy Agency, 2011b). According to Kjellsson (2002), the size of existing water boilers in Swedish single-family houses varies with the size of the family, the most common size being 200 or 300 litres. In the 1970s most of the installed boilers were 300 litres, due to comfort regulations requiring that large discharges could be met to service bathtubs. Since then, domestic hot water consumption has decreased mainly because showering has replaced the use of bathtubs and because of the widespread use of water-saving nozzles. Today, the estimated average size of the new hot water boilers replacing the old ones in such houses is estimated to be 200 litres (Kjellsson, 2002). This indicates that there may now be some free space in the storage cupboard and

this could be used by a retrofitting add-on unit described in more detail in the chapter "Technical Improvements". Furthermore, when a standard solar domestic hot water system is installed, the existing hot water storage is replaced by a solar storage tank. Such solar storages often have shapes and/or volumes differing from those of conventional storing vessels, which make installation in the available space complicated and time-consuming, and thereby increases the overall installation cost.

Taking into account the cold Swedish climate, a forced circulation flow system with a water-glycol mixture is normaly used for connecting solar collectors to the existing domestic hot water storages. Since forced circulation with an external heat exchanger is used, almost any kind of storage tank can be retrofitted when the new solar thermal system is installed. As in other studies, the annual solar fraction was used as parameter to be optimised (Morrison & Tran, 1984; Wongsuwan & Kumar, 2005; Buckles & Klein, 1980; Hobbi & Siddiqui, 2009; Duffie & Beckman, 2006; Fanney & Klein, 1988; Michaelides & Wilson, 1997; Mills & Morrison, 2003; Furbo et al., 2005; Bernardo et al., 2011). Four different system configurations were simulated in TRNSYS software and compared on the basis of the annual solar fraction. These are described in detail in Article IV. A standard solar domestic hot water system was also analysed. This investigation provided information necessary for further investigation of such systems in practice and for validating the theoretical models.

6.2 Previous retrofitting solutions

Cruickshank and Harrison (2004 and 2006) investigated thermosyphon systems in the cold climate of Canada. In 2011, the same authors studied the performance of series- and parallel-connected thermosyphon storages (Cruickshank & Harrison, 2011). Thermosyphon systems became popular in several parts of the world such as eastern Asia and Australia, mainly due to their simplicity and reliability (Qin, 1998). The thermosyphon driving force depends on the pressure difference and frictional losses between the heat exchanger side arm and the tank. Consequently, the generated flow will be a complex function of the state of charge of the tank, the temperature profile along the heat exchanger and pipes, the height difference between the top of the heat exchanger and the top of the tank, and the pressure drop in the heat exchanger, piping and connections (Cruickshank & Harrison, 2006; Fraser & Brunger, 1995; Morrison & Tran, 1984; Ogueke et al., 2009). Such dependence on the heat exchanger pressure drop and tank characteristics limits how the retrofit is carried out, where the heat exchanger is placed and which storage tanks can be used (Ogueke

et al., 2009). Consequently, a new, well performing solar hot water tank is normally required to be connected to the existing hot water boiler.

Previous retrofitting solutions commonly consisted of a new solar storage connected upstream to the existing hot water heater (Sophie, 2007). Conergy, Thermo Dynamics and Enerworks are examples of company brands of such commercial products (Conergy Australia, 2009; Thermo Dynamics Ltd, 2009; Enerworks, 2009). Since both a new solar heating storage and a control/pump group are added, more space is needed, and the cost reductions are limited.

A commercial Swedish company developed a product that makes it possible to directly connect solar collectors to existing hot water boilers via an external heat exchanger and two pumps (Värmebaronen, 2009). Since the existing hot water storage features a heating unit at its base, the working temperature of the collectors is relatively high throughout the year, which limits the solar energy output. A related product also connects solar collectors directly to existing hot water storages, but without using anti-freeze fluid and therefore without the need of a new heat exchanger (Paradigma, 2012). One of the disadvantages is that the system needs to circulate warm water for preventing the collectors from freezing. "Solaplug" is another simple retrofitting product consisting of a coil solar heat exchanger around an auxiliary electric heater (Mondol & Smyth, 2012). This unit replaces the existing electric heater at the bottom of the hot water boiler. Consequetly, less material and installation is needed but stratification is, in principle, nonexistent because the auxiliary heater is placed at the bottom. A Swedish study of a retrofitting solution achieved relatively high annual solar fractions since stratification was established in the existing storage (Krohn & Karlsson, 2003). The retrofitting was carried out by an external heat exchanger and heating unit placed in a side arm of the existing storage. In such a system, the charging process was carried out with a thermosyphon in the tank loop. The main advantages of this system were the relatively high annual performance, the low volume of the add-on retrofitting solution and a low investment cost. However, the available hot water volume was reduced, so the hot water load may not be entirely provided, especially during the winter. Also, for outlet collector temperatures below 60°C, the temperature on the top of the tank is reduced, causing the auxiliary heater to start. Another disadvantage is that the system cannot be charged during discharges, since the heating unit was not placed inside the storage. Furthermore, the risk of clogging the system with limestone may be high, since the heater was placed inside the side arm. Since the heater is not placed directly inside the storage, the risk of legionella growth may increase. Kjellsson (2002) briefely analysed different retrofitted systems in a cold climate, but the investigation did not go further in estimating their annual performances.

6.3 System configurations

When a standard hot water boiler is retrofitted for solar thermal use, the only two available connections, that were previously used only for hot water discharge to the user should now also be used for charging the storage with solar hot water. In this theoretical analysis, since an adequate technical solution for this challenge was not yet achieved, it was assumed that charge and discharge could occur simultaneously and independently, as if four connections were available. Even if this was a simplification of reality, it was considered valid for a comparison of different retrofitting configurations in relative terms. Following this analysis, the retrofitting system was built in practice and a technical solution was tested using the two available connections to enable simultaneuous charge and discharge processes. This solution is described in detail in Article V. The estimated difference in annual performance between these simplified simulation models and the models validated to the tested system are described in Chapter 7.4, "Theoretical simulation models versus the tested system".

Four different retrofitted system configurations were simulated using TRNSYS software. A conventional solar domestic hot water system was also simulated. Each system model comprised a solar collector array, storage tank/s, auxiliary heater, heat exchanger between the collector and the tank loops, circulation pump/s, and a radiation processor. The annual domestic hot water load was 3105 kWh/year, the optimized mass flow was 0.7 kg/min/m^2 collector area, the overall heat transfer coefficient of the heat exchanger was 300 W/K, and the collector area was set to 6 m^2 flat plate collectors. Two types of pump control were tested; Control (a) varied the mass flow up to 5 kg/min so that the collector outlet temperature was kept constant at 65 °C. Control (b) consisted of constant flow speed which was set to a value that maximised the annual solar fraction. Further details regarding the system components may be found in Article IV. The different configurations of all the analysed systems are shown in Figure 6.1-6.5.

The sketch of the first system (Figure 6.1) represents a model of a standard solar thermal system. The tank has an internal heat exchanger and auxiliary heater. The storage volume was set to 255 litres to match the volume of the retrofitted system with the best performance (retrofitted system 3, Figure 6.4).

Retrofitted system 1 (Figure 6.2) consists of new solar collectors fitted to an existing hot water storage in a straightforward way. An external heat exchanger connects the collectors and the tank. In this system the whole tank is constantly heated up to 60°C by the auxiliary heater placed at the bottom which makes it difficult to achieve a significant stratification level.

This means that, for this system, aiming at a constant outlet temperature of 65°C according to Control a) does not make sense.

In retrofitted system 2 (Figure 6.3), a new 3 kW auxiliary heater was added to the side arm heat exchanger, while the existing one at the bottom of the tank was turned off. The aim was to achieve stratification in the storage. The heating element of the retrofitted storage is typically the limiting component for its lifetime (Kjellsson, 2002). Since the heater is turned off in this configuration, the lifetime of the existing hot water storage may be prolonged when retrofitted. The heater and the pump on the tank loop are turned on when T_{solar} fell below T_{set} minus the dead band. Consequently, the cold water in the tank bottom flows through the heat exchanger and is heated up in the side arm heater before entering the top of the tank. The heater and the pump are turned off when T_{solar} is higher than T_{set} plus the dead band.

Retrofitted system 3 consists of a 55-litre auxiliary heater storage connected in series to the existing heater (Figure 6.4). This means that the retrofitted storage tank was exclusively used for solar hot water which was not stored together with hot water provided by the auxiliary heater. The goal of this configuration was to increase the temperature stratification in the system. When hot water was drawn off by the user, the water at the top of the retrofitted storage flowed to the bottom of the auxiliary storage and from there to the user. When the temperature in the auxiliary storage become higher than T_{set}, due to the incoming solar hot water, the auxiliary heater was turned off automatically by its thermostat.

Retrofitted system 4 (Figure 6.5) consists of adding one mixing valve to the previous system, retrofitted system 3. The cold source inlet was the retrofitted storage while the hot source inlet was the auxiliary storage. The goal was to use as much water as possible from the retrofitted tank during discharges so its temperature was lowered and the collector performance increased. In order to minimise the risk of legionella growth, the outlet temperature of the valve was set to 60°C. If both inlet temperatures were higher than 60°C, the water was taken from the retrofitted tank only and later cooled down to 50°C by the last mixing valve before going to the load. Together, the two mixing valves behave like a 4-way valve with three inlets, two from hot sources and one from a cold source. For this system, not only Controls (a) and (b) for the flow of the pump were analysed but also an extra control, Control (c). The latter functions by turning off the auxiliary heater whenever the solar storage could provide a volume of hot water equal to that of the auxiliary heater, at 60°C or higher. When the temperature of that volume in the retrofitted storage dropped below 60°C, the water in the auxiliary volume was heated up again in order to provide the necessary hot water to the load.

The extended annual solar fraction, SF_{ext}, was calculated according to Equation 6.1 (Heimrath & Haller, 2007; Weiss, 2007).

$$SF_{ext} = 1 - \frac{Q_{aux}+Q_{pump1}+Q_{pump2}}{Q_{aux,ref}} = 1 - \frac{Q_{total}}{Q_{aux,ref}} \quad (-) \qquad \text{Equation 6.1}$$

$Q_{aux,ref}$ is the annual auxiliary energy needed when no collectors are used. It can either be calculated for every different system or remain constant for a reference system. The reference system corresponds to the existing hot water boiler without solar collectors with an annual load of 3150 kWh/year for the presumed domestic hot water load described in Article IV. This corresponds to $Q_{aux,ref}$ for retrofitted system 1. On the other hand, when $Q_{aux,ref}$ is calculated separately for different systems, the solar fraction varies with everything else being constant, which leads to different results. This becomes more obvious for this particular investigation where the auxiliary volumes changed significantly and so $Q_{aux,ref}$ changed as well. The simulation results are presented in both forms in Table 6.1, with solar fraction values given for both approaches. Alternatively, the systems can be compared on the basis of their annual energy use, Q_{aux}.

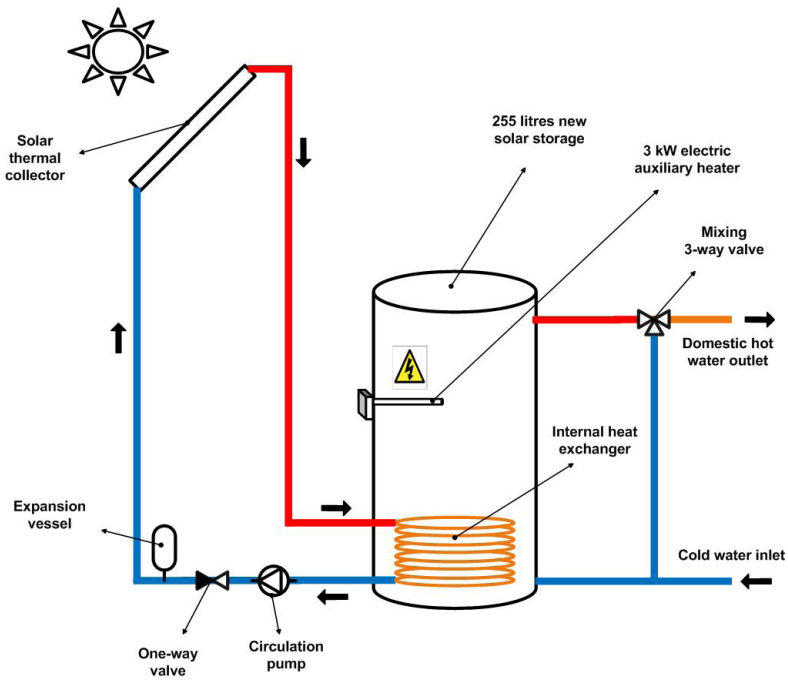

Figure 6.1 *Sketch of a standard solar domestic hot water system.*

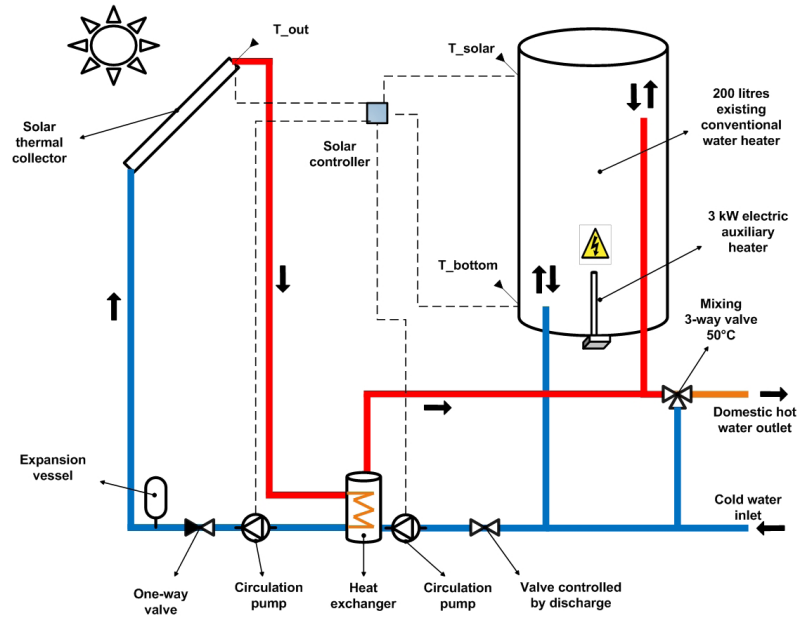

Figure 6.2 *Retrofitted system 1 - straightforward retrofitting of existing hot water heaters for domestic hot water production.*

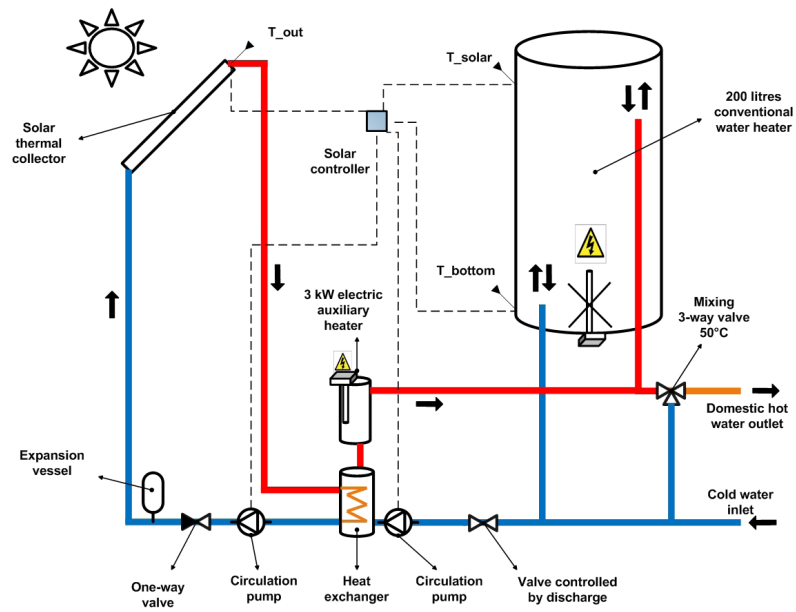

Figure 6.3 *Retrofitted system 2 - retrofitted system with auxiliary heater on the side arm for domestic hot water production.*

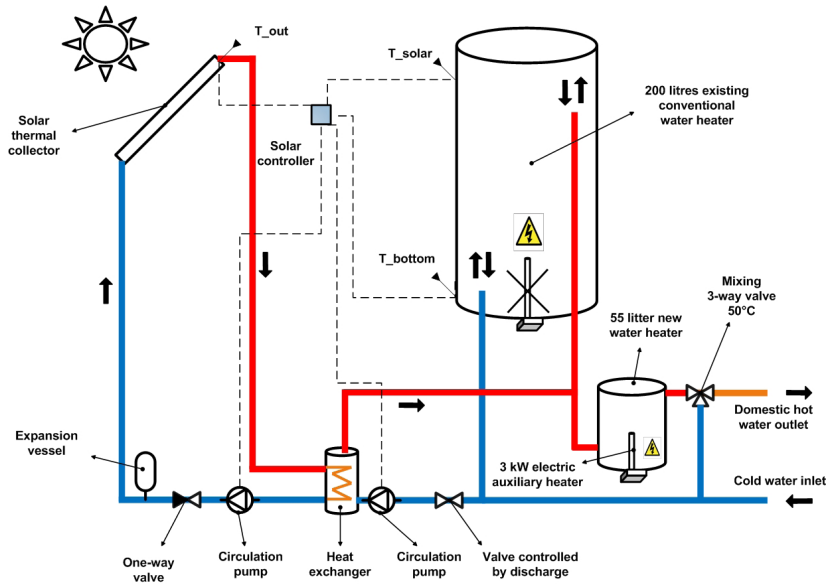

Figure 6.4 *Retrofitted system 3 - retrofitted system with an additional tank heater connected in series for domestic hot water production.*

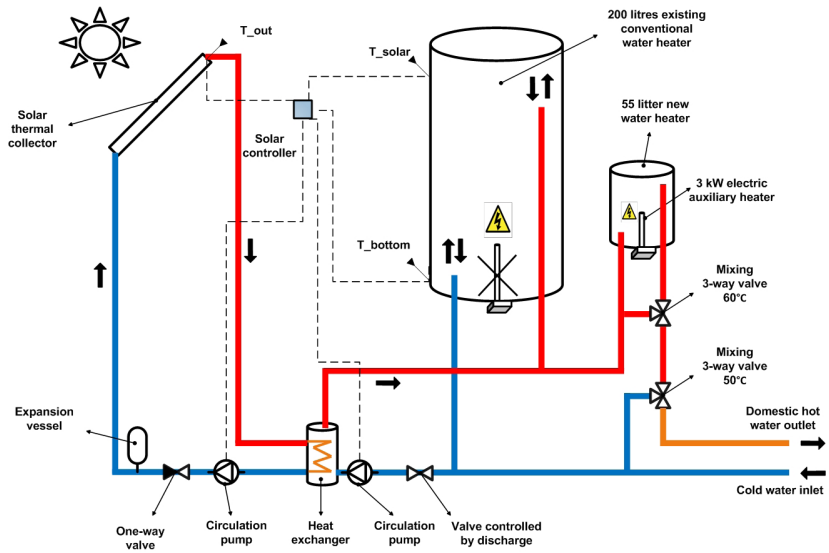

Figure 6.5 *Retrofitted system 4 - retrofitted system with an additional tank heater connected in parallel for domestic hot water production.*

6.4 Simulation results and discussion

A summary of the annual solar fraction calculations and heat losses in the storages for all systems is presented in Table 6.1. SF_{ext} corresponds to the annual solar fraction by using different values of $Q_{aux,ref}$ for each systems. In contrast, $SF_{ext,ref}$ uses a constant value for $Q_{aux,ref}$ which corresponds to the existing hot water storage without solar collectors with an annual load of 3150 kWh/year.

Table 6.1 Annual solar fraction calculations for the different retrofitting configurations.

System name	$Q_{aux,ref}$ (kWh/y)	Q_{aux} (kWh/y)	Q_{pumps} (kWh/y)	$Q_{losses\text{-}retrofit/stnd}$ (kWh/y)	$Q_{losses\text{-}aux}$ (kWh/y)	SF_{ext} (%)	$SF_{ext,ref}$ (%)
Standard system (a)	2397	1238	92	648	(-)	45	57
Standard system (b)	2397	1090	60	779	(-)	52	63
Retrofitted system 1 (b)	3105	2134	75	973	(-)	29	29
Retrofitted system 2 (a)	3507	2002	286	886	(-)	35	26
Retrofitted system 2 (b)	3507	1945	243	904	(-)	38	30
Retrofitted system 3 (a)	2037	1074	187	369	145	38	59
Retrofitted system 3 (b)	2037	877	131	447	148	51	68
Retrofitted system 4 (a)	2042	1108	181	392	135	37	58
Retrofitted system 4 (b)	2042	930	129	461	135	48	66
Retrofitted system 4 (c)	2042	914	129	461	123	49	66

The estimated annual solar fraction achieved by the standard solar domestic hot water system was 63%. This result is in accordance with previous studies of the same kind of standard SWH systems with comparable collector areas, storage type, storage volume, mean domestic hot water load and weather conditions (Helgesson, 2002; Hobbi & Siddiqui, 2009; Swedish Technical Research Centre, 2012).

For retrofitted system 1, the estimated value for the solar fraction was 29%. The main reason for such a low performance is the position of the auxiliary heater at the bottom of the tank which prevents stratification in

the storage. Also, incoming cold water at the bottom continuously demands auxiliary energy every time a draw-off takes place. Furthermore, the heat losses of the storage are high.

For retrofitted system 2, simulation results show that the annual solar fraction was 26% for Control (a) and 30% for Control (b). Heat diffusion and wall conduction in the storage limits the stratification level. Furthermore, the consumption of the pumps was significantly increased, to 243 kWh/year, which is 3.5 times higher than that of the previous system. This is because an additional pump was needed that works continuously every time auxiliary heat was required. Running the pump on the collector circuit with Control (a) was shown to decrease the collector working hours and efficiency. Control (b) was therefore shown to be more advantageous. The auxiliary volume corresponds to the volume above the temperature sensor in the upper part of the tank, which was set to 80 litres to match the corresponding auxiliary volume of the standard system. This volume satisfies regular loads while larger loads can be met by temporarily increasing the auxiliary heater temperature to 90°C or by turning on the existing auxiliary heater in the bottom of the storage.

The estimated annual solar fraction for retrofitted system 3 was 59% for Control (a) and 68% for Control (b). Since the auxiliary heater was placed in another tank, it was no longer turned on when the outlet temperature, of the collector was below 60°C. Also, the retrofitted tank worked at lower temperatures which increased the collector working hours and efficiency. This is especially relevant taking into account that the insulation levels of the existing water storage tank are unknown. Having the larger tank working at lower temperatures reduced the retrofitted storage heat losses by 50%, 447 kWh/yr (Table 6.1). Retrofitted installations oversized in the volume of the hot water storage with low levels of insulation can cause large system heat losses (Kjellsson, 2002). In addition, the new, well-insulated auxiliary storage provided the extra energy when solar energy was not available. Since this storage is configured to heat water at 60°C or higher, a high level of insulation can significantly reduce the heat losses. Furthermore, mixing caused by diffusion and wall conduction was reduced, since the auxiliary hot water at 60°C was not stored in the same tank as the cold water from the main. The system "stratification" was then partially achieved by means of two tanks with low stratification levels but working at different average temperatures.

During the summer period, when solar hot water over 60°C was available, the total solar hot water storage volume of the series-connected system was increased to 255 litres, since both tanks were connected in series and no auxiliary energy was needed. Figure 6.6 shows such a typical operation day in July where the collectors were charging the system at the same time as the user was discharging the storage. As shown in the figure, both the

retrofitted and auxiliary storages were charged during a sunny morning until the middle of a cloudy afternoon. From that point on, the pumps were stopped while the discharge process continued. At the beginning of the charging process, stratification can be seen to decrease, since water at lower temperature was placed at the top of the retrofitted storage. This is because the inlet position is placed at the top while the controller compares the bottom temperature with the collector outlet temperature in order to start the pumps. This controlling process may be improved. After the solar pump was stopped, the discharge of the retrofitted storage continued cooling down the bottom of the tank. For the described system and load, simulations show that it was necessary to use the thermal disinfection measure against Legionella 18 times during a year and that the annual solar fraction was decreased less than 3%. Since the profile of the domestic hot water load consumption was averaged to seven different draw-offs during the day, there were no short-term high consumption levels and the temperature of the domestic hot water load was always met.

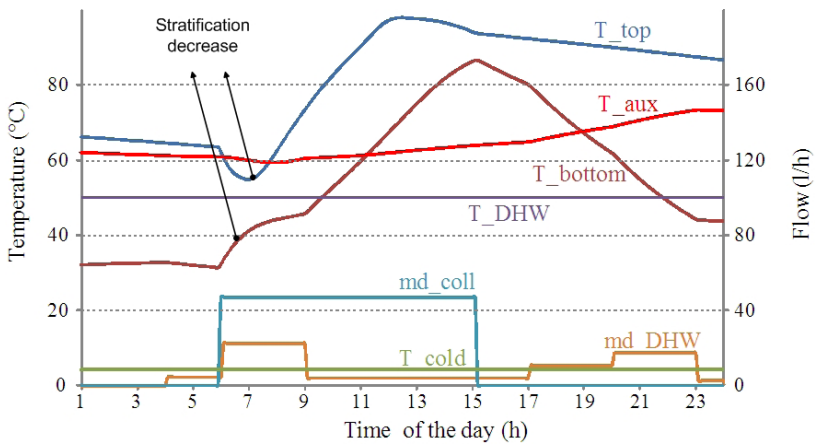

Figure 6.6 *Typical operation day of retrofitted system 3 during the summer period.*

The estimated annual solar fraction of retrofitted system 4 was 58% for Control (a), 66% for Control (b) and 66% for Control (c). Control (c) increased the annual solar fraction by less than 1%. When the auxiliary heater was turned off, the temperature dropped, due to heat losses. When it was turned back on, it reheated the water to 60°C to compensate for the heat losses during that period. The difference between turning off the heater during certain periods and compensating for the heat losses

continuously by maintaining its temperature constant at 60°C was shown not to be significant.

The achieved performance of retrofitted system 4 was lower than that of retrofitted system 3 because, during intervals where $T_{solar} > T_{set}$, the total solar hot water storage volume is not increased, since water does not go through the auxiliary heater storage. If the additional mixing valve was replaced by an electronic rotating valve that allowed water to pass through the auxiliary heater storage during such periods, the total increase in solar fraction would depend on the T_{set}. For T_{set} = 60°C, retrofitted system 4 works as retrofitted system 3 and; the solar fraction increase would be 2% and would decrease proportionally with the increase in T_{set}. It was then assumed that such a relatively low performance increase would hardly compensate for the extra costs of this electronic rotating valve. In order to minimise the risk of legionella growth, the outlet temperature of the mixing valve placed upstream was set to 60°C. If T_{solar} <60°C and T_{set} = 60°C, hot water is only taken from the auxiliary storage and since the lowest value for T_{set} is 60 °C, the risk for legionella is reduced. However, if T_{set}>60°C, water at a temperature below 60°C from the retrofitted storage can be provided to the user. In order to prevent an increase of bacterial growth, the periodical thermal disinfection program should be in place.

This investigation is most valuable for making a relative comparison between systems. How well the absolute values of the annual performances correspond with reality depends on the accuracy of several factors assumed for this study. Examples are the performance of the solar collector array, the U-values of the storages, stratification levels, the design and position of inlets and outlets, flow-induced mixing, domestic hot water load profile, and heat losses of pipes and heat exchanger. The relatively high values of annual solar fraction are due to the combination of a relatively high collector area and a low domestic hot water load.

The results showed that, when designed according to a load, the system that achieved the highest performance consisted of an additional auxiliary storage connected in series with the retrofitted tank. In such a system the existing hot water boiler was used to store the solar heat, while a smaller new auxiliary storage with an electric heater was added in series to ensure that the required outlet temperature could be met. Following this investigation, the retrofitted system was built according to the retrofitted system 3. This is described in the next chapter.

7 Retrofitted solar thermal systems – measurements and model validation

A prototype was built according to the previously described retrofitting configuration 3 which achieved the highest performance. The simulation models were simplified, since they assumed that the discharge and charge processes could occur simultaneously as if there were four available connections on the retrofitted storage. This was assumed because an adequate technical solution that used the only two connections on the existing hot water storage for both charge and discharge had not been developed at the time of the theoretical analysis. A technical solution that overcomes this challenge was then integrated in the tested system, and is described in this chapter. Several test procedures were carried out and the measurements were used to validate the adjusted simulation model of the tested system.

7.1 System construction in the laboratory

Two systems were monitored in the laboratory. These were a standard solar domestic hot water system and the developed retrofitted system according to the theoretical analysis but using a different collector array. The main goal of monitoring the standard system was to have a reference system that could be simultaneously compared with the developed system for the same solar contribution. The standard system model was not validated against measurements, since the typical performance of such a standard system is well described in literature (for example by Hobbi and Siddiqui, 2009).

7.1.1 Standard solar domestic hot water system

The main components of the system were the solar storage tank, the solar collectors and a control and operating kit. The system was designed for a typical Swedish single-family house with three to four inhabitants. The system components are described below. A sketch of the entire system including the monitoring equipment, is presented in Figure 7.3.

- CPC-thermal solar collectors (described in Article II) – In total, 9.2 m^2 of CPC-thermal load adapted collectors were installed (Figure 7.1). The collector array was tilted 50° for optimum performance over the year (Figure 10 in Article II).
- Solar storage tank – 300-litre tank featuring an internal coil heat exchanger and an electric auxiliary heater of 3 kW power (Figure 7.2).
- Control and operating kit – this unit was fitted into the collector circuit and included a circulation pump, expansion vessel, one-way valve, pressure release valve, barometer, and controller. There were three temperature sensors connected to the controller. Two of them were placed inside the tank through small immersion pipes. The other sensor was placed on the collector outlet, in direct contact with the absorber surface. The power of the pump can be regulated from 43 W to 82 W. The volume of the expansion vessel was 8 litres, with a preset pressure of 2.5 bar. The controller started the pump when the difference between the outlet collector temperature and the bottom tank temperature was greater than 4°C. The pump stopped whenever that temperature difference was less than 2°C or the top temperature of the tank reached 95°C. Propylene glycol mixed with water (40%) was used as a heating media to protect the fluid from freezing in the winter.

Figure 7.1 *9.2 m^2 of the CPC-thermal collectors at 50° tilt.*

Figure 7.2 *Storage and control unit under installation.*

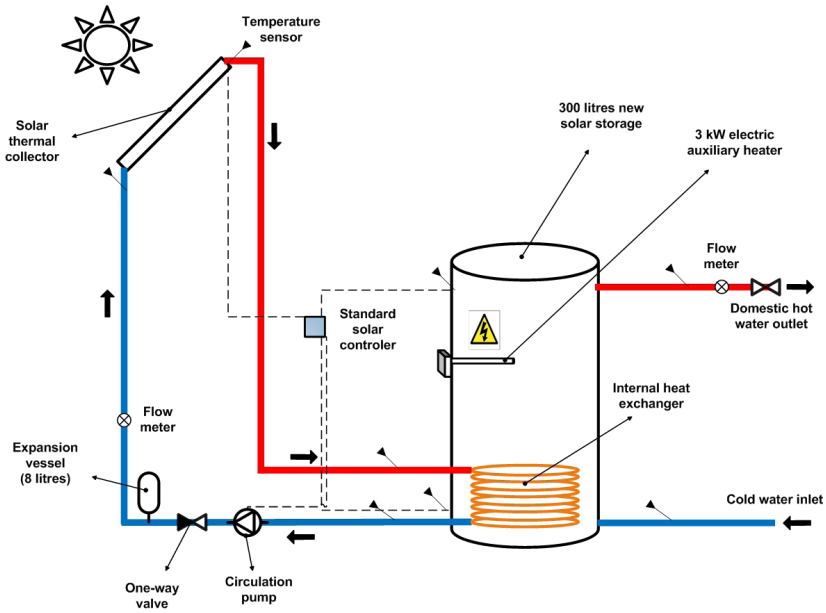

Figure 7.3 *Sketch of the standard domestic hot water system and the monitoring equipment.*

7.1.2 Retrofitted system

The retrofitted system was built in a flexible way to allow replacement of components and changes in their position (Figure 7.4). The main components of the retrofitted system are described below.

- Solar collectors – An identical collector array was used as in the previous system. These consisted of 9.2 m^2 of CPC-thermal load adapted collectors at a 50° tilt.
- Solar storage tank – According to the retrofitted system 3 (Figure 6 in Article IV), a combination of storages were implemented (Figure 7.4). A 200-litre retrofitted storage, shown on the right in Figure 7.5, was used since this is regarded as the most common tank volume in Swedish single-family electricity-heated houses (Kjellsson, 2002). A 55-litre storage with an auxiliary heater of 3 kW was used as auxiliary storage (Figure 7.5, left). The auxiliary heater of the new auxiliary storage was controlled by an internal thermostat placed at its bottom.
- Control and operating kit – This system used the same control unit as the standard solar system. The temperature sensors of the controller were placed on the surface of the retrofitted tank under the insulation

(Figure 7.5 to the right). The temperature sensor on the collector outlet was placed in direct contact with the absorber surface. The operating kit was identical to the one used in the previous systems and made of standard components.

- External heat exchanger – Since the collector loop used propylene glycol-water mixture (40%), a heat exchanger was needed. An external compact brazed-plates heat exchanger was used to ensure space savings and high performance for the heat transfer. Its total capacity was above what was needed. The intention was to make sure that the heat exchanger was not a limitation to the system performance (Liu and Davidson, 1995; Furbo, 1993; Furbo, 1994). An optimisation of the capacity of the heat exchanger is presented in the next chapter.

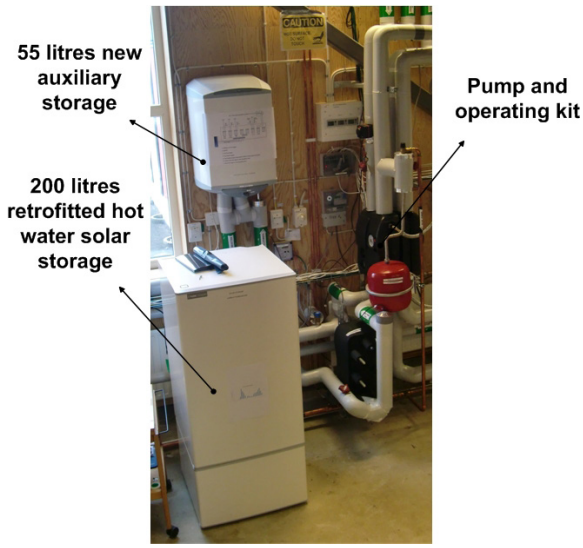

Figure 7.4 *Picture of the first prototype of the retrofitted system, which was tested in the laboratory.*

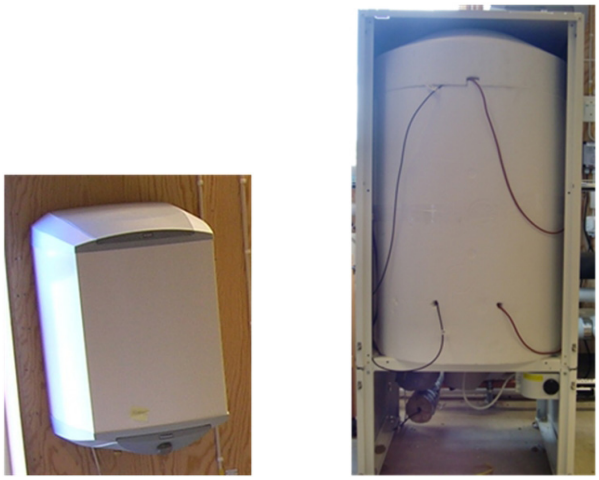

Figure 7.5 *New, added 55-litre auxiliary storage (left) and the retrofitted 200-litre tank (right). The cables to the right are used for controlling the pumps and monitoring the surface temperature of the retrofitted storage.*

Common to all systems was the way they dealt with stagnation periods. The concept of partial evaporation protection proposed by IEA task 26 was used to protect the systems (Hausner and Fink, 2002). According to this principle, the overpressure created by the collector array during stagnation forces the liquid to go inside the expansion vessel.

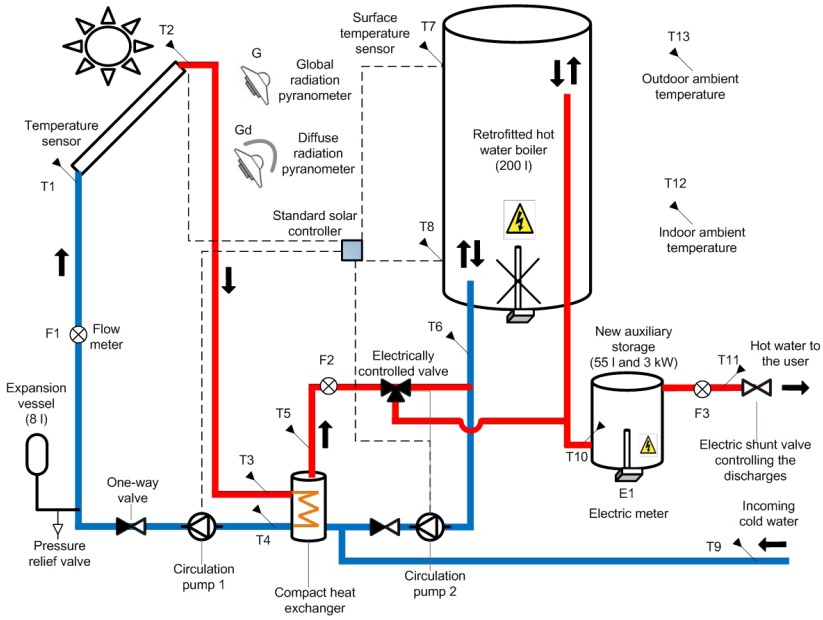

Figure 7.6 *Physical illustration of the retrofitted system as tested in the laboratory.*

An illustration of the tested retrofitted system and its measuring equipment is shown in Figure 7.6. The temperature sensors T1 and T2, together with the flow meter F1, measured the energy delivered by the collector array. T3 and T4, together with F1, measured the energy delivered to the tank circuit by the heat exchanger. T5 and T6, together with F2, measured the energy that was delivered from the heat exchanger to the tank. T7 measured the surface temperature in the upper part of the retrofitted storage and was used to stop the pump in case of overheating. T8 measured the surface temperature in the lower part of the retrofitted storage. This temperature was compared with the temperature of the outlet of the collectors in order to start or stop the pumps. T9 measured the cold water temperature. T10, together with T9 and F3, measured the energy delivered by the part of the system supported by solar thermal energy, without auxiliary heat. T11, together with T9 and F3, measured the energy delivered by the whole system. T12 measured the indoor ambient temperature while T13 measured the outside air temperature.

The electricity meter E1 measured the auxiliary energy used by the heater. The electricity used by the pumps was calculated by integrating its nominal power (43 W) during periods when a flow was measured. For the pump on the tank loop this was done by integrating its power during

periods when a flow was measured by F2 but not by F3, so that time periods corresponding to hot water discharges were excluded. The energy use of the pumps was taken into account when calculating the annual solar fraction (Equation 2 in Article IV and Equation 1 in Article V).

In order to allow solar charge during discharges an electrically controlled valve was included between heat exchanger and storage (Figure 7.6). During the charge process both pumps were powered. When a discharge took place, the controller stopped the pump on the tank loop and the incoming cold water flowed through the heat exchanger before going into the bottom of the retrofitted storage.

7.2 Measurements

Measurements were carried out continuously over nearly one year. During most of that period the system was working under "normal" conditions, i.e. as expected to operate in a typical single-family house in Sweden. In order to test the performance of the system at more extreme conditions, several test sequences were carried out. The purpose was to increase the accuracy of the parameter identification. This also introduced larger variations in the testing conditions so that the validated model would predict the performance of the system for a wider range of working conditions. The following test sequences were performed simultaneously on both the retrofitted and the standard solar domestic hot water systems. Each test sequence was repeated several times at different flow rates and temperatures. The test sequences are summarised in Table 7.1. In order to investigate the temperature profile of the water inside the storages, discharging was required after each test sequence in order to read the temperature profiles over time. This was necessary since it was not possible to introduce immersed temperature sensors inside the retrofitted storage.

Table 7.1 Summary of the performed test sequences.

Test sequence number	Main parameter investigated during the test sequence
1	Heat losses of the solar storage and retrofitted storage
2	Stratification during discharge
3	Stratification during charge
4	Decrease of the inlet temperature of the collectors when discharges occur during solar charge
5	Heat losses of the new auxiliary storage

7.2.1 Test sequence 1

In this test sequence, the retrofitted hot water storage (Figure 7.5, right) and the solar tank (Figure 7.2, left) were charged with hot water from the solar collectors in such a way that the temperature of the water inside the storages was uniform. A period without any discharge or charge followed, two to four days, depending on the test. After that period the tank was fully discharged. The main goal with this test sequence was to investigate the heat losses.

7.2.2 Test sequence 2

In this sequence, the same procedure was applied but the storages were discharged immediately after the charging, without any standby period. The main goal was to investigate stratification during discharge. Such information helped to define the number of nodes of the model of the retrofitted storage. The biggest uncertainty relates to the flow rate which influences mixing and therefore stratification.

7.2.3 Test sequence 3

In test sequence 3, the tops of the storages were partially charged with solar hot water at a temperature as stable as possible. This procedure was followed by a discharge of the tank. The main goal was to investigate the ability of the storages to build stratification during charge for different flow rates. This test also provided information about the distance between the top of the long pipe inside the retrofitted storage and the top of the tank.

7.2.4 Test sequence 4

During this test sequence, short discharge periods were actuated during solar charging for a day with high levels of solar radiation. Ideally, once a discharge occurs during solar charge, the inlet temperature to the solar collectors should be as close as possible to the temperature of the incoming cold water within a short time period. Later in this chapter, measurements are compared to simulation results of the model of the retrofitted system in Figure 7.11. The inlet temperature to the heat exchanger from the collectors varied between 40°C and 60°C with the solar radiation conditions.

7.2.5 Test sequence 5

During this test sequence, the new auxiliary storage of the developed retrofitted system was monitored during standby for different periods between four and 12 days. During these periods, no charges or discharges were performed and the temperature of the thermostat was set between 60°C and 80°C, depending on the test. The auxiliary energy required to maintain that temperature during the period was monitored. The indoor temperature was also monitored. The main goal with this test was to investigate the heat losses from that storage.

7.3 Model validation

The retrofitted system, illustrated in Figure 7.6, was modelled according to Figure 7.7. The validation followed the five steps described below. The results of the parameter identification are presented in Table 7.3 and shown in Figure 7.7.

Validation step 1 comprised selecting the target parameters that were to be identified. The target parameters are shown in Table 7.3 and represent the parameters that could be identified by the measured data and this method. An energy balance of the model according to Figure 7.7 was carried out in validation step 2. The parameters were identified in validation step 3 (Table 7.3). This was done by fitting simulation results to measurements from July to December by adjusting the target parameters. In order to do so, the absolute difference between the simulated and measured auxiliary energies was minimised using a TRNSYS application named GenOpt (Wetter, 2009). GenOpt used algorithms that iterated the target function by changing the target parameters until a minimum was found. In validation step 4, and once a set of parameters were identified, simulations and measurement results were compared for a different time period, the validation period between February and June. This was intended to test the ability of the model to describe other conditions than those used for the validation initially. Finally, in validation step 5, the identified parameters were adjusted by comparing the simulation results with measured temperature profiles during the different test sequences. For further details regarding the model validation, refer to Article V.

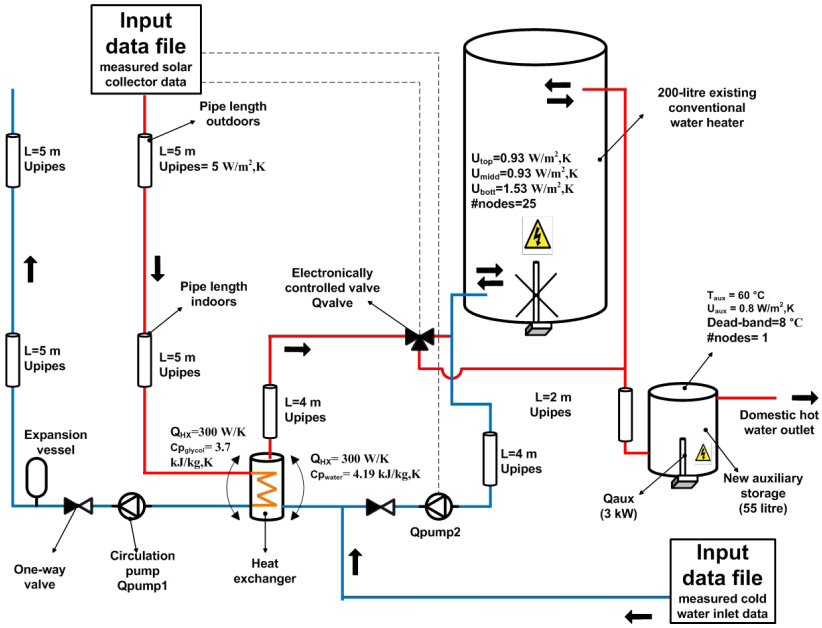

Figure 7.7 *Illustration of the validated model along with the identified parameters.*

Table 7.3 Results of the parameter identification.

Parameters	Identified	Notes
U_{pipes} (W/m^{2}K)	5	Includes heat losses from pipes and from singularities. Identified by TRNSYS-GenOpt during the period July-December.
UA_{HX} (W/K)	300	Product information. The model does not include heat losses. These were accounted for by pipe losses.
U_{top}	0.93	The heat loss coefficient of the retrofitted storage was divided in three, where the proportions between them were estimated theoretically. Parameter identified by test sequence 1.
U_{midd}	0.93	
U_{bottom} (W/m^{2}K)	1.53	
$\#nodes_{ret}$	25	Estimated based on the temperature profile from test sequence 2.
T_{aux} (°C)	60	The parameters of the new auxiliary heater were identified by test sequence 5. The dead-band was estimated by TRNSYS-GenOpt during the period July-December.
U_{aux} (W/m^{2}K)	0.8	
$Dead_{brand}$ (°C)	8	
$\#nodes_{aux}$	1	It was assumed that there was no stratification in the new auxiliary storage since the thermostat and electric heater were placed at the bottom of the tank.

As shown in Figure 7.8, the correlation between the model and measurements on a monthly basis is good. In Figure 7.9 it can be seen that when analysed on a daily basis, the correlation between them is reduced. Table 7.4 shows that TRNSYS-GenOpt iterations, together with the test sequences, identified the model parameters in such a way that the total sum of the modelled, $Q_{aux,mod}$ and measured auxiliary energy, $Q_{aux,meas}$, was very close for the identification period July-December 2010. The accuracy of the model was reduced when the system was tested at more extreme conditions during the validation period. The same applies for the modelled and measured energy provided by the system, $Q_{DHW,mod}$ and $Q_{DHW,meas}$.

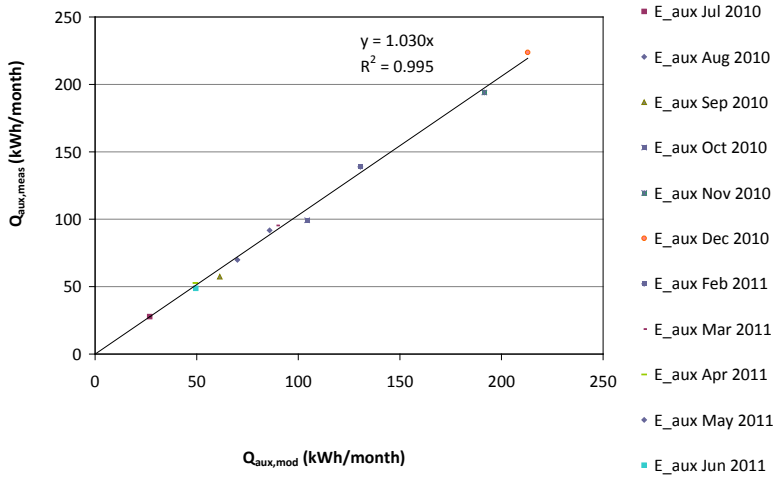

Figure 7.8 *Modelled vs. measured monthly auxiliary energy plotted for the whole period July 2010–June 2011.*

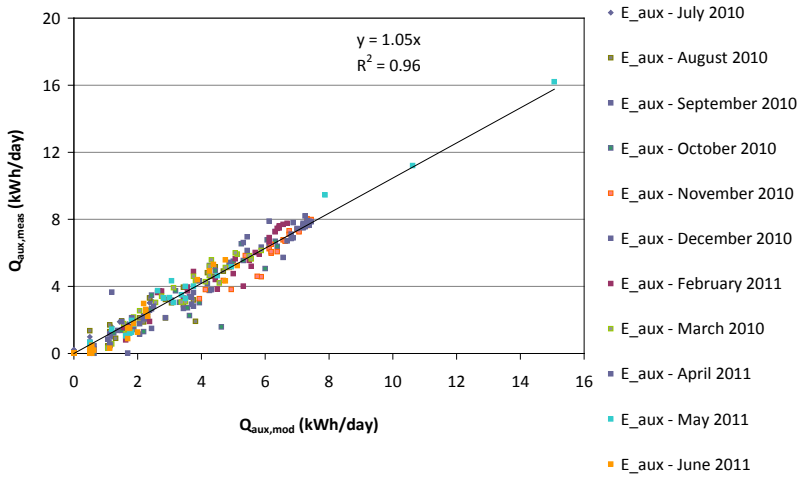

Figure 7.9 *Modelled vs. measured daily auxiliary energy plotted for the whole period July 2010–June 2011.*

Table 7.4 Sum of the modelled *vs.* measured auxiliary energy and energy provided by the whole system for the different analysed periods.

TOTAL sum (kWh)	$Q_{aux,mod}$ (kWh)	$Q_{aux,meas}$ (kWh)	$Q_{aux,error}$ (%)	$Q_{DHW,mod}$ (kWh)	$Q_{DHW,meas}$ (kWh)
Jul–Dec 2010 (identification period)	667	672 ± 7	0.7	1235	1236 ± 13
Feb–Jun 2011 (validation period)	405	427 ± 4	5.3	916	938 ± 15
Jul 2010–Jun 2011 (all data)	1072	1099 ± 11	2.5	2151	2174 ± 28

The accuracy of $Q_{aux,meas}$, was 1% of the measured value by the electricity meter. For estimating the accuracy of $Q_{DHW,meas}$ the values of T_{cold}, T_{hot} and the volume were needed. These varied during the year but in a limited temperature interval. The temperature T_{cold} varied significantly less than T_{hot} and its average value during the measuring period was 10°C, roughly. T_{hot} was commonly 60°C (temperature setting of the auxiliary heater) reaching 80°C in some periods during the summer. The accuracy shown in Table 7.4 was calculated on the assumption that T_{hot} was 60°C. If T_{hot} was assumed to be 80°C, the uncertainty would be ± 37 instead of ± 28 kWh. The tapped hot water volume was equal to 37 m^3 for the whole time period.

In the following figures, according to the validation step 5, temperature profiles of measurements are compared with those of the validated model for some of the test sequences previously mentioned in this chapter. The estimated values of the validated model are represented only by a line.

In Figure 7.10, measurements from test sequence 2 are shown together with estimations from the validated model. The slope of the temperature profile shown in the same figure suggests that the identified number of nodes that influence the stratification of the retrofitted hot water storage was adequate, for this discharge flow. The energy content was also roughly the same, however with a different temperature profile. The main reason behind this result was found to be the difference of the inlet and outlet pipe configurations between the model and reality (see Figure 7.6 and Figure 7.7). In reality, but not in the model, the extracted water from the top exchanges heat with the water at the bottom via the metalic outlet pipe that goes through the storage. This decreases stratification. During charge, water from the heat exchanger, at a higher temperature than the water inside the storage, gets colder along the way to the top of the tank. The same happens during discharge, where temperature of the water from the top of the tank is further reduced by exchanging heat with incoming cold water at the bottom of the tank before leaving the storage. Another factor reducing the accuracy of the model is that heat losses from singularities such as sensors, heat exchanger and valves were accounted for by "extra" heat losses from the pipes in the model.

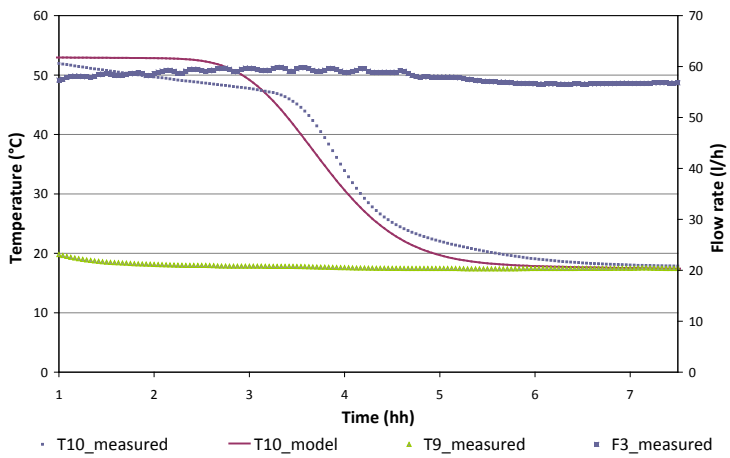

Figure 7.10 *Results from measurements and from the validated model of the retrofitted system during discharge of the retrofitted storage tank.*

In Figure 7.11, the outlet temperatures on both sides of the heat exchanger of the retrofitting system during test sequence 4 are shown. The retrofitted system, making use of the compact external heat exchanger, supplied to the inlet of the collectors, T4, a temperature close to that of the incoming discharge cold water, T9, within a short time period. The main reason for this is that the incoming cold water passed through the heat exchanger before entering the storage. Good correlations between the model and the measurements were achieved. The same response did not occur in the conventional storage tank where the incoming cold water was first mixed with the water in the bottom of the storage before cooling the coil heat exchanger, which then cools the collector loop. The response time for the temperature in the solar collector circuit was therefore longer than for the retrofitted system.

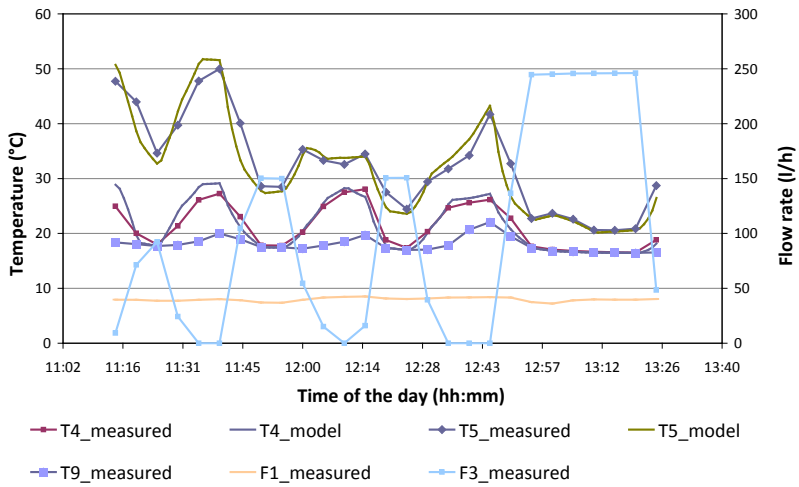

Figure 7.11 *Results from measurements and from the validated model of the external heat exchanger of the retrofitted storage tank during test sequence 4.*

Finally, measurements of the retrofitted system under normal operation conditions during part of a day with high radiation values in the summer are shown in Figure 7.12. The results from the validated model are also shown in the same figure. As predicted by the theoretical model in Figure 11 in Article IV, stratification is decreased at the beginning of the day when the solar charging starts. After that period, some stratification is achieved during charge. For lower flow rates the stratification achieved during solar charge is increased. This is not shown in Figure 7.12. The standard system

did not achieve stratification during charge since the internal coil heat exchanger is placed at the bottom.

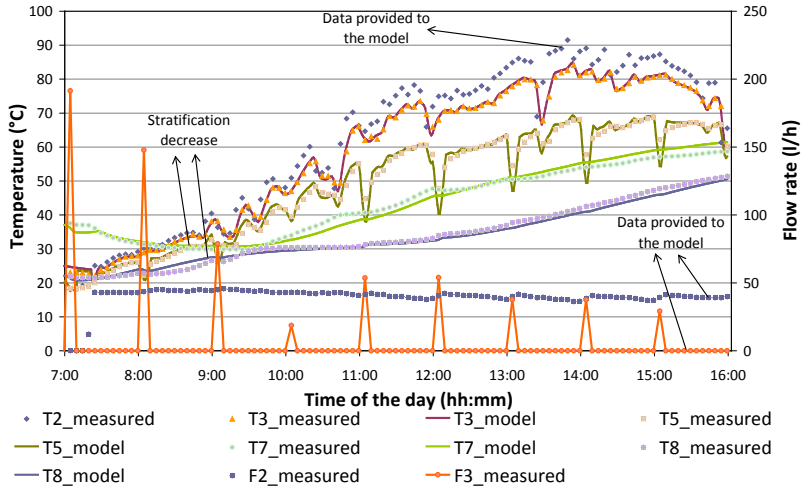

Figure 7.12 *Results of measurements and of the validated model of the retrofitted system during normal operation on a summer day. The measured values of T7 and T8 should be read as indicative figures since they are placed on the surface of the retrofitted storage.*

7.3 Theoretical simulation models *vs.* the model of the tested system

In order to comprehend how differences between the configuration of the retrofitted and the standard system influence their relative performances, a theoretical analysis was carried out. This consisted of introducing step-by-step changes in the configuration of a conventional domestic hot water system until the tested configuration of the retrofitting system was reached. It is then possible to analyse the relative performances between several system configurations including the simplified model assumed in the theoretical analysis in Article IV and the configuration of the tested system in Article V.

In order to simplify the analysis, several assumptions were made. The U-value and the total volume of the storage in each system were considered to be the same. Also, no heat losses from pipes were considered. The capacity of the heat exchangers was increased to a point where it no longer was significant to the annual performance of the system. The domestic

hot water load profile described in Figure 10 and Figure 11 of Article IV was used in both systems. For such a profile the estimated load was 3449 kWh/year. The presumed parameters used in the simulations are summarised in Table 7.5.

Table 7.5 Presumed parameters used in the simulations

Component	Retrofitted system	Standard system
U-value	1 W/m^2,K	1 W/m^2,K
Volume	350 litres (retrofitted) & 50 litres (auxiliary)	400 litres
Number of nodes	18 (retrofitted) & 2 (auxiliary)	20
Height	1.5 m (retrofitted) & 0.2 m (auxiliary)	1.7 m
Solar collector area	6 m^2 flat plate	6 m^2 flat plate
Solar collector parameters	Table 1 in Article III	Table 1 in Article III
Flow in the collector and tank circuit	102 l/h	102 l/h
Domestic hot water load profile	Figure 10 and 11 in Article V	Figure 10 and 11 in Article V
Heat exchange capacity	high	high

Five different configurations were analysed. These are shown in Figures 7.13-7.17. Configuration 1 consisted of a conventional solar domestic hot water system, as described in Article IV, assuming the parameters in Table 7.5. In configuration 2 the heat exchanger was removed but the connections to the storage were kept in the same nodes, one below the auxiliary heater and the other at the bottom. Configuration 3 consisted of adding a smaller auxiliary heater in series to an existing hot water storage with four connections. In configuration 4 the retrofitted hot water storage featured only two connections which were used in both directions for charge and discharge. When a discharge occurs, the pump in the storage circuit was stopped and a control valve was closed, forcing the incoming cold water to the bottom of the retrofitted storage. Consequently, no solar charge is possible during the time of a discharge in this configuration. Configuration 5 corresponds to the retrofitted system that was built and tested according to the previous Figure 7.7 and Article V. During discharges, the cold water went through the heat exchanger before flowing into the bottom of the retrofitted storage. This makes charge possible during discharge periods.

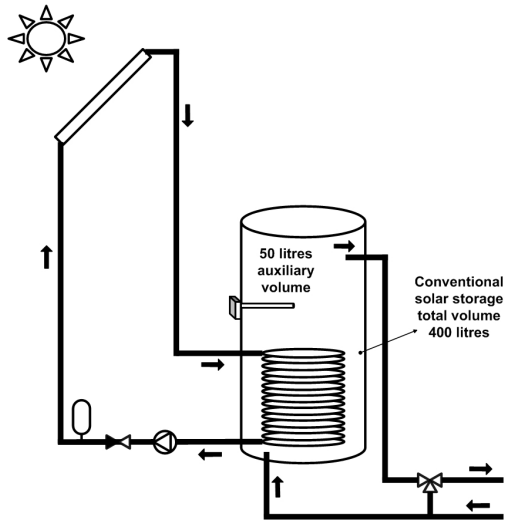

Figure 7.13 *Configuration 1: Standard solar thermal system.*

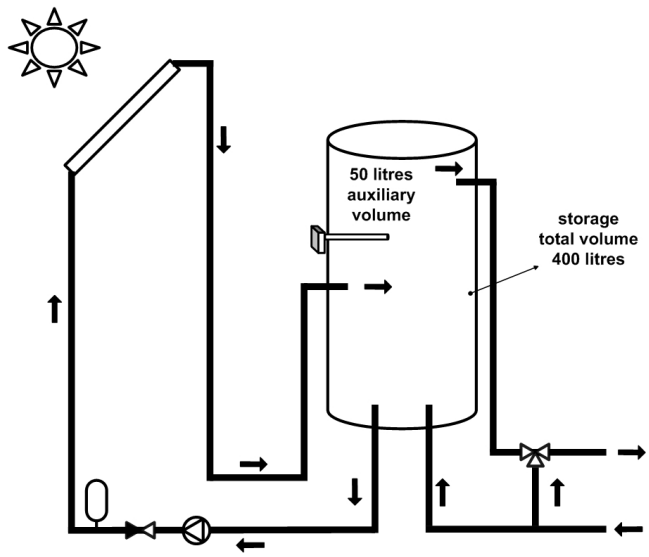

Figure 7.14 *Configuration 2: Standard solar thermal system without the coil heat exchanger.*

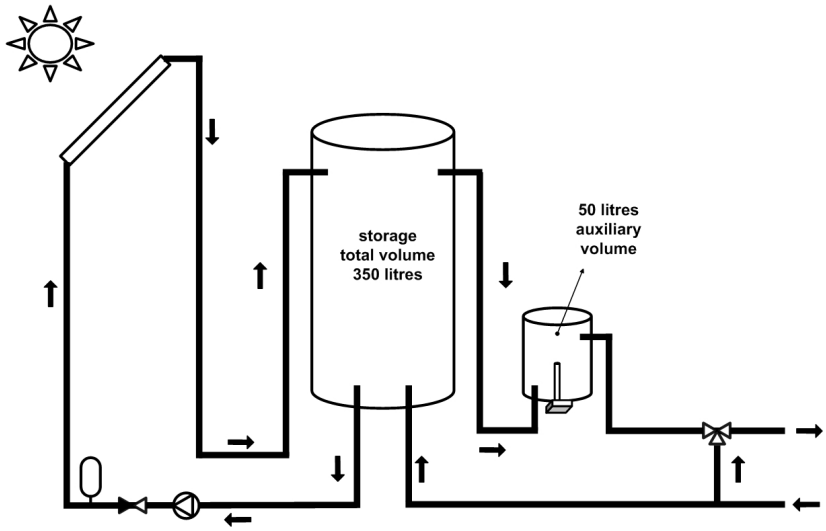

Figure 7.15 *Configuration 3: Retrofitted system where the existing storage features four connections.*

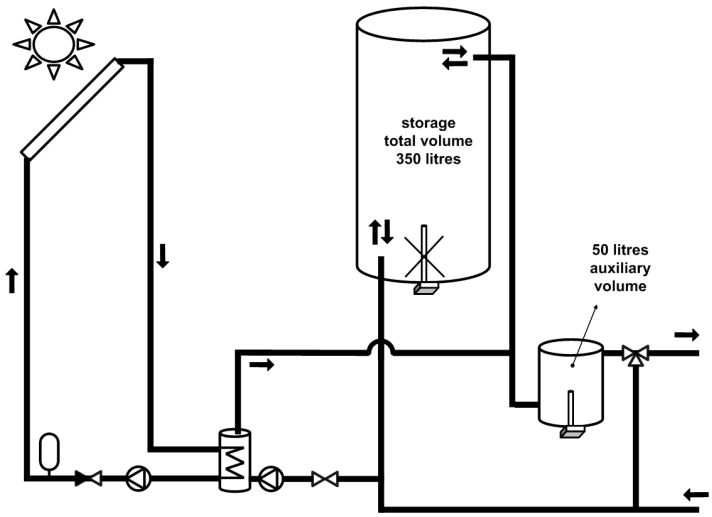

Figure 7.16 *Configuration 4: Retrofitted system where the existing storage features two connections. During discharge, the pump on the tank side is stopped and the control valve closed. Solar charge is therefore not possible during discharge periods.*

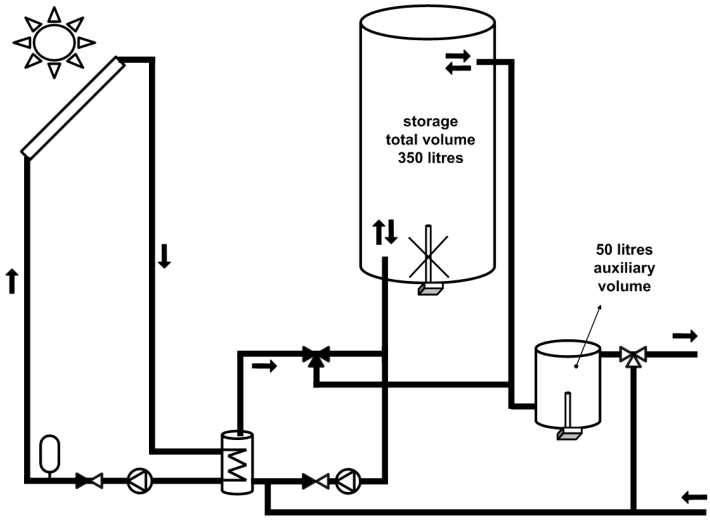

Figure 7.17 *Configuration 5: Configuration of the retrofitted solar domestic hot water system as built and tested in laboratory. During discharge the cold water always passes through the heat exchanger before going into the bottom of the retrofitted storage. Solar charge is possible during discharge periods.*

The results of the simulations are presented in Table 7.6. The annual solar fraction was calculated based on the previously described Equation 6.1. Simulation results showed that the standard system (configuration 1) achieved roughly the same performance as configuration 2. The significant performance increase achieved by configuration 3 is explained by the fact that the auxiliary heater was placed in an external storage. This reduces the heat exchange between preheated water by the collectors and the water heated by the auxiliary heater at a higher temperature. The annual solar fraction of the system with configuration 4 was significantly reduced since, in such configuration, no solar charge can occur during discharge periods. The annual solar fraction achieved by configuration 5 was close to that of configuration 3. Hence, it was concluded that the simplified configuration of the models used in the theoretical analysis described in Article IV were reasonable approximations of the retrofitted system built in the laboratory and described in Article V.

Table 7.6 Annual performance estimated by simulations models.

System	Qaux (kWh/y)	$SF_{ext,ref}$ (%)
Configuration 1	1329	62
Configuration 2	1358	61
Configuration 3	1115	68
Configuration 4	1228	63
Configuration 5	1135	66

7.4. Discussion

Temperature sensors used to control the solar charge of the retrofitted storage were placed on its surface. This part of the installation is critical for the good function of the system and may also be susceptible to errors. Alternatively, the temperature sensor that controls the charging process can be placed on the connector to the bottom of the retrofitted storage (same position as T6 in Figure 7.6). If so, the pump on the storage side should start periodically and for short time periods in order to monitor the temperature at the bottom of the retrofitted storage. To prevent boiling, another temperature sensor should be placed at the outlet of the heat exchanger on the cold side (same position as T5 in Figure 7.6). The pumps should stop when the temperature monitored by these two sensors is above a certain value during the charging process.

The objective of the validation of the model was to achieve reliable results for the estimation of the solar fraction on an annual basis while the agreement between model and measurements on a daily basis was less important. This was accomplished with the presented model. However, several limitations of the model were pointed out. Further improvements could have been carried out on the model to take into account the heat exchange between the water in the retrofitted hot water boiler storage and the pipe placed from top to bottom. However, this was considered to be unnecessary, taking into account the achieved accuracy on an annual basis. Other factors reducing the accuracy of the model are simplifications regarding the retrofitted hot water boiler and its inlets/outlets and the difficulty in estimating the dead-band of the auxiliary heater. Also, the heat losses of the heat exchanger, valves and temperature sensors were accounted for by the pipe heat losses.

8 Retrofitted solar thermal systems – system optimisation and sensitivity analysis

In this section, the methodology and results are presented for the retrofitted system optimisation with regard to energy performance, comfort level for the user, and volume of the new auxiliary storage. "Comfort" in this context relates to providing all the required hot water to the user. The analysis was focused on control strategies for auxiliary heating, reduction of heat losses, and minimum adequate volume of the new auxiliary storage. Economics was not taken into account in the optimisation. A sensitivity analysis was also performed for three different DHW load profiles, volumes of the retrofitted hot water storage between 40 litres and 400 litres, and for three different climates. The detailed analysis was described in Article V.

8.1 System optimisation

The annual solar fraction was the parameter used to compare the relative performances of several system configurations. The solar fraction definitions used in this study were not only the extended solar fraction, SF_{ext}, described by Equation 6.1, but also the solar fraction indicator, SF_i, described by Equations 8.1-8.3 (Heimrath & Haller, 2007; Weiss, 2007). The SF_{ext} takes into account not only the required energy from auxiliary heating but also the electricity use of the pumps. There is a risk that this target function in used to design a system where the desired DHW temperature is not met at all times. For larger discharges, the temperature of the water provided to the user may fall below the hot water temperature requirement during certain periods. Consequently, a penalty function for such periods was used (Heimrath & Haller, 2007; Weiss, 2007). The SF_i penalises the performance of the system when hot water provided is below the required temperature level. A highly penalising exponential function

with a factor of four was used, as previously in IEA task 26 and task 32. SF_i does not represent the real fraction of energy savings but can be used to provide an indication, in relative terms, of how well several systems meet the energy needs within comfort levels. IEA task 32 recommends verifying whether the penalty function did not exceed 5% of the total DHW load of the DHW reference system without collectors, *i.e.*, $f_{comf} \leq 0.05$, where $f_{comf} = max\left(Q_{penalty}/Q_{aux,ref}\,, 100\right)$. This comfort limit was included in the analysis.

$$SF_i = min\left(1 - \frac{Q_{aux} + Q_{pump1} + Q_{pump2} + Q_{penalty} - Q_{penalty,ref}}{Q_{aux,ref}}, 0\right)$$
$$= min\left(1 - \frac{Q_{total} + Q_{penalty} - Q_{penalty,ref}}{Q_{aux,ref}}\,, 0\right) \quad (-)$$

Equation 8.1

$$Q_{penalty} = C_p \cdot \int_0^{t_y} \dot{m} \cdot [\Delta T + (\Delta T + 1)^x - 1]\, dt \ (\mathrm{J}) \qquad \text{Equation 8.2}$$

where t_y is one year and dt the time step of five minutes. The power, x, of the penalty function was set to 4 (Heimrath & Haller, 2007; Weiss, 2007) and ΔT was defined as described in Equation 8.3.

$$\Delta T = max\left(0; T_{hot,comf} - T_{hot}\right) \ (\mathrm{K}) \qquad \text{Equation 8.3}$$

$Q_{energy,miss}$ integrates the energy for periods when the hot water temperature falls below the requirement, $T_{hot,comf} > T_{hot}$, and is defined as in Equation 8.4.

$$Q_{energy,miss} = C_p \cdot \int_0^{t_y} \dot{m} \cdot \left(T_{hot,comf} - T_{hot}\right) dt \ (\mathrm{J}) \qquad \text{Equation 8.4}$$

A base-case scenario was used for the start of the optimisation process, where adequate improvements were incremented for each analysis. This consisted of a 200-litre retrofitted hot water boiler, a new 50-litre auxiliary storage with a 3 kW electric auxiliary heater and a set temperature of 60ºC, weather data for Lund (Sweden), and 6 m^2 flat plate solar collectors. A representative DHW load profile for this analysis was chosen and is further discussed in the sensitivity analysis. The reference DHW system without solar collectors was defined as a 200-litre hot water boiler with a 3 kW auxiliary heater placed at the bottom with a total DHW load, $Q_{aux,ref}$, of 3448 kWh/year. The reference system provides nearly all the required temperature to the load during the whole year and so its penalty value, $Q_{penalty}$, was close to zero.

8.1.1 Control strategies for auxiliary heating

In order to improve the comfort level, both the auxiliary storage size and/or the temperature of the auxiliary heating can be increased. Such variation influences not only the comfort but also the energy performance. Different control strategies for auxiliary heating in both storages were tested and are described in Article V.

The analysed control that achieved the highest combined energy and comfort performance consisted of decreasing the temperature of the new auxiliary heater proportionally to the increase of the temperature in the top third of the retrofitted hot water boiler, where the upper temperature sensor was placed. This decrease was such that the combined energy content of both the auxiliary heater and the top third of the retrofitted storage were equal to the new auxiliary storage volume at maximum temperature (90°C) according to Equation 8.5. For this control strategy, the extended solar fraction SF_{ext} was 58%, the solar fraction indicator SF_i was 39%, and the penalty fraction f_{comf} was 18.9%.

$$T_{set} = max\left[\left(90 - \frac{(T_{solar} - T_{cold}) \cdot 1/3 \cdot V_{sol}}{V_{aux}}\right), 60\right] \quad (°C) \qquad \text{Equation 8.5}$$

Performance results in terms of different power rates for the heater of the new auxiliary storage are presented in Figure 8.1. As shown, higher power increased the comfort for a fairly constant value of the extended solar fraction, with the largest variation between 2 and 3 kW. However, a power greater than 3 kW might be limited by the electrical installation of the house.

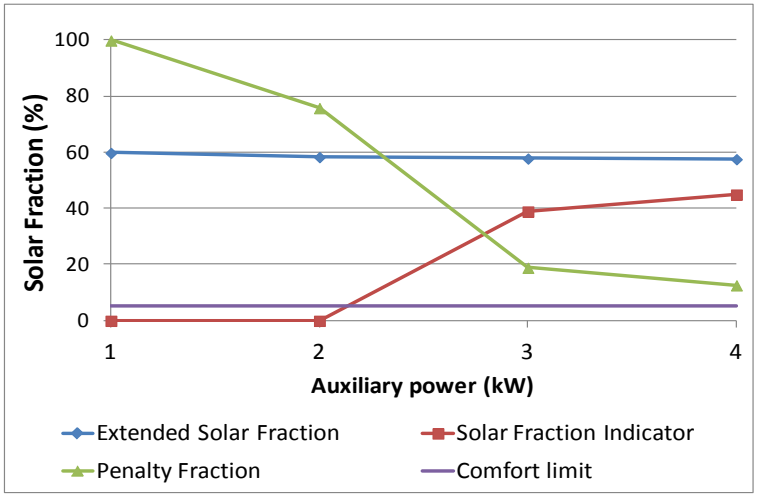

Figure 8.1 *Performance results for different power rates of the new auxiliary heater.*

If the desired comfort level is not achieved with a certain size and control of the new auxiliary storage, a preset temperature for the heater of the retrofitted hot water boiler may be a possible alternative. Several constant preset temperatures were tested, ranging from 10°C (no preheating) to 40°C. The results are illustrated in Figure 8.2 and show that, for higher preheating temperatures, the extended solar fraction decreases faster than the increase of the solar fraction indicator. Therefore, increasing the volume of the new auxiliary storage in order to increase the comfort level was investigated instead. Consequently, the above control strategy powered by a 3-kW auxiliary heater and no preheating in the retrofitted storage was found to be an appropriate optimisation step and was integrated in the base-case system for the following analysis.

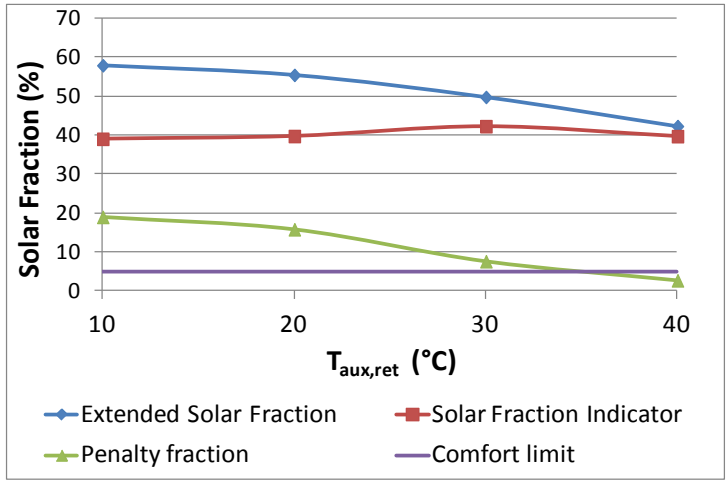

Figure 8.2 *Performance results for the different pre-heating temperatures for the heater of the retrofitted hot water boiler.*

8.1.2 Reduction of heat losses

Gathering the system components into one unit reduces the heat losses of the system. Heat losses from singularities such as sensors, heat exchanger and valves were accounted for by the heat losses of the pipes. Gathering the components into one unit reduces these heat losses. Simulations were carried out for a pipe heat loss reduction of 50% and 75% in the storage circuit. This was considered reasonable based on a 3D model improved design where the pipe length in the tank circuit was reduced by more than 75% compared with the current system. This improved design is described in section 9.3, "Future add-on unit". These changes increased the extended solar fraction by roughly two percentage points. Before reducing the pipe length, the total heat losses of all the pipes were 411 kWh/year. The correspondent UA-value was 6.13 W/K for all pipes (0.24 W/K per metre pipe). The heat losses of both storage tanks were 577 kWh/year. Of the 411 kWh/year of total heat losses from all the pipes, 115 kWh/year were from the pipes in the storage circuit with a UA-value of 2.36 W/K. These heat losses are the ones that can be reduced if the components are gathered into one unit. A 75% pipe heat loss reduction and a low energy pump in the tank circuit were integrated in the base-case system for the following analysis.

Table 8.1 Results from the heat loss reduction and pump upgrade investigation.

Case description	SF_{ext} (%)	SF_i (%)	f_{comf} (%)
0 % heat loss reduction	57.9	39.0	18.9
50 % heat loss reduction	58.4	38.8	19.6
75 % heat losses reduction	58.6	39.3	19.3
75 % heat losses reduction and low-e pump upgrade (base case)	59.7	41.8	17.9

8.1.3 Volume of the new auxiliary storage

In order to increase the comfort level, the volume of the new auxiliary storage can be increased in combination with, or as an alternative to, the increase of the heater temperature. This volume is the most important factor influencing the compactness of an add-on retrofitting unit that includes all the retrofitting components. Therefore, a low volyme is advantageous. Simulations for different volumes of the new auxiliary storage were carried out until f_{comf} was below 5%. The tested and validated volume of the new auxiliary storage was 55 litres. However, the simulated volumes in this analysis were 20, 30, 40, 50, 60 and 70 litres in order to be closer to standard marketed volumes. The number of nodes and the U-value were kept constant. The pipe heat losses were reduced by 75% and a low energy pump was used in the tank circuit.

The results are presented in Figure 8.3 and show that, for higher auxiliary volumes, the comfort level was improved for a fairly constant value of the extended solar fraction. The largest variation occurred between 40 and 50 litres. For f_{comf} below 5%, the minimum required size for the new auxiliary storage was 70 litres. This value was just above 5% for 60 litres. For an auxilary storage volyme of 70 litres, SF_{ext} equals 58%, SF_i 56% and f_{comf} 2%. During winter periods when no solar energy was available and only the new auxiliary heater provided hot water at 90°C, the system could provide a total of 187 litres at 40°C, which roughly corresponds to six simultaneous showers of 30 litres. For such a system, the number of discharges, for which the provided hot water temperature was below the requirements, was 12 out of 6485 during one year. The energy that failed to be delivered on those 12 discharges was 0.1% of the total DHW load, $Q_{aux,ref}$. To meet atypical large loads, the user has the possibility of switching on the heater of the retrofitted hot water storage.

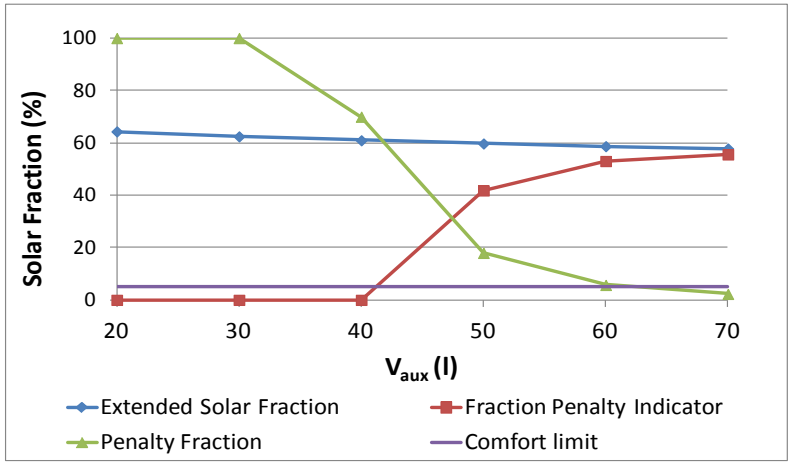

Figure 8.3 *Performance results for different auxiliary storage volumes.*

8.2 Sensitivity analysis

8.2.1 Different DHW load profiles

Since the load profile can influence the required auxiliary volume and/or power in order to meet the comfort limit, three different measured DHW load profiles were analysed, with different annual energy loads for Swedish single-family houses with three inhabitants (Stengård, 2009). These covered a full month and were extrapolated to represent one whole year, with adjustment for a seasonal factor (Swedish Energy Agency, 2009). Figures 10 and 11 in Article V show the DWH profile that was used in the base-case scenario for the optimisation process. This profile was used because its estimated annual load matches the average of the 44 measured DHW profiles in a study in Swedish single-family houses (Stengård, 2009). The total annual load for the other DHW profiles and the simulation results are presented in Table 8.2. The total number of discharges during a year for DHW profile 1 was 7390, for profile 2 there were 6485 discharges, and for profile 3 there were 3764 discharges. The energy that could not be delivered was less than 0.1% of the total DHW load, for the three profiles and 70-litre auxiliary volume.

Table 8.2 Performance of the retrofitted system for three different domestic hot water load profiles.

DHW profile	SF_{ext} (%)	SF_i (%)	$Q_{aux,ref}$ (kWh/y)	f_{comf} (%)
1	57.0	56.9	5832	0.1
2 (base case)	57.8	55.6	3449	2.2
3	71.6	70.4	2972	1.2

8.2.2 Different volumes of the retrofitted hot water storage

The existing hot water storage to be retrofitted may vary in volume. It was therefore important to be aware of the comfort and energy performance levels regarding different sizes of retrofitted boilers. A sensitivity analysis was carried out in the range of 50-400 litres of the retrofitted hot water boiler, maintaining the volume of the new auxiliary storage at 70 litres (good-comfort case). It was assumed that the height increased in proportion to the volume. The number of nodes and the U-value were kept constant. The results are illustrated in Figure 8.4 and are considered in more detail in the "Discussion" section.

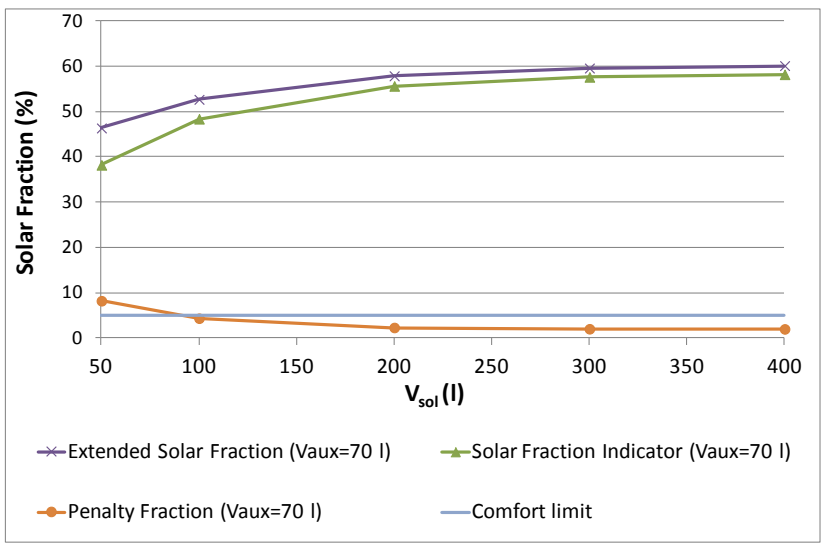

Figure 8.4. Sensitivity analysis on different volumes of the retrofitted storage.

8.2.3 Different climates

The distribution of the solar radiation throughout the year in different climates influences not only the extended annual solar fraction, SF_{ext}, but also the number of discharges below comfort level and therefore the solar fraction indicator, SF_i. The climates in Lund (Sweden, lat: 55.7° N), Lisbon (Portugal, lat: 38.7° N) and Lusaka (Zambia, lat: 15.4° S) were evaluated for collector areas of 6, 4 and 3 m^2, respectively. Such areas represent a balance between a high solar fraction and a reduced number of collectors. The tilt was close to optimal for each site and was 40° (Lund), 30° (Lisbon) and 20° (Lusaka) from the horizontal. The volumes of the new auxiliary storages that ensured that f_{comf} was below 5% were 70, 50 and 50 litres, respectively. The results for different climates are shown in Table 8.3, with a detailed description in Article V. The corresponding results for the other analysed control strategies for these climates are shown in Table 6 in Article V.

Table 8.3 Performance of the retrofitted system in different climates. The minimum size of the auxiliary storage that ensured a good level of comfort was 70 litres for Sweden and 50 litres for the other climates.

Location	Q_{total} (kWh/y)	SF_{ext} (%)	SF_i (%)	f_{comf} (%)
Lund (Sweden)	1455	57.8	55.6	2.2
Lisbon (Portugal)	765	77.8	73.6	4.4
Lusaka (Zambia)	657	81.0	76.6	4.4

8.3 Discussion

The solar fraction indicator, , evaluates the comfort level in a subjective way. It is difficult to state whether "good" comfort levels were ensured for a penalty value below 5% of the total DHW load or for other values. Also, the power factor, x, of 4 seems very penalising and exerts a big influence. For example, if a factor of 2 was used instead, a volume of 50 litres auxiliary would be close to reaching the assumed good-comfort limit. Since the scope of this study did not include new definitions of performance and comfort levels, it was decided to use previous definitions such as the ones used by IEA task 26 and 32, and mark the points within the comfort level according to them. No distinction was made between different types of energy or their sources. Nevertheless, necessary information was provided for a recalculation.

The heat loss reduction of the pipes in the storage circuit had a limited impact on the increase of the extended solar fraction. This is explained by the fact that the losses of those pipes only represent roughly one-quarter of the total pipe losses.

The volume of the new auxiliary storage had a large influence on the comfort level, and a limited impact on the extended solar fraction, due to its relatively low influence on the stored amount of solar energy throughout the year. Larger volumes of this storage provide better comfort but also greater heat losses, which cause the extended solar fraction to decrease slightly (Figure 8.3).

The sensitivity analysis on different climates showed that, for climates where the solar irradiation is more distributed throughout the year, a volume of the new auxiliary storage of 50 litres would be enough to achieve good comfort levels. The analysis also showed that, for DHW load profiles with significantly different annual loads, the comfort level was still good. In contrast to the new auxiliary storage, the volume of the retrofitted hot water storage influenced the solar storage capacity and therefore the SF_{ext}. In Figure 8.4, it was shown that, for volumes of the retrofitted hot water boiler between 100-400 litres, the SF_{ext} varied by roughly 7 percentage points. This variation was not considered critical and, since it is expected that the most common sizes of hot water storages in Sweden are 200-300 litres (Kjellsson, 2002), the retrofitting possibilities should be favourable. The impact of the volume of the retrofitted storage on the comfort level was lower than that of the new auxiliary storage. The biggest comfort constraint occured in the winter time when there is less solar hot water available and when that volume becomes therefore less important.

Engineering a compact retrofitting add-on unit is important, to reduce the space requirement and installation costs. It is difficult to evaluate the importance of the compactness of the retrofitting add-on unit for the user. This is relevant since there is a trade-off between compactness (low volume of the new auxiliary storage) and comfort. A phase-change material could possibly be used inside the new auxiliary storage to decrease its volume, but this was not investigated. This study provided the necessary information to design the system according to the importance of these factors. Once costs of production for certain market volumes can be determined, an optimisation process focused on cost efficiency can be carried out.

9. Technical improvements and cost analysis

A prototype of a new retrofitting add-on unit for connecting solar collectors with existing electric hot water storages was developed in cooperation with an industrial partner, according to the configuration of a tested retrofitted system described in Figure 1 in Article V. The objective was to develop an add-on unit that could be built in a compact and potentially cheap manner which is described in this chapter. For financial reasons, the built prototype of the add-on unit is still not very compact since it uses, where possible, standard components already available on the market. The function of the prototype was preliminarily tested in the laboratory in a qualitative way. An installation in a Swedish single-family house for detailed monitoring under authentic conditions is planned for the summer of 2013. A possible future design for the compact add-on unit was also developed.

The main difference in components between the tested retrofitted system, described in Article V, and the new retrofitting add-on unit is the use of a developed multiport valve. Also, since a compact add-on unit is used, the installation is simple and non-invasive. The multiport valve allows the retrofitted system to be switched from charge to discharge mode of operation in a completely mechanical way, without the need for electronically controlled valves. It also makes configuration of the system significantly simpler and cheaper.

A screening of international patents in the field performed by a patent company concluded that the add-on unit has good chances of being granted a patent. Two patent applications were submitted in July 2012, and are currently being processed.

For simplicity, the several elements that form the system, and which are shown in the following figures, are represented with numbers. They are listed and described briefly below for every figure.

9.1 System operation with a multiport valve

Figure 9.1 shows the retrofitted system in discharge mode using the developed multiport valve (6). This valve is responsive to pressure changes in the system and was developed for switching between charge and discharge mode. The valve is responsible for changes in the flow direction of the system and directs the water from the heat exchanger (1), via the first conduit (7), to the tank in discharge mode, or from the heat exchanger via the second conduit (8), to the tank in charge mode. This is a fully mechanical process. As shown, the flow directions of water transported in the first and second conduits are reversed by the multiport valve at the time of change in the mode of operation between charge and discharge. During the discharge mode, the multiport valve switches off the pump in the tank circuit automatically. The system components are described in Table 9.1.

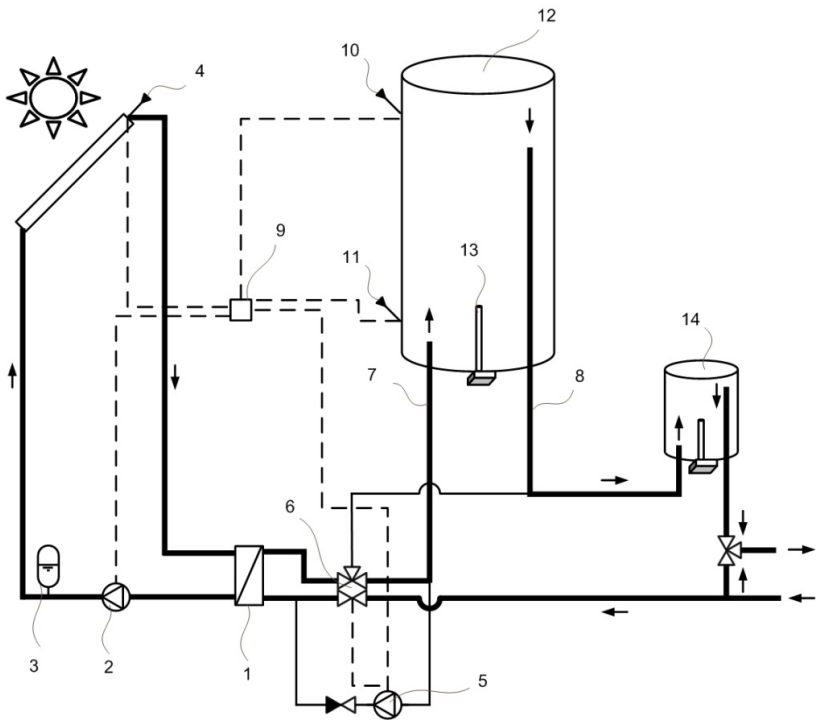

Figure 9.1 *Schematic representation of the components included in the add-on unit with the newly-developed multiport valve. The system is illustrated in discharge mode.*

Table 9.1 Description of the illustrated components in Figure 9.1.

Component number	Description
1	Compact heat exchanger
2	Circulation pump of the collector circuit
3	Expansion vessel
4	Highest temperature of the solar collector field
5	Circulation pump of the tank circuit
6	Developed multiport valve
7	First conduit for connection of the retrofitted storage with the heat consumer and the heat source
8	Second conduit for connection of the retrofitted storage with the auxiliary storage and the heat source
9	Controller
10	Surface temperature on the upper part of the retrofitted storage
11	Surface temperature on the lower part of the retrofitted storage
12	Retrofitted hot water storage
13	Heating source of the retrofitted storage
14	New auxiliary storage

9.1.1 Multiport valve

The multiport valve makes it possible to use the existing hot water boiler featuring two available connections with, in principle, the same functionalities as a standard solar storage with four available connections. Figure 9.2 shows the prototype of the valve fully mounted. The inlets / outlets of the multiport valve are described in Table 9.2.

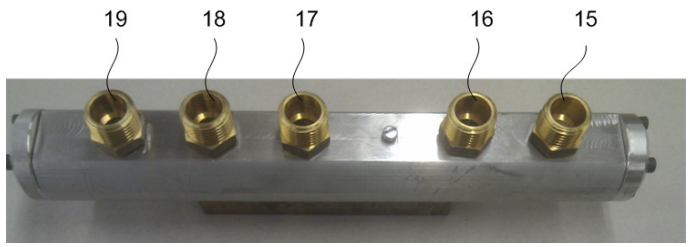

Fig. 9.2 Prototype of a fully-mounted multiport valve.

Table 9.2 Description of the illustrated components in Figure 9.2.

Component number	Description
15	Inlet of cold water flow that changes to discharge mode of operation
16	Outlet of cold water flow
17	Fluid output in charge mode of operation connected to (8)
18	Port connected to an input of fluid from the heat exchanger
19	Fluid output in discharge mode of operation connected to (7)

9.2 Future add-on unit

In order to make the installation of the system easy and non-invasive, a possible design of a compact add-on unit was developed. It is important that the add-on unit is non-invasive since new holes in the existing water boiler can cause corrosion. Furthermore, the secondary legislation on pressured tanks stipulates that such modifications are approved by the Technical Research Institute of Sweden (Kjellsson, 2002). Figure 9.3 is a front-view perspective of the add-on unit that can be integrated into an existing water supply infrastructure according to the system illustration in Figure 9.1. The components of the add-on unit are described in Table 9.3. For this particular design and dimmensions, the volyme of the auxiliary storage (14) was roughly 85 litres.

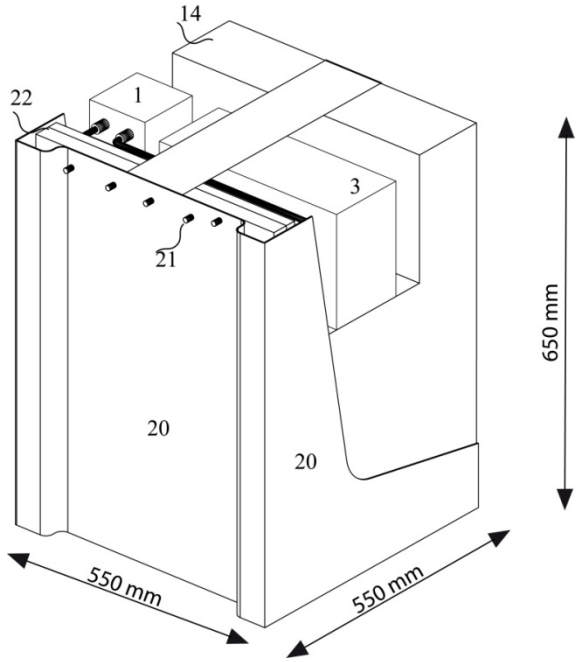

Fig. 9.3 *Front-view perspective of a possible design of the add-on unit module.*

9.3 Prototype of the add-on unit

In Figure 9.4, two identical prototypes of the add-on unit are shown. For financial reasons, another design and more space was needed for the add-on unit but functionality requirements were met. The operation of the prototype was preliminarily tested in the laboratory for the following modes of operation: charge, discharge, and charge during discharge. The new multiport valve was also tested. An installation in a Swedish single-family house is planned for the summer of 2013, which will allow quantitative monitoring under "real" conditions. The components of the add-on unit are described in Table 9.3.

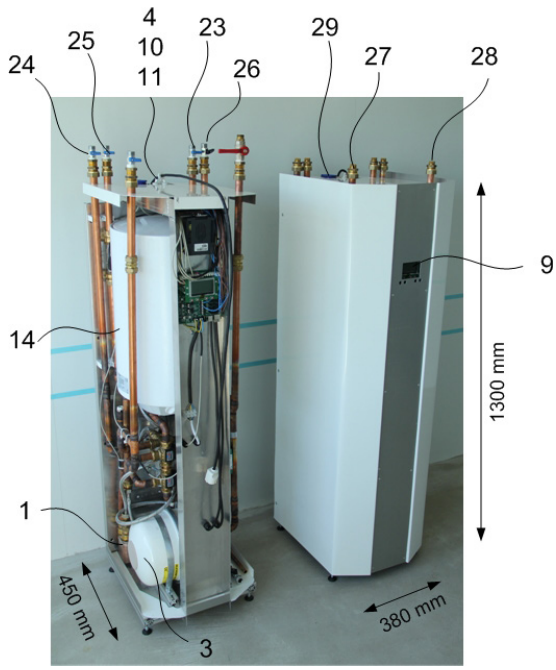

Fig. 9.4 *Two identical prototype units: to the left without the exterior cover.*

Table 9.3 Description of the components illustrated in Figure 9.4 and Figure 9.5.

Component number	Description
20	Chassis of the add-on unit
21	Connector between the add-on unit and the user/retrofitted storage
22	Moulded hydraulic block with the piping on the tank circuit and the two pumps
23	Outlet connection from the add-on unit to the solar collectors
24	Inlet connection from the solar collectors to the add-on unit
25	Inlet connection from the cold water from the main to the add-on unit
26	Outlet connection from the add-on unit to the hot water user
27	Connection of the add-on unit with the top of the retrofitted storage
28	Connection of the add-on unit with the bottom of the retrofitted storage
29	Electrical connection between the existing heating element (13), and the controller (9).

9.4 Payback-time analysis

A cost analysis was performed in order to analyse the possible investment cost reduction on solar domestic hot water systems by using the developed add-on unit. Since a cost analysis was not one of the goals of the investigation, it was carried out in a straightforward manner. The payback time of the retrofitted solar domestic hot water system was also compared with that of a standard solar domestic hot water system. The assumptions for the calculation and prices of the different parts of both systems are presented in Table 9.4 and Figure 9.5. The prices were based on a study performed by the Swedish National Board of Housing, Building and Planning (Swedish Building Regulations, 2012), which provides average prices of the various parts of solar thermal systems installed in Sweden. However, these prices were adjusted, since the statistics mainly concerned systems designed for both domestic hot water and space heating production. Therefore, the installation costs were based on Bales et al. (2012). The expected cost of removing the existing hot water storage was estimated by Kjellson (2002) to be roughly SEK 3 500 and was also taken into account. The price of the retrofitted add-on unit was based on a realistic but preliminary investigation. Its total sale price was estimated to be roughly SEK 8 000. The total estimated sale price of the retrofitted system was SEK 35 700, compared with SEK 56 200 for a standard system. Under these assumptions, a significant investment cost reduction of 36% could be achieved. The annual solar fraction of both systems was assumed to be 58%. This was the estimated annual performance of the retrofitted system in Article V, which is comparable to the performance expected from a conventional solar domestic hot water system as shown in other investigations (Helgesson, 2002; Hobbi & Siddiqui, 2009; Swedish Technical Research Centre, 2012). The annual average domestic hot water load was set to 3 449 kWh/year (Article V). The electricity price during the lifetime of the system was kept constant and assumed to be 1.6 SEK/kWh, which is the current (2012) electricity price for single-family houses (Swedish Energy Agency, 2012b). With such assumptions, the retrofitted system payback time would be roughly 11 years, compared with 18 years for a standard system, which corresponds with the estimates of the Swedish Building Regulations (2012). The prices refer to sale prices inclusive VAT. The analysis did not take into account subsidies, maintenance costs, replacement costs, interest on loans, inflation, dicount rates, residual value, and increase in the electricity price.

Table 9.4 – Assumed parameters used in the payback-time analysis.

Assumed parameters	Assumed value
Annual domestic hot water load (KWh/year)	3 449
Average electricity price during the lifetime of the system (SEK/kWh/year)	1.6
Installation costs for the standard system (SEK)	11 000
Installation costs for the retrofitted system (SEK)	6 500
Total sale price of the retrofitted system (SEK)	35 700
Total sale price of a standard system (SEK)	56 200
Relative savings on the investment cost (%)	36
Annual solar fraction of both systems (%)	58
Payback time of the retrofitted system (years)	11
Payback time of the standard system (years)	18

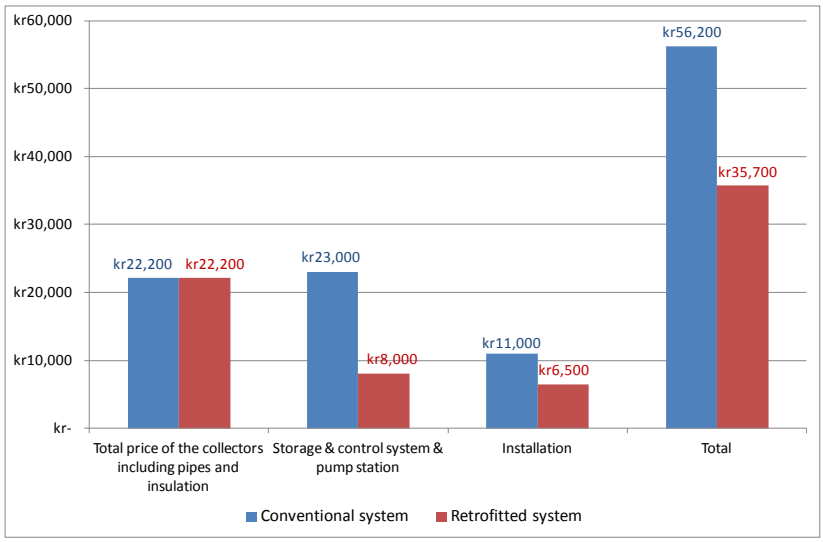

Figure 9.5 *Assumed sale price of a conventional system (in blue) and the retrofitted system (in red).*

10 Discussion and conclusions

Sweden has one of the highest electricity consumptions per capita in the world due to a high number of electrically heated houses combined with the cold Swedish climate and electricity driven industry. A retrofitted solar domestic hot water system that can save electricity in these houses has been developed and evaluated. The main principle of the system is to connect new solar collectors to existing electric hot water storages. This retrofitting has the potential to significantly reduce the investment cost. A prototype of such system was built and tested in the laboratory according to results from theoretical simulations that indicated the retrofitting configuration which should achieve the best energy performance. During the test period, necessary technical changes were carried out to the configuration of the system and, therefore, the simulation model was adjusted. This model was then validated against measurements and used to perform a system optimization and sensitivity analysis. Finally, a prototype of an add-on unit for connecting solar collectors to an existing electric hot water heater was developed. This unit is planned to be installed and monitored in real houses during the summer of 2013.

Two collectors that could be used in the retrofitted solar domestic hot water system were tested. These were a stationary concentrating CPC-PV/T hybrid and a CPC-thermal collector. Both have the same design and a low concentration factor of 1.5. The CPC-PVT hybrid aims at producing both hot water and electricity at a lower cost compared with a flat plate collector and a PV module, working side-by-side. The CPC-thermal collector aims at achieving a higher annual solar fraction than that of conventional flat plate collectors by adapting the solar thermal production to the annual load profile. A third collector, a tracking concentrating PV/T hybrid with a concentration factor of roughly 8, was also investigated. This was, in principle, a separate investigation from the previous ones. For practical reasons, this tracking hybrid is not easily integrated in single family houses but it was considered technically interesting and worth investigating as a separate study. When the project started, the main challenge with PV-systems was the high cost of the solar cells. Therefore, it was interesting to

increase the concentration factor in order to replace expensive cell area by cheaper reflector material. During recent years the market prices of solar cells have drastically decreased making the demand for decreasing the solar cell area less important.

In the previous chapters results were presented concerning the analysis of the collectors and the configurations for the retrofitting of existing hot water storages. These two investigations are independent, meaning that the collector evaluation does not influence how the retrofitting of existing hot water storages is carried out and vice-versa. In this chapter, the most important results are reviewed and their implications is discussed.

10.1 PV/T concentrating hybrids

PV/T concentrating hybrids with higher concentration factors aim at achieving higher cost effectiveness since a larger amount of relatively cheap reflector material replaces expensive solar cells. Such an example is the investigated tracking concentrating PV/T hybrid with a concentration factor of roughly 8. However, as it was shown in Article I, a higher concentration factor lowers the fraction of usable diffuse irradiation. This becomes especially important in climates such as the Swedish where the annual diffuse radiation represents roughly half of the total annual radiation (Kjellsson, 2002). As described in Article I, the studied tracking hybrid receives roughly 40% less usable annual radiation than a static optimally tilted flat surface, in Sweden. Furthermore, concentrating PV/T hybrids generally imply lower efficiencies per glazed area compared with conventional alternatives (Kostic' et al., 2010; Tripanagnostopoulos & Souliotis,2004). Results from measurements showed an electrical efficiency of roughly 8% at 25 °C with a temperature dependence of 0.3%/°C, calculated per active glazed area. The nominal efficiency of the solar cells was 16%. The measured zero loss efficiency was 56% and the U-value 2.3 W/m^2/°C, also calculated per active glazed area. The low usable radiation together with low efficiencies explains the low annual energy output per glazed area compared with conventional alternatives, described in Article I. When compared with a system formed by conventional thermal collectors and PV modules working side by side, it was shown that, for the same annual output, the side by side system used less glazed area. Since the relatively high concentration was hazardous for the cells of this hybrid, continuous flow is required in order to prevent damage through overheating. This is not possible for most domestic hot water applications in single-family houses where stagnation is likely to occur. Alternatively a failsafe mechanism to track the collector away from the sun must be developed. Also, for such

relatively high concentration factors, the volume of the hybrid becomes relatively large and a solar tracking system is required making it difficult to integrate the collector on roofs of single-family houses.

In a second study, a stationary asymmetrical CPC-PV/T hybrid collector with a concentration factor of 1.5 was investigated (Article III). Due to the low concentration factor, the cells do not require continuous cooling since the light concentration is not hazardous for them. Hence, this hybrid can withstand stagnation periods and can therefore be used in a solar domestic hot water system. Furthermore, this hybrid uses a significantly larger fraction of the diffuse solar radiation compared with the previous one. This was estimated to be roughly half of the annual diffuse solar radiation (Article III). The low concentration factor also decreases the need for a tracking system and therefore, it is easier to integrate the collector on roofs of single-family houses. Despite the previously described advantages for this hybrid, there is a disadvantage. A lower concentration factor, in association with large incidence angle modifiers (Article III) and uneven concentrated radiation, may result in a collector that does not produce significantly more electricity per cell area when compared with a standard PV module, at the same temperature. The measured electrical efficiency of this hybrid was roughly 14% at 25°C with a temperature dependence of 0.4 %/°C, calculated per active glazed area. The nominal efficiency of the solar cells was 18%.

More particularly, the reflector shape of the stationary CPC-PV/T hybrid is formed by an optical axis which, together with the tilt of the collector, decides the fraction of solar annual radiation which is used by the collector. This reflector was designed to be used in solar thermal collectors. The aim was to decrease the solar thermal production in the summer period in order to adapt the production to the annual load profile. However, since PV cells are expensive, it is more advantageous to set this hybrid collector at a low tilt that maximizes the annual production instead. This hybrid collector is made of two different parts. These are the front part of the absorber where the solar cells behave like a flat plate PV-module without concentration and the solar cells which receive concentrated radiation on the back part of the same absorber. The area of the thermal absorber is then half of what a flat plate hybrid would have used with the same cell area on top of the absorber. If the solar cells on the back part of the absorber reach the same annual production as the ones on the top, the savings in thermal absorber compared with a flat plate hybrid should compensate for the extra costs on glazing, frames and reflector. Otherwise it is more advantageous to build a flat plate hybrid collector.

Concentrating hybrid collectors are generally more suitable to be used in systems that can effectively cool the solar cells during the whole year. This can be achieved by under sizing the collector area in relation to the

load and in systems where continuous flow can be guaranteed. Also, at lower temperatures, both the electrical and thermal efficiencies are increased. Concentrating hybrids with lower concentration factors have a lower volume and are therefore more suitable to be integrated on roofs of single-family houses. The area of the hybrid should be designed to match the heat load while the generated electricity is used for household appliances or, eventually, sent to the electric grid.

10.2 CPC-thermal collector system

The use of asymmetrical CPC-thermal load adapted collectors was investigated. The performance of a conventional flat plate collector system was compared to that of the CPC-thermal collector system for domestic hot water production in a single-family house. A similar investigation was performed by Helgesson (2004). Related collector designs were investigated by Kothdiwala et al. (1995), Tripanagnostopoulos et al. (2000), Chaves & Pereira (2000), Helgesson (2002), Mills & Morrison (2003) and Nordlander (2004).

In previous studies the collector area was designed by matching the solar production to the load during the month with the highest production (Helgesson, 2004). This was done by estimating the energy output of 1 m^2 collector at 50°C mean operating temperature. A complete solar domestic hot water system was not taken into account. The increased heat losses due to a larger collector field or the stagnation periods during the year were not accounted for either. Thus, in this investigation, an annual deterioration limit when designing the collector area was assumed instead. A complete solar domestic hot water system was also taken into account. The annual solar fraction and the collector area were then calculated for various tilt angles. Since large variations in the incidence angle modifier were expected, close to the optical axis of the collector, they were measured at short time intervals and modelled by well fitting equations. A statistical annual variation of the load was also used (Article III).

Results from the CPC-thermal collector measurements show that the beam zero-loss efficiency was 64%, the diffuse incidence angle modifier was roughly 0.5, the first order heat loss coefficient was 2.8 $W/m^2/°C$ and the second order heat loss coefficient was 0.035 $W/m^2/°C^2$. These measured parameters were used to validate a simulation model of the collector. The investigation showed that the CPC-thermal collector system achieved an annual solar fraction of 71% using 17 m^2 collector area compared with 66% and 7 m^2 of flat plate collectors. Hence, the CPC-thermal collector system uses 20% less absorber area with an increase of five percentage

points in annual solar fraction compared with a standard flat plate collector system, at optimum tilt and for the same annual deterioration limit.

Helgesson (2004) concluded that, for the same optimum tilt, the CPC-thermal collector system achieved an annual solar fraction of 71% using 15 m^2. The flat plate collector system was estimated to achieve an annual solar fraction of 56% using 6.5 m^2. Thus, in Helgesson's study, the CPC-thermal collector system used 23% less absorber area than the flat plate collector system with an increase in solar fraction of 15 percentage points.

In Article II it was shown that the production of the CPC-thermal collector system was lower than the flat plate collector system during the summer period. This indicates a potential for improvement for the shape of the reflector in such a way that the decrease in usable radiation during the summer period becomes less abrupt. This conclusion is supported by Nordlander (2004). The cost decrease due to 20% lower absorber area combined with the solar fraction increase of five percentage points should compensate for extra costs of the reflector and glazed area.

It can be questioned whether the design criterion of a supposed annual deterioration limit is appropriate or not. The collector area design should be based on cost efficiency. The purpose was to quantify the stagnation periods and when they take place. The relevant analysis was a relative comparison between the CPC-thermal system and the standard flat plate system rather than concluding on the absolute values of the achieved annual solar fraction.

Since the concentration ratio of the tested CPC-thermal collector is rather low (1.5), the collector can be built in a compact way which facilitates its integration on roofs of single family houses. The lower concentration factor also makes it possible to use a larger fraction of the diffuse radiation as shown by the measured parameters. It was shown that the CPC-thermal system achieves a higher annual solar fraction using less absorber area than a flat plate collector system. Therefore, it is concluded that this collector is adequate to be part of the retrofitting solar domestic hot water system in Swedish single-family houses. The reduction in absorber area and increase in annual solar fraction should compensate for the increased costs of larger glazed areas, reflector material and frames.

10.3 Retrofitted system

Following the collector analysis, a theoretical investigation regarding the retrofitting of existing hot water storages was performed. Four system models that correspond to different retrofitting configurations were inves-

tigated and compared to a conventional solar domestic hot water system. At that stage, before practical implementation, the simulation models were simplified. Flat plate collectors were used so that the annual performance of the system could be compared with previous analysis regarding standard systems. One of the biggest challenges was to achieve stratification in existing hot water storages where the heater is normally placed at the bottom. Moreover, when standard hot water storages are retrofitted for solar thermal use, the two available connections, which were previously used for hot water discharge to the user, should now also be used for charging the storage with solar hot water. According to the theoretical analysis, the retrofitted configuration achieving the highest annual performance consisted of connecting the existing hot water storage in series with a new smaller auxiliary storage. Hence, the existing storage works together with the solar collectors at lower temperatures while the smaller additional storage works as auxiliary volume. The temperature stratification in the system is partly achieved by means of two separate tanks with limited stratification levels but working at different temperatures.

A prototype was built according to the previously described retrofitting configuration. During testing, necessary technical changes were carried out in the configuration of the system and therefore, the simulation model was revised. This model was validated against measurements and was used to optimize the performance of the system. The optimization took into account energy performance and comfort level regarding the delivered hot water temperature. Results from the optimization process showed that an appropriate control strategy is to decrease the temperature setting of the new auxiliary heater when higher solar energy is available in the retrofitted storage. A power of 3 kW was found to be suitable for the new auxiliary heater. By developing a new compact add-on unit for connecting solar collectors to an existing electrical hot water heater, it was estimated that it was possible to reduce the length of the pipes in the tank circuit, and therefore their heat losses, by 75%. In order to achieve a good comfort level, the minimum required volume of the new auxiliary storage was estimated to be at least 70 litres, in Sweden. With such improvements, the retrofitted system was estimated to achieve an annual solar fraction of 58 % using 6 m^2 of flat plate collectors in Lund, Sweden. This performance is comparable to that of standard solar domestic hot water systems for the same conditions (Helgesson, 2002; Hobbi & Siddiqui, 2009; Swedish Technical Research Centre, 2012).

The validated model with a 70-litre auxiliary storage was also used to carry out a sensitivity analysis on different domestic hot water load profiles, different volumes of the retrofitted storage and different climates. For three different domestic hot water load profiles, good comfort was achieved. Furthermore, it was estimated that a retrofitted storage of 400

litres achieved an annual solar fraction which was 7 percentage points higher than that of 100 litres. This difference in performance was not considered to be critical and it is expected that the most common sizes of boilers in Sweden are between 200-300 litres (Kjellsson, 2002). The sensitivity analysis on different climates showed an annual solar fraction of 78% in Lisbon (Portugal) and 81% in Lusaka (Zambia) for collector areas of 4 m^2 and 3 m^2, respectively. For these climates, a volume of the new additional auxiliary storage of 50 litres would be enough to achieve good comfort levels.

Several previous retrofitting solutions increase the space requirement and the cost reductions are limited in comparison with new conventional systems (Conergy, 2009; Thermo Dynamics, 2009; Enerworks, 2009). There are also retrofitting solutions which have a lower space requirement and investment cost but, since temperature stratification is not achieved, the annual performance is commonly low (Mondol and Smyth, 2012; Värmebaronen, 2013). The main advantages of the developed retrofitted system in comparison with the existing solutions are the combination of high annual performance at a low investment cost.

From the point of view of risk for legionella growth, the developed retrofitted system makes it possible to implement required prevention and control measures according to most European countries. When compared with a conventional solar storage, the risk may even be lower since a heater is placed at the bottom of both storages in the retrofitted system. These heaters can be used for thermal disinfection of the whole stored water whereas in standard solar storages the auxiliary heater only heats up part of the storage volume.

An add-on retrofitting unit, which enables an easy and non-invasive installation, was designed and built. Due to financial reasons, the developed add-on unit has a lower degree of compactness compared with what can be achieved. Engineering a compact add-on unit is important not only to decrease the heat losses but also the space requirement and installation costs. It is difficult to evaluate how important the volume of the add-on unit is for the user. This is relevant since there is a trade-off between the volume of the new auxiliary storage and comfort for the user.

A simple cost analysis was performed by comparing the investment cost and the payback time of the retrofitted system to that of a new solar domestic hot water system. For the assumptions used, the analysis showed that the investment cost including installation could be reduced by roughly one third in comparison with a conventional solar domestic hot water system. The payback time of the retrofitted system and the conventional system was estimated to be approximately 11 and 18 years respectively. Some of the assumptions such as the installation time and cost of the developed add-on unit need practical implementation to be verified.

If further improved, the developed add-on unit does not need to be exclusively used to connect new solar collectors to existing electric hot water storages in single family houses. In principle, with an adequate control and technical adjustments, the add-on unit can be adapted to connect other types of heat sources to other types of storages. The possible applications of the add-on unit may be: connection of a solar thermal collector (eventually a hybrid PVT collector) to a water storage tank provided with a heating unit; connection of a water mantled wood/pellets/gas burner to an electric hot water storage tank; connection of a solar collector and a water mantled wood/pellets/gas burner to an electric hot water storage tank.

In the first system (to the left in figure 10.1), the solar collectors can be connected, via the add-on unit, to a wood/pellets/gas burner. In that case, the wood/pellets/gas burner does not need to be intermittently used with low efficiency during the summer since the solar collectors cover the hot water demand during that period. In the second system (in the middle of the figure), an existing electric hot water storage can be connected, via the add-on unit, to a water mantled wood/pellets/gas burner. The burner could then be used for both space heating and domestic hot water production during the winter period. During the summer, the electric hot water storage could mainly cover the domestic hot water load without the need of using the burner during the period of lowest energy load. In this system, a new auxiliary storage in the add-on unit would not be entirely necessary since the heater in the existing hot water storage does not need to be turned off. In the third system (to the right in the figure), a water mantled wood/pellets/gas burner and solar collectors can be connected to an existing electric hot water storage, via the add-on unit. The burner could be used for space heating and domestic hot water production during the winter period, while the solar collectors cover the domestic hot water load during the summer period. Electricity consumption for heating could thus be essentially replaced by wood/pellets/gas and solar energy. At the time this thesis was written, the add-on unit was developed and tested for the application to the left in the figure.

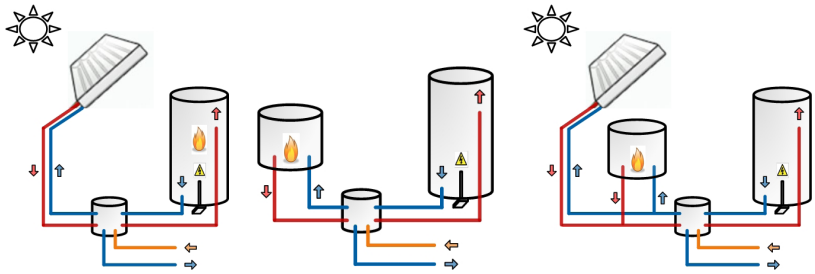

Figure 10.1 Possible applications for the developed add-on retrofitting unit.

Kjellsson (2002) summarized the necessary requirements in order to retrofit existing hot water storages for solar hot water systems. These were non-invasive connection to the existing storage, sufficient space for the extra retrofitting components and temperature stratification in the system. A non-invasive add-on unit for retrofitting existing storages was developed. Further investigations are needed in order to estimate the available space for this unit in typical houses. Temperature stratification is achieved in the developed retrofitting system and its performance is comparable to conventional solar domestic hot water systems. If the add-on unit is produced at a low cost, the savings on the investment cost, both on material and installation, are estimated to be roughly one third. The developed retrofitting solution is therefore considered to have the potential of becoming a competitive solution in the solar domestic hot water market.

11 Future work

Recommended for future work is testing of the prototype add-on unit in real houses and additional technical development that enables the add-on unit to be used for other applications described in the discussion and conclusion section.

11.1 Tests in real houses

Testing the retrofitting add-on unit in real houses will provide important information about the reliability of the developed multiport valve, required installation time, importance of the volume of the retrofitting unit, and the hot water comfort as experienced by the users.

11.2 Further development of the add-on unit

As described in the section "Technical improvements and cost analysis", the prototype of the add-on unit is still not very compact compared with what is possible. In many houses, space for the add-on unit may be limited. Work to make the unit more compact, at the lowest possible cost, should continue according to the principles described in section 9.2 "Future add-on unit".

As described in the discussion and conclusions chapter, the add-on unit does not need to be exclusively used to connect new solar collectors to existing electric hot water storages in single-family houses. In principle, with the necessary control and technical adjustments, the add-on unit can be adapted to connect other types of heat sources to other types of storages. Solar collectors can be connected via the add-on unit to existing wood/pellets/gas burners. Another type of heat source that can be connected to an existing electric water heater via the add-on unit is a water-mantled wood/pellets/gas burner. Specific control strategies and other required

technical improvements to the add-on unit for these purposes should be further investigated.

12 Published articles and open access publishing

12.1 List of articles and contribution of the author

As part of the Ph.D. work, five articles were published, three of which were in open access journals. The list of publications reflects the increased awareness of open access publishing, which is discussed in more detail below.

I. **Bernardo, R.**, Perers, B., Håkansson, H. & Karlsson, B. (2011). Performance Evaluation of Low Concentrating Photovoltaic/Thermal Systems – a case study from Sweden. *Solar Energy*, 85 (7), 1499-1510.

The *Solar Energy Journal* is a commercial journal. The co-authors helped on testing the collector and reviewing the article.

II. **Bernardo, R.**, Davidsson, H. & Karlsson, B. (2011). Performance Evaluation of a High Solar Fraction CPC-collector System. *Journal of Environment and Engineering*, 6 (3), 680-692.

Open access journal. The co-authors helped with modelling and reviewing the article.

III. **Bernardo, R.**, Davidsson, H., Gentile, N., Gomes, J., Gruffman, C., Chea, L., Mumba, C., & Karlsson, B. (2013). Measurements of the Electrical Incidence Angle Modifiers of an Asymmetrical Photovoltaic/Thermal Compound Parabolic Concentrating-Collector. *Engineering*, 5, 37-43.

Open access journal. This collector was tested in Mozambique, Africa. A small-scale laboratory was built for collector testing and for teaching purposes. The co-authors were involved in building the laboratory, testing the collector, and reviewing the paper.

IV. **Bernardo, R.**, Davidsson, H. & Karlsson, B. (2012). Retrofitting Domestic Hot Water Heaters for Solar Water Heating Systems in Single-Family Houses in a Cold Climate: A Theoretical Analysis. *Energies*, 5 (10), 4110-4131.

Open access journal. The co-authors helped with modelling and reviewing the article.

V. **Bernardo, R.** (2013). Retrofitting Conventional Electric Domestic Hot Water Heaters to Solar Water Heating Systems in Single-Family Houses – model validation and optimization. *Energies*, 6 (2), 953-972.

Open access journal.

12.2 List of articles not included in the thesis

VI. **Bernardo, R.**, Perers, B., Håkansson, H. & Karlsson, B. (2008). Evaluation of a Parabolic Concentrating PVT System. In Proceedings of the 7th Eurosun Conference *Eurosun 2008*, 7-10 October 2008, Lisbon, Portugal.

VII. Gentile N., Davidsson H., **Bernardo R.**, Gomes J., Gruffman, C., Chea L., Mumba, C. & Karlsson, B (2013). Construction of a Small Scale Laboratory for Solar Collectors and Solar Cells in a Developing Country. *Engineering*, 5, 75-80.

VIII. Davidsson, H., **Bernardo, R.** & Hellström, B (2013). Hybrid Ventilation with Innovative Heat Recovery – A System Analysis. *Buildings*, 3 (1), 245-257.

IX. Davidsson, H., **Bernardo, R.** & Hellström, B (2013). Theoretical and Experimental Investigation of a Heat Exchanger Suitable for a Hybrid Ventilation System. *Buildings*, 3 (1), 18-38.

12.3 Open access publishing

Traditionally, research work has been published in the form of articles in closed/commercial journals in the field. However, this process has a number of disadvantages. One of the most important is that access to information is limited to those who can afford it. This excludes many institutions and private persons, especially in developing countries. This makes it difficult for them to conduct research in equivalent conditions to those in developed countries. Another drawback is the principle that researchers conduct most of the work in this process, which then generates profit for the publisher. Researchers carry out the investigation, they describe it in a scientific doc-

ument, and other researchers review it. Ultimately, researchers assign the copyright of their work to a commercial publisher who will commercialise it. In some cases, research work funded by tax payers is only published in commercial/closed journals, thereby limiting access to the information for those who financed it. Some commercial journals are now allowing what is called "parallel publishing", meaning that the work can also be published elsewhere. However, some limitations often apply, such as a delay period before the paper can be published elsewhere.

Open access journals try to find a solution to some of these issues. These journals are based online, access to the information is not restricted, and they are free of most copyright and licence restrictions. Typically, the submission and reviewing process is the same as commercial journals, but the main difference is that access to its contents is free of charge. In order to cover the expenses of maintaining the journal database, editing, and correspondence with authors and reviewers, the authors pay a fee at the time of publishing. Lund University has a fund available that has previously covered 100% of this expense, but this has now been reduced to 50%. In contrast to commercial journals, these open access journals facilitate horizontal dissemination of information between researchers, since information is neither bought nor limited. Also, the review process is normally open, which greatly increases the transparency of the process. Furthermore, open access to the information increases the visibility of the research, which is one of the biggest goals of the research community. More widespread information may also prevent duplication of previous research.

On 13 September 2005, the board of Lund University decided to officially support and encourage researchers in publishing the results of their research in open access sources:

"In order to maximise the amount of accessible publications, the board of Lund University considers that:

- *if possible, Lund University should publish in free access journals for the reader;*
- *if a free access journal does not exist, the publication should preferably take place in a journal that allows parallel publishing of the article;*
- *copyright release should be avoided where the minimum demand for the authors is the right to parallel publishing;*
- *Lund University encourages that scientific journals change to a publishing method where the articles are freely available to the readers directly or in the form of parallel publishing."*

(Lund University, 2005)

Most of the open access journals are relatively new and, in most cases, have yet to establish the prestige that commercial journals have enjoyed for a long time. Also, in some cases, it was reported that some journals had a less demanding reviewing process. Therefore, the *Directory of Open Access Journals* was created (http://www.doaj.org/), which provides a catalogue of quality-controlled open access journals. Furthermore, Lund University only provides financing for the publishing fee of journals that have been subjected to quality-control analysis and if their code of conduct is in accordance with the Open Access Scholarship Publisher Association (Open Access Scholarly Publisher Association, 2013).

References

ABB (2009). Website of the company accessed 2009-2 from www.ABB.com

Abdul-Jabbar, K. (1998). Forced versus natural circulation solar water heaters: A comparative performance study. *Renewable Energy*, 14, 77-82.

Absolicon Solar Concentrator AB (2008). Website of the company accessed 2008-08 from http://www.absolicon.com

Adsten, M., Helgesson, A. & Karlsson, B. (2004). Evaluation of CPC-collector designs for stand-alone, roof- or wall installation. *Solar Energy*, 79(6), 638-647.

Affolter, P., Eisenmann, W., Fechner, H., Rommel, M., Schaap, A., Sorensen, H., Tripanagnostopoulos, Y. & Zondag, H. (2004). *PVT road map, A European guide for the development and market introduction of PV-Thermal technology.* Energy Research Centre of the Netherlands, Netherlands. Accessed 2008-01 from http://www.pvtforum.org

Aleklett, K. (2012). *Peeking at Peak Oil*. Department of Earth Sciences, Uppsala University, Sweden. Springer, New York, ISBN 978-1-4614-3423-8.

Aleklett, K. & Campbell, C. J. (2003). The peak and decline of world oil and gas production. *Minerals and Energy,* 18, 5-20. Accessed 2010-10 from http://www.peakoil.net/files/OilpeakMineralsEnergy.pdf

Arvind, C. & Tiwari, G.N. (2010). Stand-alone photovoltaic (PV) integrated with earth to air heat exchanger (EAHE) for space heating/cooling of adobe house in New Delhi (India). *Energy Conversion and Management*, 51(3), 393-409.

Arvind, C., Tiwari G.N. & Avinash, C. (2009). Simplified method of sizing and life cycle cost assessment of building integrated photovoltaic system. *Energy and Buildings*, 41(11), 1172-1180.

Bales, C., Persson, T., Firdler, F., Perers, B. & Zinko, H. (2012). *Solar Heating Systems and Storage.* Compendium for lectures, Solar Energy Research Centre, University of Dalarna, Sweden.

Bernardo, R., Davidsson, H. & Karlsson, B. (2011). Performance Evaluation of a High Solar Fraction CPC-Collector System.

Japanese Society of Mechanical Engineering – *Journal of Environment and Engineering*, 6, 680–692.

Bernardo, R.; Davidsson, H. & Karlsson, B. (2012). Retrofitting Domestic Hot Water Heaters for Solar Water Heating Systems in Single-Family Houses in a Cold Climate: A Theoretical Analysis. *Energies*, 5, 4110-4131.

Bernardo, R., Perers, B., Håkansson, H. & Karlsson, B. (2008). Evaluation of a Parabolic Concentrating PVT system. In proceedings of the 7th Eurosun Conference *Eurosun 2008*, 7-10 october 2008, Lisbon, Portugal.

Blomsterberg, Å. (2012). *Analysis of the Swedish construction industry and training on energy efficient buildings*. Accessed 2013-2 from www.energimyndigheten.se/PageFiles/110/Nul%c3%a4gesanalys.pdf

Brogren, M., Nostell, P. & Karlsson, B. (2001). Optical efficiency of a PV–thermal hybrid CPC module for high latitudes. *Solar Energy,* 69(6), 173-185.

Buckles, W. & Klein, S. (1980). Analysis of solar domestic hot water heaters. *Solar Energy*, 25, 417–424.

Burch, J.; Salasovich, J. & Hillman, T. (2005). Cold-climate solar domestic hot water heating systems: life-cycle analyses and opportunities for cost reduction. In Proceedings of *ISES Conference*, Orlando, Florida, 2005.

Cabeza, L. (2005). *Legionella in Combisystem Tanks*. Outcomes of the International Energy Agency – task 32. Accessed 2012-11 from http://www.iea-shc.org/publications/task.aspx?Task=32

Campbell Scientific (2009). Website of the company accessed 2009-2 from www. campbellsci.com

Chaves, J. & Pereira, M. C. (2000). Ultra flat ideal concentrators of high concentration. *Solar Energy,* 69(4), 269-281.

Chen, I., Hill, J., Ohlemuller, R., Roy, D. & Thomas, C. (2011). Rapid Range Shifts of Species Associated with High Levels of Climate Warming. *Science*, 333, 1024-1026.

Conergy Australia (2009). Homepage of the company, accessed 2009-2 from http://www.conergy.com.au

Coventry, J.S., Franklin, E.T. & Blakers, A. (2002). Thermal and electric performance of a concentrating PV/Thermal collector: results from the ANU CHAPS collector. In proceedings of *Australian and New Zealand Solar Energy Society Conference 2002*. Download available at http://hdl.handle.net/1885/40837.

Cruickshank, C. & Harrison, S. (2004). Analysis of a modular thermal storage for solar heating systems. *Canadian Solar Building Conference*, Proceedings of the Joint Conference of the Canadian

Solar Buildings Research Network and Solar Energy Society of Canada Inc. (SESCI), Montreal, Quebec.

Cruickshank, C. & Harrison, S. (2006). Experimental Characterization of a Natural Convection Heat Exchanger for Solar Domestic Hot Water Systems. *America Society of Mechanical Engineers*, Conference Proceedings, 425–431.

Cruickshank, C. & Harrison, S. (2011). Thermal response of a series- and parallel-connected solar energy storage to multi-day charge sequences. *Solar Energy*, 85, 180–187.

Darelid J., Löfgren, S., & Malmvall B. (2002). Control of nosocomial Legionnaires' disease by keeping the circulating hot water temperature above 55˚C: experience from a 10-year surveillance programme in a district general hospital. *Journal of Hospital Infection*, 50, 213-219.

Davidson, J.& Liu, W. (1998). *Comparison of natural convection heat exchangers for solar water heating systems*. Master's Thesis, University of Winsconsin, Madison, MI, USA. Accessed online 2012-3 from http://digital.library.wisc.edu/1793/7729

Dayan, M. (1997). *High Performance in Low Flow Solar Domestic Hot Water Systems*. Master's Thesis, University of Winsconsin, Madison, MI, USA. Accessed online 2012-3 from http://digital.library.wisc.edu/1793/7729

Duffie, J.A. & Beckman, W. A. (2006). *Solar Engineering of Thermal Process*. John Wiley and sons, inc., Interscience, New York.

Eicker, U. & Pietruschka, D. (2009). Design and performance of solar powered absorption cooling systems in office buildings. *Energy and Buildings*, 41, 81–91.

Enerworks, Solar Thermal Solutions (2009). Homepage of the company, accessed 2009-7 from http://enerworks.com

European Commission (2006). *Photovoltaic geographical information system*. Accessed 2010-09 from http://re.jrc.ec.europa.eu/pvgis/

European Renewable Energy Council (2010). *RE-thinking 2050 – a 100 % renewable energy vision for the European Union*. Accessed 2010-09 from http://www.erec.org/

European Union (2007). *The European Union climate and energy package*. Accessed 2010-09 from http://ec.europa.eu/environment/climat/climate_action.htm

Fahrenbruch, A. & Bube, R. (1983). *Fundamentals of solar cells – Photovoltaic solar energy conversion.* Department of Materials Science and Engineering, Stanford University, Stanford, California. Academic Press Inc., New York, ISBN 0-12-247680-8.

Fanney, A. & Klein, S. (1988). Thermal performance comparisons for solar hot water systems subjected to various collector and heat exchanger flow rates. *Solar Energy*, 40, 1–11.

Federal Institute for Geosciences and Natural Resources (2011). *Reserves, resources and availability of energy resources - BGR 2011*. Accessed 2013-1 from http://www.bgr.bund.de/EN/Themen/Energie/Produkte/annual_report_2011-summary_en.html

Fisher, S., Heidemann, W., Müller-Steinhagen, Perers, B., Berquist, P. & Hellström, B. (2004). Collector test method under quasi-dynamic conditions according to the European Standard EN 12975-2. *Solar Energy,* 76(1-3), 117-123.

Fraser, K., Hollands, K. & Brunger, A. (1995). An empirical model for natural convection heat exchangers in SDHW systems. *Solar Energy*, 55, 75–84.

Furbo, S., 1993. *Test of the components of the solar boiler system from Thermo Dynamics LTD*. Report number 93-20, Thermal Insulation Laboratory, Technical University of Denmark.

Furbo, S., 1994. *Test of the solar boiler system from Thermo Dynamics LTD*. Report number 270, Thermal Insulation Laboratory, Technical University of Denmark.

Furbo, S., Vejen, N. & Shah, L.J. (2005). Thermal Performance of a Large Low Flow Solar Heating System With a Highly Thermally Stratified Tank. *Journal of Solar Energy Engineering*, 127, 15–20.

Government Bill (2008). *En sammanhållen klimat – och energipolitik – Energi*. Report number 2008/9: 163, accessed 2009-09 from http://www.sweden.gov.se/content/1/c6/12/27/85/65e0c6f1.pdf

Green, M. A. (1998). *Solar Cells - Operating Principles, Technology and System Apllications*. University of New South Wales, Australia.

Hang, Y., Qu, M. & Zhao, F. (2012). Economic and environmental life cycle analysis of solar hot water systems in the United States. *Energy and Buildings*, 45, 181-188.

Hausner, R. & Fink, C. (2002). *Stagnation behaviour of solar thermal systems*. International Energy Agency, Solar Heating and Cooling Program, task 26.

Heimrath, R.; Haller, M. (2007). *The Reference Heating System, the Template Solar System of Task 32*; International Energy Agency: Paris, France. Accessed online 2012-12 from: http://archive.iea-shc.org/publications/task.aspx?Task=32.

Helgesson, A. (2004). *Optical Characterization of Solar Collectors from Outdoor Measurements*. Licentiate thesis, Lund Technical University, ISBN 91-85147-07-9.

Helgesson, A., Karlsson, B. & Nordlander, S. (2002). Evaluation of a Spring/Fall-MaReCo. In proceedings of *Eurosun 2002,* Bologna.

Hobbi, A. & Siddiqui, K. (2009). Optimal design of a forced circulation solar water heating system for a residential unit in cold climate using TRNSYS. *Solar Energy*, 83, 700–714.

International Energy Agency (2012). *Technology Roadmaps: Solar Heating and Cooling*. Accessed online 2012-11 from http://www.iea.org/publications/freepublications/publication/name,28277,en.html

International Energy Agency Statistics (2009). *Electricity information 2009*. Accessed 2010-09 from http://www.iea.org/

IPCC – Intergovernmental Panel for Climate Change (2007). *Assessment Report 4*. Accessed 2010-10 from http://www.ipcc.ch/pdf/assessment-report/ar4/syr/ar4_syr.pdf

IPCC – Intergovernmental Panel for Climate Change – Working Group 1 (2010). *Latest Findings to be assessed by WGI in AR5.* Accessed 2010-10 from http://www.ipcc.ch/pdf/presentations/COP15-presentations/stocker09unfcccCopenhagen_delegate_new.pdf

Kamstrup (2009). Website of the company accessed 2009-2 from www.kamstrup.com

Kipp&Zonnen (2009). Website of the company accessed 2009-2 from www.kippzonnen.com

Kjellsson, E. (2002). *Solar heating systems for electrically heated houses*. Report number U 02:86, Vattenfall AB.

Kjellsson, E. (2009). *Solar Collectors Combined with Ground-Source Heat Pumps in Dwellings – Analyses of System Performance*. Doctoral thesis, Lund Technical University, Building Physics, TVBH-1018, ISBN 978-91-88722-40-9.

Klein, S.A., Beckman, W.A., Mitchell, J.W., Duffie, J.A., Daffie, N.A. & Freeman, T.L. (2006). *TRNSYS, a Transient System Simulation Program*. Solar Energy Laboratory, University of Wisconsin, Madison.

Kostić, Lj. T., Pavlović, T. M. & Pavlović, Z. T. (2010). Optimal design of orientation of PV/T collectors with reflectors. *Applied Energy,* 87, 3023-3029.

Kothdiwala, A., Norton, B. & Eames, P. (1995). The effect of variation of angle of inclination on the performance of low-concentration-ratio compound parabolic concentrating solar collectors. *Solar Energy*, 55(4), 301-309.

Krohn, P. & Karlsson, B. (2003). *Solar heating system for directily heated single-family houses*. Vattenfall Utveckling AB, Research and Development Program for solar heating 2001-2003.

Ku, H. (1966). Notes on the use of propagation of error formulas. *Journal of Research of the National Bureau of Standards*, 70C (4), 263- 273. Accessed online 2012-8 from http://nistdigitalarchives.

contentdm.oclc.org/cdm/compoundobject/collection/p13011coll6/id/78003/rec/5

Lawrence Berkeley National Laboratory in University of California GenOpt—Generic Optimization Program. Accessed online 2011-6 from http://gundog.lbl.gov/GO

Leidig, K., (2001). Risk of Legionnaires' disease in Solar Water Heaters - Status report. Proceedings of the International National Agency – *Legionella Workshop*, Delft, The Netherlands, October 2001.

Lin, Q. (1998). *Analysis, Modelling and Optimum Design of Solar Domestic Hot Water Systems*. Ph.D. thesis, ISBN 87-7877-023-8.

Liu, W. & Davidson, J. (1995). Comparison of Natural Convention Heat Exchangers for Solar Water Heating Systems. In proceedings of *American Solar Energy Society Conference 1995*. Download available at http://www.p2pays.org/ref/20/19434.pdf

Lund University (2005). Official website accessed 2013-1 from http://www.lu.se/nyheter-och-press/pressmeddelanden?visa=pm&pm_id=395

Marchesi, I., Marchegiano, P., Bargellini, A., Cencetti, S., Frezza, G., Miselli, M. & Borella P. (2011). Effectiveness of different methods to control legionella in the water supply: ten-year experience in an Italian university hospital. *Journal of Hospital Infection*, 77, 47-51.

Michael, B., Theresa, G., Kathi, R., Heidi, S. & Pat, L. (2007). High-Performance Home Technologies: Solar Thermal and Photovoltaic Systems. In *Building America's Best Practices Series*, 6, U.S. Department of Energy. Accessed online 2012-7 from http://www1.eere.energy.gov/solar/solar_buildings.html

Michaelides, I. & Wilson, D. (1997). Simulation studies of the position of the auxiliary heater in thermosyphon solar water heating systems. *Renewable Energy*, 10, 35–42.

Mills, D. & Morrison, G. (2003). Optimisation of minimum backup solar water heating system. *Solar Energy,* 74(6), 505-511.

Mondol, J. & Smyth, M. (2012). Comparative Performance Analysis of Solar Heat Exchangers for Solar Domestic Hot Water Systems. In proceedings of *Eurosun ISES Conference 2012*, Rijeka, Croatia.

Morrison, G. & Tran, H. (1984). Simulation of the long term performance of thermosyphon solar water heaters. *Solar Energy*, 33, 515–526.

Nilsson, J., Håkansson, H. & Karlsson, B. (2007). Electrical and thermal characterization of a PV-CPC hybrid. *Solar Energy,* 81(7), 917-928.

Nordlander, S. (2004). *Load Adapted Solar Thermal Combisystems – Optical Analysis and Systems Optimization*. Licentiate thesis, Uppsala University, Sweden, ISSN 0346 - 8887.

Ogueke, N., Anyanwu, E. & Ekechukwu, V. (2009). A review of solar water heating systems. *Journal of Renewable and Sustainable Energy*, 1, 106-121.

Open Access Scholarly Publisher Association, 2013. Website accessed 2013-1 from http://oaspa.org/membership/code-of-conduct/

Paradignma, (2012). Home page of the company accessed 2012-11 from http://www.paradigma.de/solaranlage/aquasystem

Pentronic (2009). Website of the company accessed 2009-2 from www.pentronic.se

Perers, B. (1993). Dynamic method for solar collector array testing and evaluation with standard database and simulation programs. *Solar Energy,* 50(6), 517-526.

Perers, B. (1997). An improved dynamic solar collector test method for determination of non-linear optical and thermal characteristics with multiple regression. *Solar Energy,* 59, 163-178.

Persson, T. (2006). *Combined solar and pellet heating systems for single-family houses*. Doctoral thesis, Technical University of Stockholm, ISBN 91-7178-538-8.

Qin, L. (1998). *Analysys, modeling and optimum design of solar domestic hot water systems*. Ph.D. Thesis, Danish Technical University, Copenhagen, Danmark.

Rogers, J., Dowsett, A., Dennies, P., Lee, V. & Keevil, C., (1994). Influence of Temperature and Plumbing Material Selection on Biofilm Formation and Growth of Legionella pneumophila in a Model Potable Water System Containing Complex Microbial Flora. *Applied and Environmental Microbiology*, 60 (5), 1585-1592.

Sick, F. & Erge, T. (1998). *Photovoltaic in buildings: a design handbook for architects and engineers.* International Energy Agency task 16. ISBN 1 873936 59 1, pp 27-28.

Solar Collector, 2010. Software developed by Bengt Hellström and Hasse Kvist at the Energy and Building Design Division, Lund Technical University, Sweden.

Sophie, T. (2007). *Advanced and Sustainable Housing Renovation Handbook, a guide for designers and planners*. Accessed 2010-11 on http://www.iea-shc.org/publications/task.aspx?Task=37

Stengård, L. (2009). *Mätning av kall- och varmevattenanvändning i 44 hushåll*. Accessed online 2009-10 from http://webbshop.cm.se/System/ViewResource.aspx?p=Energimyndigheten&rl=default:/Resources/Permanent/Static/b9a064ece4d747868b5c20d1a03ab0a2/2124W.pdf

Swedish Building Regulations (2001). *Is there Legionella Bacteria in Your Waterpipes?* Accessed 2012-7 from http://www.boverket.se/Om-

Boverket/Webbokhandel/Publikationer/2001/Is-there-Legionella-Bacteria-in-Your-Waterpipes-/

Swedish Building Regulations (2012). *Evaluation of the Swedish subsidy for solar heating technology.* Report 2012:9, ISBN: 978-91-87131-20-2.

Swedish Energy Agency (2009). *FEBY – Krav Specifikation för Minienergihus.* Accessed 2010-01 from http://www.nollhus.se/dokument/Kravspecifikation%20FEBY12%20-%20bostader%20sept.pdf

Swedish Energy Agency (2011a). *Energy in Sweden 2011*. Accessed 2013-01 from http://webbshop.cm.se/System/TemplateView.aspx?p=Energimyndigheten&view=default&id=e872f0ba87dd41ce983e6cc5725393fd

Swedish Energy Agency (2011b). *Energy statistics for one- and two-dwelling buildings in 2011*. Accessed 2013-01 from http://www.energimyndigheten.se/sv/Press/Pressmeddelanden/Pressmeddelanden-2011/Ny-regional-energistatistik-for-smahus/

Swedish Energy Agency (2012a). *Space heating in Sweden 2012*. Report number EI R2012:09. Accessed 2013-01 from http://www.energimyndigheten.se/sv/Press/Pressmeddelanden/Pressmeddelanden-2012/Sallan-lonsamt-att-byta-fran-fjarrvarme/

Swedish Energy Agency (2012b). *Energy in Sweden 2012*. Accessed 2013-01 from http://webbshop.cm.se/System/TemplateView.aspx?p=Energimyndigheten&view=default&id=ac3bcc6d1511459390d08f89568c2415

Swedish Industrial Rules, 2011. *Safe water installations*. Safe Water, accessed 2012-7 from http://www.sakervatten.se/Branschregler

Swedish Technical Research Centre (2012). *Annual solar fraction for solar water heating systems*. Accessed online 2012-3 from http://www.sp.se/sv/index/services/solar/water/list/Sidor/default.aspx

Thermo Dynamics Ltd (2009). Homepage of the company, accessed 2009-5 on http://www.thermodynamics.com

The Research Council of Norway (2013). Official website accessed 2013-01 from http://www.forskningsradet.no/en/Newsarticle

The Swedish Social Board (2013). Official website accessed 2013-02 from http://www.socialstyrelsen.se/halsoskydd/vatten/legionella/skotselavvattensystem

Tripanagnostopoulos, Y. & Souliotis, M. (2004). Integrated collector storage solar systems with asymmetric CPC reflectors. *Renewable Energy*, 29, 223-248.

Tripanagnostopoulos, Y., Yianoulis, P., Papaefthimiou, S. & Zafeiratos, S. (2000). CPC solar collectors with flat bifacial absorbers. *Solar Energy*, 69, 191-203.

Tsilingiris, P.T. (1996). Design and performance of large low-cost solar water heating systems. *Renewable Energy*, 9, 617–621.

TRNSYS (2010). TRNSYS official website accessed 2010-09 from http://sel.me.wisc.edu/trnsys/

Värmebaronen (2009). Homepage of the company, accessed 2009-8 on http://www.varmebaronen.se/

Weiss, W. (2007). *Solar Heating Systems for Houses—A Design Handbook for Solar Combisystems*; James and James (Science Publishers) Ltd.: London, UK.

Wenham, S. R., Green, M. A., Watt, M. E. & Corkish, R. (2007). *Applied Photovoltaics.* University of New South Wales, School of Photovoltaic and Renewable Energy Engineering, Australia.

Wetter, M, 2009. *Generic Optimization Program Manual 3-0-2*; Simulation Research Group, Lawrence Berkeley National Laboratory: Berkeley, USA. Accessed online 2011-4 from http://engine4.org/g/genopt-generic-optimization-program-user-manual-w316-pdf.pdf

Widén, J., Lundh, M., Vassileva, I., Dahlquist, E., Ellegård, K. &Wäckelgård, E. (2009). Constructing load profiles for household electricity and hot water from time-use data—Modelling approach and validation. *Energy and Buildings*, 41(7), 753-768.

Winston, R., Miñano, J. & Benítez, P. (2005). *Nonimaging Optics*. Elsevier Academic Press, 200 Wheeler Road, 6th floor, Burlington, U.S.A., ISBN 0-12-759751-4.

Winsun Educational Software (2009). Software developed by Perers, B. at SERC, Dalarna University, Sweden. http://www.serc.se

Wolferen, H (2001). Legionella in hot tap water production. Proceedings of the International National Agency – *Legionella Workshop*, Delft, The Netherlands, October 2001.

Wongsuwan, W. & Kumar, S. (2005). Forced circulation solar water heater performance prediction by TRNSYS and ANN. *International Journal of Sustainable Energy*, 24, 69–86.

World Energy Council (2007). *Survey of Energy Resources 2007*. Accessed 2010-01 from http://www.tsl.uu.se/uhdsg/Data/WEC2007.pdf

World Energy Council (2010). *Survey of Energy Resources 2010*. Accessed 2013-01 from http://www.worldenergy.org/publications/3040.asp

Article I

Available online at www.sciencedirect.com
ScienceDirect
Solar Energy 85 (2011) 1499–1510
SOLAR ENERGY
www.elsevier.com/locate/solener

Performance evaluation of low concentrating photovoltaic/thermal systems: A case study from Sweden

L.R. Bernardo *, B. Perers, H. Håkansson, B. Karlsson

Energy and Building Design Division, Lund Technical University, Box 118, SE-221 00 Lund, Sweden

Received 1 February 2010; received in revised form 26 October 2010; accepted 6 April 2011
Available online 30 April 2011

Communicated by: Associate Editor C. Estrada-Gasca

Abstract

Some of the main bottlenecks for the development and commercialization of photovoltaic/thermal hybrids are the lack of an internationally recognized standard testing procedure as well as a method to compare different hybrids with each other and with conventional alternatives. A complete methodology to characterize, simulate and evaluate concentrating photovoltaic/thermal hybrids has been proposed and exemplified in a particular case study. By using the suggested testing method, the hybrid parameters were experimentally determined. These were used in a validated simulation model that estimates the hybrid outputs in different geographic locations. Furthermore, the method includes a comparison of the hybrid performance with conventional collectors and photovoltaic modules working side-by-side. The measurements show that the hybrid electrical efficiency is 6.4% while the optical efficiency is 0.45 and the *U*-value 1.9 W/m^2 °C. These values are poor when compared with the parameters of standard PV modules and flat plate collectors. Also, the beam irradiation incident on a north–south axis tracking surface is 20–40% lower than the global irradiation incident on a fixed surface at optimal tilt. There is margin of improvement for the studied hybrid but this combination makes it difficult for concentrating hybrids to compete with conventional PV modules and flat plate collectors.

Keywords: Evaluate solar hybrids; Photovoltaic thermal concentrators; PVT

1. Introduction

The overall problem with the use of photovoltaic (PV) systems is the high cost of the solar cells. This makes it attractive to concentrate irradiation on the PV module in order to minimise the required cell area for the same output. With increased light concentration, there will be a demand for increased cooling of the PV cells in order to lower the working temperature, prevent damage and maintain cell efficiency (Nilsson et al., 2007). Usually, a photovoltaic/thermal (PVT) concentrating system tracks and concentrates light into a water/air-cooled photovoltaic module working as a thermal absorber. Hence, not only electricity is generated from the absorber but also heat. The production of both heat and electricity is favored by lowering the operating temperature; however, a minimum water temperature, which raises the working temperature on the cells, is generally required by the given application (Affolter et al., 2004). At the end, a life cycle cost analysis is necessary to determine whether the concentrating system reduced the unit cost of produced electricity (Arvind and Tiwari, 2010; Arvind et al., 2009).

Concentrating hybrid design is an emerging technology and there are still constraints to its development and commercialization. One of the most important is the lack of an internationally accepted method to test these devices (Affolter et al., 2004). Traditionally, steady-state thermal models are used to predict the annual performance but recent studies have been introducing the use of dynamic

* Corresponding author. Tel.: +46 462227606; fax: +46 462224719.
E-mail address: Ricardo.Bernardo@ebd.lth.se (L.R. Bernardo).

0038-092X/$ - see front matter © 2011 Elsevier Ltd. All rights reserved.
doi:10.1016/j.solener.2011.04.006

Nomenclature

Monitored parameters

$P_{thermal}$	hybrid thermal power (W/m^2)
$P_{electric}$	hybrid electric power (W/m^2)
G_b	beam irradiance (W/m^2)
G_d	diffuse irradiance (W/m^2)
T_{in}	inlet temperature (°C)
T_{out}	outlet temperature (°C)
T_{amb}	ambient temperature (°C)
dV/dt	flow (m^3/s)
C_p	heat capacity (water) (J/kg °C)
ρ	density (water) (kg/m^3)
A_{Hybrid}	total glazed collector area (m^2)
$A_{active\ elect.}$	electric active glazed area
$A_{active\ thermal}$	thermal active glazed area
τ	transmittance coefficient of the glass (–)
r	reflectance coefficient of the reflector (–)
α	absorptance coefficient of the solar cells(–)

Parameters in the collector model

η_{od}	diffuse efficiency (%)
$\eta_{ob\_thermal}$	beam thermal optical efficiency (%)
$\eta_{ob\_electric}$	beam electric optical efficiency (%)
a_1	heat loss factor (W/m^2 °C)
a_2	temperature dependence of heat loss factor (W/m^2 °C^2)
$K_{ta\_thermal}$	thermal angle of incidence modifier for beam irradiance (–)
$K_{ta\_electric}$	electric angle of incidence modifier for beam irradiance (–)
$b_{o\_thermal}$	thermal angular coefficient (–)
$b_{o\_electric}$	electric angular coefficient (–)
$K_{diffuse}$	diffuse incident angle modifier (–)
K_T	electric efficiency temperature dependence (%/°C)
θ	angle of incidence onto the collector (°)

models as well (Chow, 2003). However, there is not an established method of comparing different hybrids with each other or with a traditional side-by-side system made of standard flat plate collectors and PV modules. Furthermore, there exist very few evaluations on the electric and thermal efficiency of tracking concentrating hybrids. Since there are a small number of commercialized systems, there is also a need for experimental data exchange so it is possible to draw general conclusions about concentrating hybrid performance.

For a better understanding of the conducted work in a particular case study and its contributions to the field, the main objectives of the paper are summarised below:

- To propose a testing method to characterize concentrating photovoltaic/thermal hybrids.
- To suggest a series of simulations and performance analysis for different latitudes based on the results from the testing method.
- To compare the hybrid performance with conventional PV modules and solar collectors.

Thus, several conclusions can be drawn concerning the performance of the tested concentrating hybrids, their possible applications and viability in different climates and locations.

2. Method

2.1. Experimental setup and hybrid design

This photovoltaic/thermal parabolic concentrating system tracks and concentrates light into a water-cooled photovoltaic module working as a thermal absorber. By using the heat generated in the absorber, the photovoltaic/thermal device generates not only electrical, but also thermal energy (Fig. 1). The PVT system consists of a photovoltaic module, thermal absorber, parabolic reflector, tracking system, glazed protection and supporting structure (Fig. 2). Two sections form the photovoltaic module, each one with 32 series connected cells laminated on both sides of the V-shaped thermal absorber. These sections can be interconnected both in series and parallel. The photovoltaic cells, which are specially designed for concentrated light, are made of monocrystalline silicon and have a nominal efficiency of 16% at 25 °C (Absolicon Solar Concentrator AB, 2008). The total surface area of the cells is 0.33 m^2. Water runs inside the aluminum thermal absorber where the cells are laminated. The parabolic reflector is made of a silver coated plastic film laminated on a steel sheet with a reflectance factor of 90% (Alanod Solar, 2010). The geometrical concentration ratio of the reflector is $C = 7.8$. It is important to notice that the reflector is 40 cm longer than the absorber at the edges to also make use of the irradiation in the morning and afternoon. The tracking is carried out by rotating the structure around an axis oriented in the east–west direction. The adjustment of the tilt angle is carried out periodically according to the calculated position of the sun. The parabolic trough is covered by a 4.6 m^2 glass pane with a measured transmission coefficient of 90% (Bernardo, 2007).

In this study, two hybrid areas were defined: total glazed area and active glazed area. For this particular hybrid the total glazed area (A_{Hybrid}) equals 4.6 m^2. Active glazed area was defined as the maximum glazed area that the system can make use of. This excludes surface areas where it is impossible for the irradiation to reach the absorber such as frames and gaps between solar cells and reflector edges which are longer than the absorber (Fig. 1). The electric and thermal active glazed areas are different since the

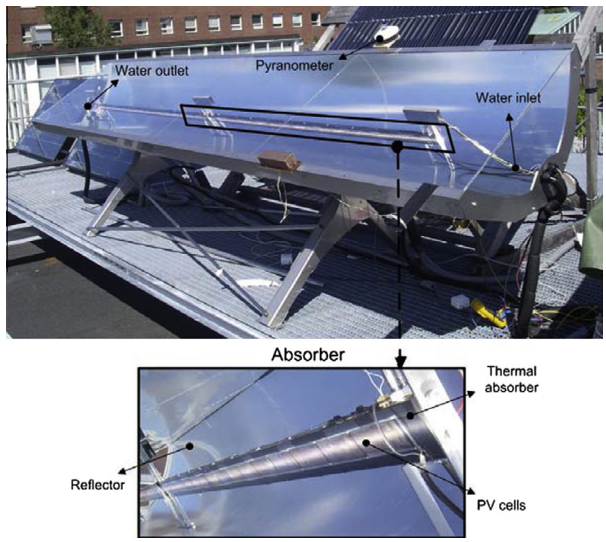

Fig. 1. PVT concentrator trough and photovoltaic cells laminated on one side of the thermal absorber.

thermal absorber is wider than cells. The electric active glazed area ($A_{\text{active elect.}}$) is 3.5 m^2 while the thermal active glazed area ($A_{\text{active thermal}}$) equals 3.7 m^2.

The relative uncertainties of the measuring instruments stated by the manufacturers are estimated for ideal measurement and installation conditions. In practice, somewhat higher relative uncertainties were assumed in order to take into account a safety margin that includes inaccuracies related to the installation and operation of those instruments at our laboratory. The pyranometer relative uncertainty was assumed to be ±2%, the flow meter ±1% and the Pt100 temperature measurement ±2%. The temperature dependence of the heat capacity and specific mass of the water was taken into account in the calculations. Hence, using the standard method of the square root of the quadratic sum for the uncertainty propagation, the global uncertainty of the efficiency measurements was estimated to be 3%.

2.2. Procedure

2.2.1. Testing and characterization method

The testing and characterization method can be seen as a modified solar collector testing method described in the following steps:

(a) Simultaneous monitoring of heat and power where the photovoltaic module operates continuously at maximum power point.
(b) Characterization of the thermal collector according to the steady-state test method (Fisher et al., 2004).
(c) Characterization of the photovoltaic module at high irradiances and variable working temperatures.
(d) Description of the thermal and electrical incidence angle modifier during one day with stable high solar intensity.
(e) Using the previous tested parameters to generate a mathematical steady-state model capable of accurately describing the thermal and electrical outputs.
(f) Validation of the model by comparison between measurements and model outputs during days with varying weather conditions.

Both the electrical and thermal outputs were measured every 6 min for different temperature conditions in the collector. The maximum electric power output extracted by the hybrid was calculated based on periodical *I–V* curve measurements. Using this value together with the incident beam irradiation, the system electrical efficiency as a function of its working temperature was determined. In reality, it is expected that an electric load is permanently connected to the PV cells and electric power is continuously extracted at maximum power point. However, measuring *I–V* curves instantaneously simplifies the whole test procedure, making it cheaper, less time consuming while still achieving an accurate result. If an electric load was continuously connected, the absorber would be colder since part of the incoming radiation would be converted to electricity. In this case, the outlet water temperature would be slightly lower than the one measured. This difference is very small and has little impact on the results. In this specific case, since the structure is closed, it was not possible to measure

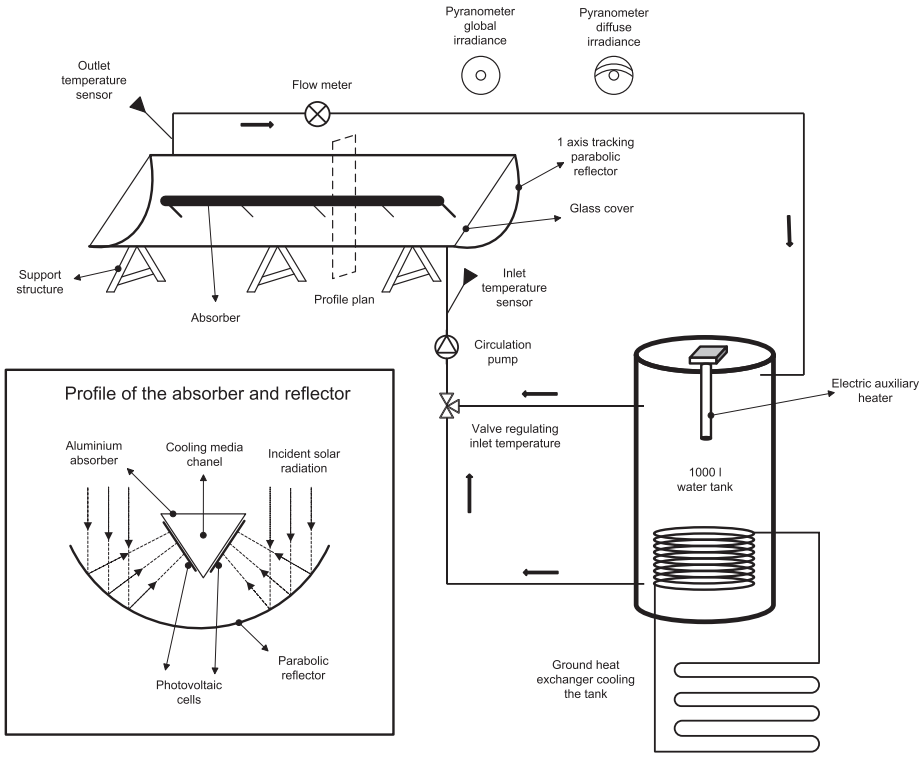

Fig. 2. Schematic diagram of the experimental setup system and its monitoring points.

the cell temperature directly. Instead, the temperature of the outlet water, running inside the thermal absorber at the moment of the electrical efficiency measurement, is presented. This is the temperature limiting the whole electric output since the cells are series connected.

Since there is no electric load continuously connected to the hybrid, all the incoming irradiation is used to produce heat. This output was calculated by Eq. (1) (Duffie and Beckman, 2006) where the monitored parameters are described in the nomenclature section at the beginning of the paper.

$$P = (\rho dV/dt \cdot C_p \cdot (T_{out} - T_{in})/A_c)(W/m^2) \quad (1)$$

The thermal power was then obtained by subtracting the measured electric power from this heat output. The incidence angle modifier (K_{ta}) for the thermal and electric efficiency was calculated with Eq. (2) (Duffie and Beckman, 2006).

$$K_{ta}(\theta) = \frac{\eta_{0b}(\theta)}{\eta_{0b}(\theta \approx 0)} \quad (2)$$

The function generally used to fit the incidence angle modifier data between 0° and 60° is given by Eq. (3) (Duffie and Beckman, 2006). The parameter b_0 shapes the curvature of the function, setting higher or lower incidence angle modifier values for the same incidence angle.

$$K_{ta}(\theta) = 1 - b_0 * \left(\frac{1}{\cos(\theta)} - 1\right) \quad (3)$$

The hybrid was continuously tested at the Energy and Building Design laboratory of Lund Technical University in Sweden (latitude 55°44′N, longitude 13°12′E) during the period 1/06/2008–13/09/2008.

2.2.2. Simulation model

By analyzing the measured data, one can determine the hybrid parameters and develop simple mathematical models capable of describing its behavior and estimate its outputs for any geographic location. The monitored parameters and the model equations are presented in Eqs. (4)–(9) (Duffie and Beckman, 2006).

$$P_{thermal} = \eta_{ob\_thermal} \cdot K_{ta\_thermal} \cdot G_b + \eta_{od} \cdot G_d - a_1 \cdot ((T_{out} + T_{in})/2 - T_{amb}) - a_2 \cdot ((T_{out} + T_{in})/2 - T_{amb})^2 \quad (4)$$

where $K_{ta\_thermal} = 1 - b_{o\_thermal} \cdot (1/\cos\theta - 1)$ (5)

$$\eta_{od} = K_{diffuse} \cdot \eta_{ob\_thermal} \quad (6)$$

$$P_{electric} = (\eta_{ob\_electrical(25\,^\circ C)} \cdot K_{ta\_electric} \cdot G_b + \eta_{od} \cdot G_d) - (K_T \eta_{ob\_electrical(25\,^\circ C)} \cdot G_b (T_{out} - 25)) \quad (7)$$

where $K_{ta\_electric} = 1 - b_{o\_electric} \cdot (1/\cos\theta - 1)$ (8)

$$\eta_{od} = K_{diffuse} \cdot \eta_{ob\_electric} \quad (9)$$

The hybrid parameters were then fed into *Winsun* (Winsun Villa Software, 2009), a TRNSYS based simulation software developed by Bengt Perers which estimates the annual thermal and electrical outputs using the described model. It is important to notice that all calculations represent collector outputs not taking into account the whole electric and thermal system. Hence, system distribution, storage losses, array shading effects and load distribution are not taken into account either. Only the energy produced by the collectors was estimated.

2.2.3. Comparison with conventional PV modules and thermal collectors

In order to compare the hybrid performance with standard thermal collectors and photovoltaic modules, simulations were also carried out for these standard components. It was assumed that the produced hot water should be used for domestic hot water applications since this can represent 90% of the potential market for these hybrids (Affolter et al., 2004). Therefore, the output temperature from the collectors should be around 65–70 °C which was assumed to imply 40 °C of mean absorber temperature depending on the flow and irradiation levels. Consequently, the hybrid solar cells, but not the individual PV module, would work at 65–70 °C. As the PV module is independent from the flat plate collector it was assumed that it could work at around 25 °C. In order to understand how the hybrid performance would change if it was used for low temperature applications, simulations were also carried out for pool heating. For this application it was assumed that the required outlet temperature would be around 30 °C which was estimated to imply 20 °C average water temperature in the hybrid since the cold water inlet is around 10 °C. The diffuse incidence angle modifier ($K_{diffuse}$) was calculated as being the inverse of the geometrical concentration ratio ($1/C$ where $C = 7.8$) (Winston et al., 2005). All the parameters for the side-by-side system were assumed to be common values for standard components.

3. Measurement results

3.1. Electrical and thermal output interaction

One of the most important aspects to take into account when studying photovoltaic/thermal hybrids is the interaction between electrical and thermal outputs (Affolter et al., 2004). When an electric load is connected to the electric circuit, electric and thermal power is extracted. This means that part of the incoming irradiation is transformed into electricity by the PV cells instead of being absorbed by the thermal receiver. Hence, the thermal output decreases as much as the extracted electrical energy. During this experiment, an electric load was connected to the PV modules during a part of the day extracting the maximum possible power from the cells. By analysing Fig. 3, one can understand the interaction between the thermal and electrical outputs of a PVT hybrid system. The outputs were calculated for total glazed area.

3.2. Electrical performance

In Fig. 4 the system electrical beam efficiency as a function of the water outlet temperature is presented. Based on this data, several collector parameters were calculated and

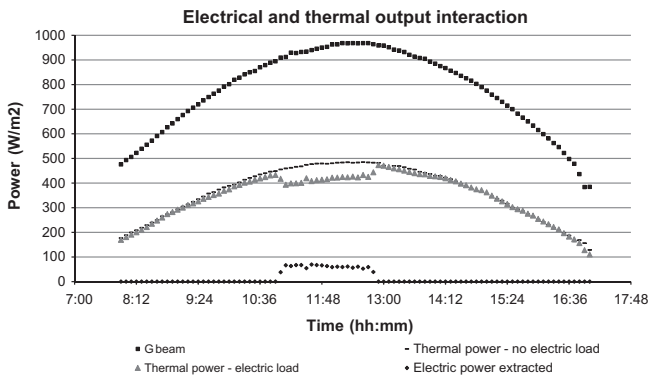

Fig. 3. Electric and thermal outputs interaction measured on two clear days with and without electric load. Power outputs per total glazed area ($A_{Hybrid} = 4.6\ m^2$).

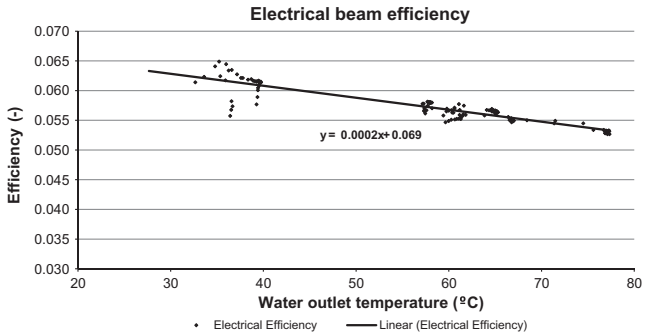

Fig. 4. Electrical beam efficiency calculated per total glazed area for different working temperatures and beam irradiation higher than 900 W/m^2.

Table 1
Measured electrical efficiency $\eta_{electric}$ (–), loss coefficient K_T (%/°C) and electrical peak power per total and active glazed area.

Electrical parameters	Expressed by total glazed area ($A_{Hybrid} = 4.6$ m^2)	Expressed by active glazed area ($A_{active\ elect} = 3.5$ m^2)
$\eta_{b\ electric}$ at 25 °C (%)	6.4 %	8.4 %
K_T (%/°C)	0.3 %/°C	0.3 %/°C
Peak power (W/m^2)	61 W/m^2	81 W/m^2

presented in Table 1. The measured electrical efficiency is 6.4% at 25 °C water outlet temperature while the electric efficiency temperature dependence equals 0.3%/°C. The measured total peak power was 61 W/m^2 of total glazed area at 28 °C inlet and 39 °C outlet water temperature and 997 W/m^2 incident beam radiation.

3.3. Thermal performance

The measured thermal beam efficiency as a function of the working temperature and incident radiation is presented in Fig. 5. Using linear approximation, the hybrid beam optical efficiency (η_{0b}) and the heat loss coefficient (U) were determined and are shown in Table 2. They equal 0.45 and 1.9 W/°C m^2 of total glazed area. The measured thermal peak power was 435 W/m^2 of total glazed area at the same conditions described above.

3.4. Incidence angle modifier

During the morning and afternoon, the reflection losses at the glass cover and absorber increase due to high angles of incidence. This effect causes a thermal and electrical output drop in the system. The measured sensitiveness of the thermal and electrical efficiency to the increase in the angle of incidence is presented in Fig. 6. The measured b_0 fitting the thermal and electric data was 0.14 and 0.28 respectively

Table 2
Measured beam optical efficiency η_{0b} (–), heat loss coefficient U (W/m^2 °C) and thermal peak power per total and active glazed area.

Thermal parameters (PV-ON)	Expressed by total glazed area ($A_{Hybrid} = 4.6$ m^2)	Expressed by active glazed area ($A_{active\ thermal} = 3.7$ m^2)
η_{0b}(–)	0.45	0.56
U (W/m^2 °C)	1.9 W/m^2 °C	2.3 W/m^2 °C
Peak power (W/m^2)	435 W/m^2	541 W/m^2

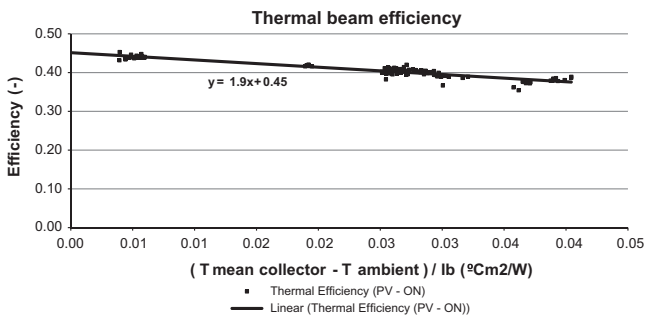

Fig. 5. Thermal beam efficiency calculated per total glazed area for different working temperatures and beam irradiation higher than 900 W/m^2.

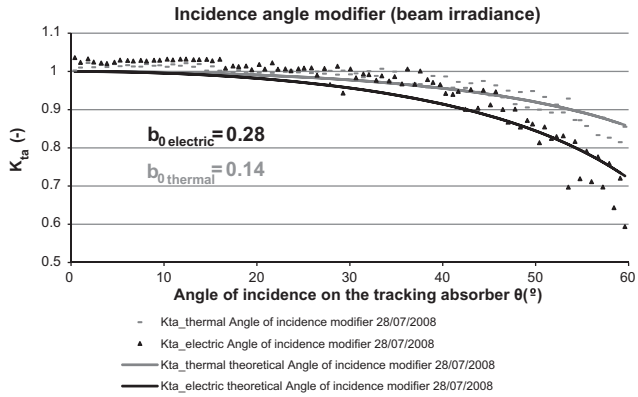

Fig. 6. Thermal and electrical incidence angle modifier for beam radiation during one clear day and $\theta < 60°$.

Table 3
Parameters for electricity production used in the simulations, expressed by total glazed area.

Model electrical parameters	η_{0b} (–)	$K_{diffuse}$ (–)	K_T (%/°C)	$b_{o\_electric}$ (–)
Hybrid electric (25 °C)	0.064	0.13	0.3 %/°C	0.28
PV module (25 °C)	0.16	0.9	0.4%/°C	0.10

Table 4
Parameters for hot water production used in the simulations, expressed by total glazed area.

Model thermal parameters	η_{0b} (–)	$K_{diffuse}$ (–)	a_1 (W/m^2 °C)	a_2 (W/m^2 °C^2)	$b_{o\_thermal}$ (–)
Hybrid thermal (PV-ON)	0.45	0.13	1.9	0	0.14
Flat plate collector	0.8	0.9	3.6	0.014	0.15

showing that higher angles of incidence have a greater impact on the electrical performance. This is mainly due to two effects. Firstly, at high angles of incidence in the morning and afternoon, the reflector edges will not redirect the incoming light to the whole length of the absorber. Hence, from the moment that the first cell in the absorber edge is not fully illuminated, the whole electrical output is affected. These are known as edge and shadow effects. Secondly, optical imprecision and tracking inaccuracies become more relevant at high angles of incidence. This effect is not as sensitive to heat as it is for electricity production since the cells are series connected and the thermal absorber is also wider.

3.5. Model validation

The hybrid measured parameters are summarized in Tables 3 and 4. The corresponding generated thermal

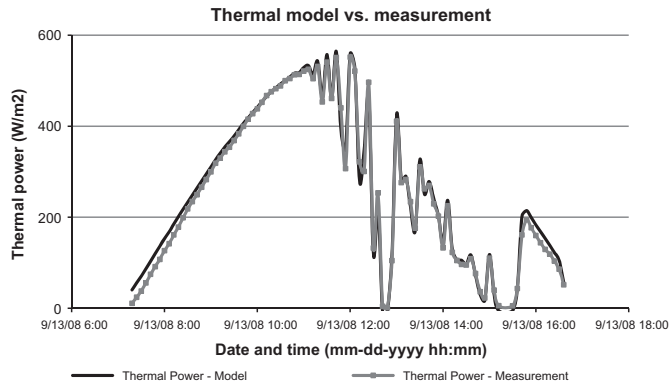

Fig. 7. Thermal model and measurements during unstable irradiation day.

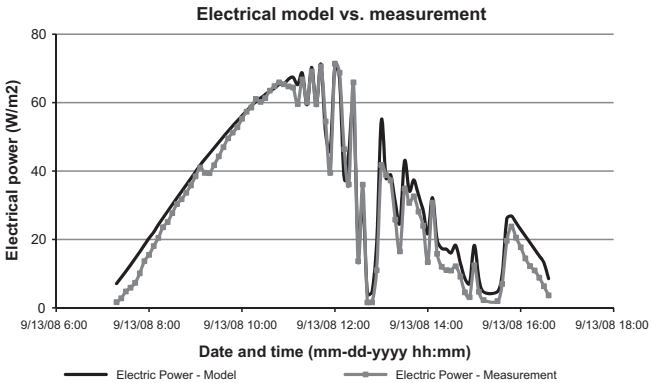

Fig. 8. Electrical model and measurements during unstable irradiation day.

and electric power outputs illustrated in Figs. 7 and 8 show that good agreement between model and measurements has been achieved even during unstable days, validating the models.

4. Performance analysis

Following the measurement test method described previously, a performance analysis procedure is proposed in this section: simulation of the annual performance for different latitudes and performance comparison with separate standard photovoltaic modules and thermal collectors.

4.1. Tracking system

The tested hybrid system is thought to work with its tracking axis oriented in the east–west direction. Simulations were carried out to estimate the received irradiation by a tracking surface with the axis horizontally oriented in both the east–west and north–south directions for several climates at different latitudes. The results are given in Table 5. Analysing the results, one can conclude that it is always better to track the sun around an axis in the north–south direction, independently on the geographical position. (10–20% better) This effect is even more relevant when the system is moved closer to the equator where the sun reaches higher altitudes. All the following simulations take into account this result, estimating the annual outputs as the hybrid would be tracking the sun in a more productive way with its axis in the north–south direction.

As it is known, concentrating solar systems can only make use of a fraction of the diffuse light. In contrast, non-concentrating systems like standard PV modules and flat plate collectors use the global irradiation. The concentrator can make use of the beam irradiation plus ($1/C$) of the diffuse irradiation ($G_b + G_d/C$) (Winston et al., 2005). This comparison is presented in Table 5. The global irradiation incident on a static surface is higher than the beam irradiation on a one-axis tracking concentrating surface. This means that, independently of its location, a non-concentrating fixed collector receives more usable irradiation than a tracking concentrating one like the studied hybrid (roughly 20–40% in this case). Closer to the equator, the beam irradiation values are higher and this result becomes less accentuated. This is even clearer as the concentration ratio increases.

4.2. Annual performance results

Based on the system parameters previously presented in Tables 3 and 4, the total annual performance for the hybrid and the traditional side-by-side system were calculated for the 3 different climates. These results are presented in Table 6. For Stockholm, the hybrid electric and thermal annual output is 45.1 kW h/m^2 yr and 187.6 kW h/m^2 yr, respectively. The PV module produces 164.5 kW h/m^2 yr while the thermal collector generates 401.6 kW h/m^2 yr.

4.3. Hybrid concentrator vs. standard PV module based on cell area

One of the most common arguments in favor of PVT concentrating systems is its higher electric output when compared with a regular PV module with the same cell

Table 5
Annual output ratio between a north–south and a east–west oriented tracking axis; annual output ratio between the usable irradiation ($G_b + G_d/C$) incident on a static and north–south tracking concentrating surface. Optimal static surface inclination from horizontal corresponds to 40° in Stockholm, 30° in Lisbon and 20° in Lusaka.

Annual output ratio	Stockholm (lat = 59.2 N)	Lisbon (lat = 38.7 N)	Lusaka (lat = 15.4 S)
Output ratio N–S/E–W tracking axis	1.10	1.14	1.19
Output ratio static/tracking concentrating surfaces	1.41	1.24	1.18

area. According to this point of view, the expensive cell area can be reduced and the thermal application can be considered just a tool to cool down the cells. Hence, if the thermal output is neglected, the hybrid can even work at a high flow rate, making the cells colder and more efficient. The production per cell area of the hybrid and the traditional PV module is presented in Table 7 and the ratio between the two annual electric outputs is shown in Fig. 9. The results show that the concentrating hybrid cells produce 3.6–4.4 times more electricity than a PV module with the same cells area. This kind of analysis provides very useful information concerning the real extra electricity production one gets with the use of the reflector in different climates. For this simulation it was considered that the standard PV module cells have 16% efficiency at 25 °C.

4.4. Hybrid concentrator vs. standard side-by-side system based on glazed area

In another point of view, since heat is the largest energy fraction produced by the hybrid, it should be considered as a valuable output taken into account when the concentrating hybrid is compared with a conventional system. Hence, the hybrid outputs were compared with an individual PV module and a solar thermal collector working separately for both domestic hot water production and pool heating. The parameters used in the simulation are presented in Tables 3 and 4. The hybrid comparison with the traditional side-by-side system based on their power outputs per total glazed area is presented in Fig. 10. This is particularly useful for areas where the available space is a strong limitation. As it is generally accepted, probably the most expensive part of these two systems is the solar cells. Hence, it makes sense to compare them taking into account that the hybrid and the PV module in the traditional system have the same cell area. This is not the only way to compare the systems but it seems to be the more reasonable one. The results show that, regardless of whether the produced hot water is used for domestic hot water application or for pool heating, the occupied ground area by the traditional side-by-side system, which generates the same electrical and thermal outputs as the hybrid, is almost the same. This result is not obvious and is further considered in the Section 5

Table 6
Hybrid and traditional side-by-side-system electric and thermal outputs per square metre of total glazed area for domestic hot water application.

Annual outputs per total glazed area	Stockholm (lat = 59.2 N)	Lisbon (lat = 38.7 N)	Lusaka (lat = 15.4 S)
Hybrid electric annual output (kW h/m^2 yr)	45.1	83.3	102.5
Hybrid thermal annual output (kW h/m^2 yr)	187.6	456.7	612.6
PV module annual output (kW h/m^2 yr)	164.5	264.8	308.3
Thermal collector annual output (kW h/m^2 yr)	401.6	887.7	1143.8

Table 7
PVT north–south concentrating hybrid and traditional PV module y output comparison based on cell area. PV module inclination from the horizontal is set to optimum values of 40° in Stockholm, 30° in Lisbon and 20° in Lusaka. $A_{cells\ hybrid} = 0.33$ m^2.

Electric annual output per cells area (kW h/m^2 yr)	Stockholm (lat = 59.2 N)	Lisbon (lat = 38.7 N)	Lusaka (lat = 15.4 S)
Hybrid tracking N–S (65 °C)	626.5	1156.1	1422.2
Traditional static PV module (25 °C)	173.2	278.7	324.5

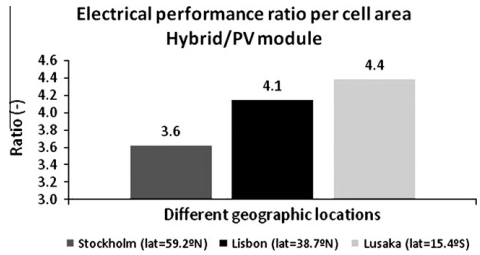

Fig. 9. Ratio between the hybrid and standard PV module annual electric production per cell area.

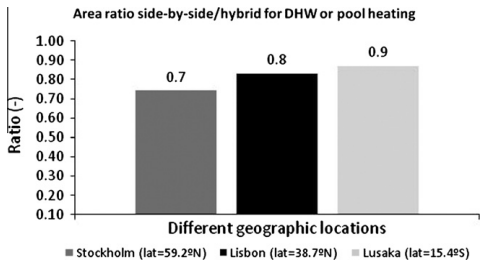

Fig. 10. Ratio between side-by-side system and hybrid total glazed areas producing the same electrical and thermal annual outputs for DHW or pool heating.

5. Discussion

In this chapter the implication of the results concerning the measured hybrid parameters, the annual performance and the comparison with conventional systems are discussed.

Using the efficiency per total glazed area one can estimate how much space one needs to reach the energy demand. It is then possible to determine, between several different hybrids, which one has the best performance for the space it uses and which hybrid is a reasonable choice for the available space. The efficiency per active glazed area may be said to be a more scientific indicator that allows a

technical comparison between hybrids based on how well they perform with the radiation they can use.

As previously reported (Yoon and Garboushian, 1994), the dependence of electricity production with temperature of concentrating hybrids is different from that in a normal photovoltaic module. For this hybrid, the electrical efficiency decrease with temperature (K_T) is approximately −0.3%/°C whereas the typical value for a standard cell without concentration is −0.4%/°C (Wenham et al., 2007). There are two different reasons for this. The electrical efficiency curve presented in Fig. 4 was calculated based on the temperature of the water and not that of the cells. Due to heat transfer resistance between these two elements, the water temperature will be somewhat lower than the cell temperature. This temperature difference is inversely proportional to the amount of heat transferred between them and it will decrease with increasing water temperature at constant solar intensity. This implicates a lower efficiency temperature dependence of the hybrid, making the slope of the line slightly smoother (Fig. 4). On the other hand, the temperature difference will increase with increasing radiation intensities at constant working temperature. This effect has a very low impact using the suggested test method since measurements were carried out only for high irradiation values according to the steady-state test method (Fisher et al., 2004). Possibly, in a future improved model, the cell efficiency should be modelled to increase with decreased irradiance intensities. The other effect is that a higher open-circuit voltage due to higher concentration actually reduces the temperature sensitivity of the cell (Yoon and Garboushian, 1994; Wenham et al., 2007). Previous experimental results have shown that the temperature influence in concentrating systems is lower, with −0.25%/°C drop in efficiency for high concentration levels at around 25 °C (Yoon and Garboushian, 1994). Hence, concentrators have an advantage when used at high temperature operation compared with a non-concentrating photovoltaic module.

The tracking system analysis shows that a one-axis tracking system should rotate around an axis aligned in the north–south direction, independently on its geographical location. If tilted towards the equator, the performance is further improved. Furthermore, a tracking concentrating system receives less usable radiation than a standard flat fixed collector. Consequently, the measured low hybrid efficiencies together with low usable irradiation generate low annual outputs. Additionally, the area covered by a conventional side-by-side system is comparable to the one used by the hybrid producing the same outputs. As a result, it is difficult for a concentrating hybrid to compete with conventional alternatives.

The optical efficiency is one of the factors that directly influence the final electric efficiency. The ideal thermal optical efficiency of the hybrid can be theoretically estimated taking into account several loss factors. These are: glass transmission, reflectance factor and the PV cells absorptance and efficiency. In the same way, it is also possible to theoretically calculate the ideal electrical efficiency of the hybrid at 25 °C. This is exemplified by Eqs. (10) and (11), respectively:

$$\begin{aligned}\eta_{\text{o\_thermal\_ideal}} &= \tau \cdot r \cdot \alpha \cdot (1 - \eta_{\text{cells\_ideal}}) \cdot A_{\text{active\_thermal}}/A_{\text{Hybrid}} \\ &= 0.90 \times 0.90 \times 0.93 \times (1 - 0.16) \times 3.7/4.6 \\ &= 0.51 \end{aligned} \quad (10)$$

$$\begin{aligned}\eta_{\text{elect.\_ideal}}(25\,^{\circ}\text{C}) &= \tau \cdot r \cdot \alpha \cdot \eta_{\text{cells\_ideal}} \cdot A_{\text{active elect.}}/A_{\text{Hybrid}} \\ &= 0.90 \times 0.90 \times 0.93 \times 0.16 \times 3.5/4.6 \\ &= 0.09 \end{aligned} \quad (11)$$

The transmittance of the glass τ was measured to be 0.90 (Bernardo, 2007), while the reflectance r is 0.90 (Alanod Solar, 2010) and the absorptance of the solar cells α was assumed to be 0.93 (Brogren et al., 2001). Dividing the active thermal area with the total glazed area makes it possible to compare the theoretical calculations with the measurements. This analysis helps to understand why the efficiencies of concentrating hybrids are lower than conventional thermal collectors and PV modules. Furthermore, the theoretical values point out a general limitation to the final efficiencies of concentrating hybrids. As shown, the difference between the measured and the theoretical efficiencies is not significant. In the thermal case, this difference can mainly be explained by the reflector shape inaccuracies. In the electric case, the difference is related to uneven distribution of solar irradiation on the cells and scattering after reflection. This is one of the challenges to overcome in this new technology. Having uniform radiation distribution over the PV module becomes especially critical for series connected cells since the one with the lowest output will limit the entire final production (Sick and Erge, 1998; Coventry et al., 2002; Nilsson, 2007). This concept is known as the "current matching problem" (Royne et al., 2005). In future models, local diodes should be installed over each cell in order to bypass the current over the poorest cells and help minimize the impact of uneven radiation. Reflector imprecision was not the only factor causing the decrease in the final electric output. Local shading effects, tracking inaccuracies, and variation between cells were also some of the obstacles found in this and other previous studies, making it difficult to achieve the efficiencies obtained when individual cells are tested under ideal conditions (Chow, 2010; Franklin and Coventry, 2002). Similar efficiency values were reported in recent studies of concentrating hybrids. Kostić et al. (2010) measured a thermal optical efficiency of 37% and an average value of the daily electrical efficiency of 3.7% in a hybrid using low concentrating flat reflectors. Also, Tripanagnostopoulos and Souliotis (2004) measured a thermal optical efficiency between 50% and 64% in solar thermal collectors using low concentrating parabolic reflectors. However, these last values would be further reduced in a PV/T hybrid since part of the irradiation would be used to produce electricity. The system design still has margin for improvement on most of its components for future developments. It is very important that cells under concentration feature very high efficiency;

the glass cover should have very high transmittance while optical errors in the reflector should be avoided and reflectance maximized. In future studies, an analysis of the aging of the cells and the efficiency decrease with time should be performed. Also, it is recommended that not only the hybrid outputs but also the performance of the whole system should be estimated. In this further investigation it is relevant to know, among other factors, what the hybrid application is, the yearly load, its daily and annual profile and the storage and auxiliary backup characteristics. Hence, it becomes possible to estimate the total system performance weighted with the investment and maintenance costs awarding different values to the electricity and thermal energy produced by the hybrid.

When it comes to possible applications for the hybrid and considering that the thermal output is much higher than the electrical output, it seems that the argument regarding the thermal output as just a benefit one can get by cooling down the cells does not make sense. It is more realistic to think that, at present, PVT hybrids can only become viable when a suitable application for the produced thermal energy is also found. The question is that the thermal system often requires a high temperature which decreases the PV module efficiency. Therefore it might be difficult to find the optimum operating point. If the generated electricity can be directly connected to the grid, then the system area should be design to cover the thermal load. When the analyzed hybrid is compared with a side-by-side system based on total glazed area the results show that, in terms of occupied space and global energy produced, there is no difference in having the hybrid working for domestic hot water production or pool heating. In this case, due to its lower U value compared with the standard flat plate collector, what is "lost" in electricity production at high temperatures is compensated for by thermal production at almost the same rate.

6. Conclusions

A complete methodology to characterize, simulate and evaluate the performance of a concentrating hybrid has been proposed and exemplified in a particular case study. The method includes a comparison with a traditional side-by-side system formed by conventional PV modules and flat plate collectors.

The evaluated hybrid of geometrical concentration 7.8 is constructed around PV cells of 16% efficiency. The evaluation results show that the optical efficiency is 0.45 and the U-value is 1.9 W/m^2 °C. The electrical efficiency is 6.4%. These values are drastically lower than for standard solar collectors and PV modules. Furthermore, the annual global irradiation incident on a tilted flat module is 20–40% higher than the beam irradiation incident on a concentrating system tracking the light around a horizontal axis aligned in the north–south direction. Hence, the low hybrid efficiencies in combination with low usable irradiation generate a low annual performance. Conventional PV modules and flat plate collectors, producing the same electric and thermal annual output as a concentrating hybrid, are comparable with the hybrid area. Even though there is a margin for improvement on the tested hybrid parameters, it is difficult for a concentrating hybrid to compete with conventional alternatives. It is very important that PV-cells under concentration have very high efficiency and that the glass cover and the reflector have very good properties. Optical errors in the reflector must be avoided and the system should be tracking around an axis aligned in the north–south direction, tilted towards the equator.

Acknowledgments

This study was supported by a Marie Curie program, *SolNet* – Advanced Solar Heating and Cooling for Buildings – the first coordinated international PhD education program on Solar Thermal Engineering. Homepage: http://cms.uni-kassel.de/unicms/?id=2141.

Johan Nilsson is acknowledged for valuable discussions and proof reading the article.

References

Absolicon Solar Concentrator AB, 2008. <www.absolicon.com>.

Affolter, P., Eisenmann, W., Fechner, H., Rommel, M., Schaap, A., Sorensen, H., Tripanagnostopoulos, Y., Zondag, H., 2004. PVT road map, A European Guide for the Development and Market Introduction of PV-Thermal Technology. Energy Research Centre of the Netherlands, Netherlands. <www.pvtforum.org>.

Alanod Solar, 2010. Technical Information Concerning the Reflector. <www.alanod-solar.com>.

Arvind, C., Tiwari, G.N., 2010. Stand-alone photovoltaic (PV) integrated with earth to air heat exchanger (EAHE) for space heating/cooling of adobe house in New Delhi (India). Energy Conversion and Management 51 (3), 393–409.

Arvind, C., Tiwari, G.N., Avinash, C., 2009. Simplified method of sizing and life cycle cost assessment of building integrated photovoltaic system. Energy and Buildings 41 (11), 1172–1180.

Bernardo, L.R., 2007. Evaluation of the Concentrating System Solar8. Master Thesis.

Brogren, M., Nostell, P., Karlsson, B., 2001. Optical efficiency of a PV-thermal hybrid CPC module for high latitudes. Solar Energy 69 (6), 173–185.

Chow, T.T., 2003. Performance analysis of photovoltaic-thermal collector by explicit dynamic model. Solar Energy 75 (2), 143–152.

Chow, T.T., 2010. A review on photovoltaic/thermal hybrid solar technology. Applied Energy 87 (2), 365–379.

Coventry, J.S., Franklin, E.T., Blakers, A., 2002. Thermal and electric performance of a concentrating PV/Thermal collector: results from the ANU CHAPS collector. In: Proceedings of Australian and New Zealand Solar Energy Society Conference, 2002. <http://hdl.handle.net/1885/40837>.

Duffie, J.A., Beckman, W.A., 2006. Solar Engineering of Thermal Process. John Wiley & Sons.

Fisher, S., Heidemann, W., Müller-Steinhagen, Perers, B., Berquist, P., Hellström, B., 2004. Collector test method under quasi-dynamic conditions according to the European Standard EN 12975-2. Solar Energy 76, 117–123.

Franklin, E.T., Coventry, J.S., 2002. Effects of highly non-uniform illumination distribution on electrical performance of solar cells. In:

Proceedings of Australian and New Zealand Solar Energy Society Conference, 2002. <http://hdl.handle.net/1885/40832>.

Kostić, Lj.T., Pavlović, T.M., Pavlović, Z.T., 2010. Optimal design of orientation of PV/T collectors with reflectors. Applied Energy 87, 3023–3029.

Nilsson, J., 2007. Optical Design for Stationary Solar Concentrators. Ph.D. Thesis, ISBN:978-91-85147-21-2, pp 23–27.

Nilsson, J., Håkansson, H., Karlsson, B., 2007. Electrical and thermal characterization of a PV-CPC hybrid. Solar Energy 81 (7), 917–928.

Royne, A., Dey, C.J., Mills, D.R., 2005. Cooling of photovoltaic cells under concentrated illumination: a critical view. Solar Energy Materials and Solar Cells 85 (4), 451–483.

Sick, F., Erge, T., 1998. Photovoltaic in Buildings: A Design Handbook for Architects and Engineers. IEA task 16. ISBN:1 873936 59 1, pp 27–28.

Tripanagnostopoulos, Y., Souliotis, M., 2004. Integrated collector storage solar systems with asymmetric CPC reflectors. Renewable Energy 29, 223–248.

Wenham, S., Green, M., Watt, M., Corkish, R., 2007. Applied Photovoltaics, Earthscan, second ed. London.

Winston, R., Miñano, J., Benítez, P., 2005. Nonimaging Optics, ISBN:0-12-759751-4.

Winsun Villa Educational Software, 2009. Perers, B., SERC Högskolan Dalarna, Sweden. <www.serc.se>.

Yoon, S., Garboushian, V., 1994. Reduced temperature dependence of high-concentration photovoltaic solar cell open circuit voltage (V_{OC}) at high concentration levels. In: Proceedings of the first WCPEC in Hawaii, 5–9 December.

Article II

Journal of Environment and Engineering
Vol. 6, No. 3, 2011

Performance Evaluation of a High Solar Fraction CPC-Collector System*

L. R. BERNARDO**, H. DAVIDSSON** and B. KARLSSON**
** Energy and Building Design Division, Department of Architecture and Build Environment
Lund Technical University, Box 118 SE-221 00 Lund, Sweden
E-mail: Ricardo.Bernardo@ebd.lth.se

Abstract
One of the most important goals on solar collector development is to increase the system's annual performance without increasing overproduction. The studied collector is formed by a compound parabolic reflector which decreases the collector optical efficiency during the summer period. Hence, it is possible to increase the collector area and thus, the annual solar fraction, without increasing the overproduction. Collector measurements were fed into a validated TRNSYS collector model which estimates the solar fraction of the concentrating system and also that of a traditional flat plate collector, both for domestic hot water production. The system design approach aims to maximise the collector area until an annual overproduction limit is reached. This is defined by a new deterioration factor that takes into account the hours and the collector temperature during stagnation periods. Then, the highest solar fraction achieved by both systems was determined. The results show that, at 50° tilt in Lund, Sweden, the concentrating system achieves 71% solar fraction using 17 m^2 of collector area compared to 66% solar fraction and 7 m^2 of a flat plate collector system. Thus, it is possible to install 2.4 times more collector area and achieve a higher solar fraction using the load adapted collector. However, the summer optical efficiency reduction was proven to be too abrupt. If the reflector geometry is properly design, the load adapted collector can be a competitive solution in the market if produced in an economical way.

Key words: Concentrating Solar Thermal, CPC, Domestic Hot Water, High Solar Fraction

Nomenclature

Monitored parameters:

Q	Collector thermal power (W/m²)
G_b	Beam Irradiance (W/m²)
G_d	Diffuse Irradiance (W/m²)
T_{in}	Collector inlet temperature (°C)
T_{out}	Collector outlet temperature (°C)
T_m	Fluid mean temperature (°C)
T_{amb}	Ambient temperature (°C)
dV/dt	Flow (m^3/s)
C_p	Heat capacity (water) (J/(kg°C))
ρ	Density (water) (kg/m^3)
A_c	Collector area (m²)

*Received 7 Feb., 2011 (No. 11-0099)
[DOI: 10.1299/jee.6.680]

Parameters in the collector model:

$F'(\tau\alpha)_n K_d$	Diffuse zero-loss efficiency (-)
$F'(\tau\alpha)_n$	Beam zero-loss efficiency (-)
$F'U_0$	Heat loss factor (W/m^2 °C)
$F'U_1$	Temperature dependence of heat loss factor ($W/m^2,°C^2$)
$g(\theta)$	Beam incidence angle modifier for the glazing
$K_b(\theta)$	Beam incidence angle modifier as a function of θ (-)
$K_b(\theta_l,\theta_t)$	Beam incidence angle modifier as a function of θ_l and θ_t (-)
$K_b(\theta_l,\theta)$	Beam incidence angle modifier as a function of θ_l and θ (-)
$K_{bl}(\theta_l,0)$	Longitudinal incidence angle modifier for beam irradiance (-)
$K_{bt}(0,\theta_t)$	Transversal incidence angle modifier for beam irradiance (-)
K_d	Incidence angle modifier for diffuse irradiance (-)
$(mC)_e$	Collector effective thermal capacitance ($J/(m^2°C)$)
θ	Angle of incidence onto the collector normal (°)
θ_l	Projection of the angle of incidence onto the longitudinal plane (°)
θ_t	Projection of the angle of incidence onto the transversal plane (°)
$R_t(\theta_t)$	Beam incidence angle modifier for the reflector
t	Simulation time-step (h)

1. Introduction

One of the most important goals to be achieved by a solar thermal system is a high annual solar fraction[1],[2], i.e. the fraction of the hot water load which is covered by solar energy. While solar thermal systems can generally achieve a high annual solar fraction in areas near the equator, in regions where the annual solar irradiation is lower it can be difficult. In most such regions, the solar contribution profile peaks during the summer months and decreases during the winter period. On the contrary, the domestic hot water load is fairly constant during the whole year which means that these two factors do not match all year round. Thus, the annual solar fraction is reduced.

It is common to design the system collector area in such way that the production over the sunniest period meets the thermal load[3],[4]. The aim of these systems is to achieve a solar fraction close to 100% during this period not taking into account overproduction at all. However, the solar hot water production and consumption profiles are very different throughout the day as well. The solar hot water production does not entirely take place at the same time as it is consumed by the users. Only a fraction of this extra energy can be stored in the solar tank. Hence, the system ends up with many hours where the collectors are in stagnation and other hours where auxiliary energy is needed. Furthermore, long stagnation periods influence long-term reliability and low maintenance operation of the collector system[5]. Common problems are overheating and permanent damage on system components, regular loss of fluid, condensation pressure chocks, deterioration of the fluid that ends up clogging the system, fluid circulation noise[6]. Hence, there is a need to define a deterioration factor taken into account when designing a new system. Using this criteria will limit the stagnation period along the year and, consequently, minimizes the risk of system malfunctions along its lifetime.

This paper describes a collector design approach that increases the solar fraction by maximizing the energy contribution of the thermal collector system but also limiting the overproduction. This is accomplished by using the collector's special reflector design at optimal tilt, collector area and flow. As a result of these optimizations, the system is able to reduce the difference between the solar hot water production and the domestic hot water

load throughout the year and still avoid overproduction under a user-determined value. Related concepts to this collector have been reported by Kothdiwala et al.[7], Tripanagnostopoulos et al.[8], Chaves and Pereira[9], Mills and Morrison[1]. The collector parameters were determined based on a dynamic testing method and multi linear regression[10]. These parameters were then fed into a validated model in TRNSYS[11] estimating the compound parabolic concentrator (CPC) system performance and comparing it with a flat plate collector system. There exists no validation model of a solar thermal system using this asymmetric CPC.

The main objective of the work was to evaluate the performance of the CPC collector system and compare it with a conventional flat plate collector system.

2. Method

2.1 Experimental setup and collector design

A solar collector design in which relatively expensive selective absorber material is replaced by cheap reflectors was studied. A compound parabolic collector with a geometrical concentration factor of 1.5 has been developed[4]. The collector consists of a reflector, a bi-facial selective absorber, a support structure and a glass cover illustrated in Fig. 1 and Fig. 2. The reflector material is made of anodised aluminium with a solar reflection equal to 0.85[12]. The parabolic reflector has an optical axis normal to the collector glass which defines the irradiation acceptance interval of the reflector. Once the incident radiation is outside this interval, the reflectors do not redirect the incoming beam radiation to the absorber, and the optical efficiency of the collector is reduced (Fig. 2). Hence, the collector's optical efficiency changes throughout the year depending on the projected solar altitude. The tilt determines the amount of total annual irradiation kept within the acceptance interval. As a result, by varying the tilt, it is possible to increase the collector area without causing overproduction in the summer when the collector has lower optical efficiency. The bi-facial selective absorber festures 0.96 solar absorptance and 0.10 reflectance to long wave radiation[13]. Since the absorber is parallel to the glass, in the upper part of the collector a pocket of hot air is created decreasing convection heat losses. The support structure is made of light wood with empty spaces in between in order to reduce its weight, wind obstruction and material costs. The glass cover is made of low iron glass with solar transmittance 0.9 at normal incidence angle[12].

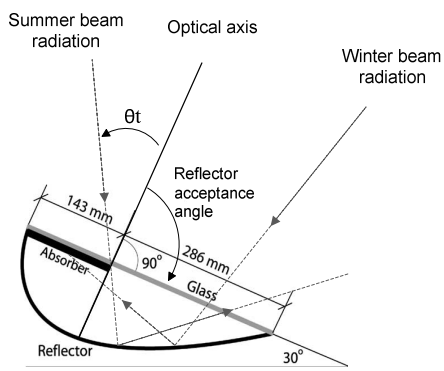

Fig. 1. Cross-section of the CPC collector.

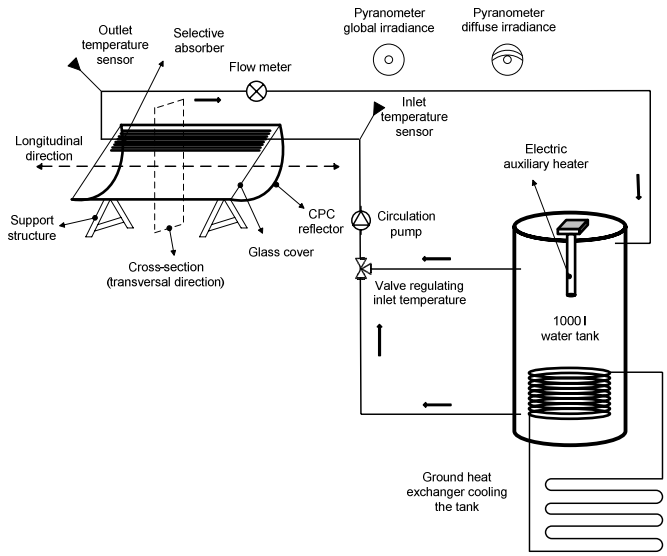

Fig. 2. Experimental setup of the CPC collector.

2.2 Testing and characterization method

Several measurements were carried out on the CPC collector in order to calculate the necessary parameters for the annual performance simulations. Measured average data was stored every 6 minutes between the 20th and the 29th of September, 2009. A simplified dynamic test method for determination of non-linear optical and thermal characteristics with multiple linear regression was used[10),(14),(15)]:

$$Q = F'(\tau\alpha)_n K_b(\theta) G_b + F'(\tau\alpha)_n K_d G_d - F'U_0(T_m - T_{amb}) - F'U_1(T_m - T_{amb})^2 - (mC)_e \frac{dT_m}{dt} \quad (W/m^2)$$

equation 1

$$Q = \frac{\rho \frac{dV}{dt} C_p (T_{out} - T_{in})}{A_c} \quad (W/m^2)$$

equation 2

McIntire[16] presented a biaxial incidence angle modifier model described in the longitudinal and transverse directions:

$$K_b(\theta_l, \theta_t) \approx K_{bl}(\theta_l, 0) \cdot K_{bt}(0, \theta_t) \quad (-)$$

equation 3

The incidence angle modifier is a factor that decreases the optical efficiency depending on the incidence angle between the beam solar radiation and the normal to the collector surface. However, this model presents disadvantages. Rönnelid et al.[17] showed that the model underestimates the optical losses in the glass and that large errors can occur at high incidence angles. This effect is reduced since the optical losses in the glass are accounted twice.

In this study an incidence angle modifier model proposed by Nilsson et al.[18] was used. The biaxial model uses the projected transverse incidence angle to determine the influence of the reflector and the real angle of incidence to determine the influence of the glazing in

the following way:

$$K_b(\theta_l,\theta) \approx R_t(\theta_t)\cdot g(\theta) \quad (-) \qquad \text{equation 4}$$

Firstly, the influence of the glazing was measured in the longitudinal direction when the transversal incident angle was kept constant. Secondly, the dependence of the reflector was measured on the transversal plane when the longitudinal incidence angle was also constant. This was carried out by testing two identical CPC collectors during the autumn equinox, both tilted 55° from horizontal (the latitude in Lund) but placing one of them horizontally and the other vertically like shown in Fig. 3. This procedure is described in detail in Helgesson[3]. Typically, the measured curves are included in the collector model using a matrix made of singular incidence angle modifiers. The rest of them are linearly interpolated. At incidence angles close to the collector acceptance angle, the incidence angle modifiers variation is abrupt. Hence, interpolating discrete values can cause large inaccuracies. In this study, the measured incidence angle modifiers were included in the model using high grade polynomial equations. Hence, interpolations were avoided and the accuracy of the model increased.

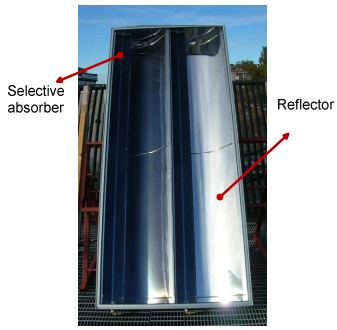

Fig. 3. CPC collector turned 90° during the autumn equinox.

2.3 Simulation model

A TRSNSYS model describing the whole solar collector system was created. Its main components are shown in Fig. 4 and listed below:

- Thermal collector – CPC collector type 832, created by Bengt Perers and further developed by Hellström, Fisher, Bales, Haller, Dalibard and Paavilainen[19]. In this study, the biaxial incidence angle modifiers described by polynomial equations were added to the model;
- Radiation processor – type 109-TMY2, Lund weather data (latitude 55°44'N, longitude 13°12'E), Sweden;
- Circulation pump – type 3b, single speed. The collector flow was design to maximise the solar fraction for each collector area and tilt angle;
- Storage tank – type 4c, stratified storage with uniform losses and variable inlets. This storage model adjusts the inlets location continuously in order to place the incoming fluid at a level as close to its temperature as possible. This improves greatly stratification in the tank and consequently the annual solar fraction. The total volume is 300 litres and 1.60 m high. The 3kW auxiliary heater is placed at the top with a set-point temperature of 60˚C;
- Domestic hot water load profile – type 14 for the daily load profile and type 14h for the yearly variation.

Vol. 6, No. 3, 2011

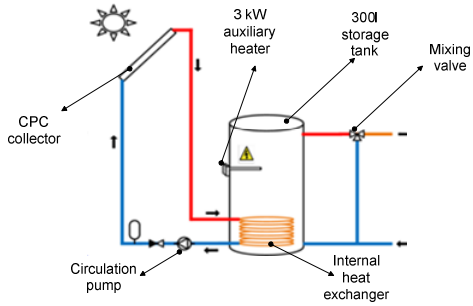

Fig. 4. Main components of the solar thermal system model.

The domestic hot water load profile was built based on the one described by Widén et al.[20] but scaled to the latest data on Swedish total hot water consumption (Stengård[21]). Seven different water draw-offs were performed during the day (Fig. 5). Furthermore, the annual hot water consumption variation effect was also introduced and it is shown in Fig. 6 (Swedish Energy Agency[22]). The total annual consumption is 2050 kWh/year. The annual limit for the deterioration factor was set to 5000°C.h/year. This value takes into account not only the number of stagnation hours but also how much the collector outlet temperature raised over 100°C during that period in the following way:

$$\sum \left(T_{out} - 100\right) \cdot t \quad \left(^{\circ}C \cdot h\right) \qquad \text{(during stagnation periods)} \qquad \text{equation 5}$$

Stagnation period was defined by the time period during which both the top of the storage tank and the outlet collector temperature were above 100°C. During this period, the collector pump is stopped. Has shown in equation 5, it was assumed that stagnation time and collector outlet temperatures above 100°C have a linear influence on the parameter. The figure 5000°C.h/year represents a reasonable maximum overproduction (100 hours of stagnation with 150°C collector temperature, for example). Finally, by simulation iterations, the maximum collector area that corresponds to the maximum solar fraction but limits the overproduction to 5000°C.h/year was determined. This design criterion is further discussed in the discussion section.

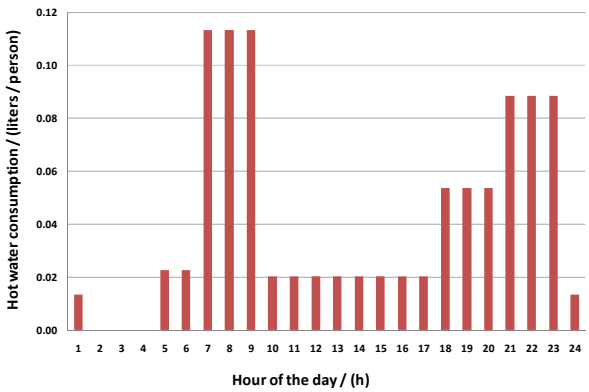

Fig. 5. Daily domestic hot water profile.

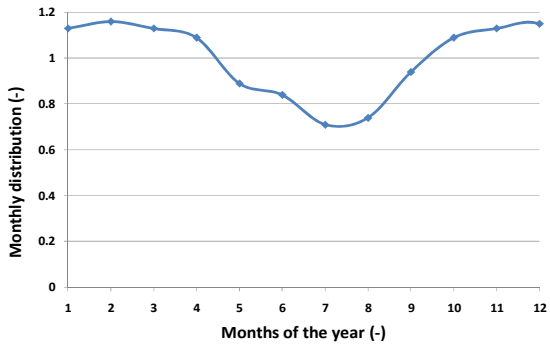

Fig. 6. Yearly domestic hot water profile.

3. Measurement results

3.1 Thermal performance

Table 1 shows the CPC collector parameters, estimated using multi linear regression on the measured data, and the parameters assumed to be typical for conventional flat plate collectors.

Table 1. Measured CPC collector parameters and assumed typical flat plate collector parameters.

Parameters and units	CPC collector (measured)	Flat plate collector (presumed)
$F'(\tau\alpha)_n$ (-)	0.64	0.8
$F'(\tau\alpha)_n K_d$ (-)	0.31	0.72
$F'U_0$ / (W/m^2,°C)	2.8	3.6
$F'U_1$ /(W/m^2,°C^2)	0.035	0.014
$k_b(\theta)$ (-)	-	0.2
$(mC)_e$ /(J/m^2 °C)	1923	8000

3.2 Incidence angle modifiers

Fig. 7 shows the longitudinal and transversal incidence angle modifiers describing the influence of glazing and reflector, respectively. The transversal incidence angle modifier was measured while the longitudinal incidence angle modifier was estimated by the Fresnel and Snell's laws.

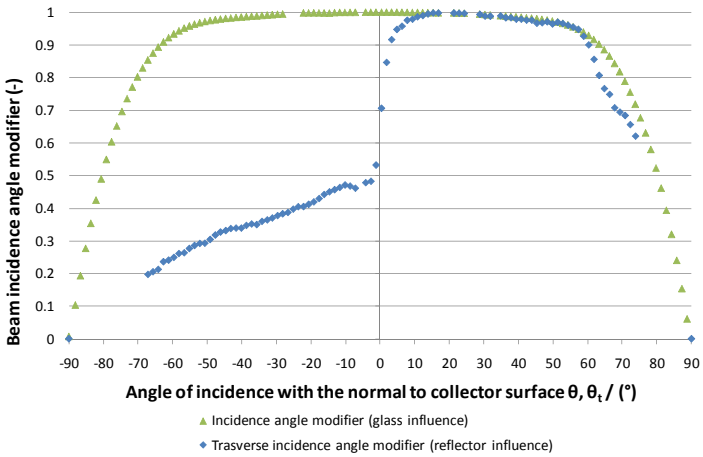

Fig. 7. Reflector and glazing beam incidence angle modifiers during autumn equinox.

3.3 Model validation

To validate the CPC collector model, the measured and modelled power outputs were compared during the test period (Fig. 8). From the analysis of Fig. 8, one can conclude that good agreement was found between the model and the measurements. In Fig. 9 the modelled and measured power output are compared during a variable irradiation day. It was assumed that the CPC collector model is the only component that requires validation. The other component models are TRNSYS standard models and have been used with great reliability in the scientific community.

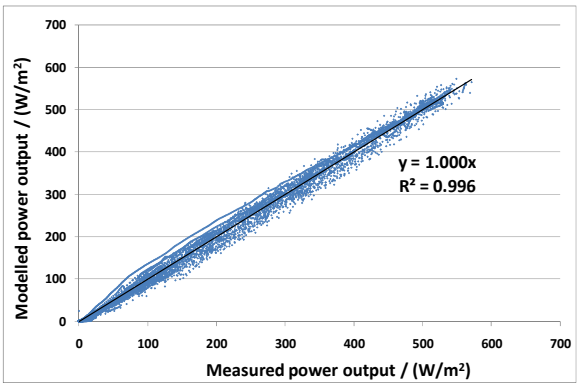

Fig. 8. Measured and modelled power output data during the testing period.

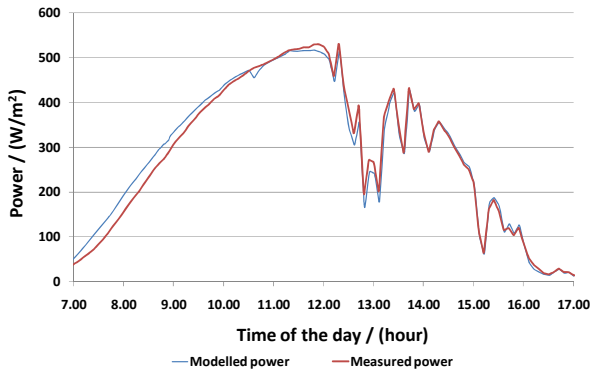

Fig. 9. Measured and modelled power output on the 20th September 2009.

4. Performance analysis and discussion

Using the collector measured parameters, TRNSYS simulations were carried out for the concentrating collector and a traditional flat plate solar thermal system situated in Lund, Sweden. The assumed design criterion limiting the collector area takes into account not only the number of stagnation hours but also the collector outlet temperature. This deterioration factor was set to 5000°C.h/year. Obviously, this design criterion can be questioned, especially when it comes to the particular chosen number of 5000°C.h/year. Also, it is uncertain if temperature and time during stagnation periods should have equal weight on this factor. Further work is needed to understand how to account for overproduction in the system design in a more precise way and to account the weight of this factor on the system design. The assumed design guideline should be seen as a first iteration step in that direction. The intention is to consider a deterioration factor when designing a new solar thermal system. The important analysis at this stage is result comparison between these two different collector systems rather than conclude about the absolute value of the solar fraction results. As both systems were design in the same way, inaccuracies that occur in one system will occur in the same way in the other one. This makes it significantly more reliable to take conclusions about the systems performances. In a future analysis taking into account the costs for every kind of component, the system will be design in order to improve its cost-effectiveness. The difference between the measured and modelled outputs during the morning illustrated in Fig. 9 is explained by the difficulty on modelling the thermal capacitance of the collector. Nevertheless, during the hours of the day where higher solar intensities and collector outputs occur, the model meets the measurements with high accuracy guaranteeing accuracy in the results.

The maximum solar fraction achieved by both systems, for several different tilts, is presented in the left axis in Fig. 10. The corresponding maximum collector area that limits the annual overproduction under 5000°C.h/year is shown in the right axis of the same figure. Analysing the results it can be concluded that when the concentrating collector is set to low tilts the optical efficiency is high during the whole year and it behaves like a flat plate collector with peak production in the summer. On the other hand, when it is set to higher tilts, the optical efficiency is reduced along the year and overproduction only occurs for large collector areas. The balance between these two situations for Lund is somewhere around 50° tilt where the optical efficiency is only reduced during the summer resulting in a high annual solar fraction and still not using extremely large collector areas. For that tilt, the

load adapted system achieves a solar fraction of 71% using 17 m^2 of collector area compared to 66% and 7 m^2 of a flat plate collector system. Contributing to these high solar fraction values is the very high stratification and well insulated model of the tank. In such a tank model, the incoming water is placed at a height in the tank that has the closest matching temperature. Also, no losses were taken into account in piping. Hence, very high stratification and consequently high solar performances were achieved. This simple tank model allowed time saving both in building the system model and the running period of the simulations.

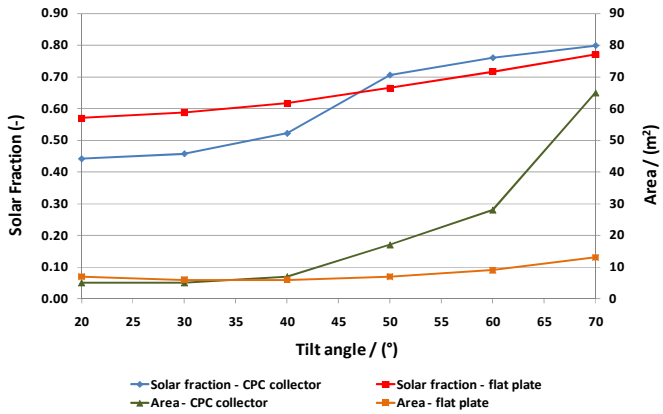

Fig. 10. Annual solar fraction and corresponding collector areas for both systems.

In Fig. 11 it is shown the annual production profile of the two solar systems for 50° tilt. One can notice the suppressed solar hot water production during the summer in the CPC collector and the overproduction moved to the spring and autumn periods. When the CPC collector system achieves higher solar fractions than the flat plate collector system, it requires, at least, 2.4 times more collector area. Taking into account that the selective absorber surface of the CPC collector is 1/3 of its total glazed area (Fig. 1), one can say that the concentrating collector makes use of less absorber area. This decrease together with higher performance must compensate the extra material such as reflector and glass as well as the possible technical difficulties of manufacturing a parabolic shape. Nevertheless, there is an exaggerated optical efficiency decrease to less than half causing underproduction during the summer. This is explained by the fact that the transverse incidence angle modifier is reduced to half when the reflector is not active (Fig. 7). Ideally, the optical efficiency should decrease during the summer but only to a level where overproduction is avoided while the domestic hot water load is fulfilled. One possible solution is to change the reflector geometry in order to have a part of the mirror active during the summer period. If the reflector geometry is improved, the CPC collector will achieve higher performances for the same collector area and become a more competitive solution when produced in a cheap way.

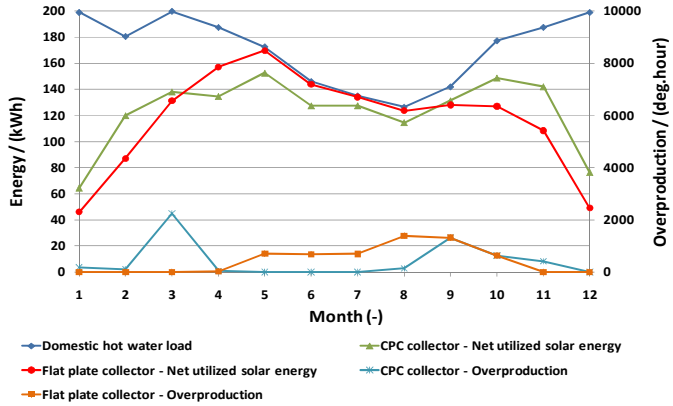

Fig.11. Energy and overproduction profiles during the year for 50° tilt, 17m^2 of collector area and 0.12 l/min,m^2 of water flow.

5. Conclusions

An evaluation of a load adapted CPC collector system was presented. The collector design aims to increase the solar fraction by adapting the solar hot water production to the load. The evaluation includes a new design approach for the collector system that estimates the collector area based on an annual overproduction limit. A comparison with a standard flat plate collector system is also included.

The results show that, at 50° tilt, it is possible to install larger collector areas of the concentrating system and achieve higher solar fractions without increasing overproduction. For this tilt, the concentrating system achieves 71% solar fraction using 17 m^2 of collector area compared to 66% solar fraction and 7 m^2 of a flat plate collector system. This means 2.4 times more collector area with a somewhat higher performance. For the same glazed area, the absorber surface of the flat plate collector is 3 times higher than that of the concentrating system. Thus, from the result analysis, one can conclude that the concentrating collector absorber area is smaller than the flat plate collector. This is one of the most expensive components of the collector. Hence, the absorber surface reduction together with the higher performance must compensate the cost increase on the other materials such as glass, parabolic reflector, frames so that the concentrating system can compete with standard flat plate collectors. Obviously, this performance comparison is sensitive to the parameters assumed for the conventional flat plate collector. Nevertheless, these values are valid for this particular collector design where the optical efficiency is reduced to less than half during the summer. This exaggerated effect causes underproduction during this period reducing the annual solar fraction. If the reflector geometry is improved, the collector can become an even more competitive solution in the market if produced in an inexpensive way.

Acknowledgments

This study was supported by a Marie Curie program, *SolNet* - Advanced Solar Heating and Cooling for Buildings - the first coordinated international PhD education program on Solar Thermal Engineering. Homepage: http://cms.uni-kassel.de/unicms/?id=2141

The Swedish Energy Agency.

References

(1) Mills, D. and Morrison, G, Optimisation of minimum backup solar water heating system, *Solar Energy* (2003), Vol. 74, No. 6, pp. 505-511.
(2) Helgesson, A., Karlsson, B. and Nordlander, S, Evaluation of a Spring/Fall-MaReCo, In: *Proceedings of Eurosun Conference* (2002), Bologna, Italy.
(3) Helgesson, A, Optical Characterization of Solar Collectors from Outdoor Measurements, *Licentiate thesis* (2004), ISBN 91-85147-07-9, pp. 293-294.
(4) Adsten, M., Helgesson, A. and Karlsson, B., Evaluation of CPC-collector designs for stand-alone, roof- or wall installation, *Solar Energy*, Vol. 79, No. 6 (2004), pp. 638-647.
(5) Hausner, R. and Fink, C, Stagnation behaviour of thermal solar systems (2000), Download available at www.aee-intec.at/0uploads/dateien119.pdf.
(6) Hausner, R. and Fink, C, Stagnation behaviour of solar thermal systems (2002), *A report of IEA SHC, task 26*.
(7) Kothdiwala, A., Norton, B., Eames, P, The effect of variation of angle of inclination on the performance of low-concentration-ratio compound parabolic concentrating solar collectors, *Solar Energy* (1995), Vol. 55, No. 4, pp. 301-309.
(8) Tripanagnostopoulos, Y., Yianoulis, P., Papaefthimiou, S. and Zafeiratos, S, CPC solar collectors with flat bifacial absorbers, *Solar Energy* (2000), Vol. 69, pp. 191-203.
(9) Chaves, J. and Pereira, M. C, Ultra flat ideal concentrators of high concentration, *Solar Energy*, Vol. 69 (2000), No. 4, pp. 269-281.
(10) Perers, B, An improved dynamic solar collector test method for determination of non-linear optical and thermal characteristics with multiple regression, *Solar Energy* (1997), Vol. 59, pp. 163-178.
(11) Klein, S. et al., 1997. TRNSYS, a Transient System Simulation, *University of Wisconsin*, Madison, USA.
(12) Hellström, B., Adsten, M., Nostell, P., Wäckelgård, E. and Karlsson, B., The impact of optical and thermal properties on the performance of flat plate solar collectors, In: *Proceedings of Eurosun Conference* (2000), Copenhagen, Denmark.
(13) Wäckelgård, E., Hultmark, G., Industrially sputtered solar absorber surface, *Solar Energy Materials and Solar Cells,* Vol. 54, No. 1-4 (1998), pp. 165-170.
(14) Perers, B, Dynamic method for solar collector array testing and evaluation with standard database and simulation programs, *Solar Energy* (1993), Vol. 50, No. 6, pp. 517-526.
(15) Duffie, J.A., Beckman, W.A, *Solar Engineering of Thermal Process* (2006) John Wiley & Sons.
(16) McIntire, W. R, Factored approximations for biaxial incidence angle modifiers, *Solar Energy* (1982), Vol. 29, No. 4, pp. 315-322.
(17) Rönnelid, M., Perers, B. and Karlsson, B, On the factorisation of incidence angle modifiers for CPC collectors, *Solar Energy* (1997), Vol. 59, No. 4-6, pp 281-286.
(18) Nilsson, J., Brogren, M., Helgesson, A., Roos, A. and Karlsson, B, Biaxial model for the incidence angle dependence of the optical efficiency of photovoltaic systems with asymmetric reflectors, *Solar Energy* (2006), Vol. 80, No. 9, pp. 315-322.
(19) Perers B. and Bales C, A Solar Collector Model for TRNSYS Simulation and System Testing, *A Report of IEA SHC - Task 26 Solar Combisystems* (2002), Download available at http://www.les.ufpb.br/portal/index2.php?option=com_docman&task=doc_view&gid=190&Itemid=30
(20) Widén, J., Lundh, M., Vassileva, I., Dahlquist, E., Ellegård, K. and Wäckelgård, E, Constructing load profiles for household electricity and hot water from time-use data—Modelling approach and validation, *Energy and Buildings* (2009), Vol 41, No. 7, pp. 753-768.

(21) Stengård, L., 2009, *Measurement of cold and hot water use in 44 apartments*, Accessed in 2009/10 from http://webbshop.cm.se/System/ViewResource.aspx?p=Energimyndigheten&rl=default:/Resources/Permanent/Static/b9a064ece4d747868b5c20d1a03ab0a2/2124W.pdf
(22) Swedish Energy Agency, 2009. *FEBY – Specific Regulations for small energy houses,* Download available at http://www.energieffektivabyggnader.se/download/18.712fb31f12497ed09a58000141/Kravspecifikation_Minienergihus_version_2009_oktober.pdf

Article III

Engineering, 2013, 5, 37-43
doi:10.4236/eng.2013.51b007 Published Online January 2013 (http://www.SciRP.org/journal/eng)

Measurements of the Electrical Incidence Angle Modifiers of an Asymmetrical Photovoltaic/Thermal Compound Parabolic Concentrating-Collector

Bernardo Ricardo[1*], Davidsson Henrik[1], Gentile Niko[1], Gomes João[2], Gruffman Christian[3], Chea Luis[4], Mumba Chabu[5], Karlsson Björn[6]
[1]Energy and Building Design, Lund University, Lund, Sweden
[2]Solarus Sunpower AB, Stockholm, Sweden
[3]Finsun AB, Älvkarleby, Sweden
[4]Universidade Eduardo Mondlane, Maputo, Mozambique
[5]University of Zambia, Lusaka, Zambia
[6]Division of Energy Engineering, Mälardalen University, Västerås, Sweden
Email: [*]Ricardo.Bernardo@ebd.lth.se

Received 2013

ABSTRACT

Reflector edges, sharp acceptance angles and by-pass diodes introduce large variations in the electrical performance of asymmetrical concentrating photovoltaic/thermal modules over a short incidence angle interval. It is therefore important to quantify these impacts precisely. The impact on the electrical performance of the optical properties of an asymmetrical photovoltaic/thermal CPC-collector was measured in Maputo, Mozambique. The measurements were carried out with the focus on attaining a high resolution incidence angle modifier in both the longitudinal and transversal directions, since large variations were expected over small angle intervals. A detailed analysis of the contribution of the diffuse radiation to the total output was also carried out. The solar cells have an electrical efficiency of 18% while the maximum measured electrical efficiency of the collector was 13.9% per active glazed area and 20.9% per active cell area, at 25˚C. Such data make it possible to quantify not only the electrical performance for different climatic and operating conditions but also to determine potential improvements to the collector design. The electrical output can be increased by a number of different measures, e.g. removing the outermost cells, turning the edge cells 90˚, dividing each receiver side into three or four parts and directing the tracking, when used, along a north-south axis.

Keywords: CPC-Collector; PVT Hybrid; Incidence Angle Modifier; Asymmetric Collector; Electrical Efficiency

1. Introduction

The electrical part of an asymmetric compound parabolic concentrating (CPC) photovoltaic/thermal hybrid (PV/T), collector has been investigated. The radiation is concentrated onto an aluminium thermal absorber on which PV cells have been laminated. The cells were laminated on both the upper and the lower side of the absorber. The front side works like a standard PV module without concentration while the backside receives solar radiation from a parabolic reflector such as illustrated in **Figure 1**. Even though the concentration factor of the collector is low, equal to 1.5, the PV cells can still reach high temperatures. This will reduce the electric production and cooling is required in order to maintain electrical efficiency. This is carried out by running water inside the thermal absorber. By using the heat generated in the absorber, the PV/T collector produces electricity and thermal heat, see **Figure 2**. The PV/T system, shown in **Figure 1** and **Figure 2**, consists of a photovoltaic module, thermal absorber, compound reflector (parabolic and circular), glazed protection and supporting structure. The reflector material is made of anodised aluminium with a solar reflection of approximately 95% [1]. The optical axis for the reflector geometry is normal to the glass of the collector. This defines the acceptance angle for the irradiation of the reflector. If the radiation falls outside this angle the reflectors do not redirect the incoming beam radiation to the backside absorber and the optical efficiency of the collector is thus reduced. Hence, the optical efficiency of the collector changes throughout the year depending on the projected solar altitude. The tilt of the collector determines the amount of total annual irradiation kept within the acceptance interval [2]. The glass cover of the collector is made of low iron glass with solar

[*]Corresponding author.

transmittance of 0.9 at normal incidence angle.

The main objective of this study was to accurately measure the optical properties for the electrical output of an asymmetric PV/T CPC-collector with the focus on edge effects, bypass diodes, acceptance angle and the contribution of diffuse radiation. This information makes it possible to understand how to further improve the collector design and estimate the expected production in different climatic and operating conditions.

2. Method

2.1. Experimental Setup and Hybrid Design

Figure 2 describes the electrical arrangement of the solar cells in one PV/T module. Since receiver 1 and receiver 2 are exactly the same only one of the receivers was tested. The figure shows the collector viewed from the top. The backside, i.e. the part that utilizes the reflector is equipped with the same PV cell arrangement. One string consists of 38 PV cells. Both the front side and the backside of the receiver consist of two PV strings each. The total number of PV cells per receiver is thus 152 cells. The PV array is made up of six cells that have been cut into 26 mm wide pieces. The manufacturer chose to do so in order to have a larger voltage and a smaller current for larger irradiation levels due to the increased concentration. The total area of PV cells on a receiver was approximately 0.58 m² and the active glazed area was approximately 0.87 m² per receiver. Active glazed area was defined as the glazed area where the incident radiation can contribute to electricity production, i.e. the area on top of the cells and the area on top of the reflector in front of the cells, excluding edges, spaces between cells and parts where there was no reflector [3]. **Figure 2** shows the electrical connection in red and the water connections in blue. T_{in} and T_{out} represent the temperature sensors placed at the inlet and outlet of the water running inside the collector. T_{mid} represents the temperature sensor at the middle of the receiver.

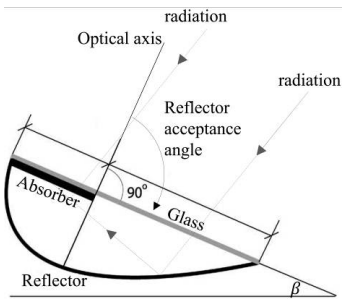

Figure 1. The geometry of the investigated PV/T hybrid solar collector.

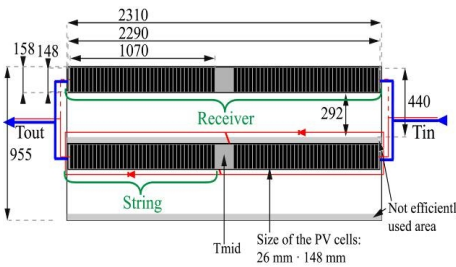

Figure 2. Top view of the PV/T hybrid collector. The water connection is in blue and the electrical connections in red.

Figure 2 also shows the size of the different electric components in the collector. The total size of the collector is 2.31 m by 0.955 m. The length of the thermal receiver is 2.290 m and the height is 0.158 m. The size of the PV cells is 0.148 m times 0.026 m. The active height of the reflector is 0.292 m. The parts of the collector which are excluded by the active glazed area are indicated in the figure. The total active height of the trough is 0.44 m, i.e. the sum of the active reflector height and the height of the PV cells.

The evaluation of the PVT hybrid collector was only performed for the electrical part. The thermal part was previously evaluated in [2] and further measurements are ongoing.

2.2. Procedure

Since there are many factors that affect the characteristic parameters of a solar collector the measurements have been performed and evaluated in a specific order. The first step was to analyze the efficiency and the temperature dependence of the PV cell module. This part was performed while the incidence angle maximizes the electrical output, i.e. close to normal incidence. Once the temperature dependence was determined, the angular dependence or more accurately, the incidence angle modifier, could be measured.

In reality, it is expected that an electric load is permanently connected to the PV cells and electric power is continuously extracted at maximum power point. However, the presented method of instantaneous I-V curve measurements simplifies the whole test procedure. These results are less expensive and less time consuming to achieve while still maintaining a good level of accuracy. If an electric load were continuously connected, the absorber would be colder since a part of the incoming radiation would be converted to electricity. This would mean lower temperatures and thus slightly lower thermal losses. This difference is however small and has little impact on the results [3]. Since the investigated collector has a closed structure it was not possible to measure the

cell temperature directly. Instead, the temperature of the outlet water was measured. This is the limiting temperature of the whole electric output since the hottest cells in the series connected string will limit the energy production.

The transverse incidence angle modifier (IAM_t) is defined by the reduction in electrical efficiency for a given irradiation caused by the increase of the incidence angle between the sun and the normal to the collector in the transverse direction (θ_t). This is exemplified in the left illustration in **Figure 3**. From 0˚ to +90˚ the sun's direction is inside the acceptance angle of the reflector and outside from 0˚ to -90˚. The IAM measurements are a combination of all angular effects such as decrease of transmission in the glazing for high incidence angles and shading effects by edges, etc.

To be able to measure IAM_t for different transverse angles the longitudinal angle had to be kept equal to zero. This was measured by facing the collector towards the solar azimuth for various tilt angles. This is illustrated in **Figure 4**.

The incidence angle modifier is applied for the direct radiation only. However, even during clear days, there is always a percentage of diffuse light that contributes to the measured power output, which becomes relevant for low concentrating collectors such as this one.

The fraction of useful diffuse radiation for the concentrating collector relative to the total diffuse radiation on the glazed cover of the collector is described by **Figure 5**. The pyranometer, labelled (A), will see $(1+\cos(\beta))/2$ of the full sky. This is the same as for the front side of the receiver, labelled (B). They thus see the same part of the diffuse sky and it would be a correct assumption when a non-concentrating collector is tested. This is however not the case for the backside of the receiver. The acceptance angle for the reflector blocks a substantial part of the sky. This part is indicated with red arrows in **Figure 5**. The radiation that will strike the backside of the receiver comes from the radiation labelled (C) and is equal to the radiation measured by the pyranometer minus half the sky due to the acceptance angle. This is true for positive tilt, i.e. the leftmost illustration in **Figure 5**. The right-hand illustration shows the case for tilting the reflector backwards. The pyranometer (D) and the front side (E) of the receiver are unaffected. However, the backside radiation (F) will be half of the sky as long as the tilt β is less than 90°. This happens since the part outside the acceptance angle is now facing the ground. Thus the part of the diffuse radiation inside the acceptance angle is always half of the sky.

The fraction, *f*, of the diffuse radiation that is useful for the collector can be calculated by summing the contributions from the front side and the backside of the receiver and dividing this by the diffuse radiation measured by the diffuse pyranometer. The front side of the receiver accounts for one third of the total glazed area while the backside, via the reflector, accounts for two thirds of the total glazed area. If the collector is rotated like the left side of the figure *f* will be:

$$f = \frac{\frac{1}{3}\left(\frac{1+\cos(\beta)}{2}\right)+\frac{2}{3}\left(\frac{1+\cos(\beta)}{2}-\frac{1}{2}\right)}{\left(\frac{1+\cos(\beta)}{2}\right)} \quad (1)$$

If the collector is rotated like the right side of the figure *f* will be:

$$f = \frac{\frac{1}{3}\left(\frac{1+\cos(\beta)}{2}\right)+\frac{2}{3}\left(\frac{1}{2}\right)}{\left(\frac{1+\cos(\beta)}{2}\right)} \quad (2)$$

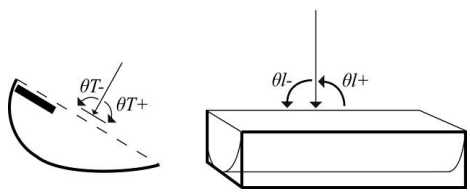

Figure 3. Transversal incidence angle to the left and longitudinal incidence angle to the right.

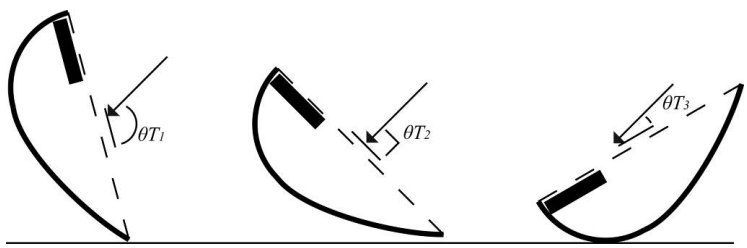

Figure 4. Tilting the collector to achieve different transverse incidence angles.

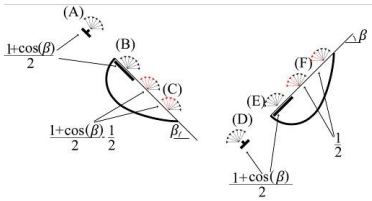

Figure 5. Fraction of useful diffuse radiation for different transverse incidence angles.

However, this is true for an infinitely long trough without any shading from the edges. This is not the case for the investigated collector. The front side of the receiver will be only slightly affected by shading and the shading effect is thus omitted. The shading of the backside will be more important. This is illustrated to the right in **Figure 6**.

The black arrow, labelled 1, close to normal incidence will be reflected to the outermost PV cell. So will all rays coming from an even lower angle, e.g. rays labelled 2 and 3. For radiation with a higher incidence angle, the rays will be either reflected to hit another cell or be stopped by the edges. I.e. the outermost cell can only see roughly half of the diffuse sky. The problem is identical for the left side of the collector. This will reduce the contribution from radiation to the backside of the receiver, i.e. (C) and (F) in **Figure 5** by approximately 50%. This will change equation (1) and equation (2) to:

$$f = \frac{\frac{1}{3}\left(\frac{1+\cos(\beta)}{2}\right)+\frac{2}{3}\left(\frac{1+\cos(\beta)}{2}-\frac{1}{2}\right)\Big/2}{\left(\frac{1+\cos(\beta)}{2}\right)} = \frac{1+2\cos(\beta)}{3(1+\cos(\beta))} \quad (3)$$

$$f = \frac{\frac{1}{3}\left(\frac{1+\cos(\beta)}{2}\right)+\frac{2}{3}\left(\frac{1}{2}\right)\Big/2}{\left(\frac{1+\cos(\beta)}{2}\right)} = \frac{2+\cos(\beta)}{3(1+\cos(\beta))} \quad (4)$$

Measurements of the IAM_t were carried out by varying the tilt β from -30° to +30°, see **Figure 5**. **Figure 7** shows a plot of equation (3) and equation (4). The variation in the fraction of the useful diffuse radiation is small for this tilt interval. Hence, the fraction of useful diffuse radiation was set to be the average of its value and equal to 50%.

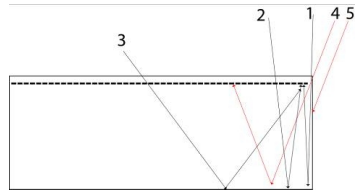

Figure 6. Shading of the PV cells due to the gables of the collector.

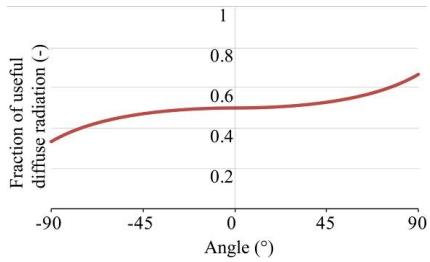

Figure 7. The fraction of useful diffuse radiation as a function of the collector tilt.

The longitudinal incidence angle modifier (IAM_l) was measured while keeping a constant θ_t which corresponds to the measured maximum value of IAM_t.

3. Results

3.1. Theoretical Estimate of the Maximum Output of the Collector

The produced electricity is the sum of the production on the front and back sides, equation (5).

$$P_{el} = P_{el\_front} + P_{el\_back} \quad (5)$$

The power from the front side is the product of the cell area, A_{cells_front}, the transmission through the glass, τ, the efficiency of the cells, $\eta_{cells\_(25^\circ C)}$, and the total incoming radiation, G_{total}, equation (6).

$$P_{el\_front} = A_{cells\_front} \cdot \tau \cdot \eta_{cells\_(25^\circ C)} \cdot G_{total} \quad (6)$$

Due to the acceptance angle for the collector the radiation has to be divided into beam and diffuse radiation. The power from the backside is thus the sum of the two, equation (7).

$$P_{el\_back} = P_{el\_back\_beam} + P_{el\_back\_diff} \quad (7)$$

The electrical output from the back cells due to the beam radiation is the product of the total width of the cells, *w*, the height of the mirror, *h*, the transmission through the glass, τ, the reflection of the reflector, *r*, the efficiency of the cells, $\eta_{cells\_(25^\circ C)}$ and the beam radia-

tion G_b. The electrical production is also dependent on the optical efficiency. The optical efficiency, $\eta_{opt.}$, was set to one in order to estimate the maximum collector output, equation (8).

$$P_{el\_back\_beam} = w \cdot h \cdot \tau \cdot r \cdot \eta_{cells\_(25^\circ C)} \cdot G_b \cdot \eta_{opt.} \quad (8)$$

The electrical output from the diffuse radiation on the cells on the backside is calculated in equation (9). This is the product of the cell area of the back side, A_{cells_back}, the transmission through the glass, the reflection of the reflector, the efficiency of the cells, the diffuse radiation and also the optical efficiency.

$$P_{el\_back\_diff} = A_{cells\_back} \cdot \tau \cdot r \cdot \eta_{cells\_(25^\circ C)} \cdot G_d \cdot \eta_{opt.} \cdot f \quad (9)$$

Inserting the values presented in **Table 1.** into equations 5-9 gives a total maximum electrical output of $P_{el} = 272\text{W}$ or $P_{el} = 156\text{W/m}^2$ active glazed area (1.74 m²).

3.2. Electrical Efficiency Dependence on Temperature

The measured electrical efficiency per cell area for the PV/T hybrid collector at 25˚C is 20.9%, **Figure 8**. Expressed per active glazed area the efficiency is 13.9%. This means that the maximum electrical power for a collector is 241 W or 139 W/m^2 active glazed area. As expected, this number is somewhat lower than the optimum output of 272 W for a perfect optical efficiency. Also, the dependence of electrical efficiency on temperature (K_T) is -0.4%/K, in good agreement with the common value for solar cells described in literature [4].

3.3. Incidence Angle Modifiers for Beam Radiation

Figure 9 shows the electrical transverse and longitudinal incidence angle modifiers for the beam radiation, IAM_t in blue and IAM_l in red. The measured values are adjusted for temperature variations. The sharp increase/decrease around 0° for the IAM_t is due to the radiation shifting from outside to inside of the acceptance angle. The IAM_l for the front side and backside receivers is shown in yellow and green respectively. As shown, the front side receiver behaves like a flat plate solar panel. The backside receiver is the main responsible for the efficiency drop during low incidence angles in the longitudinal direction.

Table 1. Data for the calculation of the theoretical maximum collector output.

A_{cells_top} (m^2)	0.288698	τ(-)	0.95	$\eta_{cells\_(25^\circ C)}$ (-)	0.18
G_{total} (W/m^2)	1000	w(m)	1.976	h(m)	0.292
r(-)	0.95	G_b (W/m^2)	900	η_{opt} (-)	1
A_{cells_back} (m^2)	0.288698				

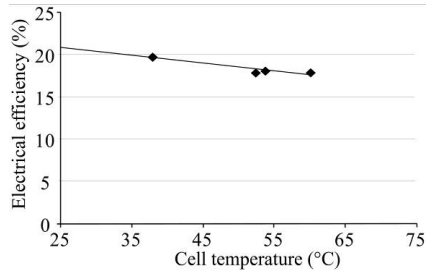

Figure 8. Electrical efficiency dependence on the water outlet temperature expressed per cell area.

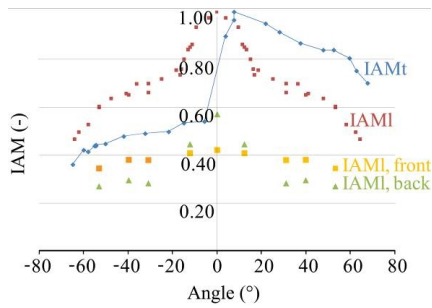

Figure 9. Electrical transverse incidence angle modifier (IAM_t) for beam radiation in blue and the longitudinal incidence angle modifier (IAM_l) in red. The IAM_l for the backside and the front side of the receiver is shown in yellow and green respectively.

4. Discussion

Figure 9 shows that when the collector is tracking around an axis aligned in the East-West direction it should maintain the projected solar height over the day between 5° and 10°. The drop in the longitudinal incidence angle modifier is due to the shading caused by the reflector edges. When $0°<\theta_l<30°$ the decrease in the IAM_l is apparent. This corresponds to partial shading on the first cell placed at the edge of the backside receiver. At around $\theta_l=30°$ the cell on the edge on the backside is totally shaded, eliminating almost completely the production of that string. Shading more cells when $\theta_l>30°$ will not imply a further production decrease on that string and thus, the total efficiency decrease slows down. If there was no diode installed on the string the drop would be double, since the strings are connected in series. I.e. the total IAM would drop to about 0.5 and not just to the 0.75 as seen in the figure. This is even more clearly seen, if the numbers for the cells on the backside of the absorber are studied. Here the value drops from 0.58 to 0.29, i.e. a 50% reduction. As can be seen from the same

figure the front side is less affected by the shading. The IAM_t shown in **Figure 9** is in agreement with previous measurements for the thermal production of a solar thermal collector with the same geometry [2].

The PV/T hybrid collector is made of two different parts. A front part where the solar cells behave like a flat plate solar panel under no concentration and a back part under concentration using a reflector. Since there is no synergic effect from combining non-concentrating solar cells with concentrating solar ones, only one of these alternatives should be the most cost-effective way of building a solar collector rather than a combination of both. The choice between a concentrating or non-concentrating system depends on the concentration factor, the fraction of diffuse and beam irradiation in the geographical location and the compactness needed for the collector.

The reflector part of the collector concentrates the radiation two times on the back side receiver. If the optical efficiency is around 50%, meaning that, under optimum conditions, the collector produces the same electrical output as a flat plate solar panel for the same temperature. This conclusion would change significantly, if the concentration factor were increased and the optical efficiency maintained. Hence, the concentration factor has an important influence on the output per cell area. One way of increasing the concentration could be to reduce the cell area on the backside of the receiver while using a tracking system. This can be done by cutting the cells in half or in thirds in the parallel direction of the busbars. The effect of the radiation profile after reflection should be further investigated.

As shown in **Figure 8**, a limitation of this study is the reduced amount of measured data for the dependence of efficiency on the temperature. Measurements were also carried out with cheaper sensors in order to verify the possibility of building low investment scientific solar laboratories in developing countries. The overall accuracy of measurement with such sensors was lowered to approximately 9%, but with a cost reduction of above 90% [5].

5. Conclusions

The optical properties of a PV/T CPC-collector were determined. These include the electrical transverse and longitudinal incidence angle modifiers, taking into account edge effects, by-pass diodes, acceptance angle and diffuse radiation contribution. The measured electrical efficiency at 25°C outlet water temperature was 20.9% per cell area and 13.9% per active glazed area. Such efficiencies occur during peak hours. During a large period of the day the output is significantly reduced by the reflector edges as shown by the IAM-measurements. This represents a big margin of improvement for the collector. By removing the cells on the edge, turning the edge cells 90°, dividing the string into three or four parts and tracking the collector around an axis oriented in the North-South direction, the collector performance can be significantly improved and is now under study. Hence, the annual production can become competitive with a flat plate solar panel while, at the same time, producing hot water.

6. Acknowledgements

The authors are grateful to the Swedish International Development Cooperation Agency for sponsoring the project.

REFERENCES

[1] Alanod, reflector manufacturer, 2012. http://alanod.com.

[2] L. R. Bernardo, H. Davidsson, B. Karlsson, "Performance Evaluation of a High Solar Fraction CPC-Collector System", *Japanese Society of Mechanical Engineers - Journal of Environment and Engineering*, 2011, Vol. 6, pp. 680-692. http://dx.doi.org/10.1299/jee.6.680

[3] L. R. Bernardo, B. Perers, H. Håkansson, B. Karlsson, "Performance Evaluation of Low Concentrating Photovoltaic/Thermal Systems: A Case Study from Sweden, *Solar Energy*, 2011, Vol. 85, pp. 1499-1510. http://dx.doi.org/10.1016/j.solener.2011.04.006

[4] S. Wenham, M. Green, M. Watt, R. Corkish, "Applied Photovoltaics", 2nd edition, Earthscan, London, 2007, ISBN 978-1844074013.

[5] N. Gentile et al., "Construction of a small scale laboratory for solar collectors and solar cells in a developing country", *Power and Energy Engineering Conference* and *Engineering*, Sanya, China, Dec 31, 2012 - Jan 2, 2013, unpublished

Nomenclature

P_{el}	Hybrid electric power	(W)
P_{el_front}	Hybrid electric power from front side receiver	(W)
P_{el_back}	Hybrid electric power from backside receiver	(W)
$P_{el\_back\_beam}$	Hybrid electric power from backside receiver due to beam radiation	(W)
$P_{el\_back\_diff}$	Hybrid electric power from backside receiver due to diffuse radiation	(W)
G_{total}	Total irradiance	(W/m²)
G_b	Beam Irradiance	(W/m²)
G_d	Diffuse Irradiance	(W/m²)
T_{in}	Inlet water temperature	(°C)
T_{out}	Outlet water temperature	(°C)
T_{mid}	Middle water temperaure	(°C)
A_{cells_front}	Cell area of the front side receiver	(m²)
A_{cells_back}	Cell area of the backside receiver	(m²)
β	Collector tilt from horizontal	(°)
f	Useful fraction of diffuse radiation	(-)
τ	Transmittance coefficient of glass	(-)
r	Reflectance coefficient of the reflector	(-)
w	Total width of the cells	(m^2)
h	Height of the reflector	(m^2)
C	Concentration factor of the collector	(-)
$\eta_{cells\_(25°C)}$	Cell efficiency at 25°C	(-)
η_{opt}	Optical efficiency	(-)
K_T	Electrical efficiency temperature dependence	(%/°C)
θ	Angle of incidence onto collector	(°)
θ_t	Transverse angle of incidence onto collector	(°)
θ_l	Longitudinal angle of incidence onto collector	(°)
IAM_l	Electrical longitudinal incidence angle modifier	(-)
IAM_t	Electrical transverse incidence angle modifier	(-)

Article IV

Energies **2012**, *5*, 4110-4131; doi:10.3390/en5104110

OPEN ACCESS

energies

ISSN 1996-1073

www.mdpi.com/journal/energies

Article

Retrofitting Domestic Hot Water Heaters for Solar Water Heating Systems in Single-Family Houses in a Cold Climate: A Theoretical Analysis

Luis R. Bernardo [1,*], Henrik Davidsson [1] and Björn Karlsson [2]

[1] Energy and Building Design Division, Lund University, Box 118 SE-221 00 Lund, Sweden; E-Mail: Henrik.Davidsson@ebd.lth.se

[2] Division of Energy, School of Sustainable Development of Society and Technology, Högskoleplan 2, Gåsmyrevreten, SE-721 23 Västerås, Sweden; E-Mail: Bjorn.Karlsson@mdh.se

* Author to whom correspondence should be addressed; E-Mail: Ricardo.Bernardo@ebd.lth.se; Tel.: +46-462227606; Fax: +46-462224719.

Received: 20 July 2012; in revised form: 15 October 2012 / Accepted: 15 October 2012 / Published: 22 October 2012

Abstract: One of the biggest obstacles to economic profitability of solar water heating systems is the investment cost. Retrofitting existing domestic hot water heaters when a new solar hot water system is installed can reduce both the installation and material costs. In this study, retrofitting existing water heaters for solar water heating systems in Swedish single-family houses was theoretically investigated using the TRNSYS software. Four simulation models using forced circulation flow with different system configurations and control strategies were simulated and analysed in the study. A comparison with a standard solar thermal system was also presented based on the annual solar fraction. The simulation results indicate that the retrofitting configuration achieving the highest annual performance consists of a system where the existing tank is used as storage for the solar heat and a smaller tank with a heater is added in series to make sure that the required outlet temperature can be met. An external heat exchanger is used between the collector circuit and the existing tank. For this retrofitted system an annual solar fraction of 50.5% was achieved. A conventional solar thermal system using a standard solar tank achieves a comparable performance for the same total storage volume, collector area and reference conditions.

Keywords: solar thermal; storage tank; water heater; retrofit; domestic hot water

Nomenclature:

T_{set}	Temperature setting of the auxiliary heater (°C)
T_{out}	Collector outlet temperature (°C)
T_{top}	Solar hot water temperature in the upper part of the retrofitted tank (°C)
V_{aux}	Volume of the auxiliary heater storage (L)
β	Collector slope from horizontal (°)
$F'(\tau\alpha)_n$	Zero loss efficiency of the collector (-)
$F'U_0$	Heat loss factor (W/m^2 K)
$F'U_1$	Temperature dependence of the heat loss factor (W/m^2 K^2)
$F'U$	Total heat loss factor (W/m^2 K)
$k_b(\theta)$	Beam incidence angle modifier as a function of θ(-)
b_0	Calibration factor for $k_b(\theta)$
θ	Angle of incidence on the collector normal (°)
t	Simulation time-step (h)
U_{top}	Average heat loss factor for the top of the storage (W/m^2 °C)
U_{side}	Average heat loss factor for the edges of the storage (W/m^2 °C)
U_{bottom}	Average heat loss factor for the bottom of the storage (W/m^2 °C)
U_{pipe}	Average heat loss factor for the piping (W/m^2 °C)
l_{out}	Total length of the pipes exposed to outdoor temperature (m)
l_{in}	Total length of the pipes exposed to indoor temperature of 20 °C (m)
C_p	Specific heat of water (J/kg K)
$HX_{capacity}$	Capacity of the heat exchanger (W/K)
P_{pump}	Maximum pump power (W)
$\dot{m}$	Mass flow rate (kg/h)
A_c	Collector area (m^2)
$Q_{aux\text{-}nonsolar}$	Required auxiliary energy to meet the load without solar collectors (kWh/y)
$Q_{aux\text{-}solar}$	Required auxiliary energy to meet the load with solar collectors (kWh/y)
Q_{pumps}	Required energy to run all the pumps in the system (kWh/y)
$Q_{losses\text{-}retrofit}$	Thermal losses from the retrofitted storage (kWh/y)
$Q_{losses\text{-}aux}$	Thermal losses from the auxiliary storage (kWh/y)
$Q_{losses\text{-}stnd}$	Thermal losses from the standard solar storage (kWh/y)
T_{top}	Temperature at the top of the retrofitted storage (°C)
T_{bottom}	Temperature at the bottom of the retrofitted storage (°C)
T_{aux}	Temperature at the new auxiliary heater storage (°C)
T_{DHW}	Temperature of the domestic hot water provided to the user (°C)
T_{cold}	Temperature of the cold water from the main (°C)
md_{coll}	Mass flow rate at the solar collector circuit (L/h)
md_{DHW}	Mass flow rate of the domestic hot water provided to the user (L/h)

1. Introduction

One of the biggest obstacles to the economic profitability of domestic solar water heating (SWH) systems is the investment cost [1–3]. The installation cost of forced circulation systems used in cold climates can represent up to 50% of the total investment cost depending on the size and type of system [4]. Also, the solar storage is one of the most expensive components in a solar water heating system [1]. Retrofitting existing domestic water heaters when new SWH systems are installed can reduce the total investment cost by decreasing both the installation and material costs. In Sweden there are more than half a million electrically heated single family houses that use conventional water heaters for domestic hot water production [5]. Such retrofitting needs to be carried out with consideration of the cold Swedish climate. In such regions the solar storage is placed indoors and a freeze protection medium runs inside the collector circuit. Since existing water heaters are not provided with a heat exchanger, an external one should be used. There are two main types of systems designed with an external heat exchanger outside the storage: thermosyphon and forced flow circulation.

Cruickshank and Harrison, in 2004 [6] and 2006 [7], investigated this type of thermosyphon systems in the Canadian cold climate. In 2011 [8], the same authors studied the performance of series and parallel connected thermosyphon storages. Thermosyphon systems became popular in several parts of the world such as Eastern Asia and Australia, mainly due to their simplicity and reliability [9]. The thermosyphon driving force depends on the pressure difference and frictional losses between the heat exchanger side-arm and the tank. Hence, the generated flow will be a complex function of the state of charge of the tank, the temperature profile along the heat exchanger and pipes, the height difference between the top of the heat exchanger and the top of the tank and the pressure drop in the heat exchanger, piping and connections [7,10,11]. Such dependence on the heat exchanger pressure drop and tank characteristics limits how the retrofit is carried out, where the heat exchanger should be placed and which storage tanks can be used [12]. Moreover, when properly designed, forced circulation systems can significantly achieve higher performances compared with natural convection driven systems [2,12–14]. This is mainly explained by the increase in energy transfer rate at a low energy driving cost. For example, a 40 W pump can generate a driving force 45 times higher than the one achieved by natural convection systems. In addition, low energy pumps are now available at a lower cost. The disadvantages of forced circulating systems are stated to be a higher degree of complexity and the demand for electricity to run the pumps and controls [2,12].

Fewer studies are focused on forced circulation systems specially designed for cold regions. Wongsuwan and Kumar [15] concluded that TRNSYS software [16] predicts accurately the performance of forced circulation systems. Buckles and Klein [17] used TRNSYS software to theoretically investigate different system configurations, and concluded that heat exchangers, with the same capacity, have similar performance whether placed inside or outside the storage. In 2009, Hobbi and Siddiqui [18] used TRNSYS to theoretically optimize the design of a forced circulation hot water system for cold climates. As in other studies, the annual solar fraction was used as design parameter to be optimized [11,15,17–24]. Of specific interest is the fact that there is a lack of studies investigating the retrofitting of existing water heaters in single-family houses for solar hot water application in cold regions.

Retrofitting solar domestic hot water systems today commonly consists on series connecting the existing system with a new solar storage upstream and using the existing hot water boiler as a backup heater [25]. Some retrofitted systems make use of thermosyphoning and are therefore dependent on a new well performing storage for that purpose [26–28]. Existing installations are often oversized in volume since large design loads have been used before and because domestic hot water consumption has been decreasing [25]. Combined with low levels of insulation, such over sizing causes large system heat losses. When using the existing storages as solar hot water storage the thermal losses in the system can be decreased since the solar water temperature is lower than the backup temperature. In cases where it is possible to know when the existing boiler is close to the end of its lifetime, it can be advantageous to change the existing storage [25].

In this research, retrofitting of conventional domestic water heaters using forced circulation SWH systems for single-family houses in the Swedish climate was theoretically investigated. This was carried out by means of two pumps, one in the tank loop and the other in the solar collector loop with a heat exchanger in between. Four different system configurations were simulated in TRNSYS software and compared based on the annual solar fraction. Since forced circulation is used, almost any kind of storage tank can be retrofitted when a new solar thermal system is installed. Also, the degree of complexity of forced circulation systems may be reduced with such a retrofit. For a better understanding of the research contribution to the field and to increase the readability of the paper, the main objectives of the study are stated below:

- To theoretically investigate different system configurations and control strategies in retrofitting conventional domestic water heaters for SWH systems in single-family houses in the Swedish climate;
- To compare the performance of the retrofitted systems with the performance of a standard solar thermal system for the same reference conditions.

This study provides necessary information to further investigate such systems in practice. It is then necessary to validate the theoretical models and carry out a life cycle cost assessment to compare the different systems. Such assessment is based on many factors that vary from country to country and can lead to different conclusions. Outside cold regions free from freezing, an anti-freeze solution and an external heat exchanger are not required. This will alter the system configuration, its performance and final costs. Other variable factors are cost of the auxiliary energy, its predicted trend during the system lifetime, the investment cost of the required equipment, the installation cost, maintenance costs, operation costs, replacement costs, subsidies, taxes on eventual loans, inflation, chosen discount rate and residual value at the end of the system's lifetime. Also, it is difficult to quantify how much the industrial development on the integration of all retrofitting components into one add-on unit would decrease the cost. In addition, the space occupied by the introduction of the extra retrofitting material such as pumps, controls and heat exchanger is a qualitative comparison parameter between the systems valued differently by the consumer. These assessments are outside the scope of this work and will be dealt with in a further stage of the investigation.

2. Methodology

Different system configurations were analysed using TRNSYS software in order to determine the annual solar fraction. Firstly, the characteristics of existing domestic water tanks in Sweden were determined. Secondly, a domestic hot water load profile representative of Swedish single-family houses was created. Lastly, the energy model of each system configuration and sensitivity analysis was described.

2.1. Existing Domestic Hot Water Heaters in Swedish Single-Family Houses

The main boundary of this investigation was to retrofit the most common type of existing domestic hot water heaters in single family houses in Sweden. To the best of our knowledge, there is no official data concerning the most common tank size in such houses. According to the Swedish domestic water heater manufacturers, installers and researchers in the field, the most common Swedish single-family house tank size is 200–300 litres, depending on the family size. The trend is that higher loads correspond to higher available storage volumes. A sensitivity analysis showed that retrofitting a 300 litre tank would give a higher annual solar fraction than using a 200 litre tank for the same load. Hence, to be on the safe side, it was decided to use a 200 litre tank for the analysis. In most of the cases, the heat is generated by a 3 kW electric auxiliary heater inside the tank.

2.2. Domestic Hot Water Load in Swedish Single-Family Houses

A profile of the domestic hot water load consumption in Swedish single-family houses was created. The profile consists of seven different draw-offs during the day (Figure 1). This represents a simplification of the hourly profile described by Widén *et al.* [29] but scaled to the latest data on the Swedish average hot water consumption of 42 litres per person per day measured in 44 single-family houses [24,30]. A sensitivity analysis showed that using a more detailed draw-off profile would have a low impact on the results and would only increase the total computational time. The measured average cold water temperature in the taps was 8.5 °C [30]. The variation in consumption during the year was also introduced based on measured data [31] and is shown in Figure 2. Swedish statistics show that the average number of inhabitants in Swedish single-family houses is three [32]. Hence, assuming that hot water is heated up to 60 °C, the annual domestic hot water consumption in these houses was estimated to be 2050 kWh/year. This value is close to previous measured values in single-family houses [33]. This energy amount does not include the extra energy necessary to compensate for the heat losses from the storage and piping system and the energy necessary to run the circulation pump in the tank loop, if one is installed. These factors were taken into account by the model in calculating the annual solar fraction of every system.

Figure 1. Daily domestic hot water profile.

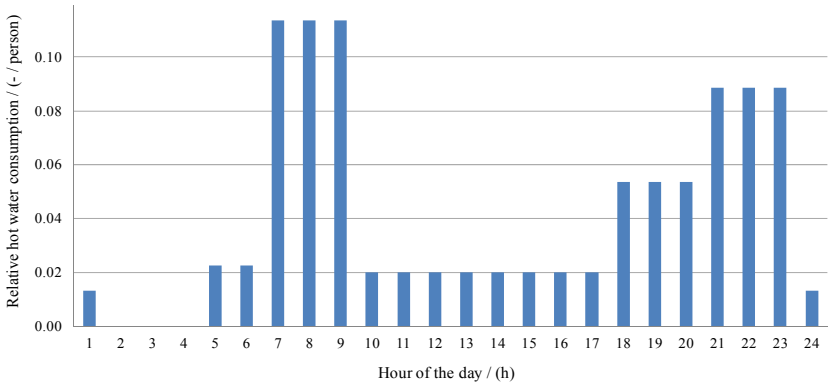

Figure 2. Yearly variation of the daily domestic hot water consumption.

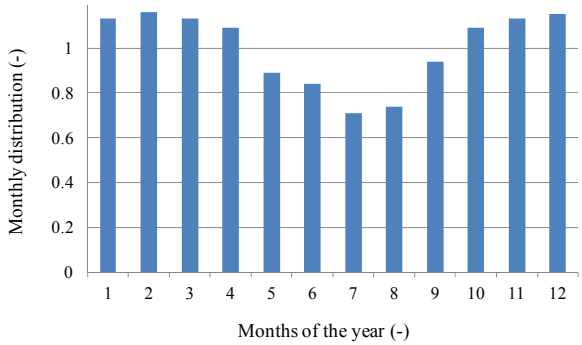

2.3. Regulations Regarding Water Heating Systems and Legionella Growth

It is known that legionella bacteria grow between 20 °C and 50 °C with maximum growth between 32 °C and 42 °C and dies above 60 °C after a certain period of exposure [34–36]. E.U. directives concerning legionella prevention are very general. In EN 806-2 is stated that "the hot water temperature in the hot water pipe work shall not drop below 50 °C" [37]. Investigation during in Swedish and Italian hospitals during ten years showed that, in order to achieve safety from legionella danger, it is unrealistic and unnecessary to completely eliminate the bacteria [38,39]. Indeed, a thermal prevention does not offers 100% protection against legionella occurrence but prevents an uncontrolled bacteria growth [37]. From the literature review it is concluded that small systems like the ones designed for solar domestic hot water represent a very low risk for bacteria growth. In France, Germany, United Kingdom and Switzerland, the risk is considered very low in single-family houses and there are no restrictions on water storage temperature [34,37,40,41]. According to a theoretical study for the specific conditions in The Netherlands, a possible risk for legionella growth should not be excluded especially in case of absence during a week in the winter [34]. The Netherlands uses probably the most extensive risk assessment in Europe and recommends that a weekly thermal

disinfection of 60 °C during 20 min is performed when the water is stored between 25 °C and 45 °C [25,37]. In such situation, "Legionella may occasionally occur in concentrations above the detection limit but there is no reason to expect high concentration levels [37]". The Swedish industry regulations recommend that a weekly thermal disinfection is performed at 60 °C during 10 min if water is stored at lower temperatures than 60 °C [42,43]. Hence, according to the literature review and taking the following measures, the system should be well protected against a dangerous level of legionella growth:

- Auxiliary heater volume kept at 60 °C;
- Hot water temperature available at the higher than 50 °C and lower than 60 °C;
- Heating up the whole storage volume to 60 °C during 20 min if the temperature of the retrofitted tank was below 60 °C during a period of one week;
- As a design guideline, the domestic hot water system should, during a maximal period of six hours, be able to heat up 10 °C cold water and deliver two times 140 litres of 40 °C water in one hour. This is the equivalent to being able to provide, every six hours, 9.75 kWh during one hour.

All systems were designed in a way that these requirements/recommendations could be met.

2.4. System Model

The retrofitted system models range from simple connections to more advanced configurations and controls. However, the complexity was never increased to a level that would be technically difficult to build in practice. Also, it was decided to avoid design configurations that would predictably cause such a rise in the investment cost that it would be hardly recouped by the increase in energy savings. Each system model was built by using different component simulation models called TRNSYS types. These are:

- *Thermal collector*—type 537 from TESS TRSYS library [44]. This solar collector model operates like a conventional flat plate collector but makes it possible to regulate a variable speed for the pump in the collector loop in order to keep the outlet temperature, T_{out}, at a user-specified value. The parameters used to describe the collector were considered to be reasonable for flat plate collectors used in a cold climate [18,24]. These are 0.8 for $F'(\tau\alpha)_n$, −3.6 for $F'U_0$, −0.014 for $F'U_1$ and −0.2 for b_0 based on average collector temperature and tested flow rate of 30 kg/h. The dependence of parameter $k_b(\theta)$ on b_0 is described by Equation (1) [19]. A sensitivity analysis was performed regarding the size of the collector and the corresponding annual solar fraction in the range 0–12 m^2.

$$\boldsymbol{K_b(\theta)} = 1 - b_0 \times \left(\frac{1}{\cos\theta} - 1\right) \quad (1)$$

- *Fully stratified standard storage tank (6 nodes)*—type 534 from TESS TRNSYS library. This model represents a common type of storage tank in standard SWH systems for domestic hot water production. The model divides the tank into isothermal nodes that thermally interact with the ones above, below and with the tank wall. It models a vertical cylindrical tank with a total volume of 255 litres and 1.60 m high. The coil heat exchanger was placed in the lower third of the tank according to the manufacturer's specifications. A 3 kW electric auxiliary heater was

fitted horizontally at 0.5 m from the top with a set-point temperature, T_{set}, of 60 °C (Figure 3). As shown by Cruickshank and Harrison [45], calculating the heat loss factor of the storage based on its insulation characteristics and materials can lead to significant errors. The number and type of inlet and outlet connections and poor insulation at the tank bottom are examples of factors that lead to such inaccuracies. Thus, the U-values were then based on the experimental results with common storages in standard SWH systems [45]. These were assumed to be 1 W/m^2 °C for the top and middle of the storage, U_{top}, U_{side} and 2.5 W/m^2 °C for the bottom, U_{bottom};

- *Fully stratified retrofitted storage tank (6 nodes)*—type 534 from TESS TRNSYS library. This storage was modelled with the same principles as the standard storage for SWH systems. However, the total volume was set to 200 litres, the height was assumed to be 1.40 m, the connections are placed at the top and bottom of the tank (Figures 4–7) and there is no internal heat exchanger. Only retrofitted system 2 uses the auxiliary heater placed at the bottom (Figure 4). In all the other systems this heater is disabled. The same U-values described above were also used for this storage;
- *Small heater storage tank (1 node)*—type 534 from TESS TRNSYS library. The total volume was set to 55 litres and the height to 0.60 m. The connections are also placed at the top and bottom of the tank (Figures 5–7). An auxiliary heater of 3 kW was used in all models since this is the most common and a higher power could create problems with the installed capacity in such houses. The auxiliary heater keeps the temperature of the storage volume at least at 60 °C to avoid legionella problems [46]. The average U-value used for this storage was 0.5 W/m^2 °C based on preliminary measurements on an existing tank. A sensitivity analysis concerning the impact on the annual solar fraction of the variation in the auxiliary heater volume and temperature was performed;
- *External heat exchanger*—type 5b, counter flow (Figures 4–7). A sensitivity analysis was performed to investigate the influence of the heat exchanger capacity on the annual solar fraction in the interval 0–600 W/K. Since the effect of glycol percentage in the anti-freeze solution of the collector circuit was previously shown to have small impact on the annual solar fraction [18], the C_p of water, 4.19 kJ/kg K, was used instead. The flow speed was set equal on both sides of the heat exchanger;
- *Circulation pumps*—type 3b, single speed. In all the systems the flow was optimized in order to maximise the annual solar fraction;
- *Controller*—type 2b, ON/OFF differential controller. The controller turns ON both the pumps when the difference between the outlet collector temperatures, T_{out}, and the bottom tank temperature, T_{bottom}, is higher than 10 °C. The charging process is ceased when this difference is lower than 3 °C. The charging is also stopped if the temperature at the top of the tank, T_{top}, reaches 100 °C.
- *Radiation processor*—type 109-TMY2 used to compute the radiation and weather data for Lund, Sweden (latitude 55°44'N, longitude 13°12'E);
- *Domestic hot water load profile*—type 14 used to generate the daily load profile (Figure 1);
- *Energy balance check*—type 28 with energy balance check based on Buckles and Klein [17] for every simulation time-step, t, of six min.

A summary of the design parameters used in the system model are presented in Table 1.

Table 1. Design parameters for the system model.

Parameter	Value
A_c	0–12 m^2
$F'(\tau\alpha)_n$	0.8 (−)
$F'U_0$	−3.6 W/m^2 K
$F'U_1$	−0.014 W/m^2 K^2
b_0	0.2 (−)
β	40 °
$\dot{m}/A_c$	0–11 kg/h m^2
P_{pump}	60 W
U_{pipe}	0.8 W/m^2 K
l_{out}	8 m
l_{in}	8 m
$HX_{capacity}$	0–600 W/K
T_{set}	60–90 °C
V_{aux}	55–75 L
U_{top}	1 W/m^2 K
U_{side}	1 W/m^2 K
U_{bottom}	2.5 W/m^2 K

The annual solar fraction takes into account the energy to produce the domestic hot water required by the load including losses and necessary energy to run pumps as well as the saved energy by the collectors. It was calculated based on Equation (2) [17].

$$f = \frac{Q_{aux-nonsolar} - Q_{aux-solar} - Q_{pumps}}{Q_{aux-nonsolar}} = 1 - \frac{Q_{aux-solar} + Q_{pumps}}{Q_{aux-nonsolar}} \quad (2)$$

2.4.1. Solar Collectors and Flow Control

The solar collectors were placed at a 40° tilt from horizontal which maximises the annual solar fraction in Lund, Sweden [47]. A sensitivity analysis was performed regarding the impact of the size of the collector array on the annual solar fraction. Once the size was determined the collector field area in all systems was kept constant in order to ensure that any difference in annual performance was caused by the system configuration and/or control. Two types of pump control were tested. Control (a) varies the flow up to 300 kg/h so that the collector outlet temperature was kept constant and equal to 65 °C. Control (b) consists of constant flow speed and is set to a value that maximises the annual solar fraction. The optimization process for control (b) was performed using Generic Optimization Program (GenOpt) [48] applied to TRNSYS. The Hooke-Jeeves algorithm [49] was used to perform iterations with different flow values until the maximum annual solar fraction of each system was reached.

2.4.2. Standard System

A model of a standard solar thermal system was created which is described by the sketch in Figure 3. The storage volume is 255 litres in order to match the volume of the retrofitted system with

the highest performance (retrofitted system 3, Figure 6). There are three temperature sensors that control the pump, two placed on the tank's surface and the other at the collector outlet.

Figure 3. Standard solar water heating system.

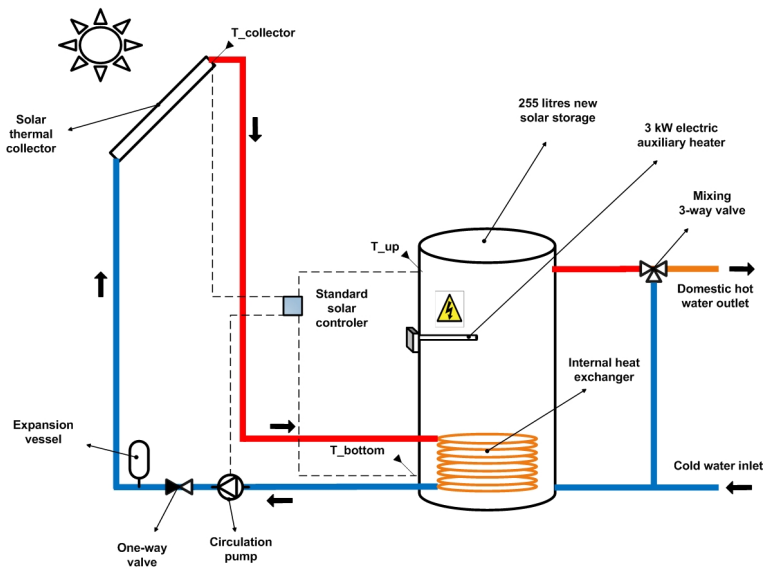

2.4.3. Retrofitted System 1

Figure 4 describes a simple and direct way of assembling the solar collectors to the existing water heaters. Also, two temperature sensors are placed on the surface of the retrofitted tank in order to control both the collector pump and the tank pump. As exemplified in Figure 3, solar storages are specially designed for solar thermal applications with, at least, two connections for the domestic hot water loop and two others for the solar collector loop. Contrarily, conventional tank heaters have only two connections for domestic hot water. The working period of the pump placed in the tank loop must be controlled with the domestic hot water draw-offs so they do not coincide. When no hot water is required, the pump is able to charge the tank. When draw-offs take place, both the pump and the control valve are shut down and the incoming cold water is pressed in the bottom of the tank replacing the outgoing domestic hot water at the top. In this system the whole tank is constantly heated up to 60 °C by the auxiliary heater placed at the bottom. This means that, for this system, running the system with control a) in order to have a constant outlet temperature of 65 °C does not make sense.

2.4.4. Retrofitted System 2

In this system, a new 3 kW auxiliary heater is added to the side-arm heat exchanger while the existing one at the bottom of the tank is turned OFF (Figure 5). The aim is to achieve stratification in the storage. The heater and the pump on the tank loop are turned ON when T_{top} falls below T_{set} minus the dead band. Consequently, the cold water in the tank bottom flows through the heat exchanger and

is heated up in the side-arm heater before entering the top of the tank. The heater is turned off when T_{top} is higher than T_{set} plus the dead band.

Figure 4. Retrofitted system 1—simple retrofitting of existing hot water heaters.

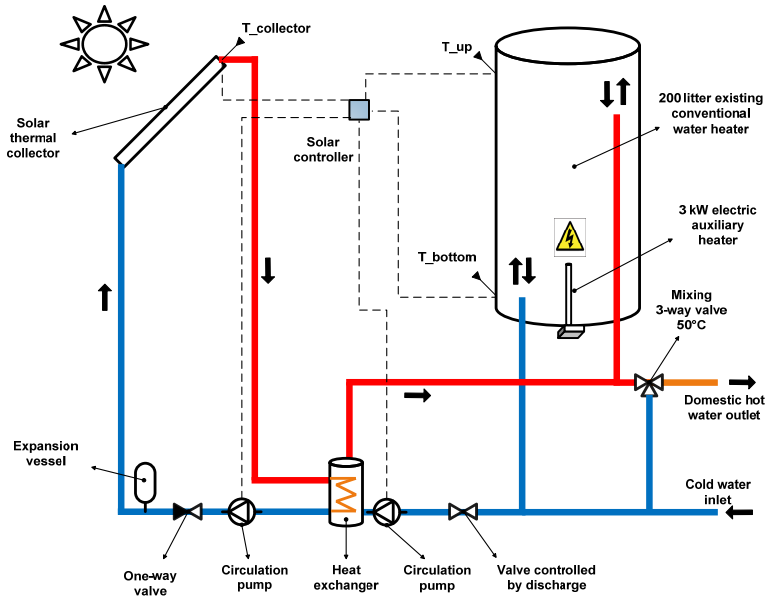

Figure 5. Retrofitted system 2—retrofitted system with auxiliary heater on the side-arm.

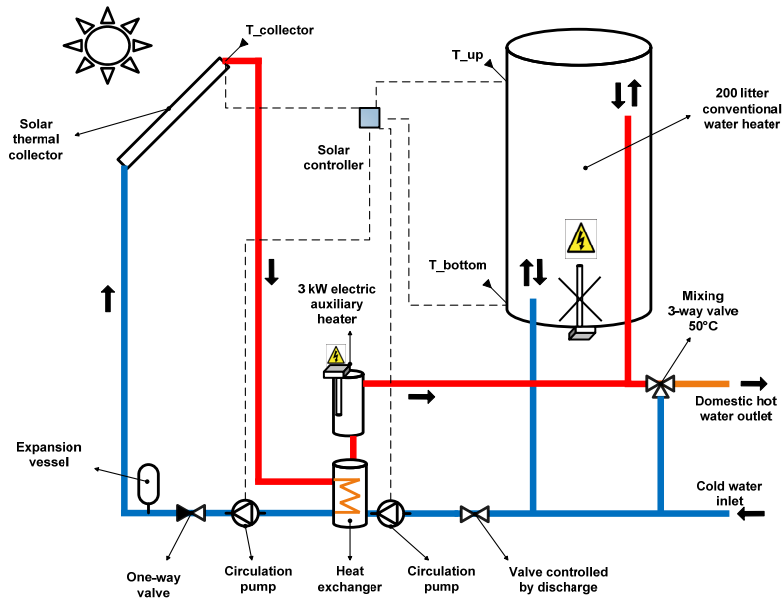

2.4.5. Retrofitted System 3

In retrofitted system 3, a 55 litre auxiliary heater storage was series connected to the existing storage (Figure 6). This means that the retrofitted storage tank is now exclusively used for solar hot water which is not stored together with hot water provided by the auxiliary heater. When hot water is drawn off by the user, the water at the top of the retrofitted storage is pushed to the bottom of the small heater and from there to the user. When the temperature in the auxiliary heater becomes higher than T_{set} due to the incoming solar hot water, the auxiliary heater is turned OFF automatically by the thermostat.

Figure 6. Retrofitted system 3—retrofitted system with an additional tank heater connected in series.

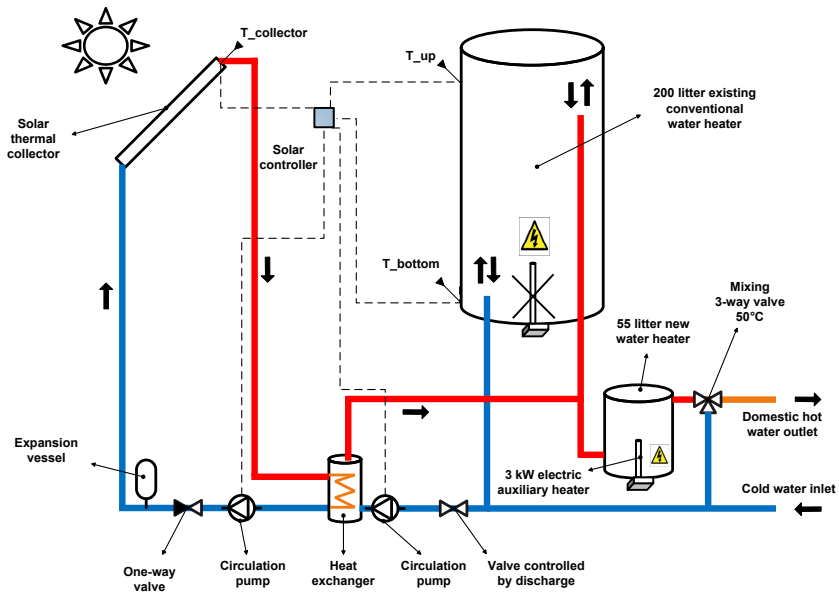

2.4.6. Retrofitted System 4

The last retrofitted system consists of adding one mixing valve in the previous system (Figure 7). The valve makes it possible to mix flows from two inlets into one outlet. The cold source inlet is the retrofitted storage while the hot source inlet is the auxiliary storage. In order to minimize the risk of legionella growth the outlet temperature of the valve was set to 60 °C. If both the inlet temperatures are higher than 60 °C the water is taken from the retrofitted tank only and later cooled down to 50 °C by the last mixing valve before going to the load.

For this system, not only controls (a) and (b) for the flow of the pump were analysed but also an extra control, control (c). The latest consists on shutting down the auxiliary heater whenever the solar storage is able to provide a volume of water equal to that of the auxiliary heater, heated up to 60 °C or

higher. When the temperature of that volume drops below 60 °C, the water in the auxiliary volume is heated up again and ready to provide the necessary hot water to the load.

Figure 7. Retrofitted system 4—retrofitted system with an additional mixing valve.

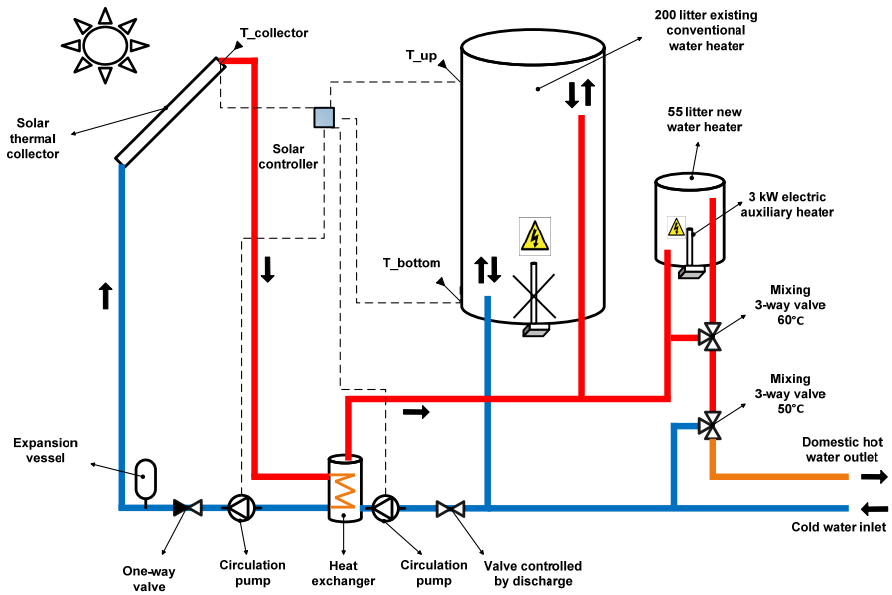

3. Results and Discussion

3.1. Standard System

3.1.1. Collector Area

The sensitivity analysis of the collector area is presented in Figure 8. The collector area was set to 6 m^2 since it represents a balance between a high annual solar fraction and collector area. The chosen collector area is not a determinant factor on comparing the different systems based on their system configurations, types of storage and control strategies. Different collector areas would impact the absolute value of the annual solar fraction but not the relative performances between the systems.

3.1.2. Mass Flow Rate

The mass flow rate per collector area ($\dot{m}/A_c$) was optimized for each system using GenOpt. The optimizing results for the standard system are shown in Figure 9. As shown in the figure, for the flow interval of 5–10.8 kg/h m^2 the annual solar fraction is kept at its maximum, 52%, within a 1% deviation. The flow used in all systems was 7 kg/h m^2 which ensures maximum annual solar fraction. Such low flow value is in agreement with previous studies where comparable flow rates were found to increase the annual performance [23,50–52]. Furthermore, the requirement on the size of components in low flow systems is reduced. This is the case of the heat exchanger capacity, pipe diameter, pump

sizes and their energy consumption [2,12,50]. The annual solar fraction result is in accordance with previous studies for the same kind of standard SWH systems with comparable collector area, storage type, storage volume, mean domestic hot water load and weather conditions [18,53].

Due to the position of the auxiliary heater, the total auxiliary volume is 102 litres. In order to reach the recommended design guideline for large loads the heater temperature should be temporarily increased to 70 °C by the user.

Figure 8. Variation of the annual solar fraction with the collector area.

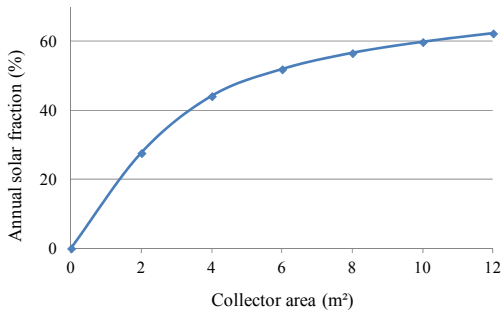

3.2. Retrofitted System 1

3.2.1. Heat Exchanger Capacity

The influence of the heat exchanger capacity on the annual solar fraction was investigated (Figure 10). The capacity for the heat exchanger was set to 300 W/K which ensures an annual solar fraction of 28.9%. This value represents 95% of the achieved annual solar fraction if the heat exchanger capacity was doubled. The heat exchanger capacity of 300 W/K was kept constant in all systems.

Since the auxiliary is placed at the bottom, the whole tank represents the auxiliary volume when solar energy is not available, which ensures that the design guideline for large loads is met.

3.3. Retrofitted System 2

For this system, simulation results show that the annual solar fraction increases to 34.8% for control (a) and 37.6% for control (b). However, stratification is limited by the fact that the auxiliary hot water is pumped inside the tank, inducing mixing. Also, heat diffusion and wall conduction in the storage limit the stratification level. Furthermore, the energy needed for the pump increased significantly to 243 kWh/year which is 3.5 times higher than that of the previous system. This is explained by the fact that one more pump is needed and that one of them works continuously every time auxiliary heat is required. Running the system with control (a) prevents disruption of stratification since the top of the tank is heated up to 60 °C and the collector outlet temperature is always higher than 65 °C. However, this increases significantly the collector losses and control (b) was shown to be more efficient.

In this system the auxiliary volume is the volume above the temperature sensor in the upper part of the tank which was set to 80 litres. This volume meets regular loads while design loads are met by temporarily increasing the auxiliary heater temperature to 90 °C or by turning ON the existing auxiliary heater in the bottom of the storage.

Figure 9. Convergence of the optimization algorithm of the annual solar fraction by varying the collector flow.

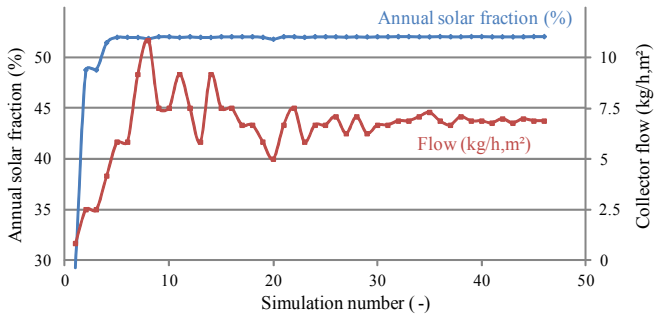

Figure 10. Variation of the annual solar fraction, for system 1, with the heat exchanger capacity.

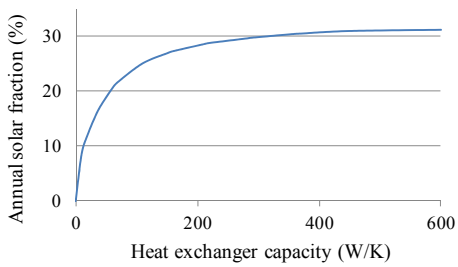

3.4. Retrofitted System 3

The estimated annual solar fraction for retrofitted system 3 is 38.1% for control (a) and 50.5% for control (b). Since the auxiliary heater is placed in another tank, it is no longer turned ON when the outlet temperature of the collector is below 60 °C. Also, the retrofitted tank works at lower temperatures which increases the collector working hours and efficiency. In addition, the new well insulated hot temperature tank provides the extra energy when solar energy is not available. Having the larger tank working at lower temperatures reduced the retrofitted storage heat losses by 50%, 457 kWh/y (Table 5). Furthermore, mixing caused by diffusion and wall conduction was also considerably reduced since the auxiliary hot water at 60 °C is not stored in the same tank as the cold water from the main. The system "stratification" is then achieved by means of two tanks with low stratification levels but working at different average temperatures.

During the summer period, when solar hot water is available over 60 °C, the total solar hot water storage volume of the series connected system is increased to 255 litres, since both tanks are connected

in series and no auxiliary energy is needed. Figure 11 shows such a typical operation day in July where the collector is charging the system simultaneously as the user is discharging the tank. As shown in the figure, both the retrofitted storage tank and auxiliary storage are charged during a sunny morning until the middle of a cloudy afternoon. From that point on, the pumps were stopped while the discharge process continued. At the beginning of the charging process it is possible to notice that stratification decreases since colder temperature is placed at the top. This is explained by the fact that the inlet position is placed at the top while the controller compares the bottom temperature with the collector outlet temperature in order to start the pumps. This controlling process will be improved and tested in practice. After the solar pump is stopped the discharge of the retrofitted storage continues cooling down the bottom of the tank.

Figure 11. Typical operation day of retrofitted system 3 during the summer period.

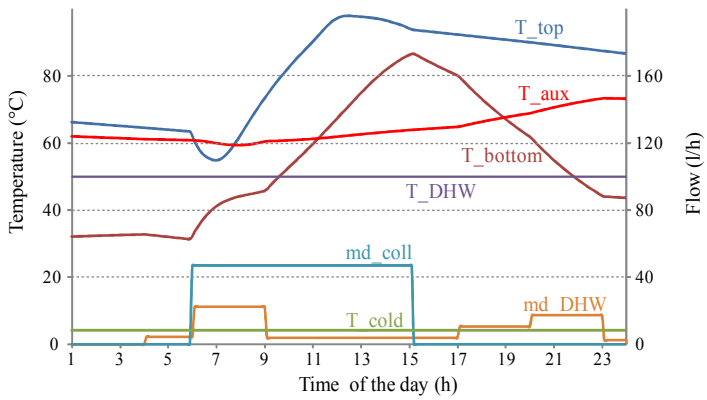

The sensitivity analysis on the auxiliary volume and temperature variation is presented in Tables 2 and 3. The annual solar fraction remains almost constant with auxiliary volume variation. For larger auxiliary volumes, the domestic hot water load increases due to higher losses. However, the solar coverage increases proportionally and the annual solar fraction remains almost constant. On the other hand, the increase in T_{set} caused a significant decrease in solar fraction. The domestic hot water load increases due to higher thermal losses in the auxiliary heater. For higher values of T_{set} less water is required from the auxiliary heat source and, since the tanks are series connected, from the retrofitted solar storage. Hence, the average temperature of the retrofitted storage becomes higher which decreases the solar contribution and increases the heat losses.

The 55 litre tank heated to 60 °C meets regular loads. When the temperature in the main is 8.5 °C, it corresponds to 92 litres mixed water at 40 °C provided to the user. When T_{set} is increased to 90 °C and, if the solar storage is discharged, the design guideline for large loads is met by 85% of the total energy. To meet this recommended design load to 100% the user can temporarily turn ON the existing auxiliary heater of the retrofitted tank. Alternatively, the 75 litre auxiliary volume heated up to 90 °C covers that demand to 100%.

For the present conditions, simulation shows that it was necessary to use the thermal disinfection measure 18 times during a year and that the annual solar fraction was decreased less than 3%.

Table 2. Annual solar fraction calculations for three auxiliary volume sizes of retrofitted system 3 with T_{set} = 60 °C.

V_{aux} (L)	$Q_{aux\text{-}nonsolar}$ (kWh/y)	$Q_{aux\text{-}solar}$ (kWh/y)	Q_{pumps} (kWh/y)	$Q_{losses\text{-}retrofit}$ (kWh/y)	$Q_{losses\text{-}aux}$ (kWh/y)	Annual Solar Fraction (%)
55	2037	877	131	447	148	50.5
65	2053	885	131	445	163	50.5
75	2070	901	131	446	179	50.1

Table 3. Annual solar fraction calculations for different auxiliary heater temperatures of retrofitted system 3 with V_{aux} set to 55 L.

T_{set} (°C)	$Q_{aux\text{-}nonsolar}$ (kWh/y)	$Q_{aux\text{-}solar}$ (kWh/y)	Q_{pumps} (kWh/y)	$Q_{losses\text{-}retrofit}$ (kWh/y)	$Q_{losses\text{-}aux}$ (kWh/y)	Annual Solar Fraction (%)
60	2037	877	131	447	148	50.5
70	2088	1007	127	477	176	45.7
80	2138	1148	122	508	208	40.6
90	2188	1296	118	538	244	35.4

3.5. Retrofitted System 4

The estimated annual solar fraction for retrofitted system 4 is 36.9% for control (a), 48.2% for control (b) and 49.0% for control (c). As shown, control (c) increased the annual solar fraction by less than 1%. When the auxiliary heater is turned OFF, the temperature drops due to heat losses. When it is turned back ON it again heats up the volume to 60 °C to compensate for the heat losses during that period. The difference between shutting down the heater during certain periods and compensating for the heat losses continuously by maintaining its temperature constant at 60 °C was shown not to be significant.

The fact that the achieved performance is lower than that of the previous system is explained by the fact that, during intervals where $T_{solar} > T_{set}$, the total solar hot water storage volume is not increased since water does not go through the auxiliary heater storage. If the additional mixing valve were replaced by an electronic rotating valve that allowed that to happen, the total maximum increase would be 2% for T_{set} = 70 °C and would decrease proportionally with the increase in T_{set}. It was then assumed that such a small saving would hardly compensate for the extra costs of this special control valve.

At T_{set} = 60 °C the system works like retrofitted system 3 and therefore a sensitivity analysis on the auxiliary volume would show the same results. On the other hand, the increase in T_{set} shows different results (Table 4). In retrofitted system 3, for higher values of T_{set}, less water is required from the auxiliary storage and therefore from the retrofitted storage. On the contrary, increasing T_{set} in retrofitted system 4 does not have the same effect since water is required from the retrofitted storage both to the mixing valve and to the auxiliary storage. Thus, the discharge rate of the retrofitted storage is not significantly changed and, consequently, neither are the heat losses or the solar contribution. Hence, the decrease in solar fraction is not so abrupt and is mostly the result of the increase in heat losses in the auxiliary storage. Also in this system, the design guideline for large loads is met as described previously in retrofitted system 3.

Table 4. Annual solar fraction calculations for different auxiliary heater temperatures of retrofitted system 4 with V_{aux} set to 55 L.

T_{set} (°C)	$Q_{aux\text{-}nonsolar}$ (kWh/y)	$Q_{aux\text{-}solar}$ (kWh/y)	Q_{pumps} (kWh/y)	$Q_{losses\text{-}retrofit}$ (kWh/y)	$Q_{losses\text{-}aux}$ (kWh/y)	Annual Solar Fraction (%)
60	2042	930	129	461	135	48.2
70	2081	992	128	470	171	46.2
80	2120	1030	128	470	208	45.4
90	2161	1068	128	470	244	44.6

As shown in Tables 2–4, the performance of retrofitted system 3 and 4 present marginal differences. The series connected system, retrofitted system 3, achieves the highest annual solar fraction but is also the most sensitive to T_{set}. This result indicates that the size of the auxiliary storage should be well designed according to the load so that increases in its temperature are not often needed. In case of big uncertainties in the real domestic hot water load, retrofitted system 4 is more suitable since the decrease in performance is less sensitive to storage temperature increase during long periods. The costs of the two systems are almost identical.

3.6. Standard and Retrofitted Systems

A summary of the annual solar fraction calculations and heat losses in the storages for all systems is presented in Table 5. How well the simulation results describe reality depends on several factors assumed for this study. Some of these are: the performance of the solar collector array, the U-values of the storages, losses by wall conduction, stratification levels, the design and position of inlets and outlets, flow induced mixing, heat losses of pipes and heat exchanger. As all retrofitted systems were built using the same components, inaccuracies that occur in one system model tend to occur in the same way in the others. This makes it significantly more reliable to draw conclusions about the relative performances of the systems. In a future analysis model validation and a detailed economic investigation will be carried out.

Table 5. Annual solar fraction calculations for all systems.

System name	$Q_{aux\text{-}nonsolar}$ (kWh/y)	$Q_{aux\text{-}solar}$ (kWh/y)	Q_{pumps} (kWh/y)	$Q_{losses\text{-}retrofit}$/ $Q_{losses\text{-}stnd}$ (kWh/y)	$Q_{losses\text{-}aux}$ (kWh/y)	Annual Solar Fraction (%)
Standard system (a)	2397	1238	92	648	(-)	44.5
Standard system (b)	2397	1090	60	779	(-)	52.0
Retrofitted system 1 (b)	3105	2134	75	973	(-)	28.9
Retrofitted system 2 (a)	3507	2002	286	886	(-)	34.8
Retrofitted system 2 (b)	3507	1945	243	904	(-)	37.6
Retrofitted system 3 (a)	2037	1074	187	369	145	38.1
Retrofitted system 3 (b)	2037	877	131	447	148	50.5
Retrofitted system 4 (a)	2042	1108	181	392	135	36.9
Retrofitted system 4 (b)	2042	930	129	461	135	48.2
Retrofitted system 4 (c)	2042	914	129	461	123	49.0

Housing all the retrofitting components, controls and required valves in one add-on unit which is then connected to the existing heater, the collectors and the user may reduce the complexity and cost of the installation.

4. Conclusions

Four different system configurations on how to retrofit existing domestic hot water heaters in single-family houses in Sweden were theoretically analysed. The simulation results quantify the impact of the different configurations and control strategies on the annual solar fraction for one set of reference conditions. From the simulation results it was concluded that it is appropriate to use forced circulation and an external heat exchanger for the retrofit. Hence, the performance of the retrofit is not dependent on the tank loop configuration or on the type of existing tank which is being retrofitted.

A high performance (high $F'(\tau\alpha)_n$ and low $F'U$) solar collector array of 6 m^2 is appropriate for the Swedish climate and domestic hot water load. For such collector area, low mass flow rates in the range of 5–10.8 kg/h m^2 maximise the annual solar fraction. Consequently, the requirement on component sizes such as the heat exchanger capacity, pipe diameter, pump size and its energy consumption is reduced. Hence, the cost of the retrofit can be further reduced. A heat exchanger capacity of 300 W/K was found to be adequate to ensure that 95% of the maximum annual solar fraction is achieved.

The annual solar fraction of the retrofitted systems ranges from 28.9% to 50.5%. The retrofit configuration achieving the highest annual performance of 50.5% consists of using the retrofitted tank for solar hot water storage and connecting it in series with a new small auxiliary heater storage tank. Hence, the larger tank works at lower average temperatures while the new smaller and well insulated tank works at higher average temperatures. This increases the solar contribution and reduces the heat losses. The annual solar fraction achieved by a stand-alone standard solar thermal system with the same collector area, storage volume and reference conditions is 52%. Hence, the performances of both systems are comparable while the retrofitted system has the potential to have a lower investment cost. In the future, a model validation and a detailed economical assessment for a Swedish case study will be performed.

Acknowledgments

This study was supported by a Marie Curie program, SolNet—Advanced Solar Heating and Cooling for Buildings—the first coordinated international PhD education program on Solar Thermal Engineering.

References

1. Hang, Y.; Qu, M.; Zhao, F. Economic and environmental life cycle analysis of solar hot water systems in the United States. *Energy Build.* **2012**, *45*, 181–188.
2. Dayan, M. High Performance in Low Flow Solar Domestic Hot Water Systems. Master's Thesis, University of Winsconsin, Madison, MI, USA, 1997.
3. Tsilingiris, P.T. Design and performance of large low-cost solar water heating systems. *Renew. Energy* **1996**, *9*, 617–621.

4. Eicker, U.; Pietruschka, D. Design and performance of solar powered absorption cooling systems in office buildings. *Energy Build.* **2009**, *41*, 81–91.
5. Swedish Energy Agency. *Energy Statistics for Single-Family Houses*; Swedish Energy Agency: Stockholm, Sweden, 2010.
6. Cruickshank, C.A.; Harrison, S.J. Analysis of a Modular Thermal Storage for Solar Heating systems. In *Proceedings of the Joint Conference of the Canadian Solar Buildings Research Network and Solar Energy Society of Canada Inc. (SESCI)*, Montreal, Canada, 2004.
7. Cruickshank, C.A.; Harrison, S.J. Experimental Characterization of a Natural Convection Heat Exchanger for Solar Domestic Hot Water Systems. *ASME Conf. Proc.* **2006**, 425–431.
8. Cruickshank, C.A.; Harrison, S.J. Thermal response of a series- and parallel-connected solar energy storage to multi-day charge sequences. *Sol. Energy* **2011**, *85*, 180–187.
9. Qin, L. Analysys, modeling and optimum design of solar domestic hot water systems. Ph.D. Thesis, Danish Technical University, Copenhagen, Danmark, 1998.
10. Fraser, K.F.; Hollands, K.G.T.; Brunger, A.P. An empirical model for natural convection heat exchangers in SDHW systems. *Sol. Energy* **1995**, *55*, 75–84.
11. Morrison, G.L.; Tran, H.N. Simulation of the long term performance of thermosyphon solar water heaters. *Sol. Energy* **1984**, *33*, 515–526.
12. Ogueke, N.V.; Anyanwu, E.E.; Ekechukwu, O.V. A review of solar water heating systems. *J. Renew. Sustain. Energy* **2009**, *1*, 106–121.
13. Abdul-Jabbar, N.K. Forced *versus* natural circulation solar water heaters: A comparative performance study. *Renew. Energy* **1998**, *14*, 77–82.
14. Davidson, J.; Liu, W. Comparison of natural convection heat exchangers for solar water heating systems University of Minesota, Minneapolis, MN, USA, 1998.
15. Wongsuwan, W.; Kumar, S. Forced circulation solar water heater performance prediction by TRNSYS and ANN. *Int. J. Sustain. Energy* **2005**, *24*, 69–86.
16. Klein, S.A. TRNSYS—Official Website. Available online: http://sel.me.wisc.edu/trnsys (accessed on 1 July 2010).
17. Buckles, W.E.; Klein, S.A. Analysis of solar domestic hot water heaters. *Sol. Energy* **1980**, *25*, 417–424.
18. Hobbi, A.; Siddiqui, K. Optimal design of a forced circulation solar water heating system for a residential unit in cold climate using TRNSYS. *Sol. Energy* **2009**, *83*, 700–714.
19. Duffie, J.A.; Beckman, W.A. *Solar Engineering of the Thermal Processes*, 3rd ed.; John Wiley & Sons Inc.: New York, NY, USA, 2006.
20. Fanney, A.H.; Klein, S.A. Thermal performance comparisons for solar hot water systems subjected to various collector and heat exchanger flow rates. *Sol. Energy* **1988**, *40*, 1–11.
21. Michaelides, I.M.; Wilson, D.R. Simulation studies of the position of the auxiliary heater in thermosyphon solar water heating systems. *Renew. Energy* **1997**, *10*, 35–42.
22. Mills, D.; Morrison, G.L. Optimisation of minimum backup solar water heating system. *Sol. Energy* **2003**, *74*, 505–511.
23. Furbo, S.; Vejen, N.K.; Shah, L.J. Thermal Performance of a Large Low Flow Solar Heating System With a Highly Thermally Stratified Tank. *J. Sol. Energy Eng.* **2005**, *127*, 15–20.

24. Bernardo, L.R.; Davidsson, H.; Karlsson, B. Performance Evaluation of a High Solar Fraction CPC-Collector System. *Jpn. Soc. Mech. Eng. J. Environ. Eng.* **2011**, *6*, 680–692.
25. Sophie, T. Advanced and Sustainable Housing Rennovation Handbook, a guide for designers and planners. Available online: http://www.iea-shc.org/publications/task.aspx?Task=37 (accessed on 1 November 2010).
26. Home page of Conergy Australia. Available online: http://www.conergy.com.au (accessed on 1 February 2009).
27. Thermo Dynamics Ltd. Solar Water Heating, Solar Pumps. Available online: http://www.thermo-dynamics.com (accessed on 1 May 2009).
28. Enerworks, Solar Thermal Solutions. Available online: http://enerworks.com (accessed on 1 July 2009).
29. Widén, J.; Lundh, M.; Vassileva, I.; Dahlquist, E.; Ellegård, K.; Wäckelgård, E. Constructing load profiles for household electricity and hot water from time-use data—Modelling approach and validation. *Energy Build.* **2009**, *41*, 753–768.
30. Swedish Energy Agency. *Measurments of Cold and Hot Water Usage in 44 Single-Family Houses in Sweden*; Swedish Energy Agency: Stockholm, Sweden, 2009.
31. Swedish Energy Agency. *Guidelines for Low Energy Houses*; Report Number EBD-R--09/26; Lund University of Technology, Lund, Sweden, 2009.
32. Swedish Statistics. *Housing and Housing Expenses*; Swedish Statistics: Stockholm, Sweden, 2006.
33. Swedish Energy Agency. *Measurements of Cold and Hot Water Usage in 10 Single-Family Houses*; Swedish Energy Agency: Stockholm, Sweden, 2008.
34. Werner, W. IEA-SHC, Task 26, Publications & Outcomes. In *Proceedings of the Industry Workshop, Solar Combisystems*, London, UK, 2011. Available online: http://www.iea-shc.org/publications/task.aspx?Task=26 (accessed on 1 February 2012).
35. Kim, B.R.; Anderson, J.E.; Mueller, S.A.; Gaines, W.A.; Kendall, A.M. Literature review—Efficacy of various disinfectants against Legionella in water systems. *Water Res.* **2002**, *36*, 4433–4444.
36. WHO. Legionella and the prevention of legionellosis. Available online: http://www.who.int/water_sanitation_health/emerging/legionella/en/index.html (accessed on 1 January 2012).
37. Warmedan, J.; Caris, R. Workshop Legionella. In *Proceedings of International Energy Agency*, *Solar and Cooling Program*, Delft, The Netherlands, 4–5 October 2001. Available online: http://www.iea-shc.org/publications/category.aspx?CategoryID=57 (accessed on 1 February 2012).
38. Darelid, J.; Löfgren, S.; Malmvall, B.E. Control of nosocomial Legionnaires' disease by keeping the circulating hot water temperature above 55 °C: Experience from a 10-year surveillance programme in a district general hospital. *J. Hosp. Infect.* **2002**, *50*, 213–219.
39. Marchesi, I.; Marchegiano, P.; Bargellini, A.; Cencetti, S.; Frezza, G.; Miselli, M.; Borella, P. Effectiveness of different methods to control legionella in the water supply: Ten-year experience in an Italian university hospital. *J. Hosp. Infect.* **2011**, *77*, 47–51.
40. Cabeza, L. Legionella in Combisystems Tanks. Available online: http://www.iea-shc.org/publications/task.aspx?Task=32 (accessed on 1 February 2012).

41. Health, Safety Executive, U.K. The Control of Legionella Bacteria in Water Systems, Approved Code of Practice and guidance. Available online: http://www.hse.gov.uk/pubns/books/l8.htm (accessed on 1 March 2012).
42. Swedish Building Regulations, Statute-book of the Swedish Building Regulations. Available online: http://www.boverket.se/Lag-ratt/Boverkets-forfattningssamling/BFS-efter-forkortning/BBR/ (accessed on 1 December 2011)
43. Safe water installation. Swedish branch rules. Available online: http://www.sakervatten.se/Branschregler (accessed on 1 March 2012).
44. TESS Libraries. Thermal Energy System Specialists TESS Component Library Package. TRNSYS: Transient System Simulation Tool. Available online: http://www.trnsys.com/tess-libraries (accessed on 1 May 2011).
45. Cruickshank, C.A.; Harrison, S.J. Heat loss characteristics for a typical solar domestic hot water storage. *Energy Build.* **2010**, *42*, 1703–1710.
46. Swedish Energy Agency. Hot Water Circulation. Available online: http://energimyndigheten.se/sv/Siteseeker/?q=legionella+sjukdom&defst=True&uaid=5E2A3C27CEB0B04C50EECEBB3DDE489B:3139322E3136382E31312E35:5246323862601135320 (accessed on 1 December 2011).
47. Bernardo, L.R.; Perers, B.; Håkansson, H.; Karlsson, B. Performance evaluation of low concentrating photovoltaic/thermal systems: A case study from Sweden. *Sol. Energy* **2011**, *85*, 1499–1510.
48. Lawrence Berkeley National Laboratory in University of California GenOpt—Generic Optimization Program. Available online: http://gundog.lbl.gov/GO (accessed on 1 June 2011).
49. Wetter, M. *Generic Optimization Program Manual 3-0-2*; Simulation Research Group, Lawrence Berkeley National Laboratory: Berkeley, UC, USA, 2009. Available online: http://engine4.org/g/genopt-generic-optimization-program-user-manual-w316-pdf.pdf (accessed on 1 April 2011).
50. Hollands, K.G.T.; Lightstone, M.F. A review of low-flow, stratified-tank solar water heating systems. *Sol. Energy* **1989**, *43*, 97–105
51. International Energy Agency. Publications & Outcomes. Available online: http://www.iea-shc.org/publications/task.aspx?Task=14 (accessed on 1 January 2012).
52. Wuestling, M.D.; Klein, S.A.; Duffie, J.A. Promising control alternatives for solar water heating systems. *J. Sol. Energy Eng.* **1985**, *107*, 215–221.
53. Swedish Technical Research Centre. Annual solar fraction for solar water heating systems. Available online: http://www.sp.se/sv/index/services/solar/water/list/Sidor/default.aspx (accessed on 1 March 2012).

Article V

Energies **2013**, *6*, 953-972; doi:10.3390/en6020953

OPEN ACCESS

energies

ISSN 1996-1073

www.mdpi.com/journal/energies

Article

Retrofitting Conventional Electric Domestic Hot Water Heaters to Solar Water Heating Systems in Single-Family Houses—Model Validation and Optimization

Luis R. Bernardo

Energy and Building Design Division, Lund University, Box 118 SE-221 00 Lund, Sweden;
E-Mail: Ricardo.Bernardo@ebd.lth.se; Tel.: +46-462227606; Fax: +46-462224719

Received: 14 December 2012; in revised form: 15 January 2013 / Accepted: 22 January 2013 / Published: 12 February 2013

Abstract: System cost reductions and development of standardised plug-and-function systems are some of the most important goals for solar heating technology development. Retrofitting hot water boilers in single-family houses when installing solar collectors has the potential to significantly reduce both material and installation costs. In this study, the TRNSYS simulation models of the retrofitting solar thermal system were validated against measurements. Results show that the validated models are in good agreement with measurements. On an annual basis a deviation of 2.5% out of 1099 kWh was obtained between the auxiliary energy from results and from the simulation model for a complete system. Using the validated model a system optimization was carried out with respect to control strategies for auxiliary heating, heat losses and volume of auxiliary storage. A sensitivity analysis was carried out regarding different volumes of retrofitted hot water boiler, DHW profiles and climates. It was estimated that, with adequate improvements, extended annual solar fractions of 60%, 78% and 81% can be achieved for Lund (Sweden), Lisbon (Portugal) and Lusaka (Zambia), respectively. The correspondent collector area was 6, 4 and 3 m^2, respectively. The studied retrofitted system achieves a comparable performance with conventional solar thermal systems with the potential to reduce the investment cost.

Keywords: solar thermal; storage tank; hot water boiler; retrofit; domestic hot water

Nomenclature:

$\dot{m}$	Mass flow rate (kg/h)
C_p	Specific heat of water (J/kg K)

T_{hot}	Hot water temperature outlet (°C)
$T_{hot,comf}$	Hot water temperature requirement (°C)
ρ	Volumic mass (kg/m^3)
V_{aux}	Volume of the new auxiliary storage (L)
T_{aux}	Thermostat temperature of the heater of the new auxiliary storage (°C)
$T_{aux,ret}$	Thermostat temperature of the heater of the retrofitted hot water boiler (°C)
V_{sol}	Volume of the retrofitted hot water boiler (L)
T_{sol}	Lowest solar hot water temperature on the top third of the retrofitted hot water boiler (°C)
U_{top}	Heat loss factor of the upper part of the retrofitted hot water boiler (W/m^2 °C)
U_{midd}	Heat loss factor of the middle part of the retrofitted hot water boiler (W/m^2 °C)
U_{bottom}	Heat loss factor of the bottom part of the retrofitted hot water boiler (W/m^2 °C)
U_{aux}	Heat loss factor of the new auxiliary storage (W/m^2 °C)
U_{pipes}	Heat loss factor of the pipes (W/m^2 °C)
Q_{HX}	Overall heat transfer coefficient of the heat exchanger (W/K)
$Dead\_band$	Dead band of the heater of the new auxiliary storage °C
$\#nodes_{ret}$	Number of nodes of the retrofitted hot water boiler (-)
$\#nodes_{aux}$	Number of nodes of the new auxiliary storage (-)
Q_{aux}	Auxiliary energy (kWh)
$Q_{aux,mod}$	Modelled auxiliary energy (kWh)
$Q_{aux,meas}$	Measured auxiliary energy (kWh)
$Q_{aux,error}$	Error between the modelled and measured auxiliary energy (%)
$Q_{DHW,mod}$	Modelled provided energy by the system to the user (kWh)
$Q_{DHW,meas}$	Measured provided energy by the system to the user (kWh)
$Q_{DHW,error}$	Error between the modelled and measured provided energy by the system to user (%)
$Q_{aux,ref}$	Auxiliary energy of the reference hot water boiler without solar collectors (kWh/y)
$Q_{energy,miss}$	Total annual energy that was not provided to the load (kWh/y)
Q_{pump1}	Yearly electrical consumption of the pump in the collector circuit (kWh/y)
Q_{pump2}	Yearly electrical consumption of the pump in the tank circuit (kWh/y)
Q_{total}	Yearly sum of the consumption of the pumps and the auxiliary heat (kWh/y)
$Q_{penalty}$	Penalty function of the solar domestic hot water system (kWh/y)
$Q_{penalty,ref}$	Penalty function of the domestic hot water system without solar colelctors (kWh/y)
f_{comf}	Fraction between the penalty function and the total domestic hot water (DHW) load of the DHW reference system (%)
x	Power of the penalty function (-)
SF_{ext}	Extended solar fraction (%)
SF_i	Solar fraction indicator (%)

1. Introduction

According to the Technology Roadmap of the Solar Heating and Cooling program [1], one of the strongest bottlenecks for solar heat technology deployment is the initial cost and economic profitability [2,3]. Some of the main goals for solar heating technology are a system reduction cost of 30%, development of standardised kits and plug-and-function systems. Retrofitting existing domestic hot water (DHW) boilers using plug-and-play docking units has the potential to meet these goals. The investment cost can be significantly reduced both in material and installation costs [1,4,5]. The largest part of the solar thermal market involves retrofitting situations where the investment cost is the main bottleneck [6]. Using a plug-and-play kit for such situations could make it possible to combine a large market with lower investment costs [7]. Just in Sweden there are more than half a million electrically heated single family houses that use conventional water heaters for domestic hot water production [8].

Previous retrofitting solutions commonly consisted of connecting in series the existing hot water system with new upstream solar storage and using the existing hot water boiler as a backup heater [9]. Some make use of thermosyphoning for solar hot water charging. “Conergy”, “Thermo Dynamics” and “Enerworks” are examples of company brands of such commercial products [10–12]. The driving force created by thermosyphoning depends on the pressure losses and therefore on the geometrical characteristics of the tank where the solar hot water is stored [13–16]. Consequently, a new good performance solar hot water tank is normally required to be connected to the existing hot water boiler [10–12]. Since both a new solar heating store and a new docking unit are added, the space requirements are increased and the cost reductions limited. Furthermore, when properly designed, forced circulation systems can significantly achieve higher performances compared with natural convection driven systems [14,17–19].

A product named “Paradigma” has the advantages of retrofitting the existing hot water boiler that was previously used for space heating applications by directly connecting the solar collector to the boiler without using anti-freeze fluid and therefore without the need of a new heat exchanger and storage [20]. The system circulates warm water to prevent the collectors from freezing. The lower temperature of the system is the return temperature from space heating while the outlet temperature from the collectors needs to be higher than the temperature inside the boiler for DHW use. One of the disadvantages of the system is the need of solar collectors with low heat losses since they work at higher temperatures. The system uses vacuum tube collectors with reflectors which work during less than half of the time compared with a conventional system. If flat plate collectors were used instead, the annual performance would be reduced to roughly by half [20]. Also, for space heating systems, a heat pump is a competitive solution. “Solaplug” is a simple retrofitting product consisting of a coil solar heat exchanger around an auxiliary electric heater [21]. This unit replaces the existing electric heater at the bottom of the hot water boiler. Hence, the material and installation decrease but stratification is in principle nonexistent since the auxiliary heater is placed at the bottom.

A theoretical analysis, based on TRNSYS simulations, was performed earlier on several retrofitting system possibilities using forced circulation flow [4]. The results showed that, when designed according to a load, a system where an additional storage is connected in series with the retrofitted tank achieves the highest performance. In such a system the existing hot water boiler is retrofitted to store the solar heat while a smaller new auxiliary storage with an electric heater is added in series to

make sure that the required outlet temperature can be met (Figure 1). When a standard hot water boiler is retrofitted for solar thermal use, the two connections that were previously used only for hot water discharge to the user should now also be used for charge the storage with solar energy. In the theoretical analysis [4], since a technical solution for the flow reversion was not yet achieved, it was assumed that charge and discharge could occur simultaneously and independently. Even if this was a simplification of reality it was valid for a comparison of different retrofitting configurations in relative terms. The system was now built in practice and a technical solution was tested to reverse the flow in the connections of the retrofitted storage. The principle is described in the next section and illustrated in Figure 1. A compact add-on unit that minimizes space requirement and installation costs is advantageous, although there is a trade off between compactness, energy performance and comfort, *i.e.*, the capability to provide the required hot water temperature to the load. In order to accurately optimize the system energy performance taking into account comfort and compactness, testing and validation of the model was required.

The main objectives of the study were to carry out the validation of the system model and to use it for a system optimization and a sensitivity analysis. The system optimization focused on control strategies for auxiliary heating, heat loss reduction and minimum adequate size of the new auxiliary storage. The sensitivity analysis investigated different DHW load profiles, the size of retrofitted hot water boilers and different climates.

2. System Validation

In this section, the methodology and the results of the model validation are described. A physical description of the system along with an illustration of the model is presented. The validation method consisted of minimizing a target function defined as the absolute difference between the simulated and measured auxiliary energies. The identified parameters that minimize the target function are presented. Also, modelled *versus* measured results are illustrated graphically and numerically for different time intervals.

2.1. System Description

The retrofitted system consists of connecting in series a new auxiliary storage with a heater to the existing hot water boiler (Figure 1). This means that the existing boiler is used exclusively for storage of solar hot water, while the new boiler is used for assuring the desired temperature of the hot water. When hot water is drawn off by the user, the water at the top of the retrofitted hot water boiler is pushed to the bottom of the new auxiliary storage and from there to the user.

The two connections of the retrofitted hot water boiler need to be adapted for both hot water discharge and solar energy charge. This was carried out by reversing the direction of the flow in the connections every time a discharge occurs by means of a special valve. During a discharge, the cold water inlet goes to the bottom of the retrofitted hot water boiler via the external heat exchanger. Hence, solar charging during a discharge is possible (Figure 1). However, during such periods, the charging flow on the tank side is given by the load and not by the pump. In this way the mechanism for the flow reversion, as well as the DHW profile, influences how the charging process occurs and therefore the

annual solar fraction. Hence, for increased accuracy, samples from the latest measured DHW loads in 44 Swedish single-family houses were used for selecting the investigated DHW profiles [22,23].

Figure 1. Physical illustration of the retrofitted system tested at the laboratory.

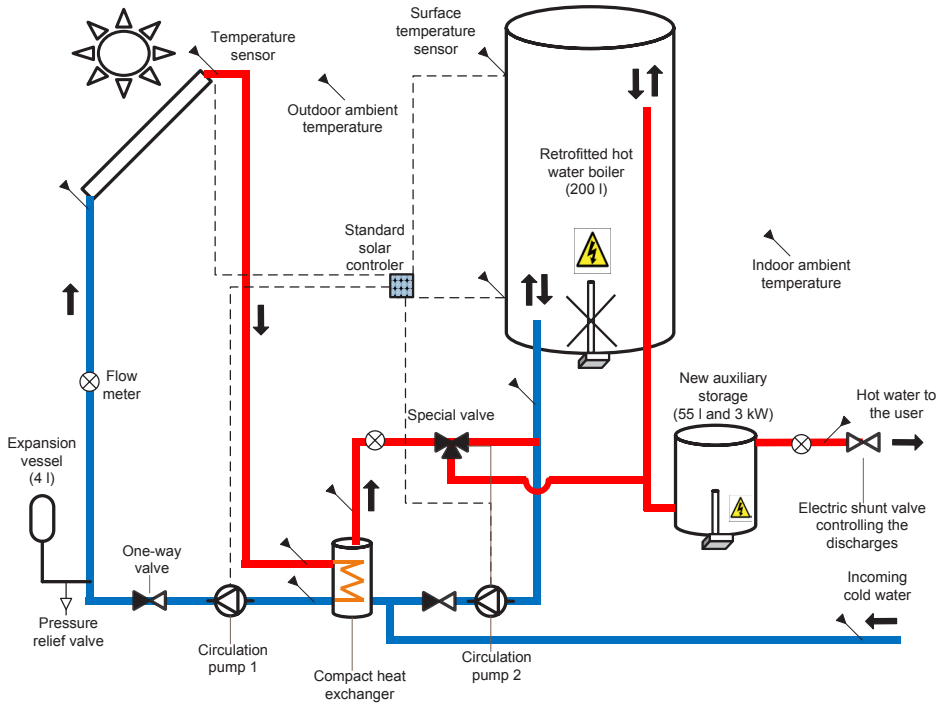

2.2. Validation of the Simulation Model

The retrofitted system, illustrated in Figure 1, was modelled according to Figure 2. The first step of the validation was to select the target parameters that were to be identified. The target parameters are shown in Table 1 and represent the parameters that were more easily identified by measurements. Also, these were possible to be estimated theoretically allowing the iteration to start with a realistic value. Secondly, an energy balance of the model was carried out. The parameter identification was then carried out between July and December by means of fitting the simulation results to measurements by adjusting the target parameters. This was performed by minimizing a target function using a TRNSYS application called Genopt [24–26]. The target function was defined as the absolute difference between the simulated and measured auxiliary energies. Genopt uses algorithms that iterate the target function by changing several system parameters until a minimum is found. Once a set of parameters were identified, simulations and measurement results were compared for a different time period, the validation period between February and June. During this period, tests were carried out at more extreme conditions such as long charge and discharge periods at different flow rates as well as long stand-by periods. This was intended to test the ability of the model to describe other conditions

than the ones used for the validation initially. Finally, simulation results were compared with measured temperature profiles during different test sequences.

Figure 2. Illustration of the validated model along with the identified parameters.

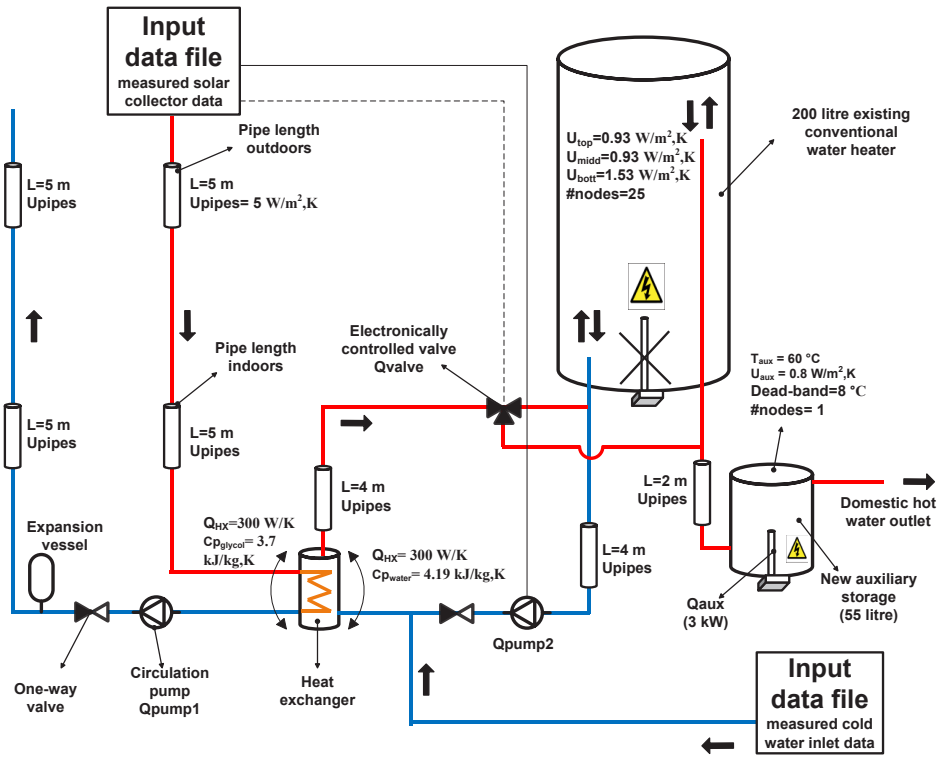

The measured data that was fed into the model according to Figure 2 were the valve control data, the collector fluid and cold water mass flow rates and the temperatures of the collector, cold water, outdoor and indoor ambient. During measurements, data logging was performed every five minutes during roughly one year for 12 temperature sensors, three flow meters and one electric meter.

The results of the parameter identification by matching simulation results with measurements are presented in Table 1 and shown in Figure 2. TRNSYS-Genop did not have enough accuracy for defining three different U-values for the retrofitted tank. Therefore, the proportions between them were estimated theoretically so that the target function could identify only one parameter. The identified parameters are in agreement with the ones measured by Cruickshank and Harrison [27] who showed that three different U-values sufficiently describe the heat losses of a thermal storage.

Table 1. Results from the parameter identification.

Parameters	Identified	Notes
U_{pipes} (W/m^{2}K)	5	Includes heat losses from pipes and from singularities.
Q_{HX} (W/K)	300	Product information. The model does not include heat losses. These are accounted for pipe losses.
U_{top}	0.93	The heat loss coefficient of the retrofitted storage was divided in three where the proportions between them were estimated theoretically.
U_{midd}	0.93	
U_{bottom} (W/m^{2}K)	1.53	
$\#nodes_{ret}$	25	Calculated based on the temperature profile from test discharges.
T_{aux} (°C)	60	Parameters of the new auxiliary heater.
U_{aux} (W/m^{2}K)	0.8	
$Dead\_band$ (°C)	8	
$\#nodes_{aux}$	1	Assumed that there is no stratification since the thermostat and electric heater are placed at the bottom of the tank.

As shown in Figure 3, the correlation between the model and measurements on a monthly basis is good. In Figure 4 one can see that when presented on a daily basis, the correlation is reduced. One factor that contributes to this is the temperature accuracy of the model. The slope of the temperature profile shown in Figure 5 suggests that the identified number of nodes that control the stratification of the retrofitted hot water boiler was approximate. The energy content is also roughly the same, however with a different temperature profile. This is mainly due to the difference of the inlet and outlet pipe configurations between the model and reality. In reality, contrarily to the model, the extracted water from the top exchanges heat with the water at the bottom via the metalic outlet pipe that goes through the store and therefore decreases stratification.

Figure 3. Modelled *vs*. measured monthly auxiliary energy plotted for the whole period July 2010–June 2011.

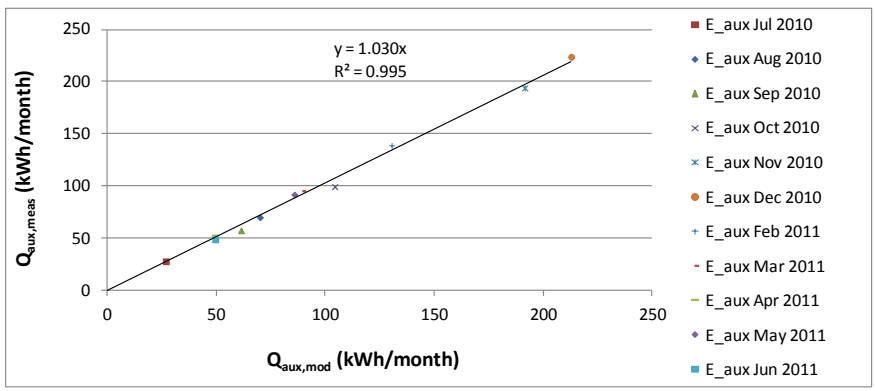

Figure 4. Modelled *vs*. measured daily auxiliary energy plotted for the whole period July 2010–June 2011.

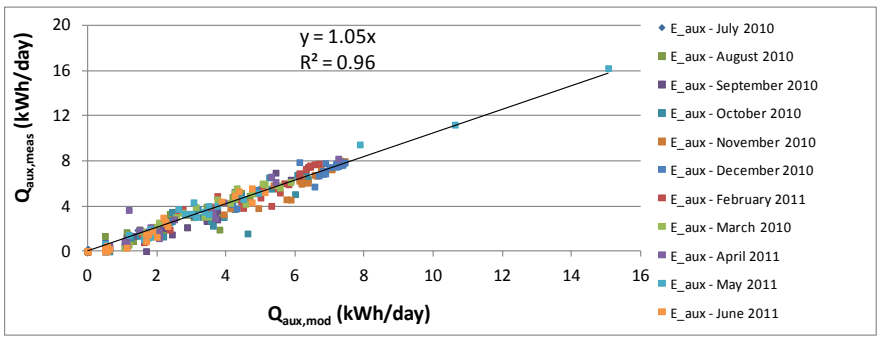

Figure 5. Measured and modelled temperature profiles of water being discharged from the 200 litres retrofitted hot water boiler previously homogenously heated to 53 °C.

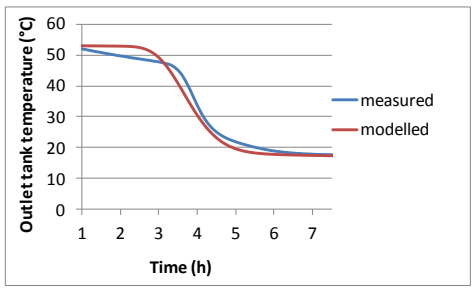

Table 2 shows that TRNSYS-Genopt iterations identified the model parameters in such a way that the total sum of the modelled, $Q_{aux,mod}$ and measured auxiliary energy, $Q_{aux,meas}$, was very close for the identification period July-December 2010. The accuracy of the model is reduced when the system was tested at more extreme conditions during the validation period. The same applies for the modelled and measured energy provided by the system, $Q_{DHW,mod}$ and $Q_{DHW,meas}$.

Table 2. Sum of the modeled *vs*. measured auxiliary and provided energy for the different analysed periods.

TOTAL sum (kWh)	$Q_{aux,mod}$ **(kWh)**	$Q_{aux,meas}$ **(kWh)**	$Q_{aux,error}$ **(%)**	$Q_{DHW,mod}$ **(kWh)**	$Q_{DHW,meas}$ **(kWh)**	$Q_{DHW,error}$ **(%)**
Jul–Dec 2010 (identification period)	667	672 ± 7	0.7	1235	1236 ± 8	0.1
Feb–Jun 2011 (validaion period)	405	427 ± 4	5.3	916	938 ± 6	2.4
Jul 2010–Jun 2011 (all data)	1072	1099 ± 11	2.5	2151	2174 ± 14	1.1

3. System Optimization

In this section, the methodology and results for the system optimization are presented. This took into account energy performance, comfort level to the user and add-on unit compactness. The analysis was focused on control strategies for auxiliary heating, reduction of heat losses and minimum adequate size of the new auxiliary storage. Economics were not accounted in this investigation.

The solar fraction was used in order to compare the relative performances of several system configurations. This expression compares the annual energy use of a solar domestic hot water (SDHW) system with a reference DHW system without solar collectors. The solar fraction definitions used in this study were the extended solar fraction, SF_{ext}, and solar fraction indicator, SF_i, described by Equations (1) to (4) [28,29].

The first one takes into account not only the required energy from auxiliary heating but also the electricity use by the pumps. There is a risk that this target function leads to a system where the desired DHW temperature is not met at all times. For larger discharges the temperature of the water provided to the user may fall below the hot water temperature requirement during certain periods. Hence, a penalty function for such periods was used [28,29]. The SF_i penalises the performance of the system when hot water is provided below the required temperature level. A highly penalising exponential function with a factor of four was used as previously in IEA task 26 and task 32. SF_i does not represent the real fraction of energy savings but can be used to provide information in relative terms regarding how well several systems meet the energy needs within comfort levels. In IEA task 32 it was recommended to verify if the penalty function did not exceed 5% of the total DHW load of the DHW reference system without collectors, *i.e.*, the penalty fraction, $f_{comf} \leq 0.05$, where $f_{comf} = max\left(Q_{penalty}/Q_{aux,ref}, 100\right)$. This comfort limit is included in the analysis:

$$SF_{ext} = 1 - \frac{Q_{aux} + Q_{pump1} + Q_{pump2}}{Q_{aux,ref}} = 1 - \frac{Q_{total}}{Q_{aux,ref}} \tag{1}$$

$$\begin{aligned} SF_i &= min\left(1 - \frac{Q_{aux} + Q_{pump1} + Q_{pump2} + Q_{penalty} - Q_{penalty,ref}}{Q_{aux,ref}}, 0\right) \\ &= min\left(1 - \frac{Q_{total} + Q_{penalty} - Q_{penalty,ref}}{Q_{aux,ref}}, 0\right) \end{aligned} \tag{2}$$

$$Q_{penalty} = C_p \cdot \int_0^{t_y} \dot{m} \cdot [\Delta T + (\Delta T + 1)^x - 1]\, dt \tag{3}$$

where t_y is one year and dt the time step of five minutes. The power, x, of the penalty function was set to 4 [28,29] and ΔT defined as:

$$\Delta T = max\left(0; T_{hot,comf} - T_{hot}\right) \tag{4}$$

$Q_{energy,miss}$ integrates the energy for periods when the hot water temperature falls below the requirement, $T_{hot,comf} > T_{hot}$, and is defined as:

$$Q_{energy,miss} = C_p \cdot \int_0^{t_y} \dot{m} \cdot \left(T_{hot,comf} - T_{hot}\right) dt \tag{5}$$

Energies **2013**, *6* **962**

A base case scenario was used for the start of the optimization process where adequate improvements were incremented for each analysis. This consists of a 200 litres retrofitted hot water boiler, a 50 litres new auxiliary storage with a 3 kW electric auxiliary heater, Lund climate (Sweden) and 6 m^2 solar collectors. A representative DHW profile for this analysis was chosen and is further discussed in the sensitivity analysis. The reference DHW system without solar collectors was defined as a 200 litres hot water boiler with a 3 kW auxiliary heater placed at the bottom with a total DHW load, $Q_{aux,ref}$, of 3448 kWh/y.

3.1. Control Strategies for Auxiliary Heating

In order to improve the comfort level, both the storage size and/or the temperature of the auxiliary heating can be increased. Such variation influences not only the comfort but also the energy performance. Different control strategies for auxiliary heating in both storages were tested.

For controlling the heater of the new auxiliary storage two alternatives were analysed (Figure 6). Both were based on decreasing the temperature setting of the auxiliary heater when higher solar energy was available. Alternative 1 decreases the temperature of the new auxiliary heater proportionally to the increase of the temperature in the highest third of the retrofitted hot water boiler, where the upper temperature sensor is placed. This decrease is such that the combined energy content of both the auxiliary heater and the top third of the retrofitted storage are equal to the new auxiliary storage volume at maximum temperature (90 °C) according to the following equation:

$$T_{aux} = max\left[\left(90 - \frac{(T_{sol} - T_{cold}) \cdot {}^{1}/_{3} \cdot V_{sol}}{V_{aux}}\right), 60\right] \quad (6)$$

Alternative 2 simply consists of decreasing the auxiliary temperature from 90 °C to 60 °C when the top third of the solar storage is at 60 °C or higher. Hence, the risk of decreasing the comfort level is reduced in comparison with control 1. The results regarding the different control strategies for the heater of the new auxiliary storage are presented in Table 3, where also the alternatives of a constant auxiliary temperature of 60 °C and 90 °C are included. Control 1 was shown to be the best control in achieving a balance between high solar fraction and comfort level. The energy that could not be delivered for the alternative with the lowest comfort level, 60 °C, was 3.1% of the total DHW load.

Table 3. Results for the different auxiliary heater control strategies.

Control	SF_{ext} (%)	SF_i (%)	f_{comf} (%)
90 °C	47.3	32.2	15.2
60 °C	63.7	0.0	100.0
control 1	57.9	39.0	18.9
control 2	49.4	34.4	15.1

A sensitivity analysis on having different power rates for the heater of the new auxiliary storage is presented in Figure 7. As shown, a higher power increases the comfort for a fairly constant value of the extended solar fraction with the largest variation between 2 and 3 kW. However a higher power than 3 kW might be limited by the electrical installation of the house.

Figure 6. Alternative 1 and 2 for the control of the new auxiliary heater depending on its volume and available solar energy.

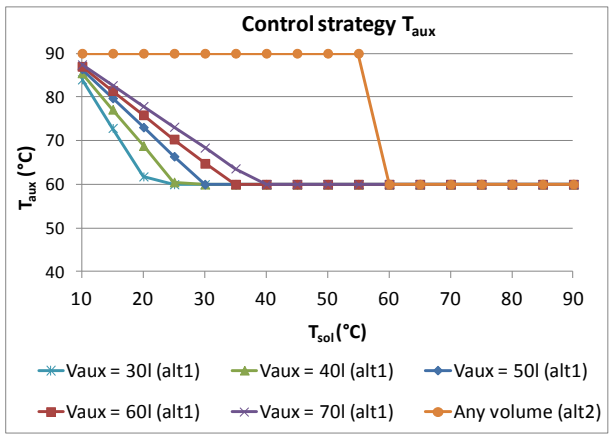

Figure 7. Sensitivity analysis on the power rates of the new auxiliary heater.

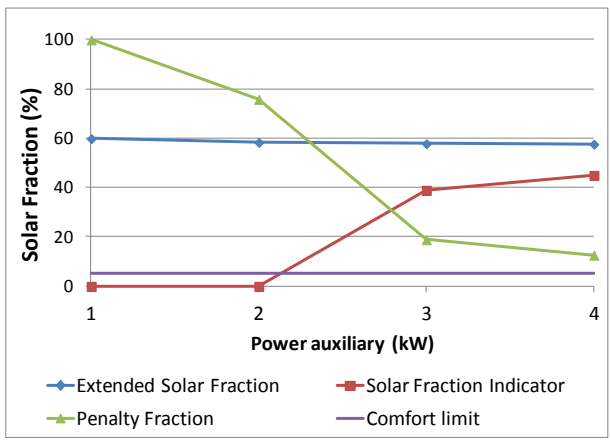

If the desired comfort level is not achieved with a certain size and control of the new auxiliary storage, a pre-set temperature for the heater of the retrofitted hot water boiler can be a solution. Several constant pre-set temperatures were tested ranging from 10 °C (no preheating) to 40 °C. The results are illustrated in Figure 8 and show that for higher pre-heating temperatures the extended solar fraction decreases faster than the increase in the solar fraction indicator. Control was thus found to be an appropriate optimization and was integrated in the base case system for the following analysis.

Figure 8. Performance results for the different pre-heating temperatures for the heater of the retrofitted hot water boiler.

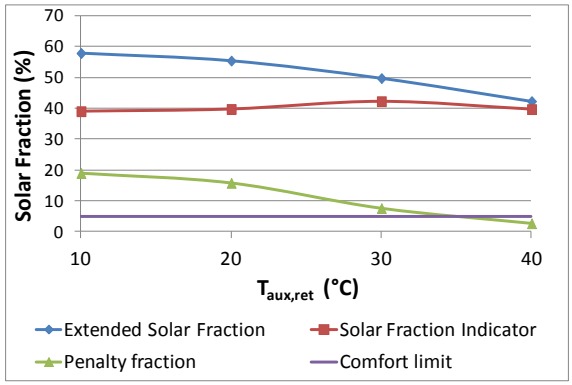

3.2. Heat Loss Reduction

The system was optimized with respect to the reduction of the heat losses by gathering the system components into one unit and using control 1. Heat losses from singularities such as sensors, heat exchanger and valves were accounted by the heat losses from the pipes. Gathering the components into one unit decreases these heat losses. Simulations were carried out for the pipe heat loss reduction by 50% and 70%. This was considered reasonable based on a preliminary 3D model improved design where the pipe length was reduced with more than 75% of the current system. The impact on the annual solar fraction of using a low energy pump (19 W) on the tank side was also tested [30]. The results are presented in Table 4. A 75% pipe heat losses reduction and a low energy pump were integrated in the base case system for the following analysis. These changes increased the extended solar fraction by roughly 2%.

Table 4. Results from the heat loss reduction and pump upgrade investigation.

Case description	SF_{ext} (%)	SF_i (%)	f_{comf} (%)
0% heat loss reduction	57.9	39.0	18.9
50% heat loss reduction	58.4	38.8	19.6
75% heat losses reduction	58.6	39.3	19.3
75% heat losses reduction and low-e pump upgrade (base case)	59.7	41.8	17.9

3.3. Different Volumes of the New Auxiliary Storage

In order to increase the comfort level, the volume of the new auxiliary storage can be increased in alternating fashion or in combination with the increase of the heater temperature. This volume is the most important factor influencing the compactness of the add-on unit that includes all the retrofitting components and is therefore advantageous to minimize it. Simulations for different volumes of the new auxiliary storage were carried out until the value of f_{comf} was below 5%. The tested and validated

volume of the new auxiliary storage was 55 litres. However, the simulated volumes in this analysis were 20, 30, 40, 50, 60 and 70 litres in order to be closer to standard marketed volumes. The number of nodes and the U-value were kept constant. The heat losses of the storage increase for larger surface areas. The pipe heat losses were reduced with 75% and a low energy pump was used on the tank circuit.

The results are presented in Figure 9 and show that for higher volumes the comfort level is improved for a fairly constant value of the extended solar fraction. The largest variation occurs between 40 and 50 litres. For f_{comf} below 5%, the minimum required size for the new auxiliary storage is 70 litres. For such configuration, SF_{ext} equals 58%, SF_i 56% and f_{comf} 2%. During winter periods when no solar energy is available and only the new auxiliary heater provides hot water (at 90 °C), a total of 187 litres at 40 °C can be provided by this system which roughly corresponds to six showers of 30 litres at the same time. For such system the total amount of discharges, for which the provided hot water temperature was below the requirements, were 12 out of 6485 during one year. The energy that was failed to be delivered due to this temperature drop was 0.1% of the total DHW load, $Q_{aux,ref}$. To meet unusual large loads the user has the possibility to turn on the heater of the retrofitted hot water boiler.

Figure 9. Sensitivity analysis on different auxiliary storage volumes.

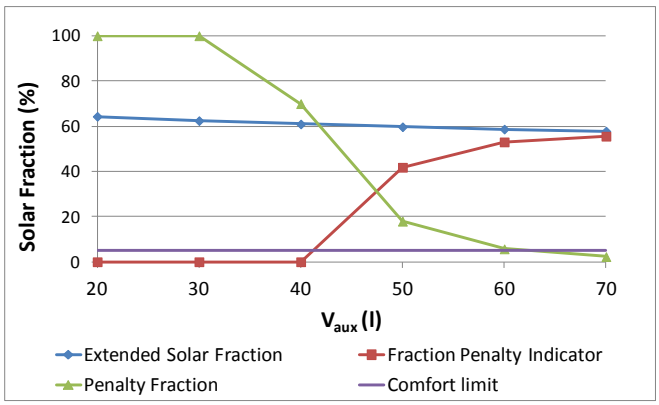

4. Sensitivity Analysis

A sensitivity analysis was performed for three different DHW load profiles, several volumes of the retrofitted hot water boiler between 40 litres and 400 litres and for three different climates.

4.1. Different DHW Load Profiles

Since the load profile can influence the system performance, three different measured DHW load profiles were analysed with different annual energy loads for single-family houses with three inhabitants. These cover a full month and were extrapolated to represent one whole year while adjusted by a seasonal factor [31]. Figures 10 and 11 show DWH profile 2. This was used in the base case scenario for the optimization process since its estimated annual load matches the measured average of

the 44 measured DHW profiles [22]. For simplicity, only DHW profile 2 is presented in detail. The total annual load for the other DHW profiles and the simulation results are presented in Table 5. The total number of discharges during a year for DHW profiles 1, 2 and 3 are 7390, 6485 and 3764, respectively. The energy that could not be delivered was less than 0.1% of the total DHW load, for the three profiles.

Figure 10. Illustration of the measured monthly domestic hot water profile 2 which was used in the annual simulations.

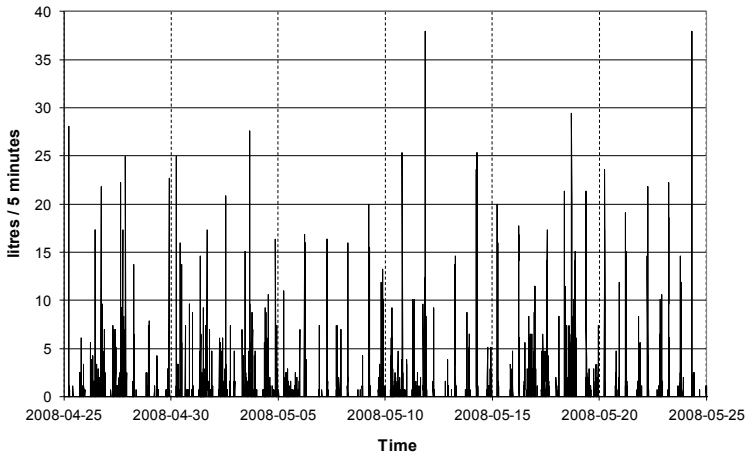

Figure 11. Illustration of the accumulated volume per flow rate for the measured monthly domestic hot water profile 2 which was used in the annual simulations.

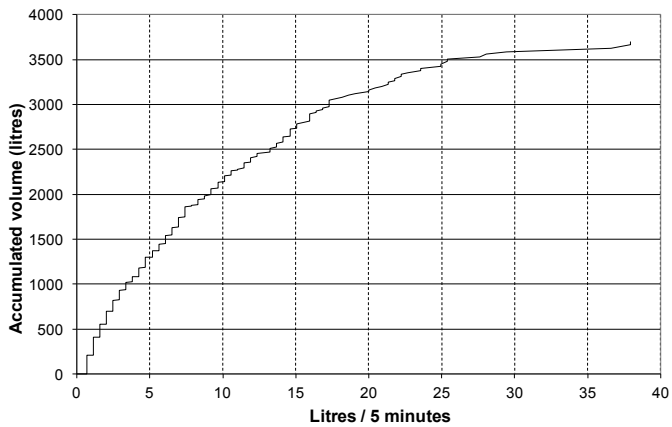

Table 5. Performance of the retrofitted system for three different domestic hot water profiles.

DHW profile #	SF_{ext} (%)	SF_i (%)	$Q_{aux,ref}$ (kWh/y)	f_{comf} (%)
1	57.0	56.9	5832	0.1
2	57.8	55.6	3449	2.2
3	71.6	70.4	2972	1.2

4.2. Different Volumes of the Retrofitted Hot Water Boiler

The existing hot water boiler for the retrofitting can vary in size. It is therefore important to be aware of the comfort and energy performance levels regarding different sizes of retrofitted boilers. A sensitivity analysis was performed in the range of 50–400 litres for 70 litres volume of the new auxiliary heater (good comfort case). It was assumed that the height increased in proportion to the volume. The number of nodes and the U-value were kept constant. The heat losses of the storage increase for larger surface areas. The results are illustrated in Figure 12 and further considered in the Discussion section.

Figure 12. Sensitivity analysis on different volumes of the retrofitted storage.

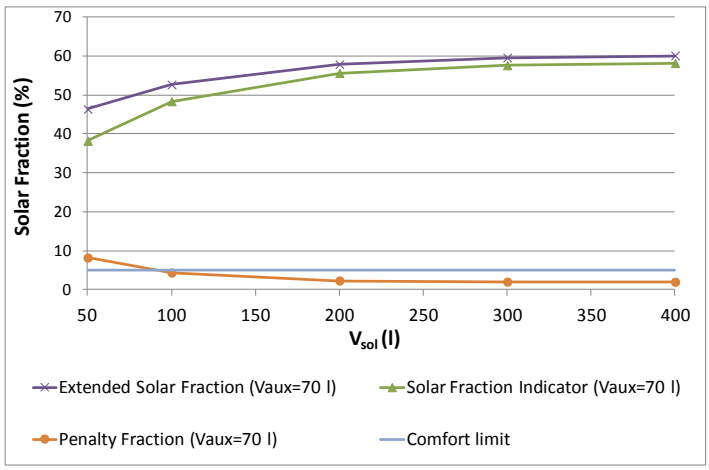

4.3. Different Climates

The distribution of the solar radiation throughout the year in different climates influences not only the extended annual solar fraction, SF_{ext}, but also the number of discharges below comfort level and therefore the solar fraction indicator, SF_i. The climates in Lund (Sweden, lat: 55.7° N), Lisbon (Portugal, lat: 38.7° N) and Lusaka (Zambia, lat: 15.4° S) were evaluated for collector areas of 6, 4 and 3 m^2, respectively. Such areas represent a balance between a high solar fraction and a reduced number of collectors. The tilt was close to optimal for each site and equal to 40°, 30° and 20° from horizontal, respectively. The volume of the new auxiliary storage that ensured that f_{comf} was below 5% were 70, 50 and 50 litres, respectively. The results in different climates and for different control strategies are shown in Table 6.

Table 6. Performance of the retrofitted system in different climates for different auxiliary heating controls.

Location	Control type	Q_{total} (kWh/y)	SF_{ext} (%)	SF_i (%)	f_{comf} (%)
Lund (Sweden)	90 deg	1847	46.4	43.5	3.0
	60 deg	1246	63.9	0.0	100.0
	control 1	1455	57.8	55.6	2.2
Lisbon (Portugal)	90 deg	1304	62.2	59.0	3.2
	60 deg	248	80.3	15.5	64.9
	control 1	765	77.8	73.6	4.4
Lusaka (Zambia)	90 deg	1280	62.9	60.6	2.3
	60 deg	603	82.5	63.7	18.9
	control 1	657	81.0	76.6	4.4

5. Discussion

A limitation on the TRNSYS-Genopt validation method is that other combinations of identified parameters could possibly provide a better fit to the measured results. Also, further improvements could have been carried out on the model to take into account the heat exchange between the water in the retrofitted hot water boiler storage and the pipe placed from top to bottom (Figure 1). However, this was considered to be unnecessary taking into account the model accuracy that was required. The goal with the model validation was to achieve reliable results for the solar fraction at an annual basis while the agreement between model and measurements at a daily basis was less important. This was accomplished with the presented model.

Since the validated model was used for other boundary conditions than during the test, it is difficult to quantify its uncertainty, especially since the DHW load profile used in tests was significantly different from the one in simulations. Some factors decreasing its accuracy are the model simplifications regarding the retrofitted hot water boiler and its inlets/outlets, the assumption of a constant numerical relation between the three U-values of the retrofitted hot water boiler, the assumption that the upper and middle U-values would be the same and the difficulty to estimate the dead-band of the auxiliary heater, since there was no sensor placed inside the new auxiliary heater tank. Both the identified values for the pipe and storage U-values are however in accordance with previous studies [27,28].

The solar fraction indicator, SF_i, evaluates the comfort level in a subjective way. It is difficult to state whether "good" comfort levels are ensured for a penalty value below 5% of the total DHW load or for other value. Also, the power factor, x, equal to 4 seems very penalizing and has a big influence in this result. In fact, if the power factor was reduced to 2, a 50 litres volume of the new auxiliary storage would be enough to guarantee that f_{comf} was below 5% in Lund instead of 70 litres as it was shown. Since the scope of this study did not include new definitions of performance and comfort levels, it was decided to use previous definitions such as the ones used by IEA task 24 and 32 and mark the points within the comfort level according to them. No distinction was made between different types of energy or their sources. Nevertheless, necessary information is provided for a recalculation.

Among the analysed controls, Control 1 was shown to be the best in achieving a balance between high solar fraction and comfort level. This is due to the fact that lower auxiliary temperatures in the

series connection configuration allow higher volumes of cold water inlet in the solar storage which increases the solar collector working hours and efficiency. The user has also the option of manually regulating the termostat of the new auxiliary heater from 60 to 90 °C. Also, for a great increase in capacity, the heater of the retrofitted hot water boiler can also be turned on. It is difficult to predict how a user will regulate the thermostat or even eventually change its own consumption pattern with such auxiliary controls [32]. More advanced controls such as predictive behaviour controls could be further investigated and tested in a real application [33].

The volume of the new auxiliary storage has a large influence on the comfort level and a limited impact on the extended solar fraction due to its low influence on the stored amount of solar energy. Higher volumes of this storage provide a better comfort but also higher heat losses which causes the extended solar fraction to decrease sligtly (Figure 9). This strong influence on comfort can be a disadvantage since it requires an increase in volume of the retrofitting add-on unit. On the other hand it allows the comfort level to be mainly controlled by the manufacturer. The manufacturer can also control the insulation level of the new auxiliary storage which is, among other factors, significantly more important for the system performance than that of the retrofitted hot water boiler [34].

The sensitivity analysis on different climates showed that for climates where the solar irradiation is more distributed along the year, a volume of the new auxiliary storage of 50 litres would be enough to achieve good comfort levels. The analysis also showed that for DHW load profiles with significantly different annual loads the comfort level is still good. Finally, and contrarily to the new auxiliary storage, the volume of the retrofitted hot water boiler significatly influences the solar storage capacity and therefore the SF_{ext}. It was shown in Figure 12 that, for volumes of the retrofitted hot water boiler between 100–400 litres, the SF_{ext} varies by roughly 7 percentage points. This variation does not seem to be critical and, since it is expected that the most common sizes of boilers in Sweden are between 200–300 litres [35], the retrofitting possibilities should be favourable. The volume of the retrofitted hot water boiler also impacts the comfort level but decreasingly for higher volumes of the new auxiliary storage. The biggest comfort problem occurs in the winter time when there is less available solar hot water and when therefore that volume is less important.

To engineer a compact add-on unit is importnant not only for the heat losses decrease but also to decrease the space requirement and installation costs of the add-on unit. It is difficult to evaluate how important the compactness of the retrofitting component is for the user. This is relevant since there is a trade off between compactness (low volume of the new auxiliary storage) and energy performance and comfort. This study provides the necessary information to design the system according to the importance of these factors. Once costs of production for certain market volumes can be determined, an optimization process focused on cost efficiency can be carried out.

6. Conclusions

A retrofitted solar thermal system was evaluated and the simulation models validated against measurements. These results were used to carry out a sensitivity analysis on several improvement possibilities. The adjusted model was shown to be in agreement with the measurements with a deviation of 2.5% out of 1099 kWh of auxiliary energy on an annual basis.

The results from the optimization process showed that one of the investigated control strategies for auxiliary heating increased the extended solar fraction significantly by roughly 11 percentage points with a relatively small compromise on the comfort level. Also, by gathering the retrofitting components into one unit the pipe heat losses were estimated to decrease. In combination with a low energy pump the extended solar fraction was estimated to increase by roughly two percentage points. Furthermore, for the climate of Lund in Sweden, the minimum adequate size of the new auxiliary storage that achieves good comfort was found to be 70 litres equipped with a 3 kW heater. With such improvements and retrofitting a hot water boiler of 200 litres using 6 m^2 of collector area the system achieved an extended solar fraction of 58%.

The sensitivity analysis on different volumes of retrofitted hot water boilers showed that between 100–400 litres the extended solar fraction was reduced roughly by 7 percentage points while achieving good comfort levels, even for other DHW load profiles. For climates where the annual irradiation is more distributed, a volume of 50 litres of the new auxiliary storage would be enough to reach comfort levels for the climates in Lisbon (Portugal) and Lusaka (Zambia). For these climates, extended solar fractions of 78% and 81% can be achieved with the use of 4 and 3 m^2 collector areas, respectively.

The studied retrofitted system achieves therefore a comparable performance with conventional solar thermal systems in single-family houses with the potential to significantly reduce the investment cost for solar heating of domestic hot water.

Acknowledgments

Chris Bales and Bengt Hellström are acknowledged for guidance while writing the manuscript, while Åke Blomsterberg is acknowledged for the proofreading. I am grateful to the Swedish Energy Agency for providing measured data regarding the DHW profiles in single-family houses.

References

1. *Technology Roadmaps: Solar Heating and Cooling*; International Energy Agency: Paris, France, 2012. Available online: http://www.iea.org/publications/freepublications/publication/name.28277.en.html (accessed on 28 November 2012).
2. Hang, Y.; Qu, M.; Zhao, F. Economic and environmental life cycle analysis of solar hot water systems in the United States. *Energy Build.* **2012**, *45*, 181–188.
3. Tsilingiris, P.T. Design and performance of large low-cost solar water heating systems. *Renew. Energy* **1996**, *9*, 617–621.
4. Bernardo, L.R.; Davidsson, H.; Karlsson, B. Retrofitting domestic hot water heaters for solar water heating systems in single-family houses in a cold climate: A theoretical analysis. *Energies* **2012**, *5*, 4110–4131.
5. Eicker, U.; Pietruschka, D. Design and performance of solar powered absorption cooling systems in office buildings. *Energy Build.* **2009**, *41*, 81–91.
6. Burch, J.; Salasovich, J.; Hillman, T. Cold-Climate Solar Domestic Hot Water Heating Systems: Life-Cycle Analyses and Opportunities for Cost Reduction. In *Proceedings of International Solar Energy Society* (*ISES*) *Solar Word Conference*, Orlando, FL, USA, 6–12 August 2005.

7. Michael, B.; Theresa, G.; Kathi, R.; Heidi, S.; Pat, L. High-Performance Home Technologies: Solar Thermal and Photovoltaic Systems. In *Building America's Best Practices Series*; U.S. Department of Energy: Washington DC, USA, 2007. Available online: http://www1.eere.energy.gov/solar/solar_buildings.html (accessed on 17 July 2012).
8. *Energy Statistics for Single-Family Houses*; Swedish Energy Agency: Stockholm, Sweden, 2010. Available online: http://213.115.22.116/System/TemplateView.aspx?p=Energimyndigheten&view=default&id=8613121560eb43158f8d5c775820e3f7 (accessed on 1 February 2012).
9. Sophie, T. *Advanced and Sustainable Housing Renovation Handbook*, *a Guide for Designers and Planners*; International Energy Agency: Paris, France, 2010. Available online: http://www.iea-shc.org/publications/task.aspx?Task=37 (accessed on 1 November 2010).
10. Homepage of Conergy Australia. Available online: http://www.conergy.com.au (accessed on 1 February 2009).
11. *Solar Water Heating, Solar Pumps*; Thermo Dynamics Ltd.: Halifax, Canada. Available online: http://www.thermodynamics.com (accessed on 1 May 2009).
12. Enerworks, Solar Thermal Solutions. Available online: http://enerworks.com (accessed on 1 July 2009).
13. Fraser, K.F.; Hollands, K.G.T.; Brunger, A.P. An empirical model for natural convection heat exchangers in SDHW systems. *Sol. Energy* **1995**, *55*, 75–84.
14. Ogueke, N.V.; Anyanwu, E.E.; Ekechukwu, O.V. A review of solar water heating systems. *J. Renew. Sustain. Energy* **2009**, *1*, 106–121.
15. Cruickshank, C.A.; Harrison, S.J. Experimental Characterization of a Natural Convection Heat Exchanger for Solar Domestic Hot Water Systems. In *Proceedings of ASME International Design Engineering Technical Conferences and Computers and Information in Engineering*, Philadelphia, PA, USA, 10–13 September 2006; pp. 425–431.
16. Morrison, G.L.; Tran, H.N. Simulation of the long term performance of thermosyphon solar water heaters. *Sol. Energy* **1984**, *33*, 515–526.
17. Dayan, M. High Performance in Low Flow Solar Domestic Hot Water Systems. Master's Thesis, University of Winsconsin, Madison, MI, USA, 1997. Available online: http://digital.library.wisc.edu/1793/7729 (accessed on 2 March 2012).
18. Khalifa, A. Forced *versus* natural circulation solar water heaters: A comparative performance study. *Renew. Energy* **1998**, *14*, 77–82.
19. Davidson, J.; Liu, W. *Comparison of Natural Convection Heat Exchangers for Solar Water Heating Systems*; University of Minesota: Minneapolis, MN, USA, 1998. Available online: http://www.osti.gov/bridge/servlets/purl/676960-ayAvwF/webviewable (accessed on 4 April 2012).
20. Homepage of Paradignma—AquaSystem. Available online: http://www.paradigma.de/solaranlage/aquasystem (accessed on 28th November 2012).
21. Mondol, J; Smyth, M. Comparative Performance Analysis of Solar Heat Exchangers for Solar Domestic Hot Water Systems. In *Proceedings of Eurosun International Solar Energy Society* (*ISES*) *Conference*, Rijeka, Croatia, 17–21 September 2012.
22. *Measurments of Cold and Hot Water Usage in 44 Single-Family Houses in Sweden*; Swedish Energy Agency: Stockholm, Sweden, 2009, ISSN 1403-1892, ER:2009:26. Available online: http://webbshop.cm.se/System/ViewResource.aspx?p=Energimyndigheten&rl=default:/Resources/Permanent/Static/b9a064ece4d747868b5c20d1a03ab0a2/2124W.pdf (accessed on 2 February 2011).

23. *Measurements of Cold and Hot Water Usage in 10 Single-Family Houses*; Swedish Energy Agency: Stockholm, Sweden, 2008. Available online: http://webbshop.cm.se/System/TemplateView.aspx?p=Energimyndigheten&view=default&cat=/Rapporter&id=d53ecd5488b64010b76fbdadaa14d776 (accessed 2008).
24. *GenOpt—Generic Optimization Program*. Lawrence Berkeley National Laboratory at the University of California, Berkeley: Berkeley, CA, USA. Available online: http://gundog.lbl.gov/GO (accessed on 1 June 2011).
25. Klein, S.A. *A Transient Systems Simulation Program*; The University of Wisconsin Madison: Madison, WI, USA. Available online: http://sel.me.wisc.edu/trnsys (accessed on 1 July 2010).
26. *Thermal Energy System Specialists TESS Component Library Package*; Transient System Simulation Tool: Madison, WI, USA. Available online: http://www.trnsys.com/tess-libraries (accessed on 1 May 2011).
27. Cruickshank, C.A.; Harrison, S.J. Heat loss characteristics for a typical solar domestic hot water storage. *Energy Build.* **2010**, *42*, 1703–1710.
28. Heimrath, R.; Haller, M. *The Reference Heating System, the Template Solar System of Task 32*; International Energy Agency: Paris, France. Available online: http://archive.iea-shc.org/publications/task.aspx?Task=32 (accessed on 12 December 2012).
29. Weiss, W. *Solar Heating Systems for Houses—A Design Handbook for Solar Combisystems*; James and James (Science Publishers) Ltd.: London, UK, 2007.
30. Wilo Technical Online Catalogue. Available online: http://productfinder.wilo.com/en/GB/productrange/000000010002929a00040023/fc_range_pumplist (accessed on 28 November 2012).
31. Swedish Energy Agency. *Guidelines for Low Energy Houses*; Report Number EBD-R--09/26; Lund University of Technology: Lund, Sweden, 2009.
32. Olmos, L.; Ruester, S.; Liong, S.-J.; Glachant, J.-M. Energy efficiency actions related to the rollout of smart meters for small consumers, application to the Austrian system. *Energy* **2011**, *36*, 4396–4409.
33. Prud'homme, T.; Gillet, D. Advanced control strategy of a solar domestic hot water system with a segmented auxiliary heater. *Energy Build.* **2001**, *33*, 463–475.
34. *Solar Heating Systems—Educational Notes*; Department of Civil Egineering, Technical University of Denmark: Lyngby, Denmark. Available online: http://www.kurser.dtu.dk/2011–2012/11117.aspx?menulanguage=en-gb (accessed on 28 November 2012).
35. Bernardo, L.R. *Retrofitted Solar Thermal System for Domestic Hot Water for Single Family Electrically Heated Houses*; Report EBD-T--10/13; Lund University of Technology: Lund, Sweden, 2010.